Insulin-Like Growth Factor 2 mRNA-Binding Protein 2 as a Regulator of Macrophage Function: Potential Implications for Tumor Progression

Dissertation

zur Erlangung des Grades

des Doktors der Naturwissenschaften

der Naturwissenschaftlich-Technischen Fakultät

der Universität des Saarlandes

von

Hanna Sonja Schymik

Saarbrücken

2025

Tag des Kolloquiums:	22.10.2025
Dekan:	Prof. Dr.-Ing. Dirk Bähre
Berichterstatter:	Prof. Dr. Alexandra K. Kiemer
	Prof. Dr. Christian Ducho
Vorsitz:	Prof. Dr. Andriy Luzhetskyy
Akad. Mitarbeiter:	Dr. Sabrina Schnur

Die Daten der vorliegenden Dissertation wurden im Zeitraum von September 2020 bis März 2025 am Institut für Pharmazeutische Biologie der Universität des Saarlandes unter der Betreuung von Prof. Dr. Alexandra K. Kiemer erhoben.

Contents

Abstract

Macrophages are key regulators of the tumor microenvironment, influencing tumor progression through their metabolic and immunological profiles. This thesis examines the role of the RNA-binding protein IGF2BP2 (Insulin-like Growth Factor 2 mRNA-Binding Protein 2) in macrophage function, with a focus on metabolism, migration, and tumor interaction.

Initial experiments revealed species-specific regulation: stimulation with lipopolysaccharide (LPS) increased Igf2bp2 levels in murine macrophages while reducing its expression in human cells. In contrast, M2 polarization, induced by interleukin-4, upregulated IGF2BP2 in both species.

Myeloid-specific IGF2BP2 knockout (KO) in mice led to increased glycolysis, impaired mitochondrial respiration, and reduced expression of tumor-associated macrophage (TAM) markers. Lipidomic profiling revealed altered membrane composition, correlating with reduced migration *in vitro*. This was confirmed *in vivo* via intravital microscopy.

In a lung carcinoma model, IGF2BP2-deficient female mice showed reduced tumor growth, fewer TAMs, and a shift toward pro-inflammatory macrophages. No effect was observed in males.

Pharmacological inhibition of IGF2BP2 in human macrophages impaired mitochondrial function and reduced pro-angiogenic gene expression.

These findings identify IGF2BP2 as a regulator of macrophage activity and tumor progression, suggesting its potential as an immunotherapeutic target.

Zusammenfassung

Makrophagen sind zentrale Regulatoren des Tumormikromilieus und beeinflussen das Tumorwachstum über ihre metabolischen und immunologischen Eigenschaften. Diese Arbeit untersucht die Rolle des RNA-bindenden Proteins IGF2BP2 (Insulin-like Growth Factor 2 mRNA-Binding Protein 2) in der Funktion von Makrophagen mit Fokus auf Metabolismus, Migration und Tumorinteraktion.

Erste Experimente zeigten eine speziesabhängige Regulation: Die Stimulation mit Lipopolysaccharid (LPS) erhöhte die *Igf2bp2*-Expression in murinen Makrophagen, während sie in humanen Zellen reduziert wurde. M2-Polarisierung durch Interleukin-4 führte in beiden Spezies zur Hochregulation von IGF2BP2.

Ein myeloidspezifischer Knockout (KO) von IGF2BP2 in Mäusen resultierte in erhöhter Glykolyse, beeinträchtigter mitochondrialer Atmung und reduzierter Expression tumorassoziierter Marker. Lipidom-Analysen zeigten eine veränderte Membranzusammensetzung, korreliert mit verminderter Migration *in vitro*. Dies wurde durch intravitale Mikroskopie *in vivo* bestätigt.

Im Lungenkarzinom-Modell wiesen IGF2BP2-defiziente weibliche Mäuse reduziertes Tumorwachstum, weniger TAMs und eine Polarisierung zu proinflammatorischen Makrophagen auf. Bei männlichen Tieren zeigte sich kein Effekt.

Die Hemmung von IGF2BP2 in humanen Makrophagen beeinträchtigte die mitochondriale Funktion und senkte die Expression proangiogener Gene. IGF2BP2 erweist sich damit als Regulator der Makrophagenfunktion und potenzielles immuntherapeutisches Target.

1 Introduction

1.1 Cancer: A Global Health Challenge

Cancer represents the second leading cause of death worldwide, with a significant and steadily increasing global burden. In 2022, approximately 19.98 million new cancer cases and 9.74 million cancer-related deaths were reported globally (Ferlay et al., 2021; Ritchie et al., 2023), accounting for approximately one in six deaths worldwide (Boussios et al., 2024; Pyarilal et al., 2025). The impact of cancer is particularly severe in low- and middle-income countries, which face considerable challenges in cancer care, contributing to an increasing burden of disease in these regions (Jackman et al., 2024; Tečić Vuger et al., 2024).

Among various cancer types, lung, breast, colorectal, prostate, and stomach cancers are the most prevalent globally, with lung cancer being the most diagnosed malignancy, accounting for approximately 12.4% of all new cancer cases and 18.7% of cancer deaths globally in 2022 (Ferlay et al., 2021). Cancer incidence continues to rise, and predictions indicate that the number of cases and deaths could nearly double in the next 20 years, underscoring the urgency of addressing this public health issue (Chanu and Singh, 2024).

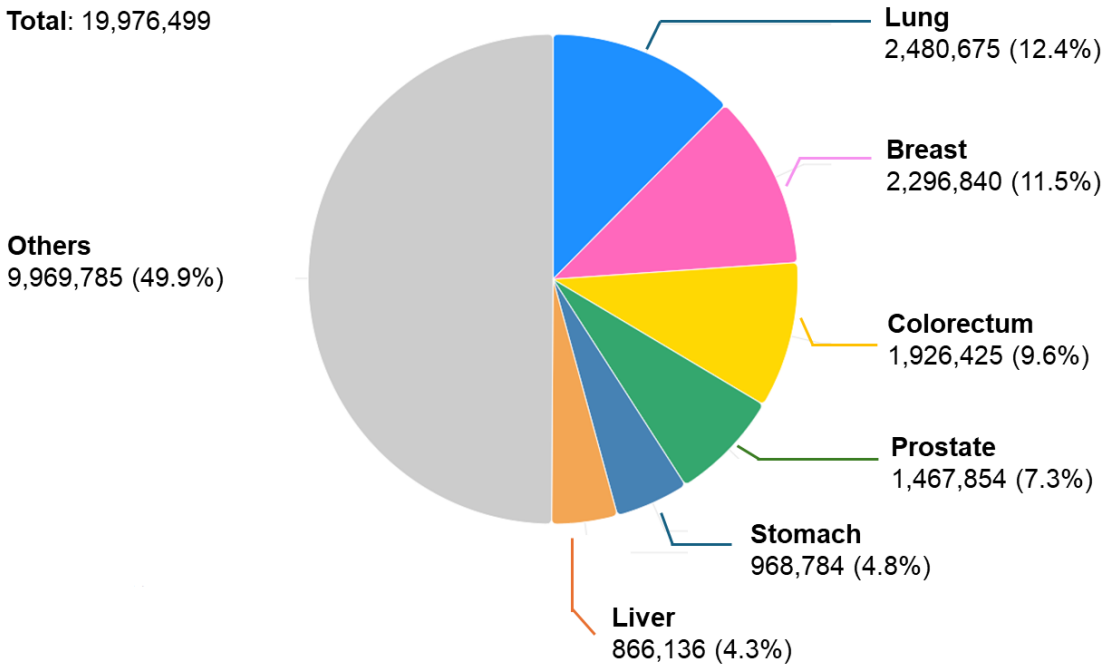

Figure 1. Tumor incidence in 2022. Data was obtained from the GLOBOCAN 2022 study (Ferlay et al., 2021).

1.2 Inflammation and Immune Evasion: Interconnected Hallmarks of Cancer

Hanahan and Weinberg's landmark framework, the "hallmarks of cancer," describes the core biological features that underline tumor initiation, progression, and metastasis. These hallmarks include sustaining proliferative signals, evading growth suppression, resisting programmed cell death, promoting replicative immortality, inducing angiogenesis, enabling invasion and metastasis, escaping immune destruction, tumor-promoting inflammation, and reprogramming cellular energy metabolism (Gyorffy et al., 2024; Hanahan and Weinberg, 2011; Meirson et al., 2020).

Within this framework, the immune system plays a dichotomous role, capable of both suppressing and actively promoting tumor growth. On the one hand, a robust immune response can eliminate nascent tumor cells; on the other hand, persistent inflammatory processes foster a microenvironment that supports tumor development (Hanahan and Weinberg, 2011; Nakamura and Smyth, 2019). Prolonged inflammation often results in an immunosuppressive niche in which cancer cells evade immune surveillance by downregulating antigen presentation, secreting immunosuppressive cytokines, or recruiting regulatory immune cells (Greten and Grivennikov, 2019; Zhang et al., 2017). This environment promotes tumor cell survival, stimulates angiogenesis, promotes genomic instability, and perpetuates immune evasion (Greten and Grivennikov, 2019; Zhao et al., 2021a). Mechanistically, tumor cells can downregulate major histocompatibility complex (MHC) molecules and harness regulatory T cells (Tregs) or myeloid-derived suppressor cells (MDSCs), collectively weakening anti-tumor immunity (Attiq and Afzal, 2023; Maueröder et al., 2014). As a result, cancers adept at immune evasion often exhibit resistance to therapy and can exploit chemotherapy-induced inflammation to further amplify immunosuppressive pathways (Edwardson et al., 2019).

From a therapeutic standpoint, targeting both inflammation and immune evasion with anti-inflammatory agents, immune checkpoint inhibitors, or a combination thereof offers a way to reinvigorate the anti-tumor immune response (Coussens et al., 2013; Crusz and Balkwill, 2015; Zhao et al., 2021b). Accordingly, clinical and preclinical studies increasingly demonstrate that the combination of anti-inflammatory strategies, such as nonsteroidal anti-inflammatory drugs (NSAIDs), with conventional chemotherapeutic agents can enhance therapeutic efficacy or

exert direct anticancer effects, thereby reinforcing chronic inflammation as a critical driver of malignancy (Piskovatska et al., 2023; Ramos-Inza et al., 2021; Thiruchenthooran et al., 2023).

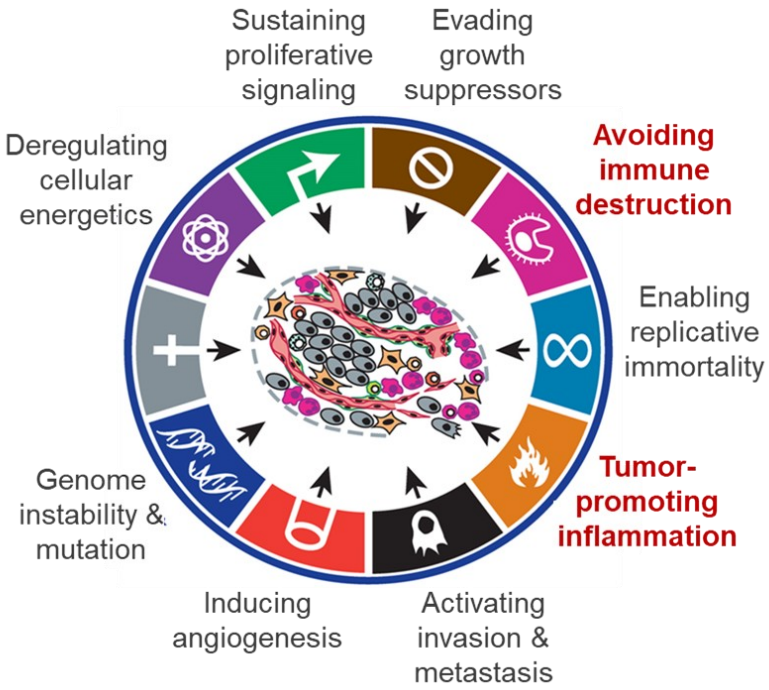

Figure 2. Hallmarks of cancer. Adapted from (Hanahan and Weinberg, 2011).

1.3 The Tumor Microenvironment

The tumor microenvironment (TME) is a complex and dynamic network that influences cancer initiation, progression, and therapeutic outcomes. In addition to malignant cells, it includes immune cells, fibroblasts, endothelial cells, and structural components, such as the extracellular matrix (Neophytou et al., 2021a; Rasheed and Koyyala, 2020). The TME has been shown to play a critical role in the development of malignancy by changing its composition during cancer progression (Arneth, 2020; Zhao et al., 2024).

Within this multicellular network, immune cells can act as both tumor suppressors and tumor promoters, depending on their activation status and the signals they receive from neighboring cells (Galli et al., 2020; Lei et al., 2020). For example, cytotoxic T lymphocytes (CTLs) and certain natural killer (NK) cell subsets actively recognize and eliminate tumor cells by releasing cytotoxic granules and pro-inflammatory cytokines (Bhargav et al., 2023; Hinshaw and Shevde, 2019). Conversely, Tregs and MDSCs can promote an immunosuppressive niche by secreting anti-inflammatory mediators, such as IL-10 and TGF-β, which dampen CTL and NK activity, thereby facilitating immune evasion (Lei et al., 2020; Ren et al., 2021). Similarly, macrophages

exhibit a functional spectrum, with M1-like phenotypes exerting tumoricidal activities and M2-like phenotypes promoting immunosuppression and angiogenesis (He and Zhang, 2021; Neophytou et al., 2021b).

Cancer-associated fibroblasts (CAFs) add another layer of complexity to the TME. Once considered a uniform cell type, CAFs are now recognized as diverse populations that reshape tumor architecture through the deposition of collagen, matrix cross-linking, and the secretion of pro-angiogenic signals (Goenka et al., 2023; Zhao et al., 2023). They also modulate immune cell recruitment and function, further driving cancer progression.

Given its central role in shaping tumor behavior, the TME has become a target for innovative therapeutic strategies. Immunomodulatory treatments, such as immune checkpoint inhibitors and adoptive cell therapies, aim to reprogram the TME into a more immunogenic and therapeutically responsive state (Rasheed and Koyyala, 2020; Ren et al., 2021).

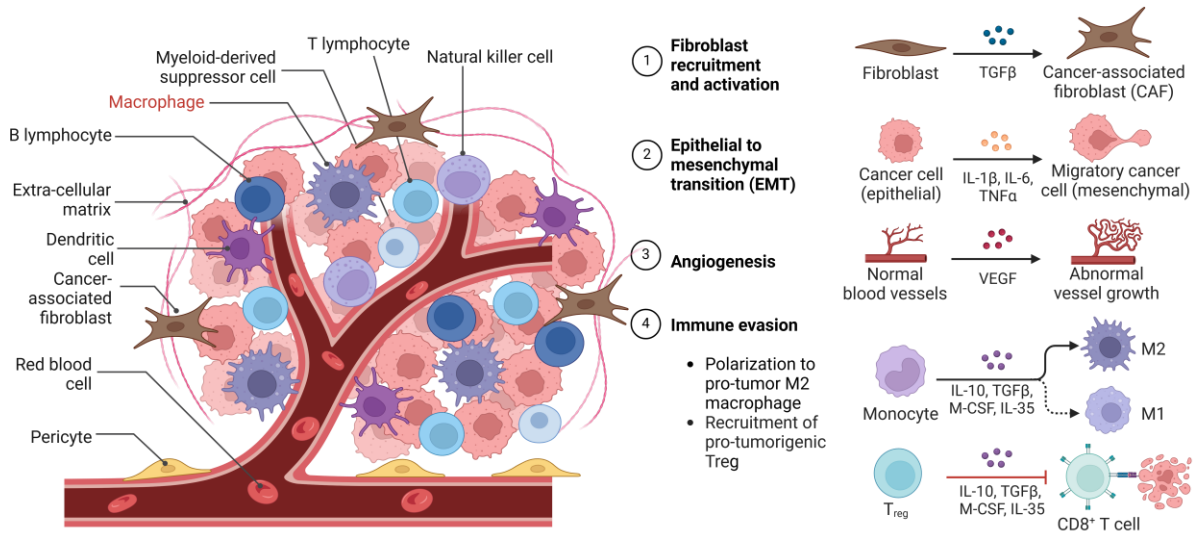

Figure 3. The tumor microenvironment (TME). Adapted from (Herrera et al., 2019).

1.4 Macrophages

Macrophages are highly adaptive immune cells that play a pivotal role in maintaining tissue homeostasis, defending against pathogens, and orchestrating tissue repair (Sreejit et al., 2020; Watanabe et al., 2019). They arise from two developmentally distinct sources: embryonic progenitor cells and bone marrow-derived hematopoietic stem cells (HSCs). During embryogenesis, primitive macrophages originate from erythro-myeloid progenitors in the yolk sac and fetal liver and subsequently reside in various tissues, including the brain, liver, and skin

(Goldmann et al., 2016; Hoeffel and Ginhoux, 2015). These tissue-resident macrophages, including microglia in the brain and Kupffer cells in the liver, are established prenatally and possess the capacity for self-renewal, thereby maintaining their populations independently of adult hematopoiesis throughout life (Park et al., 2022; Sheng et al., 2015).

In contrast, bone marrow-derived macrophages originate from HSCs, which give rise to circulating monocytes that infiltrate tissues during inflammation or injury and subsequently differentiate into macrophages *in situ* (Doyle et al., 2024; Shapouri-Moghaddam et al., 2018). The relative contribution of each origin varies by tissue and physiological context. For example, lung macrophages have mixed developmental origins, whereas the central nervous system is predominantly populated by yolk sac-derived microglia, except for plexus macrophages (Evren et al., 2019; Goldmann et al., 2016).

Functionally, macrophages serve as professional phagocytes, engulfing pathogens, apoptotic cells, and debris to maintain tissue integrity (Van Broeckhoven et al., 2021; Kapellos et al., 2016a). They also bridge innate and adaptive immunity by presenting antigens *via* MHC class II molecules to activate T cells. Moreover, macrophages modulate immune responses by secreting a diverse array of cytokines that can either promote inflammation or support resolution and tissue repair, depending on their activation state and environmental signals (Herb and Schramm, 2021; Yang et al., 2023).

1.4.1 Macrophage Polarization

The functional heterogeneity of macrophages arises from their plasticity, which enables them to dynamically adapt their phenotype and function in response to environmental signals, allowing them to undertake diverse functions such as pathogen clearance, tissue repair, and immune regulation (Murray, 2017; Shapouri-Moghaddam et al., 2018). To conceptualize this diversity, a widely used framework categorizes macrophages into two major subsets: "classically activated" M1 and "alternatively activated" M2 macrophages (Strizova et al., 2023a; Yunna et al., 2020).

M1 macrophages, also known as "classically activated" macrophages, are primarily induced by microbial stimuli such as lipopolysaccharide (LPS), interferon-γ (IFN-γ), and granulocyte-macrophage colony-stimulating factor (GM-CSF) (Lee, 2019; Wang et al., 2023a). This polarization activates a robust Th1-skewed proinflammatory program essential for defense against intracellular pathogens and tumor cells. M1 macrophages secrete high levels of

proinflammatory cytokines (TNF, IL-1α, IL-1β, IL-6, IL-12, IL-23) and inducible enzymes such as cyclooxygenase-2 (COX-2) and inducible nitric oxide synthase (iNOS), the latter of which generate reactive oxygen and nitrogen species (ROS, NO) and confer potent microbicidal and tumoricidal activity (Murray, 2017; Viola et al., 2019; Yao et al., 2019). Functionally, M1 macrophages enhance antigen presentation by upregulating MHC class II, CD40, CD80, and CD86, while producing chemokines (e.g., CXCL9-11, CCL2-5) that recruit and activate effector T cells (Montoya et al., 2019; Zhang et al., 2021a). At the transcriptional level, M1 polarization is orchestrated by signaling pathways and transcription factors, including NF-κB, STAT1, IRF5, AP-1, and ATF2, which activate genes involved in immune activation, chemotaxis, and metabolism (Li et al., 2018; Rajabalee et al., 2023).

Metabolically, M1 macrophages switch to aerobic glycolysis to produce biosynthetic precursors necessary for inflammatory responses. This metabolic reprogramming is driven in part by endogenous nitric oxide (NO), which inhibits key mitochondrial enzymes such as pyruvate dehydrogenase (PDH) and aconitase 2, thereby suppressing oxidative phosphorylation (OXPHOS) and channeling glucose-derived carbon into glycolysis (Palmieri et al., 2020; Soto-Heredero et al., 2020). Metabolic intermediates, such as succinate and itaconate, not only fuel energy demands but also stabilize HIF-1α and promote IL-1β production, thereby further amplifying inflammation (Huang et al., 2024; Luan and Medzhitov, 2016).

In addition to their antimicrobial role, M1 macrophages also have anti-tumor properties. They can phagocytose cancer cells, release pro-apoptotic cytokines, and modulate the tumor microenvironment (Choo et al., 2018; Gunassekaran et al., 2021). Novel therapeutic approaches exploiting these properties include chimeric antigen receptor-macrophage (CAR-M) therapy, in which macrophages are genetically engineered to express receptors targeting specific tumor antigens, thereby enhancing their anti-tumor efficacy (Chettri et al., 2024; Huo et al., 2023). In addition, extracellular vesicles (EVs) derived from M1 macrophages and loaded with therapeutic microRNAs or chemotherapeutic agents are being investigated as innovative vehicles for targeted cancer immunotherapy (Jorquera-Cordero et al., 2022; Tang et al., 2024).

M2 macrophages (alternatively activated macrophages) are induced by Th2 cytokines, such as IL-4, IL-10, and IL-13, which, in part, initiate an anti-inflammatory program *via* STAT6 and IRF4 (Lee, 2019; Yao et al., 2019). M2 macrophages exhibit high expression of scavenger receptors, including CD163, CD204, and CD206, which promote efficient efferocytosis and contribute to tissue homeostasis (Mehrotra and Ravichandran, 2022; Taban et al., 2022).

Consistent with their pro-resolving role, M2 macrophages secrete anti-inflammatory mediators, including IL-10 and TGF-β. They upregulate enzymes such as arginase-1 (Arg-1) and indoleamine 2,3-dioxygenase (IDO), which deplete local L-arginine and tryptophan, respectively, limiting NO production and T-cell-mediated inflammation to promote a more immune-tolerant, tissue-repairing environment (Arlauckas et al., 2018; Summer et al., 2025; Yu et al., 2019). Functionally, M2 activation promotes tissue repair, angiogenesis, and immunotolerance, in part through the production of chemokines such as CCL17, CCL22, and CCL24, which recruit regulatory T cells (Strizova et al., 2023a; Tong et al., 2021). However, this pro-repair capacity can become maladaptive if chronically maintained, leading to fibrosis or tumor-promoting immunosuppression (Komohara et al., 2016; Mantovani et al., 2013).

Metabolically, M2 macrophages rely on OXPHOS and fatty acid oxidation (FAO) pathways, which are partially regulated by the transcription factor PPARγ (Mills and O'Neill, 2016; Pérez and Rius-Pérez, 2022). This metabolic reprogramming enables efficient ATP production and sustained activity, distinguishing it from glycolysis-dependent M1 macrophages.

While the M1/M2 classification provides a practical conceptual framework, accumulating evidence shows that macrophages often exist along a continuum, co-expressing features of both subtypes, or shifting functional programs over time (Murray, 2017; Strizova et al., 2023b; Yunna et al., 2020). Recognizing this plasticity is crucial for effective therapeutic strategies, as targeting a single subtype can overlook the full range of macrophage functions and highlight the need to address their entire spectrum of activation states.

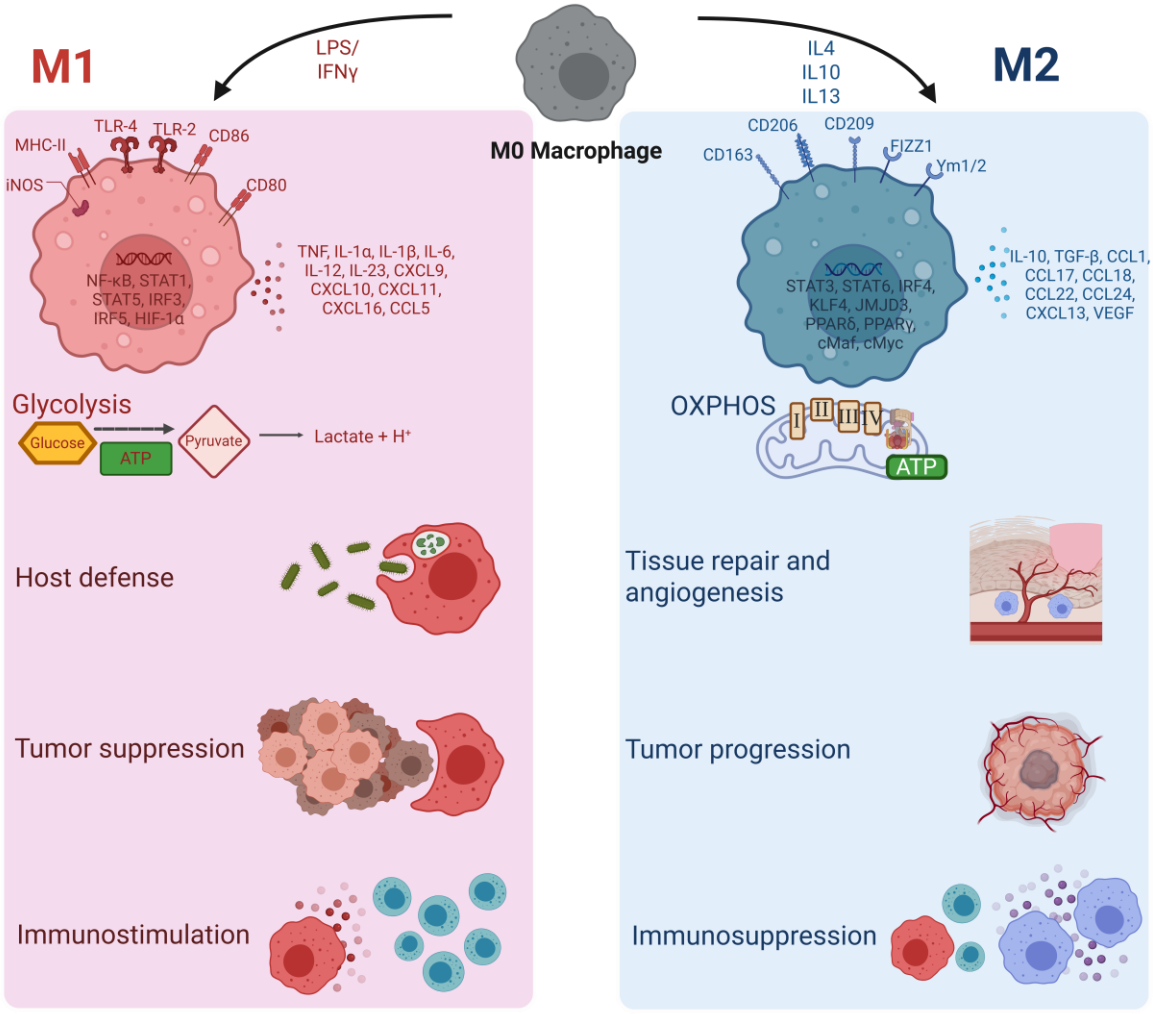

Figure 4. Macrophage polarization and function. Adapted from (Yao et al., 2019; Yunna et al., 2020).

1.4.2 Tumor-associated Macrophages

Tumor-associated macrophages (TAMs) are a prominent and functionally diverse population of immune cells within the TME, primarily derived from circulating monocytes that are recruited by chemokines such as CCL2, CCL5, CXCL12, and CSF-1, which play a key role in promoting cancer progression (Cassetta and Kitamura, 2018; Lin et al., 2019; Mantovani et al., 2017). While monocyte-derived macrophages are the primary source of TAMs, current findings highlight the significant contribution of tissue-resident macrophages of embryonic origin, which exhibit unique functional profiles shaped by both their developmental ontogeny and the TME in which they reside (Laviron and Boissonnas, 2019; Vogel and Weichhart, 2023).

Once recruited into the TME, macrophages exhibit considerable plasticity and are often characterized by an M1-M2 framework: classically activated TAM-M1 macrophages display

pro-inflammatory and tumoricidal functions, whereas alternatively, activated TAM-M2 macrophages exhibit immunosuppressive functions that support tumor growth (Pan et al., 2020; Pathria et al., 2019). However, recent single-cell transcriptomic analyses have revealed that TAMs frequently occupy mixed or intermediate phenotypes shaped by spatial localization, tumor stage, and local signals (Azizi et al., 2018; Bao et al., 2021; Xiao et al., 2022).

M2-like TAMs are characterized by their ability to support tumor progression through multiple interrelated mechanisms, making them critical players in cancer biology. These macrophages produce anti-inflammatory cytokines such as IL-10 and TGF-β, establishing an immunosuppressive microenvironment that significantly attenuates cytotoxic T-cell responses and allows tumors to evade immune detection (Chen et al., 2019a; Yang et al., 2020c). Furthermore, M2-like TAMs express inhibitory ligands such as PD-L1/2 and SIRPα, which directly inhibit T-cell activation, proliferation, and function, thereby further impairing effective anti-tumor immune responses (Mantovani et al., 2017; Yang et al., 2020c). In addition, through the secretion of chemokines such as CCL20 and CCL22, they actively recruit and promote the expansion of regulatory T cells (Tregs), thereby enhancing immune tolerance and promoting a tumor-permissive microenvironment (Chen et al., 2019b).

Furthermore, TAMs play a pivotal role in promoting tumor angiogenesis through the secretion of classical pro-angiogenic factors, such as vascular endothelial growth factor (VEGF), platelet-derived growth factor (PDGF), and various matrix metalloproteinases (MMPs), as well as emerging angiogenic mediators including basic fibroblast growth factor (bFGF), interleukin-1β (IL-1β), and chitinase-like proteins like YKL-40 (Larionova et al., 2021; Riabov et al., 2014; Zhao et al., 2024). VEGF-A remains a crucial angiogenesis regulator, driving endothelial cell migration and proliferation. Meanwhile, MMPs (e.g., MMP-2, -3, -7, -9) promote angiogenesis by remodeling the extracellular matrix, facilitating endothelial cell infiltration and subsequent formation of the vascular network (Augoff et al., 2022; Deryugina et al., 2014).

In addition, TAMs help maintain cancer stem cell (CSC) niches, thereby enhancing tumor resilience and resistance to therapy (Basak et al., 2023; McWhorter and Bonavida, 2024). They support CSC maintenance in part by creating a metabolically favorable microenvironment characterized by enhanced OXPHOS and fatty acid metabolism, which aligns with the metabolic preferences of CSCs. Moreover, TAMs secrete factors such as CCL2, which can activate AKT/β-catenin signaling to promote epithelial-mesenchymal transition (EMT) and

enhance CSC self-renewal (Allavena et al., 2021; Hasan et al., 2022; Luo et al., 2022; Marrone et al., 2024).

Clinically, a high density of M2-like TAMs correlates with poor prognosis in several cancers, including triple-negative breast cancer, ovarian, gastric, and lung cancer, as well as diffuse large B-cell lymphoma (Hwang et al., 2020; Jääskeläinen et al., 2024; Marchesi et al., 2015; Yin et al., 2017; Yuan et al., 2017). This unfavorable association is primarily attributed to the reduced responsiveness of tumors to conventional therapies, such as chemotherapy and radiotherapy, in the presence of abundant M2-like TAMs. Mechanistically, TAMs exert a protective influence on tumor cells by secreting soluble mediators, including IL-6, TNF, and COX-2, that can partially inhibit apoptosis and enhance cell survival under therapeutic stress (Cendrowicz et al., 2021; Yang et al., 2020c). Moreover, TAMs facilitate chemoresistance by upregulating ATP-binding cassette (ABC) transporters, which actively efflux chemotherapeutic agents, thereby reducing intracellular drug concentrations (Chen et al., 2024; Zhang et al., 2023). Under hypoxic conditions, TAMs overexpress dihydropyrimidine dehydrogenase (DPD), an enzyme that metabolizes and inactivates 5-fluorouracil, further limiting treatment efficacy (Malier et al., 2020, 2021).

Given their critical role in cancer progression, therapy resistance, and immune evasion, TAMs represent a promising therapeutic target. Emerging clinical trials are actively exploring innovative strategies to modulate TAM functions, including approaches to deplete these cells, reprogram their polarization from pro-tumorigenic M2 to anti-tumorigenic M1 phenotypes, disrupt their recruitment or metabolic pathways (Jumaniyazova et al., 2025; Kzhyshkowska et al., 2024). One promising approach is PF-07265807, a selective dual inhibitor of the TAM-expressed receptor tyrosine kinases MERTK and AXL, which is being evaluated in combination with the PD-1 inhibitor sasanlimab and the VEGF inhibitor axitinib in a phase I trial in advanced renal cell carcinoma (Hirohashi et al., 2023; McDermott et al., 2023). Targeting these pathways holds the promise of simultaneously alleviating immunosuppression and inhibiting angiogenesis. However, therapeutic modulation of TAMs remains challenging due to their functional heterogeneity and dynamic plasticity. Continued research is essential to refine these approaches and identify robust, predictive biomarkers to guide patient stratification and maximize clinical benefit.

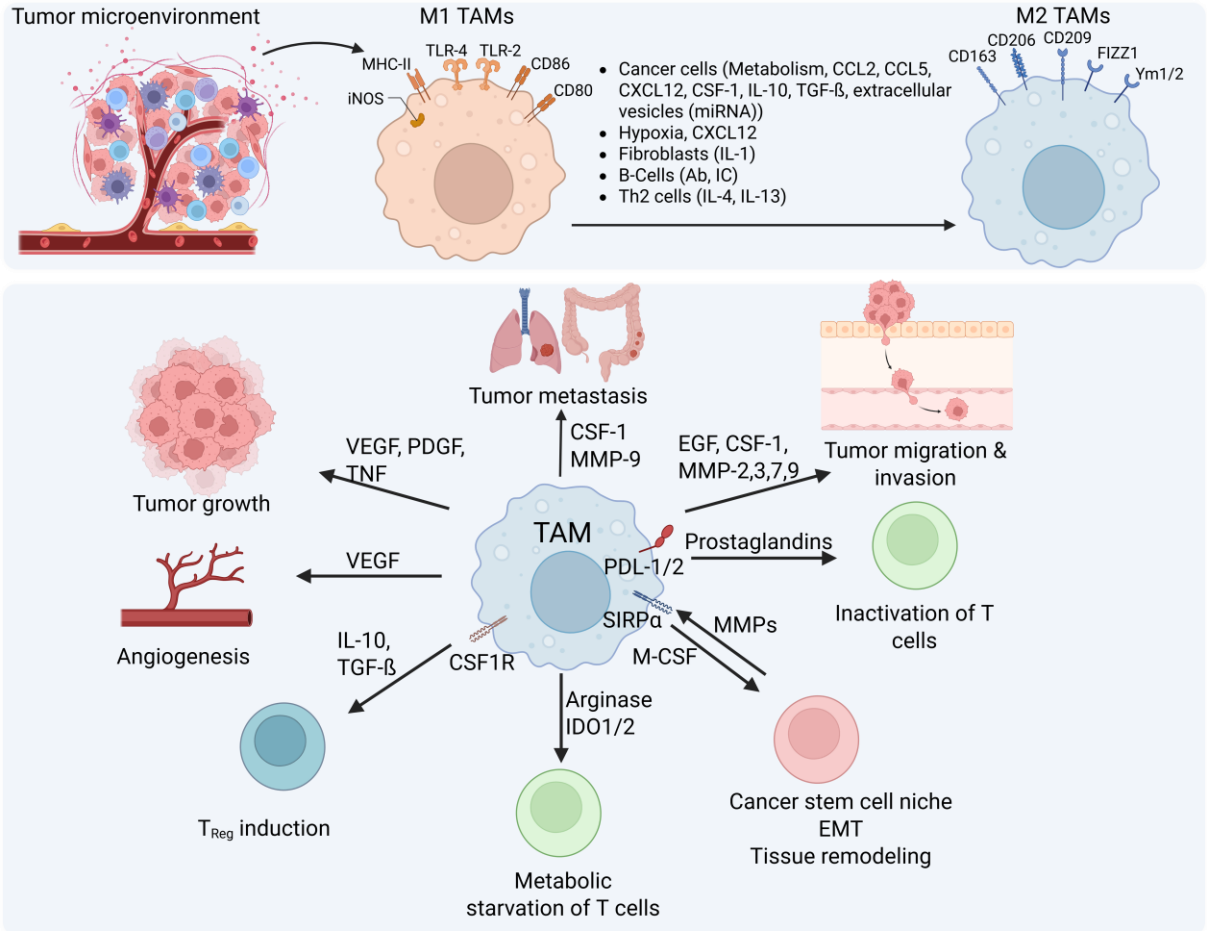

Figure 5. TAM polarization and their role in tumor progression. Adapted from (Chen et al., 2019a; Mantovani et al., 2017).

1.5 The *Insulin-like Growth Factor 2* mRNA Binding Protein 2 (IGF2BP2)

Insulin-like growth factor 2 mRNA-binding proteins (IGF2BPs/IMPs) are a family of highly conserved RNA-binding proteins (RBPs) consisting of three mammalian paralogs: IGF2BP1, IGF2BP2, and IGF2BP3. IGF2BP2 stands out as a multifunctional regulator of post-transcriptional gene expression. By modulating RNA localization, stability, and translation, IGF2BP2 orchestrates various cellular processes, including metabolism, differentiation, and tumorigenesis (Cao et al., 2021; Latifkar et al., 2022). It interacts with multiple RNA species, including messenger RNAs (mRNAs), long non-coding RNAs (lncRNAs), and microRNAs (miRNAs), reflecting its broad regulatory scope (Sun et al., 2024; Wang et al., 2021a).

The IGF2BP2 gene, located on chromosome 3q27.2, encodes a 66 kDa protein, with alternatively spliced isoforms such as a 62 kDa variant resulting from exon skipping (Wang et

al., 2021a). Structurally, IGF2BP2, like its paralogs IGF2BP1 and IGF2B3, contains two RNA recognition motifs (RRMs) and four K-homology (KH) domains that are essential for its high-affinity RNA binding and post-transcriptional regulatory functions (Korn et al., 2021; Zorc et al., 2024).

Although IGF2BP2 is primarily localized in the cytoplasm, it can translocate to the nucleus under stress conditions, suggesting a potential role in nuclear RNA processing (Cao et al., 2018; Krumbein et al., 2023). Additionally, IGF2BP2 has been identified in mitochondria and regulates mitochondrial mRNA and energy metabolism (Cao et al., 2018). Similar to IGF2BP1 and IGF2BP3, IGF2BP2 is expressed during embryonic development and reactivated in various tumor types. However, in contrast to IGF2BP1 and IGF2BP3, IGF2BP2 remains detectable at low levels in several metabolically active adult tissues under physiological conditions (Czepukojc et al., 2019; Degrauwe et al., 2016; Shao et al., 2023).

A hallmark of IGF2BP2 is its role as an m^6A reader. It selectively binds to GG(m^6A)C motifs on mRNAs, increasing their stability and translation. This interaction is part of a broader m^6A epi-transcriptomic regulatory system involving 'writers' (methyltransferases), 'erasers' (demethylases), and 'readers' such as IGF2BP2 (An and Duan, 2022; He et al., 2018). Through this mechanism, IGF2BP2 plays a critical role in regulating key biological functions, including stem cell maintenance, inflammatory signaling, and oncogenic transformation (Li et al., 2024e).

IGF2BP2 is emerging as a key post-transcriptional regulator in physiological and pathological processes. Its functions in metabolic homeostasis, immune regulation, and cancer progression underscore its relevance as a potential therapeutic target across various diseases (Ma et al., 2024; Wang et al., 2021a).

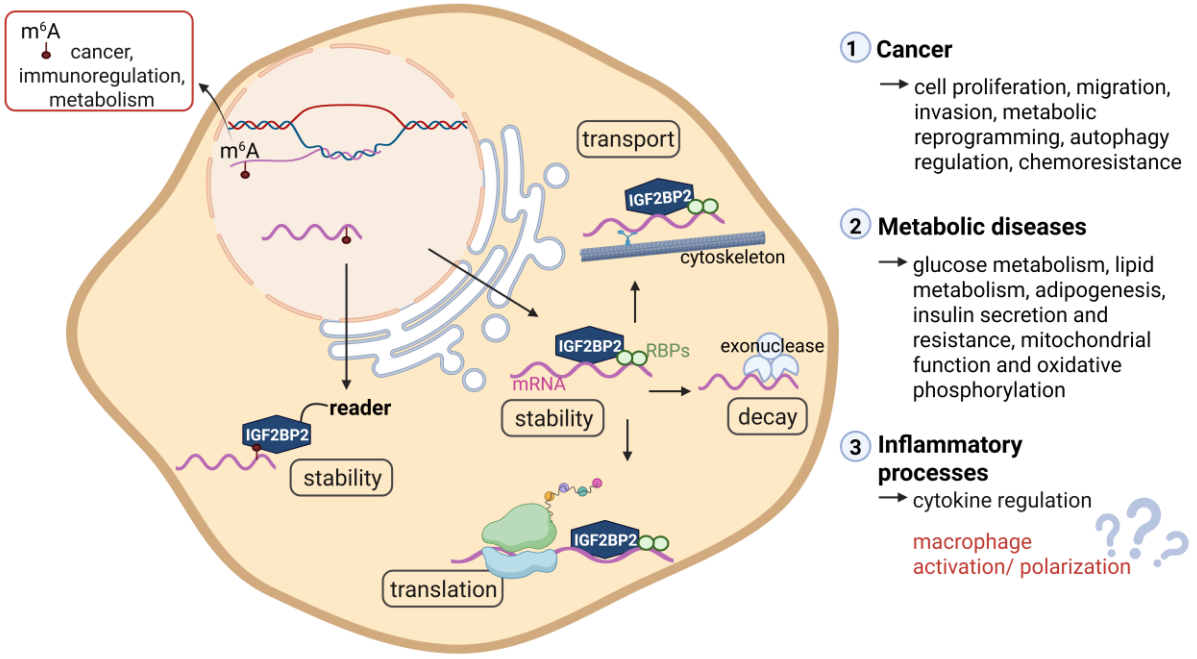

Figure 6. Post-transcriptional regulation of mRNA by IGF2BP2. Adapted from (Du et al., 2024; Zhu et al., 2023).

1.5.1 IGF2BP2 as a Tumor Marker and Regulator of Cancer Progression

IGF2BP2 has gained increasing attention as a prominent tumor-associated RBP with significant implications for cancer biology and clinical oncology. As an m^{6}A reader, IGF2BP2 stabilizes and enhances the translation of oncogenic transcripts, thereby driving cancer cell proliferation, invasion, metastasis, and resistance to therapy in a variety of malignancies (Cui et al., 2021; Li et al., 2019). Notably, the alternatively spliced isoform p62 was first identified as a tumor-associated autoantigen in hepatocellular carcinoma (HCC), where it is strongly overexpressed and associated with poor prognosis. Transgenic mouse models overexpressing p62 develop fatty liver, steatohepatitis, and enhanced tumor formation, suggesting a pivotal role in hepatocarcinogenesis (Kessler et al., 2013a; Laggai et al., 2014a; Simon et al., 2014a; Tybl et al., 2011). Beyond liver cancer, elevated IGF2BP2 expression has been documented in colorectal, breast, pancreatic, lung, and oral cancers, highlighting its potential as a diagnostic marker and therapeutic target (Cui et al., 2021; Han et al., 2022; W. Lin et al., 2024; Xia et al., 2024; Xu et al., 2019).

Mechanistically, IGF2BP2 exerts its oncogenic functions through both m^{6}A-dependent and independent pathways. It stabilizes transcripts of key cancer-associated genes, such as MYC, SOX2, FEN1, and CDK6, thereby supporting cell cycle progression, maintaining stemness, and

facilitating metabolic reprogramming (Wang et al., 2019; Xia et al., 2024; Zhang et al., 2022; Zhou et al., 2022). Additionally, IGF2BP2 facilitates the activation of key signaling pathways, including the PI3K/Akt, FAK/Src, and IGF1R-RhoA-ROCK pathways, which contribute to epithelial-mesenchymal transition (EMT), cellular migration, and tumor survival (Lin et al., 2024; Liu et al., 2022; Xu et al., 2019). Consistent with these findings, recent CRISPR/Cas9-based studies confirmed that IGF2BP2 is essential for tumor cell proliferation, as its knockout severely impaired growth and colony formation in liver, colorectal, and lung cancer cells (Chanda et al., 2024).

IGF2BP2 is critical in mediating chemoresistance by stabilizing m^{6}A-modified RNAs involved in mitochondrial function, stress response, autophagy regulation, and apoptotic pathways. In particular, it increases the stability and expression of long non-coding RNAs such as *DANCR*, *TUG1*, and *MALAT1*, which contribute to cell survival during chemotherapy (Han et al., 2022a, 2022b; Liu et al., 2022a). For instance, elevated IGF2BP2 levels confer resistance to apoptosis induced by chemotherapeutic agents such as doxorubicin by activating the ERK1/2 pathway in hepatocellular carcinoma (Kessler et al., 2013b). Clinically, high IGF2BP2 levels in primary tumors correlate with a poor response to chemotherapeutic agents such as 5-fluorouracil and oxaliplatin, while genetic depletion of IGF2BP2 can sensitize colorectal cancer cells to these treatments (Kendzia et al., 2023). Recent studies suggest that IGF2BP2 can modulate autophagy by stabilizing m^{6}A-modified transcripts of autophagy-related genes. Its loss increases autophagosome formation and flux in several tumor models (Han et al., 2022; Li et al., 2024; Xia et al., 2022). While autophagy is often viewed as a pro-survival process, suppressing autophagy can paradoxically promote chemoresistance by accumulating damaged cellular components, which ultimately enhance tumor cell survival (Vempati and Malla, 2020).

IGF2BP2 has emerged as an essential regulator of tumor metabolism, with studies suggesting its involvement in orchestrating both glycolysis and oxidative phosphorylation (OXPHOS) in response to cancer-specific metabolic demands. It has been reported to increase the expression of glycolytic enzymes such as *GLUT1*, *HK2*, and *ALDOA* and to modulate glutamine metabolism through targets such as *MYC* and *GPT2*, which support tumor cell proliferation (Weng et al., 2022; Zhu et al., 2023). In addition, IGF2BP2 has been implicated in maintaining mitochondrial functionality by stabilizing transcripts of respiratory chain components, including *NDUFA2*, *CPT1A*, and *NDUFS3*, thereby promoting OXPHOS and ATP production (Huang et al., 2022; Janiszewska et al., 2012). More recently, IGF2BP2 was identified as a synthetic dependency in PLK1-overexpressing tumors, where its loss reduces PLK1 expression

and impairs mitochondrial function, ultimately suppressing cell proliferation and survival (Cunningham et al., 2025). Given PLK1's well-established role in driving chromosomal instability (CIN), these findings suggest that IGF2BP2 is involved in maintaining CIN-associated tumor phenotypes. Earlier evidence demonstrating that IGF2BP2 promotes genomic instability and an aggressive tumor phenotype in hepatocellular carcinoma models further supports this idea (Kessler et al., 2015).

Clinically, high IGF2BP2 expression is associated with advanced tumor stage, poor prognosis, and reduced treatment response in several cancer types, including hepatocellular carcinoma, gastric cancer, and glioblastoma (Czepukojc et al., 2019; Dahlem et al., 2022; Kessler et al., 2015; Zhang et al., 2022; Zhou et al., 2022c). These findings underscore its growing value as a prognostic biomarker and a molecular target for cancer therapy. Targeting IGF2BP2 or its downstream RNA networks may help overcome drug resistance, improve treatment response, and advance precision oncology.

1.5.2 IGF2BP2: A Multifaceted Metabolic Regulator in Health and Disease

IGF2BP2 has emerged as a crucial regulator of metabolic processes and diseases, including type 2 diabetes mellitus (T2DM), obesity, non-alcoholic fatty liver disease (NAFLD), cancer metabolism, and cardiac dysfunction (Dai et al., 2015; Krumbein et al., 2023; Simon et al., 2014b, 2014a; Tybl et al., 2011; Wang et al., 2021a; Zhou et al., 2022a).

Genetic polymorphisms within IGF2BP2, primarily single nucleotide polymorphisms (SNPs) such as rs4402960 and rs1470579, have consistently shown associations with increased susceptibility to T2DM (Velmurugan et al., 2025; Ertural et al., 2024). The high expression of IGF2BP2 in pancreatic islets underscores its regulatory function in β-cell proliferation and insulin secretion, primarily by enhancing the translation of transcripts such as PDX1 (Bailetti et al., 2022; Regué et al., 2021; Wang et al., 2021a).

In adipose tissue, IGF2BP2 promotes adipogenesis by influencing the differentiation of mesenchymal stem cells into adipocytes, thereby contributing to fat accumulation and the development of obesity. Knockout models further highlight its role: IGF2BP2 KO mice resist diet-induced obesity and show improved insulin sensitivity, highlighting its functional relevance in metabolic regulation (Dai et al., 2015; Regué et al., 2023).

In liver tissue, IGF2BP2 has been identified as a key contributor to the development of NAFLD by orchestrating lipid metabolic pathways and inflammatory responses. It promotes hepatic

steatosis through several complementary mechanisms: suppression of ABCA1 expression *via* miR-33a/b interaction promotes cholesterol accumulation and dyslipidemia (Yang et al., 2020); stabilization of *CD36* mRNA enhances fatty acid uptake in hepatocytes (Wang et al., 2023b); and upregulation of ELOVL6, an enzyme involved in fatty acid elongation, further drives lipid accumulation (Laggai et al., 2014b). Notably, IGF2BP2-deficient mice resist diet-induced steatosis, highlighting its pathogenic role in hepatic lipid accumulation and metabolic dysfunction (Dai et al., 2015).

Furthermore, in cardiac tissue, IGF2BP2 expression is upregulated under stress and regulates mitochondrial transcripts essential for OXPHOS. Its overexpression disrupts mitochondrial integrity and partially mediates dilated cardiomyopathy, highlighting its role in cardiac energy homeostasis (Krumbein et al., 2023).

1.5.3 IGF2BP2 in Inflammation and Immune Regulation

IGF2BP2 has increasingly been recognized as a critical modulator of inflammatory signaling, partly through its activity as an m^{6}A reader that stabilizes key transcripts involved in immune regulation and cellular stress responses. Recent studies highlight the multifaceted and context-dependent role of IGF2BP2 in inflammatory diseases and disorders.

In rheumatoid arthritis, IGF2BP2 expression is significantly reduced in inflamed synovial tissue, correlating with heightened cytokine production and increased migration of fibroblast-like synoviocytes. Mechanistically, IGF2BP2 stabilizes *GSTM5* mRNA, thereby enhancing antioxidant responses and mitigating inflammation (Nan et al., 2024).

In periodontitis, IGF2BP2 displays stage-specific roles: its depletion in early stages increases inflammatory cytokine levels, whereas its presence in advanced disease stages suppresses osteoclast differentiation, limiting tissue destruction. These dual effects are attributed to stabilizing immunomodulatory transcripts such as *CD5L* and *CD36* (Ma et al., 2024).

In ulcerative colitis, IGF2BP2 acts as a protector by stabilizing *GPX4* mRNA. This reduces oxidative stress and prevents ferroptosis. This mechanism reduces mucosal inflammation, positioning IGF2BP2 as a potential therapeutic target for inflammatory bowel diseases (Liu and Zeng, 2024).

In contrast, in non-alcoholic steatohepatitis (NASH), IGF2BP2 plays a pro-inflammatory role. It stabilizes *Tab2* mRNA, activates NF-κB signaling, and promotes *CCL2* expression, driving

hepatic inflammation and fibrosis. Knockdown of IGF2BP2 alleviates liver injury, highlighting its pathogenic role in NASH (Czepukojc et al., 2019; Simon et al., 2014a; Zhou et al., 2022a).

Within the TME, IGF2BP2 promotes cancer-associated inflammation. In breast cancer, for example, it increases the expression of *CCL20* and *CXCL10*, thereby promoting tumor growth and immune cell infiltration (Gao et al., 2022). In lung adenocarcinoma, it stabilizes *LOX1* mRNA, aiding neutrophil recruitment and the establishment of a pro-inflammatory niche (Qian et al., 2024).

An emerging area of interest is the role of IGF2BP2 in macrophage biology. While this field is still in its early stages, recent studies suggest that IGF2BP2 modulates macrophage polarization in a context-dependent manner. It promotes an M1-like, pro-inflammatory phenotype in sepsis by stabilizing *TIM1* mRNA within the METTL3/IGF2BP2/TIM1 axis (Du et al., 2024). In contrast, in chronic inflammatory conditions such as colitis and allergic inflammation, IGF2BP2 facilitates M2 macrophage polarization by stabilizing *TSC1* and *PPARγ* transcripts in an m^{6}A-dependent manner, thereby promoting tissue repair and anti-inflammatory responses (Wang et al., 2021). Loss of IGF2BP2 skews macrophage polarization toward a dominant M1 phenotype, exacerbating inflammatory outcomes such as DSS-induced colitis.

IGF2BP2 also shapes the immunosuppressive landscape of the TME by promoting the recruitment of immunosuppressive M2-like and SPP1$^+$ macrophages, which are associated with angiogenesis, immune evasion, and poor prognosis, particularly in bladder cancer (Li et al., 2024). Mechanistically, IGF2BP2 stabilizes *NRP1* mRNA, driving M2 polarization and enhancing tumor progression (Fu et al., 2024). Additionally, in pancreatic cancer, IGF2BP2 interacts with lncRNA-PACERR to stabilize oncogenic transcripts, such as KLF12 and MYC, thereby driving M2 polarization and immune suppression (Liu et al., 2022). Furthermore, IGF2BP2 modulates the molecular composition of cancer-derived extracellular vesicles (EVs) in colorectal cancer, reprogramming macrophages toward a tumor-associated phenotype and promoting cancer cell migration (Mashayekhi et al., 2024).

Taken together, IGF2BP2 connects critical biological pathways, including cancer progression, metabolic regulation, and inflammation, highlighting the importance of further investigation to unravel the underlying molecular mechanisms. Understanding how IGF2BP2 orchestrates these macrophage-driven processes may provide new therapeutic avenues for treating inflammatory diseases and malignancies.

1.6 Objectives

This study aimed to investigate the multifaceted role of IGF2BP2 in macrophage biology and tumor progression, focusing on its influence on metabolism, migration, immune modulation, and its role in shaping the tumor microenvironment. Using a combination of *in vitro* and *in vivo* approaches in both human and mouse models, we aimed to investigate the molecular and functional implications of IGF2BP2 in different experimental contexts.

(I) Part I of this study provided a comparative analysis of IGF2BP2 regulation in human versus murine macrophages, challenging previously published findings by Wang et al. (2021) through the presentation of new experimental data and emphasizing species-specific differences in IGF2BP2 expression during acute and chronic inflammatory conditions.

(II) Part II of this study aimed to investigate the role of IGF2BP2 in tumor progression by utilizing a murine Lewis lung carcinoma (LLC1) model in female mice with a myeloid-specific IGF2BP2 knockout (KO). We hypothesized that IGF2BP2 deficiency in macrophages disrupts metabolic programming, impairs migratory capacity, and influences TAM polarization, thus impairing tumor growth.

(III) Part III of this study aimed to investigate the role of IGF2BP2 in tumor growth and progression using male WT and IGF2BP2 KO mice in the LLC1 tumor model. By comparing these findings with results from female mice (Part II), we sought to elucidate sex-specific differences in tumor biology and immune regulation associated with IGF2BP2.

(IV) Part IV of this study aimed to evaluate the therapeutic potential of IGF2BP2 inhibition in modulating TAM-like polarization and metabolic function in human macrophages. Using three validated inhibitors (compounds 4, 6, and 9), this study investigated their effects on macrophage polarization and metabolism to explore IGF2BP2 as a therapeutic target.

2 Part I: Comparative Analysis of IGF2BP2 Regulation in Human versus Murine Macrophages

2.1 Published Work in this Dissertation

In our published commentary on the study by Wang et al., *Comment on: The m6A Reader IGF2BP2 Regulates Macrophage Phenotypic Activation and Inflammatory Diseases by Stabilizing TSC1 and PPARγ*, we address key species-specific differences in the regulation of IGF2BP2 during macrophage activation. While IGF2BP2 is upregulated in alternatively activated (M2) macrophages in both human and murine systems to a similar extent, marked differences are observed under classically activated (M1) inflammatory conditions.

Wang et al. demonstrated that in murine bone marrow-derived macrophages (BMMs), treatment with LPS induces an increase in IGF2BP2 expression on both mRNA and protein levels. In contrast, our analysis revealed that in human monocyte-derived macrophages (HMDMs), LPS exposure leads to reduced *IGF2BP2* mRNA levels, while protein levels remain largely unchanged. This downregulation coincided with an increased expression of the pro-inflammatory cytokines *TNF* and *IL6* and decreased levels of the anti-inflammatory cytokine *TGFβ*, suggesting a shift toward a pro-inflammatory phenotype. Further analyses of transcriptomic data across multiple acute infection and inflammation models consistently confirmed a reduction of *IGF2BP2* expression in human macrophages. Interestingly, in chronic inflammatory conditions, such as chronic obstructive pulmonary disease, Crohn's disease, and rheumatoid arthritis, *IGF2BP2* expression was upregulated in both species. These findings underscore the context-dependent and dual role of IGF2BP2 in inflammation, highlighting the need to consider species-specific regulatory mechanisms. Thus, while murine models provide valuable insights, the translational interpretation for human systems must be approached cautiously.

This work was published in *Advanced Science* and is included in this doctoral thesis:

Hanna S. Schymik, Charlotte Dahlem, Ahmad Barghash, and Alexandra K. Kiemer (2022). Comment on: The m6A Reader IGF2BP2 Regulates Macrophage Phenotypic Activation and Inflammatory Diseases by Stabilizing TSC1 and PPARγ.
Advanced Science. 2022, 9(8):e2104372.
doi:10.1002/advs.202104372

COMMENT

ADVANCED SCIENCE Open Access

www.advancedscience.com

Comment on: The m6A Reader IGF2BP2 Regulates Macrophage Phenotypic Activation and Inflammatory Diseases by Stabilizing TSC1 and PPARγ

*Hanna S. Schymik, Charlotte Dahlem, Ahmad Barghash, and Alexandra K. Kiemer**

Recently, first insights into the regulation and the role of the RNA-binding protein IMP2 in macrophage activation have been published by Wang et al. This study addresses differences in the regulation of IMP2 between the human and murine system. While the expression of IMP2 in anti-inflammatory macrophages is synchronous in mice and men, IMP2 expression is regulated differently in inflammatory macrophages.

With recently published data in *Advanced Science*, Wang et al. for the first time report a role of the insulin-like growth factor 2 (IGF2) mRNA-binding protein 2 (IGF2BP2/IMP2/VICKZ2) in macrophage activation.[1]

As a highly conserved RNA binding protein, IGF2BP2 plays an essential role in the translation, stabilization, localization, modification, and processing of various mRNA targets and, accordingly, influences physiological and pathophysiological processes in the context of metabolism and malignancy.[2–4] However, beyond the knowledge on its promotion of inflammatory processes in fatty liver disease and autoantibody-induced glomerulonephritis, little is known about the role of IGF2BP2 in inflammatory conditions.[5,6]

Wang et al. suggest that a loss of *Igf2bp2* leads to an enhanced inflammatory M1 phenotype of murine macrophages by stabilizing *Tsc1* and *Pparg*.[1]

Here, we would like to report our data on the regulation of *IGF2BP2* in polarized human monocyte-derived macrophages (HMDMs) and our analysis of *IGF2BP2* expression levels in various inflammatory conditions in the human system. These data suggest a more complex view of IGF2BP2 in inflammation and, to some extent, contradict the conclusions of Wang et al.

In HMDMs treated with bacterial lipopolysaccharide (LPS) for up to 24 h, we found a significant reduction in *IGF2BP2* mRNA expression (**Figure 1A**), while protein levels were not changed (Figure 1B). Similarly, analysis of a proteomics dataset from the human macrophage-like THP-1 cell line polarized toward M1 by LPS and IFNγ for either 6 h or 48 h revealed no difference in IGF2BP2 protein levels (Figure S1, Supporting Information).

At early activation time points, *IGF2BP2* reduction in HMDMs was accompanied by the induction of the inflammatory cytokines TNF and IL6 and a reduction of the anti-inflammatory cytokine TGFB (Figure 1C). Importantly, prolonged LPS stimulation for 24 h represents a rather desensitized macrophage activation state, as confirmed by the absence of *TNF* and *IL6* expression (Figure 1C).[7] These findings are in contrast to the IGF2BP2 mRNA and protein induction upon LPS treatment of murine bone marrow-derived macrophages (BMDMs), as demonstrated by Wang et al.[1]

The expression of *TSC1*, which was suggested by Wang et al. to facilitate IGF2BP2 action, correlated with *IGF2BP2* and was distinctly reduced upon LPS treatment (Figure 1D).

To exploit whether this decline of *IGF2BP2* expression during inflammation is specific for LPS-facilitated inflammatory cell activation, we analyzed *IGF2BP2* expression in several publicly available data sets, in which human blood, monocytes, or macrophages were infected with either Gram-positive or Gram-negative bacteria or viruses, causing various types of Toll-like receptor (TLR) activation.[8,9] The presence of acute inflammation was confirmed by an elevated *TNF* expression of the specific samples. Our analyses demonstrate a reduced *IGF2BP2* levels in all models of acute inflammation, although statistical significance was not reached in all of them (**Figure 2**). Taken together, in contrast to the murine data from Wang et al., our analyses of human samples suggest a downregulation of *IGF2BP2* during acute inflammation.

In addition to their role in acute inflammation, macrophages can exhibit a broad polarization spectrum, with the M1 and M2 phenotypes representing two extreme ends. Classically activated (M1) macrophages act as effector cells in the Th1 response and are usually generated in vitro by the stimulation with LPS and

H. S. Schymik, C. Dahlem, A. K. Kiemer
Department of Pharmacy
Pharmaceutical Biology
Saarland University
Saarbruecken 66123, Germany
E-mail: pharm.bio.kiemer@mx.uni-saarland.de

A. Barghash
School of Electrical Engineering and Information Technology
German Jordanian University
Amman 11180, Jordan

The ORCID identification number(s) for the author(s) of this article can be found under https://doi.org/10.1002/advs.202104372

DOI: 10.1002/advs.202104372

ADVANCED SCIENCE NEWS
www.advancedsciencenews.com

ADVANCED SCIENCE
www.advancedscience.com

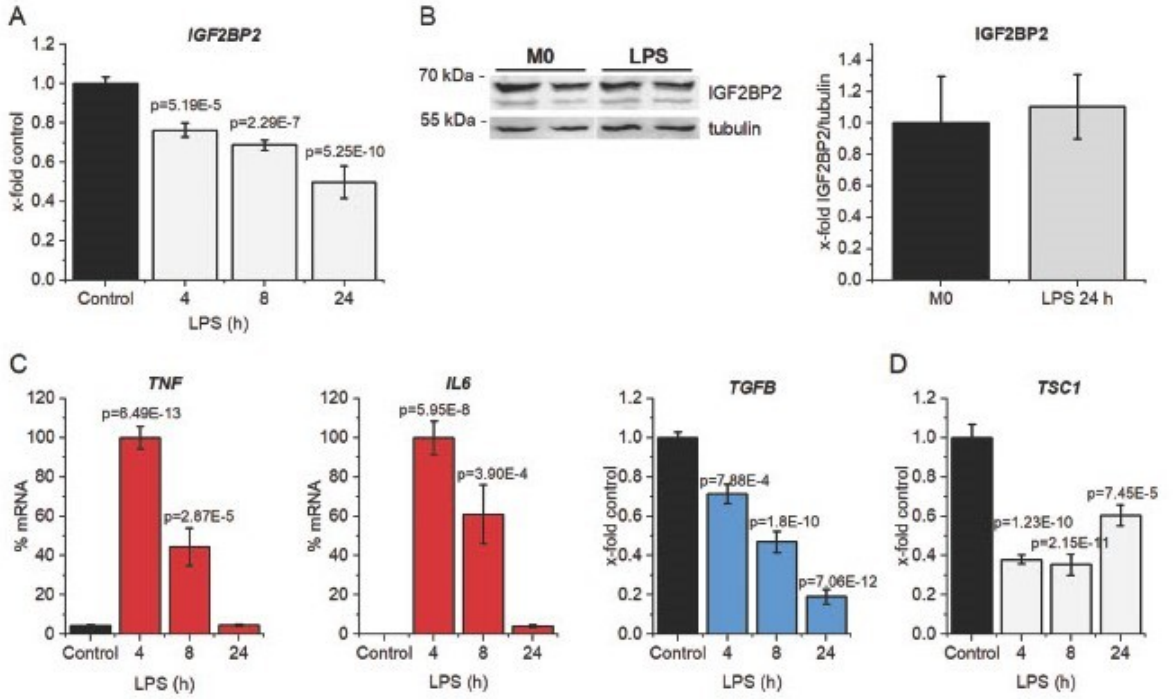

Figure 1. *IGF2BP2 in activated human macrophages.* Human monocyte-derived macrophages (HMDMs) were treated with 100 ng mL^{-1} LPS for the indicated time. IGF2BP2 expression was determined on A) gene and B) protein level (24 h). Expression data were normalized to *ACTB* or tubulin, respectively, and are represented as means ± SEM (x-fold control). C) *TNF*, *IL6*, *TGFB*, *and* D) *TSC1* were quantified upon LPS treatment. Data are represented as means ± SEM (x-fold 4 h LPS for *TNF* and *IL6*; x-fold control for *TGFB* and *TSC1*). Statistical analysis was performed by ANOVA analysis followed by Bonferroni's post hoc test; $n = 4$, triplicates (4 h; 8 h LPS); $n = 2$, triplicates (24 h).

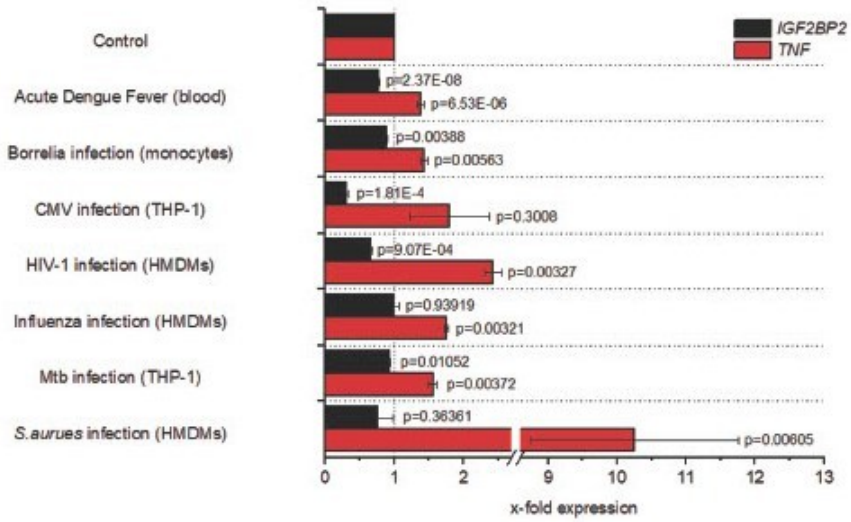

Figure 2. *Expression levels of IGF2BP2 after infection. IGF2BP2* and *TNF* expression levels were compared with the respective healthy non-infected controls, which were set to 1. Expression analysis of *IGF2BP2* and *TNF* in whole blood samples of patients with acute dengue fever (GSE51808, $n = 9$ (healthy), 18 (infected)); of human isolated monocytes infected with *Borrelia burgdorferi* (20 h) (GSE103483, $n = 3$ (control, infected)); of the macrophage-like THP-1 cell line infected with *Cytomegalovirus* (24 h) (GSE141236, $n = 3$ (control, infected)); of HMDMs infected with *HIV-1*-BaL-HAS (18 h) (GSE158434, $n = 3$ (control, infected)); of HMDMs infected with Influenza H5N1 (6 h) (GDS3595, $n = 3$ (control, infected)); of the THP-1 cell line infected with *Mycobacterium tuberculosis* (Mtb) H37Rv (GDS4781, $n = 3$ (control, infected)); of HMDMs infected with *Staphylococcus aureus* (*S. aureus*) (8 h) (GDS4931 $n = 5$ (control, infected)). Data are represented as means ± SEM. *P*-values were calculated by Student's t-test for each dataset.

ADVANCED SCIENCE NEWS
www.advancedsciencenews.com

ADVANCED SCIENCE Open Access
www.advancedscience.com

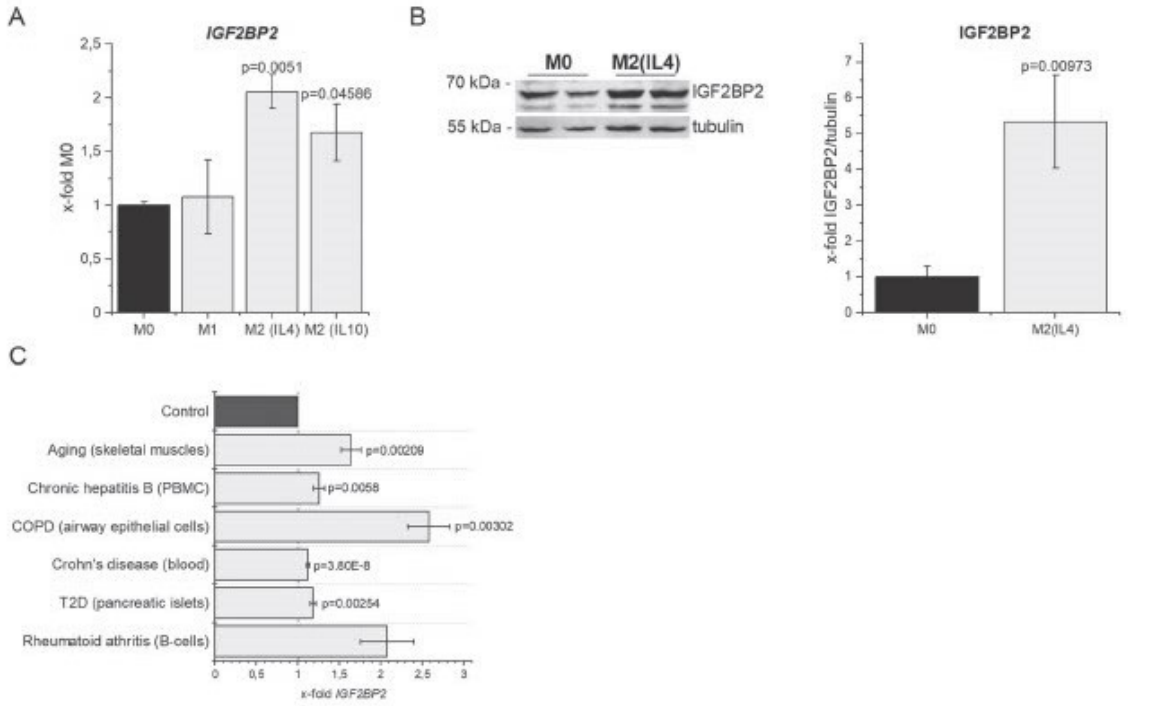

Figure 3. *IGF2BP2 expression in alternatively activated macrophages and various chronic inflammatory diseases.* HMDMs were polarized for 24 h and IGF2BP2 expression was determined on A) gene and B) protein level. Expression data were normalized to *18S* or tubulin, respectively, and are represented as means ± SEM (x-fold M0). Statistical analysis was performed by ANOVA analysis followed by Bonferroni's post hoc test, $n = 2$, triplicates (M2 (IL-4)), $n = 4$, duplicates (M2 (IL-10)). C) *IGF2BP2* expression levels were compared with the respective healthy controls, which were set to 1. Expression analysis of *IGF2BP2* of old skeletal muscles (GDS5218, $n = 7$ (young) $n = 6$ (old) female); peripheral blood mononuclear cells (PBMCs) of patients with chronic hepatitis B (GSE114783, $n = 10$ (chronic hepatitis B), $n = 3$ (healthy)); airway epithelial cells of patients with COPD (GSE5058, $n = 6$ (COPD), $n = 12$ (healthy)); of whole blood samples of patients with Crohn's diseases (GSE126124: $n = 40$ (Crohn's diseases), $n = 32$ (healthy)); of pancreatic islets of patients with type 2 diabetes (T2D, GDS3882, $n = 6$ (Diabetes), $n = 6$ (healthy)); of B-cells of patients with rheumatoid arthritis (GSE4588, $n = 7$ (arthritis), $n = 9$ (healthy)). Data are represented as means ± SEM. *P*-values were calculated by Student's *t*-test for each dataset.

IFNγ. Different M2 macrophage subsets can be generated using IL4 or IL10 for polarization.[10]

The analysis of *IGF2BP2* expression revealed that human M1 macrophages display no alterations in expression, while M2 polarized human macrophages show a significant induction on gene and protein level (**Figure 3**A,B). These data on human M2 macrophages are consistent with the data of Wang et al. as well as the observation that treatment by IFNγ alone induces *IGF2BP2* in both human and murine macrophages (see Figure S2, Supporting Information). IFNγ and LPS typically synergize and result in a pro-inflammatory macrophage "super-activation". IFNγ treatment by itself induces different signaling than LPS: It activates the STAT1 transcription factor and induces the opening of chromatin. This so-called priming not necessarily induces a transcriptional activity but rather "bookmarks" inflammatory genes for LPS-induced gene transcription.[11] The observation that IFNγ treatment by itself does in fact induce *IGF2BP2* warrants future investigations.

The anti-inflammatory M2 phenotype plays a role in chronic inflammation by supporting tissue remodeling and repair.[12] In line with the findings by Wang et al., *IGF2BP2* is elevated in conditions of chronic inflammation, such as aging, chronic hepatitis B, obstructive pulmonary disease (COPD), Crohn's diseases, type 2 diabetes, and rheumatoid arthritis (Figure 3C).

In conclusion, our data suggest that *IGF2BP2* is differentially regulated in acute inflammation in humans versus mice. Mouse macrophages in general show a limited responsiveness toward LPS, which has been suggested to be due to a rapid induction of negative feedback regulators.[13] Since *IGF2BP2* is consistently induced in both murine and human M2 macrophages, which are desensitized toward activation, the induction of IGF2BP2 in murine macrophages by LPS might contribute to the attenuated responsiveness of murine macrophages.

In contrast to LPS treatment, there is a high consistency of *IGF2BP2* expression in chronic inflammatory conditions between mouse and man. Future studies are required to gain insight into the role of IGF2BP2 at different stages of inflammation.

Supporting Information

Supporting Information is available from the Wiley Online Library or from the author.

Acknowledgements

This work was supported by grants from the Deutsche Forschungsgemeinschaft (KI702). The figure for the table of contents was created with BioRender (BioRender.com).

Conflict of Interest

The authors declare no conflict of interest.

Data Availability Statement

Research data are not shared.

Keywords

human macrophages, IFNγ I IGF2BP2, LPS, macrophage polarization, mouse macrophages, species difference

Received: October 1, 2021
Revised: December 4, 2021
Published online: January 17, 2022

[1] X. Wang, Y. Ji, P. Feng, R. Liu, G. Li, J. Zheng, Y. Xue, Y. Wei, C. Ji, D. Chen, J. Li, *Adv. Sci.* **2021**, *8*, 2100209.
[2] N. Dai, *Trends Endocrinol. Metab.* **2020**, *31*, 670.
[3] M. Hafner, M. Landthaler, L. Burger, M. Khorshid, J. Hausser, P. Berninger, A. Rothballer, M. A. Jr, A. Jungkamp, M. Munschauer, A. Ulrich, G. S. Wardle, S. Dewell, M. Zavolan, T. Tuschl, *Cell* **2010**, *141*, 129.
[4] S. M. Kessler, S. Laggai, A. Barghash, C. S. Schultheiss, E. Lederer, M. Artl, V. Helms, J. Haybaeck, A. K. Kiemer, *Cell Death Dis.* **2015**, *10*, e1894.
[5] R. Bechara, N. Amatya, R. D. Bailey, Y. Li, F. E. Y. Aggor, D. Li, C. V. Jawale, B. M. Coleman, N. Dai, N. S. Gokhale, T. C. Taylor, S. M. Horner, A. C. Poholek, A. Bansal, P. S. Biswas, S. L. Gaffen, *Sci. Immunol.* **2021**, *6*, 1287.
[6] Y. Simon, S. M. Kessler, R. M. Bohle, J. Haybaeck, A. K. Kiemer, *Gut* **2014**, *63*, 861.
[7] S. K. Biswas, E. Lopez-Collazo, *Trends Immunol.* **2009**, *30*, 475.
[8] M. A. Dobrovolskaia, A. E. Medvedev, K. E. Thomas, N. Cuesta, V. Toshchakov, T. Ren, M. J. Cody, S. M. Michalek, N. R. Rice, S. N. Vogel, *J. Immunol.* **2003**, *170*, 508.
[9] M. J. Paul-Clark, S. K. McMaster, E. Belcher, R. Sorrentino, J. Anandarajah, M. Fleet, S. Sriskandan, J. A. Mitchell, *Br. J. Pharmacol.* **2006**, *148*, 1067.
[10] J. Hoppstädter, A. Dembek, M. Höring, H. S. Schymik, C. Dahlem, A. Sultan, N. Wirth, S. A. Fityan, B. Diesel, G. Gasparoni, J. Walter, V. Helms, H. Huwer, M. Simon, G. Liebisch, M. H. Schulz, A. K. Kiemer, *EBioMedicine* **2021**, *72*, 103578.
[11] L. B. Ivashkiv, *Nat. Rev. Immunol.* **2018**, *18*, 545.
[12] A. Sica, A. Mantovani, *J. Clin. Invest.* **2012**, *122*, 787.
[13] K. Schroder, K. M. Irvine, M. S. Taylor, N. J. Bokil, K. L.e Cao, K. Masterman, L. I. Labzin, C. A. Semple, R. Kapetanovic, L. Fairbairn, A. Akalin, G. J. Faulkner, J. K. Baillie, M. Gongora, C. O. Daub, H. Kawaji, G. J. McLachlan, N. Goldman, S. M. Grimmond, P. Carninci, H. Suzuki, Y. Hayashizaki, B. Lenhard, D. A. Hume, M. J. Sweet, *Proc. Natl. Acad. Sci. USA* **2012**, *109*, E944.
[14] C. Dahlem, W. X. Siow, M. Lopatniuk, W. K. F. Tse, S. M. Kessler, S. H. Kirsch, J. Hoppstädter, A. M. Vollmar, R. Müller, A. Luzhetskyy, K. Bartel, A. K. Kiemer, *Cancers (Basel)* **2020**, *12*, 1288.
[15] J. Hoppstädter, A. Dembek, R. Linnenberger, C. Dahlem, A. Barghash, C. Fecher-Trost, G. Fuhrmann, M. Koch, A. Kraegeloh, H. Huwer, A. K. Kiemer, *Front. Immunol.* **2019**, *10*, 1634.
[16] I. D. Green, N. Pinello, R. Song, Q. Lee, J. M. Halstead, C. T. Kwok, A. C. H. Wong, S. S. Nair, S. J. Clark, B. Roediger, U. Schmitz, M. Larance, R. Hayashi, J. E. J. Rasko, J. J. Wong, *Nucleic Acids Res.* **2020**, *48*, 6513.
[17] Y. Perez-Riverol, A. Csordas, J. Bai, M. Bernal-Llinares, S. Hewapathirana, D. J. Kundu, A. Inuganti, J. Griss, G. Mayer, M. Eisenacher, E. Pérez, J. Uszkoreit, J. Pfeuffer, T. Sachsenberg, S. Yilmaz, S. Tiwary, J. Cox, E. Audain, M. Walzer, A. F. Jarnuczak, T. Ternent, A. Brazma, J. A. Vizcaíno, *Nucleic Acids Res.* **2019**, *47*, D442.
[18] E. W. Deutsch, Csordas A., Z. Sun, A. Jarnuczak, Y. Perez-Riverol, T. Ternent, D. Campbell, M. Bernal-Llinares, S. Okuda, S. Kawano, R. L. Moritz, J. J. Carver, M. Wang, Y. Ishihama, N. Bandeira, H. Hermjakob, J. A. Vizcaíno, *Nucleic Acids Res.* **2017**, *45*, D1100.
[19] J. Cox, M. Mann, *Nat. Biotechnol.* **2008**, *26*, 1367.

2.2 Author Contributions

I contributed to this publication by designing and conducting all experiments, unless otherwise stated, and performing data analysis and interpretation. I was responsible for drafting the manuscript and preparing all figures. In addition, I coordinated communication and collaboration with co-authors throughout the review and revision process.

Charlotte Dahlem prepared the IGF2BP2 Western blot, assisted in manuscript writing, and contributed to the supervision of the project. Ahmad Barghash conducted the bioinformatic analysis of a publicly available proteomic dataset. Prof. Dr. Alexandra K. Kiemer initiated the study, provided overall scientific supervision, and contributed to manuscript writing. Her support was crucial to the project's successful completion.

Prof. Dr. Alexandra K. Kiemer provided funding for this project through grants from the Deutsche Forschungsgemeinschaft (KI702). Additional acknowledgments are provided in the original publication.

3 Part II: IGF2BP2 Deficiency in Macrophages Impairs Migration, Reprograms Metabolism, and Limits Tumor Progression

3.1 Submitted Work in this Dissertation

In our submitted manuscript "IGF2BP2 Deficiency in Macrophages Impairs Migration, Reprograms Metabolism, and Limits Tumor Progression", we investigated the multiple roles of the RNA binding protein IGF2BP2 in shaping macrophage metabolism, migration, and TAM polarization. Using mice with a myeloid-specific deletion of IGF2BP2 (IGF2BP2 MΦ-KO), we investigated how IGF2BP2 influences macrophage function in the context of the tumor microenvironment.

Transcriptomic profiling *via* RNA sequencing revealed profound changes in IGF2BP2-deficient macrophages, particularly affecting mitochondrial function, glycolysis, and cellular motility pathways. Functionally, IGF2BP2-deficient macrophages exhibited a metabolic shift toward glycolysis, evidenced by increased extracellular acidification rates (ECAR) and impaired OXPHOS. Despite unchanged mitochondrial DNA content, IGF2BP2-deficient macrophages showed reduced mitochondrial membrane potential and reactive oxygen species production, indicating compromised mitochondrial respiration.

In TAM-like macrophages, IGF2BP2 deletion impaired the expression of key TAM markers (e.g., *Mrc1*, *Mmp2*, *Il10*) and was accompanied by persistent metabolic changes, including increased glycolytic activity and decreased mitochondrial respiration. The lipidomic analysis further revealed a remodeling of membrane lipids characterized by increased free cholesterol and decreased polyunsaturated phosphatidylethanolamines and phosphatidylcholines alterations known to reduce membrane fluidity and impede cellular migration.

In a subcutaneous LLC1 model, IGF2BP2 MΦ-KO mice developed significantly smaller tumors than WT controls. Flow cytometric analysis revealed a marked reduction in $F4/80^+$ macrophages in tumor tissue, while immunohistochemical staining demonstrated decreased $CD31^+$ endothelial cell density, indicating impaired TAM infiltration and angiogenesis. These alterations were accompanied by a phenotypic shift toward a more pro-inflammatory TAM profile.

As a result of these observations, we investigated macrophage motility as a potential mechanistic contributor. IGF2BP2-deficient macrophages exhibited significantly reduced migration capacity in both *in vitro* scratch assays and *in vivo* models. Using a dorsal skinfold chamber model, IGF2BP2 MΦ-KO mice displayed reduced leukocyte rolling and adhesion in

response to inflammatory stimuli, underscoring the *in vivo* relevance of impaired macrophage migration.

This work demonstrates that IGF2BP2 is a critical regulator of macrophage metabolic programming, polarization, and migration. Its deletion not only alters macrophage function but also has significant effects on tumor growth and the recruitment of immune cells. These findings position IGF2BP2 as a promising target for therapeutic strategies to modulate macrophage activity in cancer.

This work was submitted in June 2025 and is included in this doctoral dissertation as a manuscript under review.

Hanna S. Schymik, Selina Wrublewsky, Marcus Höring, Gerhard Liebisch, Gilles Gasparoni, Caroline Bickelmann, Hanah Robertson, Charlotte Dahlem, Jörn Walter, Volkhard Helms, Matthias W. Laschke, Emmanuel Ampofo, Jessica Hoppstädter, Alexandra K. Kiemer. IGF2BP2 Deficiency in Macrophages Impairs Migration, Reprograms Metabolism, and Limits Tumor Progression, (submitted, 2025).

IGF2BP2 Deficiency in Macrophages Impairs Migration, Reprograms Metabolism, and Limits Tumor Progression

Hanna S. Schymik[1], Selina Wrublewsky[2], Marcus Höring[3], Gerhard Liebisch[3], Gilles Gasparoni[4], Caroline Bickelmann[2], Hanah Robertson[1], Charlotte Dahlem[1], Jörn Walter[4], Volkhard Helms[1], Matthias W. Laschke[2,5,6], Emmanuel Ampofo[2], Jessica Hoppstädter[1], Alexandra K. Kiemer[1,5,6*]

[1]Department of Pharmacy, Pharmaceutical Biology, Saarland University, Saarbrücken, Germany.

[2] Institute for Clinical & Experimental Surgery, Saarland University, Homburg, Germany.

[3] Institute of Clinical Chemistry and Laboratory Medicine, University Hospital Regensburg, Regensburg, Germany.

[4] Department of Genetics/Epigenetics, Saarland University, Saarbrücken, Germany.

[5] Center for Gender-Specific Biology and Medicine, Saarland University, Homburg, Germany.

[6] Pharma Science Hub, Saarland University, Saarbrücken, Germany.

***Correspondence:**
Alexandra Kathrin Kiemer, Pharmaceutical Biology, Saarland University, D-66123 Saarbrücken, Germany. E-mail: pharm.bio.kiemer@uni-saarland.de.

The authors declare no potential conflicts of interest.

1 Abstract

Insulin-like growth factor 2 mRNA-binding protein 2 (IGF2BP2) plays a pivotal role in macrophage polarization and function. This study investigates the consequences of myeloid-specific IGF2BP2 deletion on macrophage (MΦ) metabolism, polarization, and tumor progression.

Bulk RNA sequencing of IGF2BP2 MΦ-knockout (KO) macrophages revealed significant alterations in gene expression profiles, particularly impacting pathways associated with glycolysis, mitochondrial function, cell motility, and cell migration. Functional assays confirmed increased glycolytic activity and a concomitant reduction in maximal respiration and reserve respiratory capacity, indicating a metabolic shift towards glycolysis. Furthermore, IGF2BP2 deficiency impaired tumor-associated macrophage (TAM)-like polarization, as evidenced by decreased expression of TAM markers, such as *Mrc1*, *Mmp2*, and *Il10*. Lipidomic analyses revealed significant remodeling of membrane lipids in IGF2BP2-deficient macrophages, characterized by increased free cholesterol and reduced levels of polyunsaturated phosphatidylethanolamines and phosphatidylcholines, consistent with impaired membrane fluidity and migratory capacity.

In vivo, IGF2BP2 MΦ-KO mice exhibited reduced tumor growth in a subcutaneous Lewis lung carcinoma model, accompanied by decreased TAM infiltration and a shift towards a pro-inflammatory macrophage phenotype. Additionally, IGF2BP2-deficient macrophages showed impaired migratory capacity both *in vitro* and *in vivo*. These findings underscore the critical role of IGF2BP2 in regulating macrophage metabolism, polarization, and function within the tumor microenvironment, suggesting its potential as a therapeutic target in cancer.

2 Introduction

Macrophages are essential components of the immune system, playing a central role in immune defense, inflammation, and tissue homeostasis. Their ability to polarize into distinct functional states, including the classically activated M1 and alternatively activated M2 phenotypes, enables them to adapt to diverse physiological and pathological conditions (1,2). In the tumor microenvironment, macrophages often adopt a tumor-associated phenotype (TAM), predominantly immunosuppressive and pro-tumorigenic. These cells contribute to tumor progression by promoting angiogenesis, immune evasion, and extracellular matrix remodeling (3,4). Despite considerable progress in understanding macrophage biology, the molecular mechanisms governing their polarization and metabolic reprogramming remain incomplete.

The insulin-like growth factor 2 mRNA-binding protein 2 (IGF2BP2/IMP2) is an RNA-binding protein that regulates gene expression post-transcriptionally, primarily through recognition of N6-methyladenosine (m6A) modifications (5). IGF2BP2 is implicated in diverse cellular processes, including metabolism, differentiation, and oncogenesis, with dysregulated expression linked to poor prognosis in various cancers, such as colorectal, lung, bladder, and hepatocellular carcinoma (6–8). Beyond its role in cancer, IGF2BP2 is a key regulator of metabolic pathways, influencing glucose tolerance, insulin sensitivity, and fatty acid oxidation, and is associated with metabolic disorders, such as diabetes and obesity (9).

Understanding the molecular mechanisms that govern macrophage function in cancer is crucial, particularly for aggressive cancers with high mortality rates. Among these, lung cancer stands out as both the most frequently diagnosed malignancy and the leading cause of cancer-related deaths worldwide. In 2022, lung cancer accounted for approximately 2.48 million new cases, representing 11.6% of all cancer diagnoses globally (10,11). Notably, increased expression of IGF2BP2 has been consistently observed in lung cancer tissues, especially in cases resistant to conventional treatments. This elevated IGF2BP2 expression is associated with tumor progression and therapy resistance, highlighting its potential as a critical factor in lung cancer pathogenesis (12,13). Although targeted therapies and immune checkpoint inhibitors have advanced treatment options, the majority of lung cancer patients still face poor outcomes due to resistance mechanisms, often driven by TAM infiltration (14,15).

Emerging evidence also indicates that IGF2BP2 is involved in inflammatory regulation, influencing immune responses in rheumatoid arthritis, periodontitis, ulcerative colitis, and steatohepatitis (16–19). This regulation is primarily mediated through the stabilization of mRNAs encoding inflammatory mediators. However, its role in macrophage polarization—particularly in TAMs—remains poorly understood. Given the critical function of TAMs in linking chronic inflammation to cancer progression, elucidating the influence of IGF2BP2 on macrophage behavior could provide novel insights into tumor immunology and potential therapeutic targets. Notably, our previous work demonstrated that IGF2BP2 is highly expressed in M2 macrophages and chronic inflammatory diseases (20), further suggesting its potential involvement in shaping the tumor microenvironment.

In this study, we investigate the functional role of IGF2BP2 in macrophages and its impact on the tumor microenvironment, aiming to uncover its potential as a regulator of immune responses in cancer.

3 Materials & Methods

3.1 Materials

All materials and reagents used in this study were obtained from commercial suppliers. RPMI-1640 cell culture media (#R0833) and DMEM (high Glucose) cell culture media (#D6546-0500) were purchased from Sigma-Aldrich, along with L-glutamine (#G7513), penicillin/streptomycin (#P4333), Accutase (#A6964), Trypsin-EDTA (#T3924), and Antimycin A (#A8674, sourced from Streptomyces sp.). Filtrated bovine serum (FBS, #P040-37500) was obtained from PAN Biotech. Blasticidin S hydrochloride (#R21001) was acquired from Thermo Fisher Scientific.

3.2 Mice

Mice were housed under a 12-hour light/dark cycle and *ad libitum* access to food and water. Myeloid-specific IGF2BP2 knockout (KO) mice were generated by crossing B6.Cg-Igf2bp2tm1.1Thor/J mice (The Jackson Laboratory), which carry loxP sites flanking exons 4 and 5 of the *Igf2bp2* gene, with 29P2-Lyz2tm1(cre)Ifo/J mice (The Jackson Laboratory). Control wild-type (WT) mice were littermates that did not carry floxed alleles and either expressed or lacked Cre recombinase. IGF2BP2 MΦ-KO mice were validated by assessing protein and mRNA levels. Sex- and age-matched littermates were used for all experiments except for tumor studies conducted exclusively in female mice. All animal procedures were approved by the local animal welfare committee (AZ 2.4.1.1; AZ06-2020; AZ04-2023; Saarland State Office for Social Affairs, Health, and Consumer Protection).

3.3 Cell Culture Conditions

Cells were cultured at 37°C in a humidified 5% CO_2 atmosphere in RPMI-1640 medium supplemented with 10% FBS, 2 mM L-glutamine, and 100 units/ml penicillin G, 100 µg/ml streptomycin, unless stated otherwise.

3.4 Isolation and Cultivation of Bone Marrow-Derived Macrophages

Bone marrow cells were isolated from three- to four-month-old WT or IGF2BP2 MΦ-KO mice. Cells were flushed from femurs and tibias using a standard medium (RPMI 1640 supplemented with 10% fetal bovine serum [FBS], 100 U/ml penicillin G, 100 µg/ml streptomycin, and 2 mM glutamine). After centrifugation at 200×*g* for 10 minutes, erythrocytes were lysed by incubation in hypotonic buffer (155 mM NH_4Cl, 10 mM $KHCO_3$, and 1 mM Na_2EDTA) for 3 minutes at 37°C. The remaining cells were resuspended in a standard medium supplemented with macrophage colony-stimulating factor (M-CSF, 50 ng/ml, Miltenyi Biotech. #130-101-704) and transferred to a 75 cm^2 culture flask overnight for initial attachment. Non-adherent cells were collected the following day and cultured in a 150 cm^2 culture flask for 5-6 days in an M-CSF-containing medium to promote differentiation into bone marrow-derived macrophages (BMMs), as described before (21). Differentiated cells were detached using Accutase, resuspended in a standard medium supplemented with 50 ng/ml M-CSF, and seeded as indicated. To polarize or activate BMMs, the differentiation media was supplemented with 20 ng/ml recombinant interferon (IFN)-γ (Biomol, #87389.20) and 100 ng/ml lipopolysaccharide (LPS) (from E. coli K12, Invivogen, #tlrl-peklps) for M1 polarization, either 20 ng/ml interleukin-4 (IL-4) (Miltenyi Biotech, #130-093-921) for M2 polarization, or left without further supplementation for M0 macrophages. TAM-like macrophages were generated with tumor-conditioned media (TCM) supplemented with 50 ng/ml M-CSF. TCM was generated by seeding 0.5-1 × 10^6 murine Lewis lung carcinoma (LLC1) cells into a T75 culture flask and growing

until confluency for three days. Subsequently, the supernatant was discarded, and a standard growth medium was added to the cells. After 48 hours, the medium was sterile-filtered (0.22 µm) to remove cell debris and used immediately for macrophage polarization.

3.5 RNA Sequencing (RNA-Seq)

Next-generation sequencing (NGS) was performed to analyze the transcriptome of BMMs from WT and IGF2BP2 MΦ-KO mice, as previously described (22). 5×10^5 BMMs were seeded in a 12-well plate and treated with 20 ng/ml IL-4 for 8 hours the following day or left untreated to generate M0 macrophages. Total RNA was isolated using the High Pure RNA Isolation Kit (Roche, #11828665001) according to the manufacturer's protocol. RNA quality was assessed using the 2100 Bioanalyzer (Agilent) with the RNA 6000 Nano Kit (Agilent, #5067-1513), and only RNA samples with an RNA integrity number (RIN) > 9 were used for further analysis. For library preparation, 500 ng of RNA was used. Poly(A) enrichment was performed using the NEBNext Poly(A) mRNA Magnetic Isolation Module (New England Biolabs, #E7490) following the manufacturer's instructions. According to the manufacturer's protocol, cDNA libraries were generated using the NEBNext Ultra Directional RNA Library Prep Kit for Illumina (New England Biolabs, #E7420). First- and second-strand cDNA synthesis was followed by adapter ligation and PCR amplification (12 cycles) to generate the final library. PCR products were purified using Agencourt AMPure XP beads (Beckman Coulter, #A63881). Sequencing was performed in single-end mode (1 × 75 nt) using the NextSeq 500 (Illumina).

3.6 RNA-Seq Data Processing and Analysis

Raw sequencing reads were demultiplexed and assessed for quality using FastQC v0.11.2. Reads were processed using the Grape-nf pipeline (v1.1.3) with Nextflow (v20.10.0) and aligned to the GRCm38/mm10 genome assembly. Differential expression analysis was performed using DESeq2 (v1.40.2) based on the read counts obtained after alignment. Principal component analysis (PCA) was conducted using transcripts per million (TPM) values of all annotated protein-coding genes. All statistical analyses were performed using the R programming language, as previously described (23). DESeq2 analysis identified differentially expressed genes (DEGs, $p < 0.05$) in IGF2BP2 MΦ-KO vs. WT macrophages under untreated and IL-4-treated conditions. TPM values of DEGs were then subjected to unsupervised k-means clustering using iDEP 1.12, independently for untreated and IL-4-treated cells. Pathway enrichment analysis was performed using Ingenuity Pathway Analysis (IPA), version 76765844 (QIAGEN, June 2023), to identify significantly enriched canonical pathways.

3.7 Seahorse Measurement

The Glycolytic and Mito Stress Tests (Agilent, #103020-100, #103010-100) were conducted using the Agilent Seahorse® XF96 Analyzer and corresponding assay kits, following the manufacturer's protocols. Cells were seeded into Agilent Seahorse XF96 cell culture microplates (#103793-100), and the culture medium was replaced with Seahorse assay medium one hour prior to measurement.

For metabolic analyses involving IGF2BP2 KO, 5×10^5 cells per well were seeded for the Glycolytic Stress Test, whereas 0.2×10^4 cells per well were used for the Mitochondrial Stress Test. BMMs were treated with IL-4 and LLC1 supernatant for 8 hours.

During the Mito Stress Test, cells were treated with 1.5 µM carbonyl cyanide-4-(trifluoromethoxy)phenylhydrazone (FCCP). Oxygen consumption rate (OCR) and extracellular acidification rate (ECAR) were quantified using the Seahorse Wave software (Agilent Technologies).

Data normalization was performed based on cell areas obtained from brightfield images and analyzed with Gen5 software (version 3.14) on a Cytation 1 imaging system (BioTek).

3.8 Measuring Mitochondrial DNA Copy Number

Genomic DNA was extracted from 5×10^5 BMMs per well of a 12-well plate using the DNA Mini Prep Plus Kit (Zymo Research, #D4069), following the manufacturer's instructions. Mitochondrial DNA (mtDNA) copy number was determined by quantitative real-time PCR (qRT-PCR), measuring the expression levels of mitochondrial genes *mt16S* and *mtND1*, with *Hk2* as the nuclear reference gene. Primer sequences are provided in Supplemental Table 1. The mtDNA copy number was calculated as the ratio of mtDNA content (mean expression of *mt16S* and *mtND1*) to genomic DNA (gDNA), represented by *Hk2* expression. This method was adapted from the protocol described by Quiros et al. (2017).

3.9 Measurement of Mitochondrial Function

MitoTracker™ Deep Red and MitoTracker™ Green (Invitrogen, #M22426 and #M7514, respectively) were prepared according to the manufacturer's instructions. BMMs were seeded in 6-well plates at a density of 1×10^6 cells per well. The following day, cells were incubated with 100 nM MitoTracker™ Green and MitoTracker™ Deep Red for 30 minutes at 37°C. Untreated controls were included. Cells were detached using a cell scraper (TPP®), washed, and resuspended in phosphate-buffered saline (PBS). Flow cytometry was performed on an LSR-Fortessa™ (BD Biosciences) using FACS Diva 8.0.1 software (BD Biosciences). A minimum of 1×10^4 events were recorded per sample. Data analysis and pseudocolor plot generation were conducted using FlowJo 10.10.0 software.

3.10 Measurement of Mitochondrial Superoxide

To assess mitochondrial reactive oxygen species (ROS) production, cells were incubated with 5 µM MitoSOX™ Red mitochondrial superoxide indicator (Invitrogen, #M36008) in PBS containing 2% FBS. Antimycin A (AA, 10 µM) was used as a positive control and added simultaneously. BMMs were seeded at a density of 5×10^5 cells per well in 96-well plates and incubated overnight. Following treatment, real-time imaging was performed using the Incucyte® S3 Live-Cell Analysis System (Essen BioScience) with brightfield and red fluorescence channels (10× objective, 400 ms acquisition time). The total integrated intensity was measured after 15 minutes of treatment and normalized to the cell confluence (%) at the start of the experiment to account for variations in cell density.

3.11 Western Blot

For Western blot analysis, BMMs were seeded at 1×10^6 cells per well in a 6-well plate and incubated overnight. Western blots for IMP2/p62 were performed as previously described using antibodies specific for IMP2/p62 (25,26). Western blot for phosphor-p44/42 MAPK (Thr202/Tyr204, 20G11, Cell Signaling, #4376S) and p44/42 MAPK (Erk1/2, L34F12, Cell Signaling, #4696S), phosphor-NF-κB p65 (Ser536, 93H1, Cell Signaling, #3033S), and NF-κB p65 (L8F6, Cell Signaling, #6956S) were performed as previously described (27). An anti-α-tubulin monoclonal antibody (DM1A, Sigma-Aldrich, #T9026) was used as a loading control.

Immobilon FL-PVDF membranes (Millipore, Burlington, MA, #IPFL00010) were blocked for 1.5 hours in Rockland blocking buffer for near-infrared Western blotting. Following incubation overnight at 4 °C with primary antibody dilutions (1:1000 in Rockland blocking buffer) and incubation for 1.5 hours at room temperature with IRDye 680- or IRDye 800- (LI-COR Biosciences, #926-68071, #926-32210) conjugated secondary antibodies (1:10,000 in Rockland blocking buffer).

3.12 qRT-PCR

BMMs were seeded at 5×10^5 cells per well for RNA isolation in 12-well plates. Total RNA was isolated using the High Pure RNA Isolation Kit (Roche; #11828665001) or the Total RNA Quick-RNA Miniprep Kit (Zymo Research; #R1055), following the manufacturer's protocols. The concentration and purity of the isolated RNA were assessed using a NanoDrop™ spectrophotometer (Thermo Fisher Scientific). Equal amounts of RNA were reversely transcribed into complementary DNA (cDNA) using the High Capacity cDNA Reverse Transcription Kit (Thermo Fisher Scientific; #4368813) with the addition of an RNase inhibitor (Invitrogen; #10777-019), as per the manufacturer's instructions. Quantitative real-time PCR (qRT-PCR) was performed using 5× HotFirePol EvaGreen qPCR Plus Mix (no ROX) (Solis BioDyne; #082500020), as described previously (28,29), and primers listed in Supplemental Table 1. Reactions were conducted in a CFX96 Touch™ Real-Time PCR Detection System (Bio-Rad). Gene expression data were normalized to the housekeeping genes *RNA18S*, or *Ppia*.

3.13 Enzyme-Linked Immunosorbent Assay (ELISA)

BMMs were seeded in 96-well plates at a density of 5×10^5 cells per well and incubated overnight. The following day, cells were treated with 100 ng/ml LPS for 4 hours. After incubation, supernatants were collected for analysis. Following the manufacturer's protocol, tumor necrosis factor (TNF)-α secretion was quantified using an ELISA kit (BioLegend; #430904).

3.14 Griess Assay

BMMs were seeded in 96-well plates at a density of 5×10^5 cells per well the day before treatment. The following day, cells were treated with 100 ng/ml LPS and 25 ng/ml IFN-γ. After 24 hours of incubation, nitrite, a stable metabolite of nitric oxide (NO), was quantified.

For the assay, 90 µl of 1% sulfanilamide in 5% phosphoric acid (H_3PO_4) and 90 µl of 0.1% N-(1-naphthyl) ethylenediamine dihydrochloride in water were added to 100 µl of cell culture supernatant. The mixture was incubated at room temperature for 10 minutes, and the absorbance was measured at 560 nm using a GloMax® Discover Microplate Reader (Promega). As described previously, a standard curve was generated using sodium nitrite ($NaNO_2$) on the same plate for quantification (30).

3.15 Lipidomic Analysis of BMMs

BMMs were seeded in a 25 cm^2 cell culture flask at a density of 2×10^6 cells in 5 ml of medium one day before treatment. The following day, M0 macrophages were maintained in a standard medium, and TAM-like macrophages were generated by culturing macrophages for 24 hours in the LLC1-conditioned supernatant. Cell pellets were then collected and stored for further analysis.

For quantitative lipidomics, internal standards were added prior to lipid extraction. An amount of 100 µg protein was subjected to lipid extraction according to the protocol by Bligh and Dyer (31).

The analysis of lipids was performed by direct flow injection analysis (FIA) using a triple quadrupole mass spectrometer (FIA-MS/MS) and a high-resolution hybrid quadrupole-Orbitrap mass spectrometer (FIA-FTMS). FIA-MS/MS was performed in positive ion mode using the analytical setup and strategy described previously (32). A fragment ion of *m/z* 184 was used for lysophosphatidylcholines (LPC) (33). The following neutral losses were applied: Phosphatidylethanolamine (PE) and lysophosphatidylethanolamine (LPE) 141, phosphatidylserine (PS) 185, phosphatidylglycerol (PG) 189, and phosphatidylinositol (PI) 277 (34). Sphingosine-based ceramides (Cer) and hexosylceramides (Hex-Cer) were analyzed using a fragment ion of *m/z* 264 (35). PE-based plasmalogens (PE-P) were analyzed according to the principles described by Zemski-Berry (36). Cardiolipin (CL) was monitored by diglycerol fragment ions (37). Glycerophospholipid species annotation assumed of even-numbered carbon chains only.

A detailed description of the FIA-FTMS method was published recently (38). Triglycerides (TG), diglycerides (DG), and cholesterol esters (CE) were recorded in positive ion mode *m/z* 500-1000 as $[M+NH_4]^+$ at a target resolution of 140,000 (at 200 *m/z*). CE species were corrected for their species-specific response (39). Phosphatidylcholines (PC), PC ether (PC O), and sphingomyelins (SM) were analyzed in negative ion mode *m/z* 520-960 as $[M+HCOO]^-$ at the same resolution setting. Analysis of free cholesterol (FC) was performed by multiplexed acquisition (MSX) of the $[M+NH_4]^+$ of FC and the deuterated internal standard (FC[D7]) (39). Free fatty acids (FA) were analyzed in negative ion mode *m/z* 150-450 as $[M-H]^-$ dissolved in methanol/chloroform = 5/1 (v/v) containing 0.005% dimethylamine.

3.16 Migration Measurements

Migration was analyzed using the IncuCyte® S3 system. BMMs were seeded at a density of 1×10^5 cells per well in an ImageLock 96-well plate. Scratches were created using the WoundMaker® tool (IncuCyte Migration Kit). Following scratch creation, cells were washed twice with media to remove debris. Cell migration was monitored for 4 hours under standard incubation conditions. The extent of scratch area coverage (%) was assessed by analyzing the cell-covered area using IncuCyte migration software. Quantification was used to determine the migration rate and the extent of scratch area coverage over time.

3.17 Dorsal Skinfold Chamber and LPS-Induced Striated Skin Muscle Inflammation

WT and IGF2BP2 MΦ-KO mice (mean age: 5 months; average body weight: 25 g) were anesthetized *via* intraperitoneal injection of ketamine (100 mg/kg) and xylazine (12 mg/kg), followed by dorsal skinfold chamber implantation.

Briefly, two symmetrical titanium frames were positioned on the extended dorsal skinfold of anesthetized mice to create a double-layered skinfold. One layer, consisting of the skin, subcutis, and retractor muscle, was removed entirely within a circular area of 15 mm in diameter. This exposed area was then covered with a removable cover slip and secured with a snap ring, allowing direct microscopic access to the microcirculation within the chamber. Following the procedure, all animals were allowed to recover for 48 hours.

After the recovery period, the chamber tissue of WT and IGF2BP2 MΦ-KO mice was topically exposed to 10 µg/ml LPS for 0.5 hours to induce local inflammation. Briefly, anesthetized mice were immobilized on a plexiglas stage, and the dorsal skinfold chamber was affixed to the microscopic stage. To enhance contrast, retrobulbar intravenous injections of 0.05 ml 5% fluorescein

isothiocyanate (FITC)-labeled dextran (150,000) were administered to stain blood plasma, along with 0.05 ml 0.1% rhodamine 6G to stain leukocytes.

Intravital fluorescence microscopy was performed to assess leukocyte-endothelial interactions, blood vessel diameters, and macromolecular leakage under baseline conditions (19 hours before LPS exposure) and at 0.5, 3, and 24 hours post-LPS treatment, as previously described (40). Leukocyte rolling and adhesion were quantified using the established methods described (40,41). Vessel diameters were measured in micrometers (μm).

3.18 LLC1-Tumor Model

A murine cancer model was established by subcutaneous injection of luciferase-expressing Lewis lung carcinoma (LLC1) cells (CRL-1642-LUC2™, ATCC) into 8- to 10-week-old female WT and IGF2BP2 MΦ-KO mice. The LL2-Luc cell line was authenticated for viability, growth characteristics, mycoplasma contamination, species identity, and sterility. Cells were cultured under standard conditions according to ATCC guidelines. Before injection, subconfluent LLC1 cells were maintained for 2–3 weeks, harvested, filtered through a 40-μm cell strainer (BD Biosciences), washed, and resuspended in PBS. Tumor induction was performed by subcutaneous injection of 5×10^5 cells into the right flank of each mouse. Tumor growth was monitored by measuring tumor dimensions with digital calipers, and volumes were calculated using the formula: (height × width^2)/2.

Bioluminescence imaging (BLI) was conducted on day 14 post-injection to assess tumor burden. Mice were administered 3 mg of D-luciferin potassium salt (Revvity, #122799) *via* subcutaneous injection, and bioluminescent signals were captured using the IVIS Spectrum in vivo imaging system (PerkinElmer). Image acquisition and quantification were performed using Living Image 4.5 software (PerkinElmer).

3.19 Flow Cytometry

Tumor cells were isolated from murine tumor tissue on day 14. Tumors were enzymatically dissociated using the Murine Tumor Dissociation Kit (#130-096-730, Miltenyi Biotec) and the gentleMACS Octo Dissociator (Miltenyi Biotec) according to the manufacturer's instructions. Following dissociation, cells were washed with PBS and stained with Zombie Yellow viability dye (BioLegend, #423101) for 20 minutes at room temperature in the dark. A blocking step was performed using BD Fc Block™ (#553142, BD Biosciences) for 10 minutes at room temperature. Cells were incubated with fluorophore-conjugated antibodies for extracellular staining in FACS Wash buffer (PBS containing 2.5% FBS and 0.05% sodium azide). The following antibodies were used: APC anti-mouse/human CD11b (Clone M1/70, BioLegend, #101212, 2 μg/ml), PE anti-mouse F4/80 (Clone BM8, BioLegend, #123110, 2.5 μg/ml), APC anti-mouse CD206 (MMR) (Clone C068C2, BioLegend, #141707, 2.5 μg/ml), Brilliant Violet 421™ anti-mouse CD86 (Clone GL-1, BioLegend, 2 μg/ml, #105031), APC anti-mouse CD4 (Clone RM4-5, BioLegend, #100515, 2 μg/ml), Brilliant Violet 421™ anti-mouse CD8a (Clone 53-6.7, BioLegend, #100737, 5 μg/ml), and PE anti-mouse NK-1.1 (Clone PK136, BioLegend, #108707, 2 μg/ml). After staining, cells were washed and resuspended in 1% paraformaldehyde (PFA) in PBS.

For intracellular CD68 staining, cells were fixed in 1% PFA for 30 minutes at 4°C, followed by permeabilization with saponin buffer (FACS Wash with 0.2% [w/v] saponin) for 10 minutes. Subsequently, cells were blocked in PBS supplemented with 20% FBS and 0.02% saponin for

30 minutes, then incubated with Alexa Fluor® 594 anti-mouse CD68 (Clone FA-11, BioLegend, #137020, 5 µg/ml) for additional 30 minutes.

Flow cytometric analysis was performed using a BD LSRFortessa™ (BD Biosciences). Data acquisition and analysis were conducted using BD FACSDiva™ software (BD Biosciences), and median fluorescence intensities of singlet cells were used to quantify surface marker expression.

3.20 Immunohistochemistry

Tumor tissues were fixed in 4% PFA at 4°C for 24 hours. Following fixation, the samples were dehydrated, embedded in paraffin, and sectioned into 3-µm-thick slices. The tissue sections were treated with citrate buffer (pH 6.0) for antigen retrieval at 95°C for 30 minutes. To block non-specific binding, sections were incubated with goat serum for 1 hour at room temperature. CD31 expression was detected by incubating the sections with a primary antibody against CD31 (1:300, Clone SZ31, Dianova, #DIA310) overnight at 4°C. The primary antibody was visualized using a Cy3-conjugated goat anti-rat secondary antibody (1:1000, Jackson ImmunoResearch Labs, #712-165-153), applied for 1 hour at room temperature, as previously described (42). Fluorescence imaging was performed using a BX60F fluorescence microscope (Olympus), and CD31-positive cells were quantified using FIJI software (NIH).

4 m^{6}A Motif Enrichment Analysis

To investigate whether DEGs in IGF2BP2 KO macrophages are enriched for m^{6}A consensus motifs, a motif enrichment analysis was conducted using the MEME Suite tool SEA (43). Bulk RNA-Seq data from WT and IGF2BP2 KO BMMs were analyzed under untreated and IL-4-stimulated conditions. DEGs were defined using DESeq2 (padj < 0.05, $|\log2FC| \geq 2$). The 3' untranslated regions (3'UTRs) of significantly up- and downregulated DEGs were extracted from the Gencode M10 annotation (44,45), with non-differentially expressed genes serving as controls.

Enrichment of the canonical m^{6}A motif (DRACH (46)) was assessed using the Simple Enrichment Analysis (SEA(43)) tool within the MEME Suite, and motif occurrences were identified using FIMO (Find Individual Motif Occurrences) (47). Only motifs with a p-value $<$ 1e-4 (uncorrected) were considered for further analysis. A significant enrichment of DRACH motifs (47) was observed in the 3'UTRs of downregulated genes in IGF2BP2 KO BMMs ($p = 0.0362$), suggesting a potential role for IGF2BP2 as a stabilizing reader of m^{6}A-modified transcripts (48).

4.1 Statistics

Data are presented as means ± SEM (bar graphs). The normality of the data distribution was assessed using the Shapiro-Wilk test. A Student's T-test was applied for normally distributed data for comparisons between two groups, while the Mann-Whitney U test was used for non-normally distributed data. Statistical significance across multiple groups was determined by one-way ANOVA (for single time point comparisons) and two-way ANOVA (for multiple time points), followed by Bonferroni post-hoc tests for normally distributed data. Outliers were identified using Grubbs' test.

Unless stated otherwise, all statistical analyses and visualizations were performed using OriginPro 2020b (OriginLab, Northampton, MA, USA).

4.2 Data Availability Statement

Raw and processed data from the RNA-sequencing generated in the study were deposited in the Gene Expression Omnibus (GEO) database under the accession code GSE292558.

5 Results

5.1 Differentially Expressed Genes in WT and IGF2BP2 KO Macrophages.

Our previous study (20) demonstrated that IGF2BP2 expression is upregulated in human M2 macrophages (MΦ) following interleukin-4 (IL-4) treatment. To characterize the impact of IGF2BP2 expression in an anti-inflammatory context, we generated mice with a myeloid-specific deletion of IGF2BP2. IGF2BP2 MΦ-knockout (KO) mice showed a significant reduction to near-undetectable levels of *Igf2bp2* expression at both the protein and mRNA levels in BMMs compared to wild-type (WT) BMMs (Fig. 1A, B). Consistently, IL-4 treatment of WT BMMs led to increased *Igf2bp2* expression at both the mRNA and protein levels (Fig. 1C, D).

We performed RNA-Seq on WT and IGF2BP2 KO BMMs under untreated conditions and after IL-4 treatment. Using the DESeq2 approach, we identified 2,739 differentially expressed genes (DEGs, $p < 0.05$) in untreated cells and 2,136 in IL-4-treated cells (Supplementary file S1). Principal component analysis (PCA) revealed clear genotypic grouping patterns closely linked to differences in gene expression between WT and IGF2BP2 KO BMMs (Fig. 1E, F).

We then performed hierarchical k-means clustering (Fig. 1G, H) to analyze the biological processes associated with the loss of IGF2BP2 in untreated and IL-4-treated cells. Figures 1I and 1J show representative gene ontology (GO) terms for biological processes for selected clusters (fold change > 2, FDR < 0.05), providing insights into the functional categories affected by IGF2BP2 expression (see Supplementary file S2 for the complete list). Notably, our analysis revealed significant metabolic alterations in IGF2BP2 KO macrophages. Specifically, genes associated with metabolic processes and mitochondrial function, including cellular respiration and mitochondrial translation, were upregulated in IL-4-treated IGF2BP2 KO macrophages (Cluster 6). Additionally, KEGG pathway analysis identified an increase in glycolysis and gluconeogenesis (Supplementary Fig. 1A, B). Differential pathway analysis using Ingenuity Pathway Analysis (IPA) further confirmed the upregulation of metabolic pathways in KO macrophages, including glycolysis and gluconeogenesis (Supplementary Fig. 1C, D).

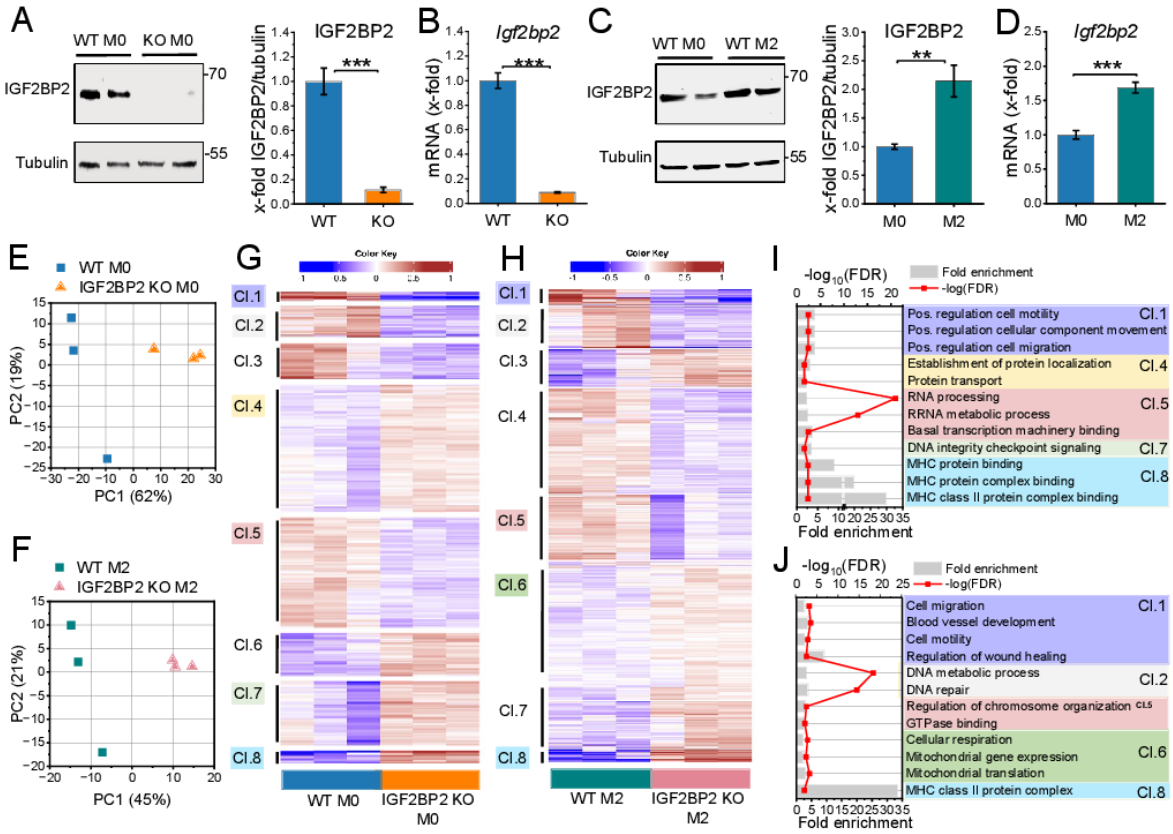

Figure 1. Differentially Expressed Genes in WT and IGF2BP2 KO Macrophages. BMMs from WT and IGF2BP2 MΦ-KO mice were cultured in standard media (M0) or treated with IL-4 (8 h, 20 ng/ml) to induce M2 polarization. **(A-D)** IGF2BP2 expression was assessed at the **(A, C)** protein level (n = 10 mice per group; n = 3 mice per group, duplicates), normalized to tubulin, and **(B, D)** mRNA level (n = 3 mice per group; n = 4 mice per group, duplicates), normalized to *RNA18S* (B) or *Ppia* (D). Data are expressed as fold change relative to untreated WT M0. **(E, F)** PCA of transcripts per million (TPM) values for all annotated protein-coding genes (>0.5 TPM; n = 3 mice per group). **(G, H)** K-means clustering of DEGs identified by DESeq2 analysis (input data = TPM) in **(E, G)** untreated and **(F, H)** IL-4-treated BMMs. **(I, J)** Selected Gene Ontology (GO) terms for biological processes, molecular functions, and cellular components enriched in the clusters (Cl) identified in **(G, H)**. Fold enrichment values are shown, and enrichment significance is represented by false discovery rate (FDR) values (fold change > 2, FDR < 0.05). **(A-D)** Data are presented as mean ± SEM. Statistical analysis was performed using Student's *t*-test (*$p < 0.05$; **$p < 0.01$; ***$p < 0.001$).

5.2 Metabolic Reprogramming in IGF2BP2 KO Macrophages: Increased Glycolysis and Impaired Mitochondrial Function

Genes within the glycolytic pathway were significantly upregulated in both M0 and M2 macrophages in IGF2BP2 KO cells (Fig. 2A, 2B; Supplementary Fig. 2A), with nine genes upregulated in M0 macrophages and thirteen genes upregulated in M2 macrophages. To assess the functional implications of these transcriptomic changes, we evaluated glycolytic activity by measuring the extracellular acidification rate (ECAR) using Seahorse Glycolytic Stress Test. The results showed a significant increase in glycolysis, glycolytic capacity, and glycolytic reserve in M2 KO macrophages (Fig. 2C, E). These results suggest an increased reliance on glycolysis for energy production in IGF2BP2 KO macrophages.

Cells can dynamically switch between glycolysis, taking place in the cytosol, and oxidative phosphorylation (OXPHOS), localized within mitochondria, to meet energy demands (49). Given that metabolic homeostasis appears disrupted in KO cells, we further examined mitochondrial function by assessing their oxygen consumption rate (OCR). In line with the observed increase in glycolytic activity, IGF2BP2 KO macrophages exhibited a significant reduction in maximal respiration and reserve respiratory capacity in both untreated and M2 KO conditions (Fig. 2D, F). No significant differences were observed in basal respiration or ATP production rates in KO macrophages (Fig. 2F, G), indicating a specific impairment of mitochondrial respiratory capacity rather than overall energy production. Despite these functional changes, the mitochondrial DNA (mtDNA) content remained unchanged, and only a slight reduction in mitochondrial mass was observed (Fig. 2H, I). The mitochondrial membrane potential ($\Delta\psi m$), driven by the proton gradient generated during OXPHOS, was also decreased in IGF2BP2 KO macrophages, consistent with the observed reduction in OXPHOS activity (Fig. 2J). Moreover, mitochondrial superoxide generation, i.e., reactive oxygen species (ROS) produced during electron flow through the electron transport chain (ETC), was significantly reduced (Fig. 2K, L). This decrease reflects the lower electron flow associated with reduced OXPHOS through ETC. Transcriptomic analysis further revealed the upregulation of genes involved in mitochondrial translation and mitochondrial organization in IGF2BP2 KO macrophages. Among these, genes encoding components of the ETC were significantly increased (Supplementary Fig. 2B, C), potentially representing a compensatory mechanism to counterbalance the reduced mitochondrial function.

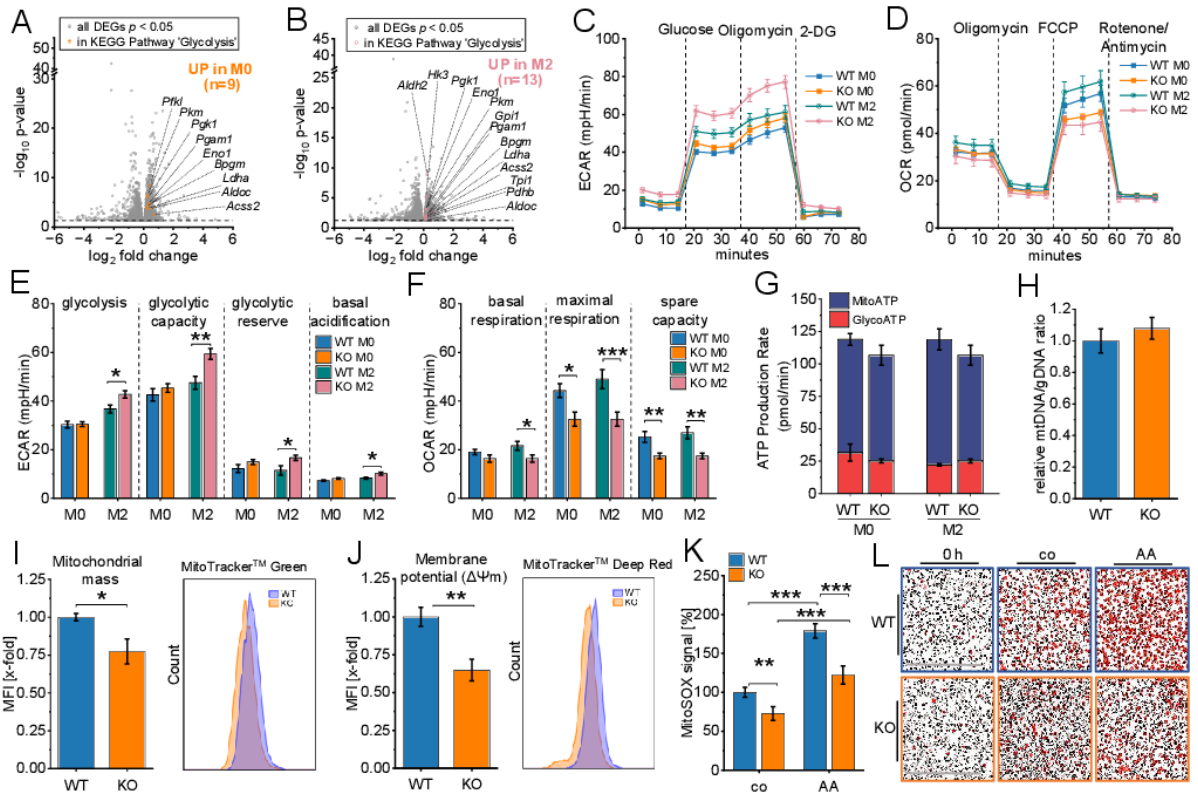

Figure 2. Metabolic reprogramming in IGF2BP2 KO macrophages. (A, B) Volcano plots of DEGs (shown in gray), with significantly upregulated glycolytic pathway genes highlighted in M0 (orange, A) and M2 (purple, B) macrophages (n = 3 mice per group). **(C, E)** Extracellular acidification rate (ECAR) during the glycolysis stress test and **(D, F)** Oxygen consumption rate (OCR) during the mitochondrial stress test in untreated (M0) and IL-4-treated BMMs, measured using the Seahorse XF Pro Analyzer (n = 4 mice per group, triplicates). **(H)** Quantitative RT-PCR detection of the relative mtDNA/gDNA ratio in BMMs (n = 8 mice per group, duplicates). **(I, J)** Flow cytometric measurements of mitochondrial mass **(I)** and mitochondrial membrane potential **(J)** relative to WT BMMs (n = 5-6 mice per group, duplicates), with pseudocolor plots of representative samples. **(K, L)** The MitoSOX™ signal was measured using live-cell imaging with the Incucyte® S3 system 15 minutes after adding MitoSOX or Antimycin A (AA). Fluorescence intensities relative to WT (set to 100%) are shown. **(L)** Representative Images. The fluorescence signal is shown in red. Scale bar = 400 µm (n = 4 mice per group, quadruplicates). *p* values were determined using one-way ANOVA followed by Bonferroni post-hoc tests (E, F, K) or student's t-test (I, J) (* $p < 0.05$; ** $p < 0.01$; *** $p < 0.001$).

5.3 IGF2BP2 Deficiency Alters TAM-like Polarization and Metabolic Reprogramming

Analysis of publicly available transcriptomic data (GSE162669, GSE162698; (22)) indicates that IGF2BP2 expression is elevated in TAMs isolated from lung adenocarcinoma tissue compared to alveolar macrophages (AMs) from adjacent normal lung tissue (Fig. 3A). A similar upregulation was observed in TAM-like macrophages, where primary human monocyte-derived macrophages (HMDMs) were polarized towards a TAM-like phenotype using tumor-conditioned medium (TCM) from the lung adenocarcinoma cell line A549 (Fig. 3B).

To further explore the role of IGF2BP2 in murine TAM polarization, BMMs were stimulated with TCM from Lewis lung carcinoma (LLC1) cells to induce a TAM-like phenotype. qPCR analysis revealed a significant upregulation of *Igf2bp2* mRNA after TAM-like polarization (Fig. 3C). A panel of TAM-associated genes was analyzed by qPCR, revealing increased expression of several TAM-like markers (*Ccl2, Hif1a, Mmp9, Mrc1, Tgfb, Vegfa*) upon polarization (Supplement Fig. 3). Notably, IGF2BP2 KO BMMs exhibited a significant reduction in key TAM-like markers, including *Mrc1*, *Mmp2*, and *Il10* (Fig. 3D).
Given the metabolic shift observed in IGF2BP2 KO M2 macrophages, we assessed the glycolytic activity in KO TAM-like macrophages using the Glycolytic Stress Test. ECAR measurements indicated a significant increase in glycolysis and glycolytic capacity in KO TAM-like macrophages compared to WT TAM-like macrophages (Fig. 3E, F). Consistent with elevated glycolytic activity, qPCR analysis demonstrated an upregulation of glycolytic markers, including *Accs2*, *Aldh2*, *Aldoc*, *Bpgm1*, *Gapdh*, *Gpi1*, and *Pgk1*, in KO TAM-like macrophages (Fig. 3G). Mitochondrial respiration was evaluated using the Seahorse XF Cell Mito Stress Test. KO TAM-like macrophages exhibited a significant reduction in maximal respiration and reserve respiratory capacity (Fig. 3H-J). Furthermore, ATP production analysis revealed a decrease in mitochondrial-driven ATP (MitoATP) levels in KO TAM-like macrophages (Fig. 3J).

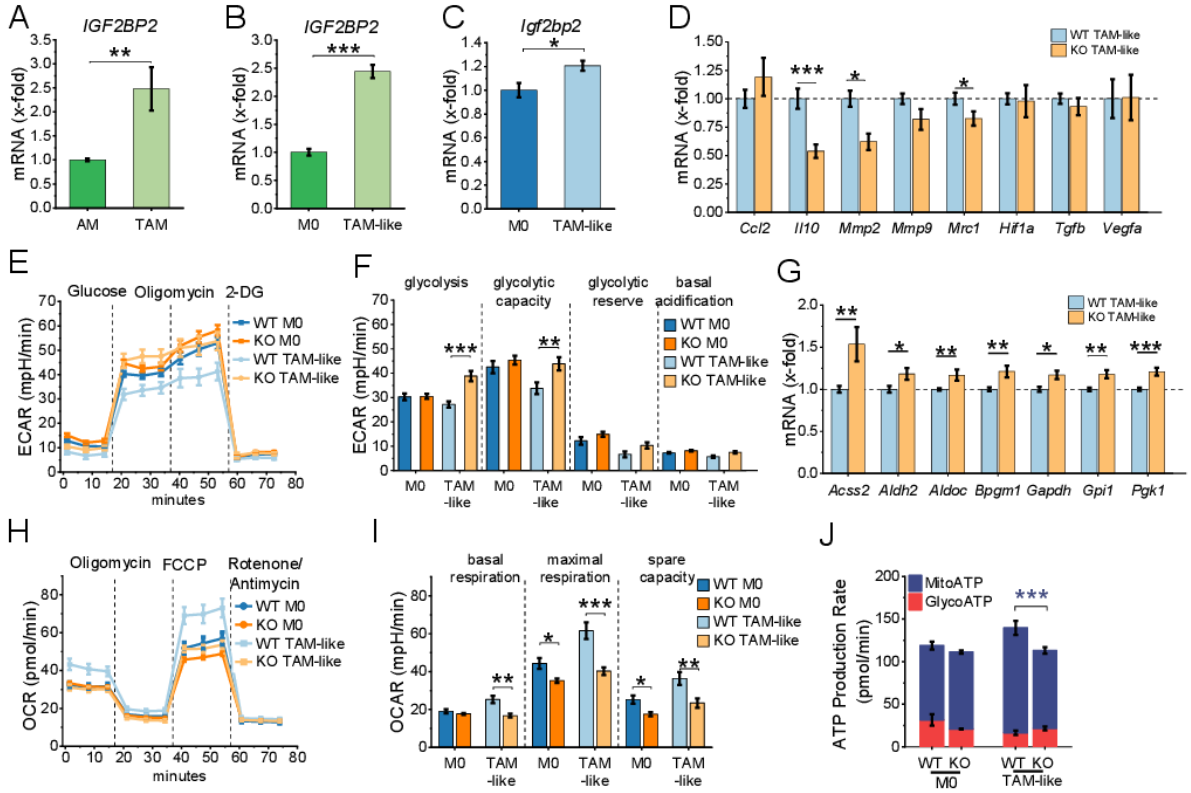

Figure 3. IGF2BP2 Regulates TAM-like Polarization and Metabolic Reprogramming. (A) Gene expression in macrophages from lung adenocarcinoma (TAMs) and adjacent non-tumor tissue (AMs) using publicly available RNA-seq data from dataset GSE162669 (n = 3 donors per group, triplicates). **(B)** Gene expression of HMDMs polarized with TCM from A549 cells for 24 h, using data from GSE162698 (n = 3 individual donors). **(C–J)** BMMs were cultured in standard medium (M0) or TCM from LLC1 cells (TAM-like) for 8 hours. mRNA expression was measured by qPCR and normalized to *Ppia*. **(C)** *Igf2bp2* expression is presented as fold change relative to M0 (n = 4 mice per group, duplicates). **(D)** Expression of TAM-like macrophage markers is shown as a fold change of WT TAM-like (n = 6 mice per group, duplicates). **(E, F)** ECAR during the Glycolysis Stress Test and **(H–J)** OCR during the mitochondrial stress test were measured in M0 and TAM-like macrophages using the Seahorse XF Pro Analyzer (n = 4 mice per group, triplicates). **(G)** mRNA expression of glycolytic markers, expressed as x-fold change relative to TAM-like macrophages (n = 4 mice per group, duplicates). Data are presented as mean ± SEM. Statistical significance was determined by Student's t-test (A-D, G) and ANOVA (F, I, J) (*$p < 0.05$; **$p < 0.01$; ***$p < 0.001$).

5.4 Lipidomic Profiling Reveals Altered Membrane Lipid Composition in IGF2BP2 KO Macrophages

Lipid metabolism plays a crucial role in shaping the phenotype and function of TAMs (50). To explore the lipidomic changes associated with TAM polarization and to assess the impact of IGF2BP2 on macrophage lipid metabolism, we conducted a comprehensive lipidomic analysis of WT and IGF2BP2 KO macrophages in both their native M0 and TAM-like states. TAM-like macrophages were generated by culturing BMMs in TCM from LLC1.

Hierarchical clustering and heat map analysis showed a clear separation between M0 and TAM-like macrophages in WT and IGF2BP2 KO (Fig. 4A, B, Supplementary file 4). TAM-like polarization induced changes in glycerolipid content, especially an increase in triglycerides, consistent with enhanced lipid storage (51), the overall distribution of major lipid classes remained relatively comparable between WT and IGF2BP2 KO macrophages (Supplementary Fig. 4A, B).

Significant differences between the groups were observed for membrane lipids: Free cholesterol (FC) levels were significantly elevated in KO TAM-like macrophages but not in KO M0 cells (Fig. 4C, D).

Within the phospholipid classes, phosphatidylethanolamine (PE) species containing long-chain polyunsaturated fatty acids were consistently reduced in IGF2BP2-deficient macrophages (Fig. 4E-H). Species likely to contain arachidonic acid (e.g., PE 38:4, PE 40:4, PE 40:5) and docosahexaenoic acid (e.g., PE 40:6) were particularly affected. When grouped by double bond number, PE species with four or more double bonds (DB4-DB7) were significantly decreased in both KO M0 and TAM-like cells (Fig. 4F, H).

A similar pattern was observed for phosphatidylcholines (PCs), the most abundant class of membrane phospholipids: Highly unsaturated PC species-including PC 38:4, PC 38:5, PC 38:6, PC 40:5, and PC 40:6-were significantly decreased in both KO M0 and KO TAM-like macrophages (Fig. 4I-L). Grouped analysis further confirmed that DB4-DB6 PCs were consistently lower in IGF2BP2-deficient cells (Fig. 4J, L).

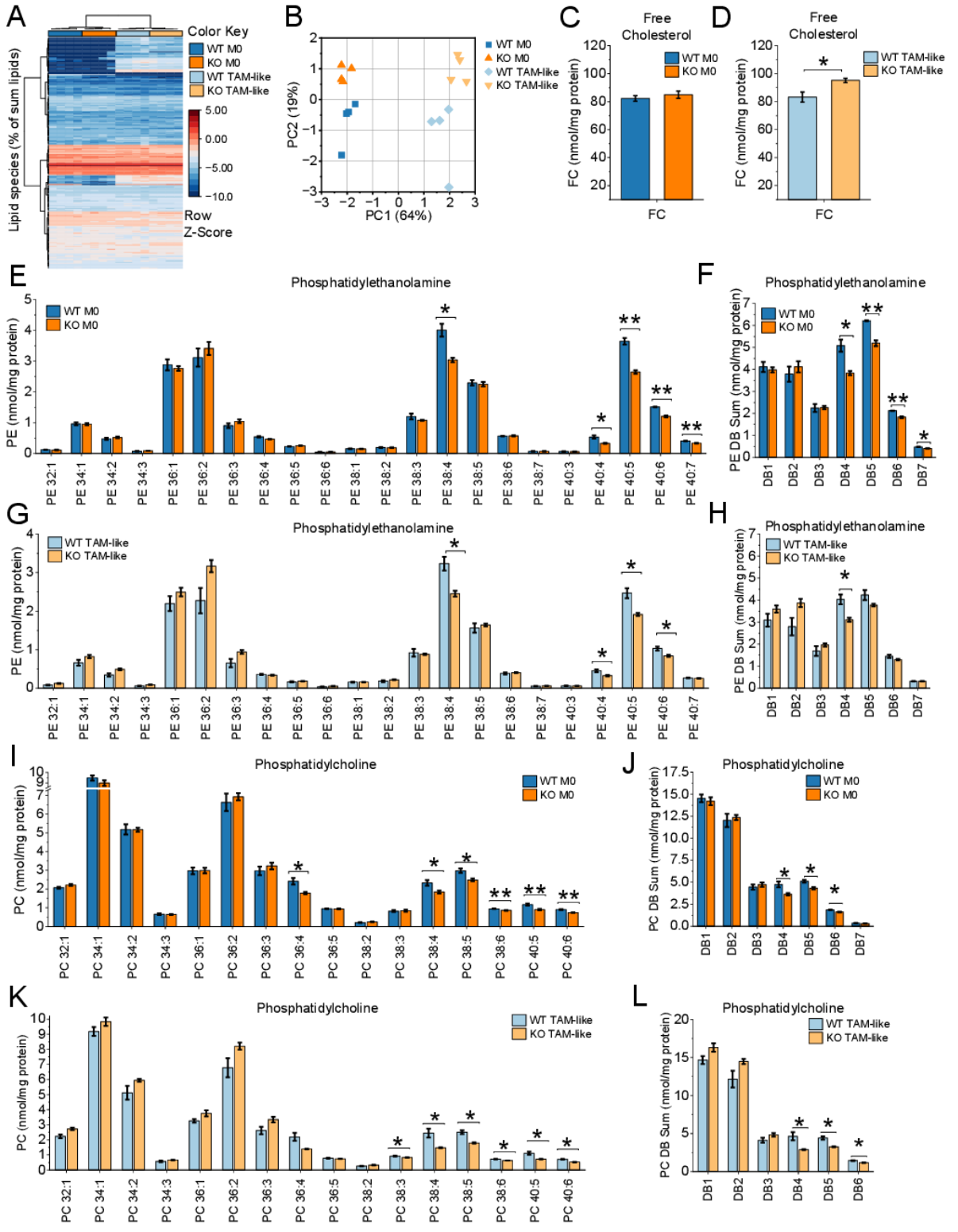

Figure 4. IGF2BP2 Deficiency Alters Membrane Lipid Composition in Macrophages (M0 and TAM-like). BMMs were cultured either in standard medium (M0) or in TCM from LLC1 cells for 24 hours to

induce TAM-like polarization. Lipid concentrations in WT and IGF2BP2 KO M0 and TAM-like macrophages were analyzed by mass spectrometry. **(A)** Hierarchical clustering of log_2-transformed lipid data expressed as a percentage of total lipids, using Ward's linkage and Euclidean distances. Samples are color-coded: WT M0 (dark blue), KO M0 (orange), WT TAM-like (light blue), and KO TAM-like (yellow). **(B)** PCA of log_2-transformed lipid concentrations (nmol/mg protein) across all lipid species. **(C, D)** Quantification of free cholesterol (FC) in WT and IGF2BP2 KO macrophages under M0 and TAM-like conditions. **(E–H)** Concentrations of phosphatidylethanolamine (PE) species (E, G) and PE species grouped by double bond (DB) number (F, H). **(I–L)** Concentrations of phosphatidylcholine (PC) species (I, K) and PC species grouped by DB number (J, L). Lipid concentrations are expressed as nmol/mg protein. Statistical significance was determined by ANOVA with Bonferroni's post hoc test (F–J). (*$p < 0.05$; **$p < 0.01$; ***$p < 0.001$).

5.5 Myeloid-Specific IGF2BP2 MΦ-KO Reduces Tumor Growth of Murine Subcutaneous Lewis Lung Carcinoma

To further investigate the role of IGF2BP2 in TAMs and its impact on myeloid cells within the tumor microenvironment (TME) and tumor progression, we used an LLC1 tumor model. We injected luciferase-expressing LLC1 cells subcutaneously into WT and IGF2BP2 MΦ-KO mice. As shown in Figure 5A-C, IGF2BP2 MΦ-KO mice developed significantly smaller tumors with reduced volume and weight compared to WT controls. Bioluminescence imaging on day 14 confirmed a lower tumor burden in MΦ-KO mice, as indicated by reduced radiance and photon flux quantification (Fig. 5D).

Flow cytometric analysis was performed to characterize the immune cell composition within the tumors. IGF2BP2 MΦ-KO mice exhibited a significant reduction in TAMs, defined as $CD11b^+F4/80^+$ or $CD11b^+CD68^+$ (Figure 5E-H). Given the well-established pro-tumorigenic role of TAMs (52), this reduction may contribute to the observed decrease in tumor growth. Further phenotypic analysis of TAMs using the CD86 and CD206 markers revealed a modest but significant increase in the $CD86^+CD206^-$ population in MΦ-KO mice, suggesting a shift toward an M1-like (classically activated) phenotype (Fig. 5I, J).

Beyond macrophages, myeloid-specific IGF2BP2 deficiency also affected other immune populations. Notably, the numbers of $CD4^+$ helper T cells and $CD8^+$ cytotoxic T cells were significantly reduced in MΦ-KO compared to WT tumors (Fig. 5K-N). Additionally, $NK1.1^+$ natural killer (NK) cells were markedly reduced in MΦ-KO tumors (Figure 5O, P).

To evaluate tumor vascularization, we performed CD31 immunofluorescence staining. MΦ-KO tumors exhibited a significantly lower CD31-positive endothelial cell area compared to WT, indicating impaired angiogenesis (Fig. 5Q, R). Consistently, gene expression analysis showed a slight reduction in *Fgf2*, *Hif1a*, and *Mmp2*, while *Mmp9* expression was significantly decreased in IGF2BP2 MΦ-KO tumors (Supplementary Fig.5).

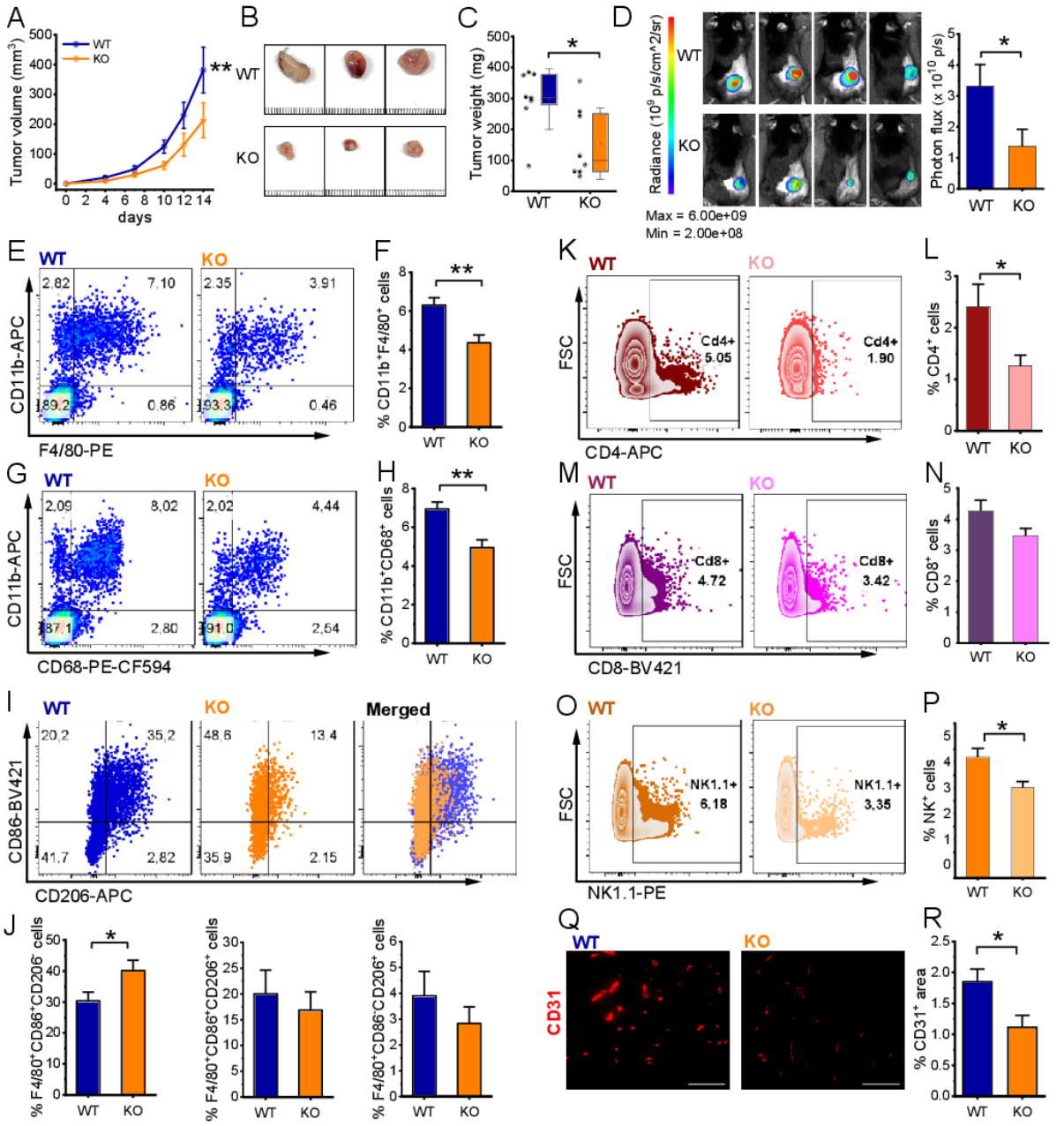

Fig. 5. IGF2BP2 MΦ-KO reduces tumor growth, alters immune cell infiltration, and impairs angiogenesis in LLC1 tumors. Luciferase-expressing Lewis lung carcinoma (LLC1) cells were injected subcutaneously into WT and IGF2BP2 MΦ-KO mice. **(A)** Tumor volume. **(B)** Representative images of resected subcutaneous tumors, scale bar = 1 mm per line). **(C)** Comparison of tumor weights between WT and IGF2BP2 MΦ-KO mice. **(D)** Bioluminescence imaging of luciferase-expressing LLC1 cells following luciferin injection, with photon flux intensity quantified on day 14. **(E–J)** For flow cytometric analysis, tumors were collected and dissociated on day 14. **(E, G,** left panel) Representative dot plots showing TAMs, gated as $CD11b^+F4/80^+$ or $CD11b^+CD68^+$ populations **(F, H,** right panels) TAM quantification. **(I, J)** TAMs were classified into $F4/80^+CD86^+CD206^-$, $F4/80^+CD86^+CD206^+$, and $F4/80^+CD86^-CD206^+$ subpopulations. **(I)** Representative plots. **(J)** Quantification data. **(K-P)** Quantification of $CD4^+$, $CD8^+$, and $NK1.1^+$ immune cell populations **(K, M, O)** Representative plots. **(L, N, P)** Quantification data. **(Q)** Representative image of fluorescently stained CD31-positive endothelial cells (red); scale bar = 100 µm. **(R)** Quantification of CD31-

positive endothelial cell area ((A-J) n = 8 mice per group, (Q) n = 8 WT, n = 7 MΦ-KO mice per group, from two independent experiments). Statistical significance was determined using two-way ANOVA for multiple time points (A) and Student's *t*-test for comparisons in (C-R) (*$p < 0.05$; **$p < 0.01$; ***$p < 0.001$).

5.6 Impaired Cell Migration in IGF2BP2 MΦ-KO Macrophages *in Vitro* and *in Vivo*

Tumor progression is closely linked to immune cell recruitment and migration (53). As shown above (Fig. 4), IGF2BP2-deficient macrophages exhibited significant alterations in membrane lipid composition, including increased free cholesterol and decreased polyunsaturated phospholipids concentration, alterations known to impair membrane fluidity and potentially impede cellular motility (54–56). Given these biophysical changes, along with the reduced number of immune cells observed in IGF2BP2 MΦ KO tumors, we next investigated whether IGF2BP2 deletion directly affects macrophage migration.

RNA-Seq revealed a significant downregulation of genes associated with cell motility, migration, and movement of cellular components in cluster1 in IGF2BP2 KO macrophages (Fig. 1I, J). Specifically, 12 genes within the GO term "cell migration" were significantly reduced in M0 macrophages (Fig. 6A). To assess the functional consequences of these transcriptional changes, we performed a scratch assay *in vitro*, which demonstrated significantly reduced migratory capacity in IGF2BP2 KO macrophages compared to WT controls (Fig. 6B, C).

To examine leukocyte migration *in vivo*, we utilized the dorsal skinfold chamber model, allowing real-time visualization of leukocyte-endothelial interactions within striated muscle tissue. Migration was stimulated *via* topical LPS application. Previous experiments confirmed that WT and IGF2BP2 KO macrophages exhibited a comparable pro-inflammatory response to LPS, including similar cytokine mRNA expression, TNF secretion, and activation of ERK and NF-κB signaling pathways (Supplementary Fig. 6).

Using intravital fluorescence microscopy, we analyzed key leukocyte migration processes, including rolling, adherence, and transmigration. To investigate the impact of IGF2BP2 depletion on myeloid cell migration, we utilized the LysMCre system, which induces IGF2BP2 deletion primarily in macrophages, neutrophils, and monocytes. This enabled us to assess the migration dynamics of these cell populations in real-time using the dorsal skinfold chamber model (Fig. 6D-G, Supplementary Fig. 7). The specificity of the LysMCre system for myeloid cells was previously validated (57).

As expected, venous and arteriolar diameters remained comparable between WT and IGF2BP2 MΦ-KO mice (Fig. 6E, Supplementary Fig. 7A). However, the IGF2BP2 MΦ-KO mice showed a significantly reduced number of rolling and adherent leukocytes in venules at 3 and 24 hours after exposure to LPS (Fig. 6F, 6G). In addition, the number of adherent leukocytes in arterioles was significantly reduced in the KO group at 3 and 24 hours (Supplementary Fig. 7C).

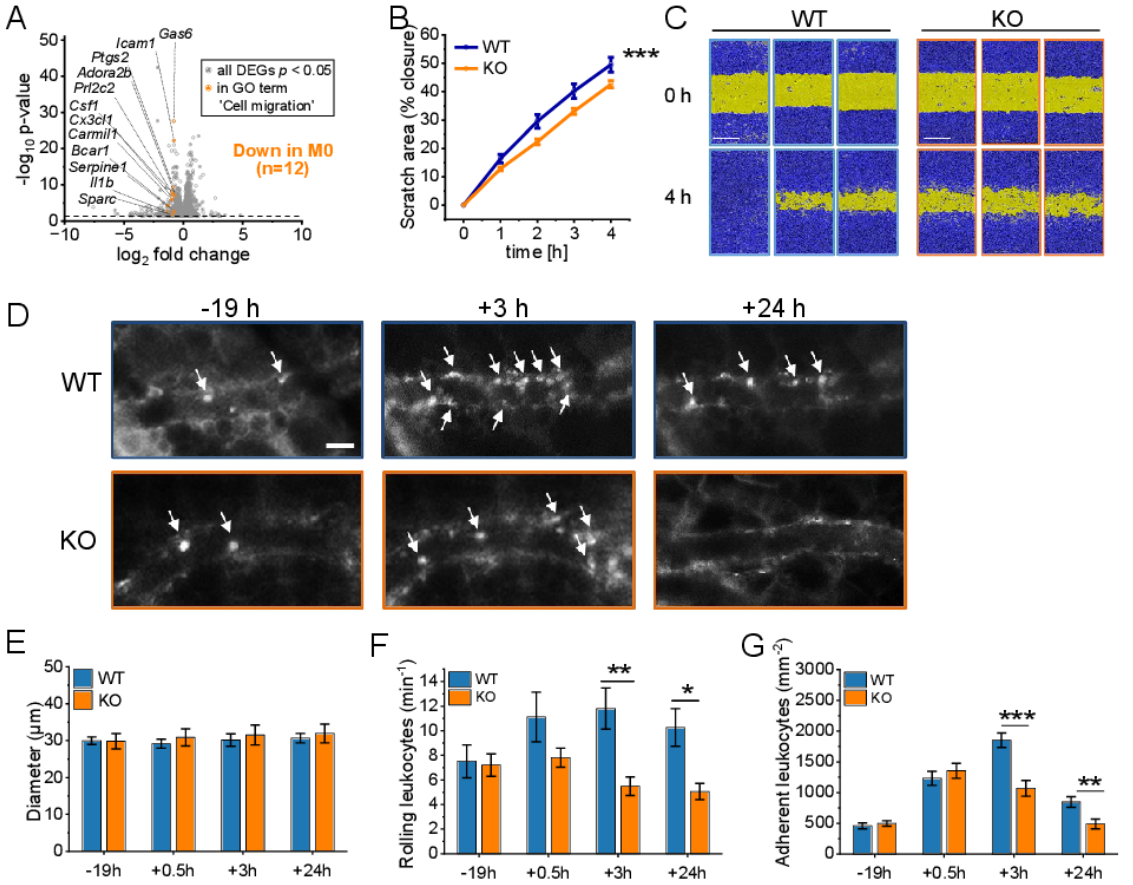

Figure 6. IGF2BP2 Deficiency Impairs Macrophage Migration and Reduces Leukocyte Recruitment *in Vivo*. **(A)** Volcano plots of DEGs (shown in gray), with significantly downregulated genes in the GO term "cell migration" (GO:0030335) highlighted in orange for M0 macrophages (n = 3 mice per group). **(B, C)** Live-cell microscopy-based analysis of cell migration. Following scratch, scratch area coverage (%) of WT and IGF2BP2 KO BMMs was monitored in an IncuCyte® S3 system over 4 hours. Representative images are shown; scale bar = 400 µm (n = 7 mice per group, triplicates). **(D)** Intravital fluorescence microscopic images of postcapillary venules in the dorsal skinfold chamber of WT and IGF2BP2 MΦ-KO mice 19 h before and 3 and 24 h after LPS treatment. Green-light epi-illumination with staining of leukocytes (arrows) by rhodamine 6G. Scale bar = 30 µm. Quantification of **(F)** rolling leukocytes, **(G)** adherent leukocytes in dorsal skinfold chambers of WT and IGF2BP2 MΦ-KO mice (n = 8 mice per group) that were exposed to treatment of LPS 0.5 hours. WT and IGF2BP2 MΦ-KO animals were analyzed at corresponding time points. Measurements were obtained using intravital fluorescence microscopy and computer-assisted image analysis. Data are presented as mean ± SEM. Statistical significance was determined using two-way ANOVA for multiple time points (B) or Student's t-test for individual time points (G, H, I) (*$p < 0.05$; **$p < 0.01$; ***$p < 0.001$).

6 Discussion

Our study highlights the critical role of IGF2BP2 in regulating macrophage metabolism, polarization, and migration, with specific implications for TAMs and tumor progression. Using myeloid-specific IGF2BP2 MΦ-KO mice, we demonstrate that IGF2BP2 deficiency drives a metabolic shift favoring glycolysis over OXPHOS, impairs macrophage migration, and alters TAM polarization, leading to reduced tumor growth.

IGF2BP2 as a Regulator of Macrophage Metabolism

Macrophages exhibit remarkable metabolic plasticity, adapting their energy pathways to environmental cues. Pro-inflammatory M1 macrophages rely on glycolysis and increased glucose uptake, whereas anti-inflammatory M2 macrophages depend on fatty acid oxidation (FAO) and OXPHOS for energy (58).

IGF2BP2 plays a critical role in metabolic transitions, with its KO in macrophages leading to enhanced glycolysis (increased ECAR) and impaired mitochondrial respiration (decreased OCR). KO cells display reduced membrane potential, indicating mitochondrial dysfunction, alongside lower mitochondrial ROS levels, suggesting decreased electron flow through the ETC. This aligns with previous findings showing that a reduction in mitochondrial membrane potential increases activation of the mitochondrial permeability transition pore, which inhibits oxidative phosphorylation, leading to lower mitochondrial ROS production and disrupted electron flow (59). Despite these functional impairments, the mitochondrial DNA content remained stable, with only a slight reduction in mitochondrial mass, indicating that IGF2BP2 primarily regulates mitochondrial activity rather than biogenesis. This metabolic reprogramming aligns with previous findings in other cellular contexts, where IGF2BP2 enhances glycolysis by regulating *ALDOA* expression in hepatic stellate cells (60) and stabilizing lncRNA *DANCR* to modulate glycolytic enzyme expression in acute myeloid leukemia (61). Additionally, IGF2BP2 has promoted aerobic glycolysis through *GLUT1* mRNA stabilization, further reinforcing its role as a pivotal metabolic regulator across various disease models (9). More recently, IGF2BP2 was identified as a critical factor in PLK1-overexpressing tumors, where its loss led to a marked reduction in PLK1 expression. This disruption further impaired mitochondrial metabolism and suppressed tumor cell proliferation and survival (62).

IGF2BP2 Modulates TAM Polarization and the Tumor Microenvironment

Our study further revealed that IGF2BP2 plays a role in macrophage polarization. IGF2BP2 expression was elevated in TAM-like macrophages, and its deletion led to a reduction in key TAM markers, including *Mrc1*, *Mmp2*, and *Il10,* and a glycolytic shift.
TAMs facilitate tumor progression by secreting cytokines that enhance tumor cell proliferation and suppress immune responses (63). Myeloid-specific IGF2BP2 deletion significantly reduced tumor growth in the LLC1 model, with MΦ-KO mice exhibiting smaller tumors, reduced tumor burden and TAM infiltration, and an increased number of inflammatory TAMs. However, MΦ-KO tumors exhibited a reduction in $CD4^+$ and $CD8^+$ T cells, as well as NK cells, indicating that IGF2BP2 deletion impacts not only macrophages but also the broader immune landscape. A likely explanation for reduced T- and NK cell infiltration in IGF2BP2 MΦ-KO tumors is the altered recruitment capacity of TAMs. TAMs contribute to T cell recruitment *via* chemokines, such as CCL5, CCL2, and CXCL9/10 (64). Thus, a decrease in TAM numbers, regardless of polarization, may reduce chemokine production and lower T-cell recruitment.

These findings align with previous studies highlighting the role of IGF2BP2 in macrophage polarization. Our prior research (20) showed that IGF2BP2 expression is elevated in M2 macrophages and chronic inflammation but downregulated in acute inflammatory responses, indicating a context-dependent role in macrophage activation.

Consistent with this, IGF2BP2 has been shown to promote an M2 phenotype in various contexts. Elevated IGF2BP2 expression in cancer cells modulates extracellular vesicle secretion, driving macrophages toward a TAM-like phenotype and promoting tumor progression (65). Similarly, IGF2BP2 stabilizes NRP1 mRNA, facilitating M2 macrophage polarization and enhancing bladder cancer malignancy (8). In addition, high IGF2BP2 expression correlates with immunosuppressive M2-like macrophages, angiogenesis, and immune evasion in bladder cancer (66). Further supporting the role of IGF2BP2 in macrophage polarization, IGF2BP2 deletion enhances M1 polarization and promotes inflammation in colitis while reducing IL-4-induced M2 activation, suggesting that IGF2BP2 facilitates the M1-to-M2 transition (67).

Our findings also suggest species-specific differences in IGF2BP2 regulation. While IGF2BP2 expression was not induced in HMDMs after 24 hours of LPS treatment (20), it was upregulated in murine BMMs after 4 hours of LPS treatment without significantly altering the pro-inflammatory response. This contrasts with the findings of Wang et al., where IGF2BP2 MΦ-KO BMMs exhibited increased pro-inflammatory cytokine expression (68), and with studies in THP-1 cells, where IGF2BP2 acts as an m^{6}A reader that binds to methylated TIM1 mRNA, enhancing its stability and thereby promoting M1 polarization and inflammation (69). Consistent with this, our data show that transcripts strongly downregulated in IGF2BP2 KO macrophages are significantly enriched in m^{6}A motifs, supporting a role for IGF2BP2 as an m^{6}A-reader stabilizing these mRNAs (Supplementary file 5). These discrepancies highlight the complexity of the role of IGF2BP2's role in macrophage polarization, influenced by differences in experimental models, polarization conditions, and species-specific responses. Murine macrophages generally exhibit a limited LPS response due to the rapid induction of negative feedback regulators (70). Moreover, human macrophages activated by LPS rely on oxidative phosphorylation rather than glycolysis for ATP generation (71), potentially contributing to the observed differences between murine and human macrophages.

IGF2BP2 and Macrophage Migration

Macrophage migration is essential for tumor progression, as alterations in motility can significantly affect immune responses and cancer development (72). Our findings demonstrate that KO macrophages exhibit markedly impaired migration both *in vitro* and *in vivo*. In the dorsal skinfold chamber model, MΦ-KO mice had fewer rolling and adherent leukocytes at inflammation sites. RNA-Seq analysis revealed downregulation of migration-related genes in KO macrophages, which was further confirmed by a scratch assay showing reduced migration. Consistent with previous findings that IGF2BP2 activates RhoA/ROCK signaling (73), our Ingenuity Pathway Analysis (IPA) of IGF2BP2 KO macrophages revealed significant downregulation of pathways associated with actin-based cell motility, particularly those involving RhoA.

Beyond cytoskeletal signaling, membrane lipid composition emerged as a critical determinant of migratory capacity (54–56). Lipidomic profiling revealed significant reductions in polyunsaturated phosphatidylethanolamine (PE) and phosphatidylcholine (PC) species, particularly those containing four or more DB arachidonic and docosahexaenoic acyl chains in KO BMMs. We observed elevated free cholesterol (FC) concentrations in KO TAM-like macrophages. Such an increase in FC, characterized by a rigid and planar molecular structure, increases lipid packing and decreases

membrane fluidity, negatively affecting dynamic cellular activities, including migration (74–76). Indeed, both PE and PC have been implicated in promoting cellular motility through increased membrane flexibility and curvature (74–76). Notably, a balanced phospholipid-to-free cholesterol (PL/FC) ratio has previously been reported to be essential for efficient macrophage phagocytosis (77). Thus, the observed lipid changes, notably the decreased polyunsaturated phospholipid species and increased cholesterol concentrations, collectively suggest impaired membrane fluidity and diminished functional plasticity of IGF2BP2-deficient macrophages.

These migratory defects were not attributable to altered acute inflammatory activation: upon LPS stimulation, both WT and KO BMMs mounted comparable pro-inflammatory responses, and no phenotypic changes were detected.

These findings are consistent with previous research suggesting that IGF2BP2 plays a pivotal role in immune cell recruitment to the TME, potentially through cytokines like CCL2 (66). For instance, in oral squamous cell carcinoma, high IGF2BP2 expression was linked to reduced immune cell infiltration, suppressed immune responses, and fewer $CD8^+$ T cells (78).

Another intriguing aspect of our findings relates to macrophage polarization, as metabolic reprogramming in KO TAM-like macrophages suggests a shift toward a more pro-inflammatory phenotype. While the exact relationship between macrophage phenotype and migration remains unclear, evidence suggests that morphology and motility are closely linked. For example, pro-inflammatory M1 macrophages typically exhibit more persistent and directed movement than anti-inflammatory M2 macrophages (79,80). This raises the possibility that IGF2BP2 may modulate migration not only through direct signaling pathways but also by influencing macrophage polarization and subsequent morphological changes.

Summary

In summary, our study identifies IGF2BP2 as a key regulator of macrophage metabolism, polarization, and migration, with significant implications for TAM function and tumor progression. IGF2BP2 deletion induces a metabolic shift toward glycolysis, impairs TAM-like polarization, and disrupts macrophage migration, collectively contributing to reduced tumor growth.

These findings highlight IGF2BP2 as a potential therapeutic target for modulating macrophage function in cancer.

7 Authors' Disclosures

A.K. Kiemer reports on grants from DFG during the conduct of the study. The other authors reported no disclosures.

8 Authors' Contributions

H.S. Schymik: Conceptualization, data curation, formal analysis, validation, investigation, visualization, methodology, writing–original draft, writing–review and editing. **S. Wrublewsky:** Data curation, formal analysis, investigation, methodology, writing–review and editing. **M. Höring:** Data curation, formal analysis, investigation, methodology. **G. Liebisch:** Data curation, formal analysis, investigation, methodology. **C. Bickelmann:** Data curation, formal analysis, investigation, methodology. **C. Dahlem:** Supervision, investigation, methodology. **M. W. Laschke:** Investigation, methodology, writing–review and editing **G. Gasparoni:** Data curation, formal analysis,

investigation, methodology. **J. Walter:** Investigation, methodology. **E. Ampofo:** Investigation, methodology, supervision. **J. Hoppstädter:** Conceptualization, resources, software, formal analysis, supervision, validation, investigation, visualization, methodology, writing–original draft, writing–review and editing. **A.K. Kiemer:** Conceptualization, resources, supervision, funding acquisition, validation, investigation, visualization, methodology, writing–original draft, project administration, writing–review and editing.

9 Acknowledgments

The study was funded, in part, by the DFG (Deutsche Forschungsgemeinschaft, #KI 702; 411093008).

10 References

1. Ni R, Jiang L, Zhang C, Liu M, Luo Y, Hu Z, et al. Biologic Mechanisms of Macrophage Phenotypes Responding to Infection and the Novel Therapies to Moderate Inflammation. Int J Mol Sci. Switzerland; 2023;24.

2. Cerdeira CD, Brigagão MRPL. Targeting Macrophage Polarization in Infectious Diseases: M1/M2 Functional Profiles, Immune Signaling and Microbial Virulence Factors. Immunol Invest. England; 2024;53:1030–91.

3. Zhao X, Ren T, Li S, Wang X, Hou R, Guan Z, et al. A new perspective on the therapeutic potential of tumor metastasis: targeting the metabolic interactions between TAMs and tumor cells. Int J Biol Sci. Australia; 2024;20:5109–26.

4. Li M-Y, Ye W, Luo K-W. Immunotherapies Targeting Tumor-Associated Macrophages (TAMs) in Cancer. Pharmaceutics. Switzerland; 2024;16.

5. Duan M, Liu H, Xu S, Yang Z, Zhang F, Wang G, et al. IGF2BPs as novel m(6)A readers: Diverse roles in regulating cancer cell biological functions, hypoxia adaptation, metabolism, and immunosuppressive tumor microenvironment. Genes Dis. Netherlands; 2024;11:890–920.

6. Kendzia S, Franke S, Kröhler T, Golob-Schwarzl N, Schweiger C, Toeglhofer AM, et al. A combined computational and functional approach identifies IGF2BP2 as a driver of chemoresistance in a wide array of pre-clinical models of colorectal cancer. Mol Cancer [Internet]. BioMed Central; 2023;22:1–14. Available from: https://doi.org/10.1186/s12943-023-01787-x

7. Chanda S, Lepikhov K, Dahlem C, Schymik HS, Hoppstädter J, Geber AK, et al. Gene Editing and Small Molecule Inhibitors of the RNA Binding Protein IGF2BP2/IMP2 Show its Potential as an Anti-Cancer Drug Target. Front Biosci - Landmark. 2024;29:1–16.

8. Fu D, Shi X, Yi X, Wu D, He H, Zhou W, et al. m6A reader IGF2BP2 promotes M2 macrophage polarization and malignant biological behavior of bladder cancer by stabilizing NRP1 mRNA expression. BMC Urol. 2024;24:1–12.

9. Wang J, Chen L, Qiang P. The role of IGF2BP2, an m6A reader gene, in human metabolic diseases and cancers. Cancer Cell Int [Internet]. BioMed Central; 2021;21:1–11. Available from: https://doi.org/10.1186/s12935-021-01799-x

10. Zhang S. Adenocarcinoma. In: Zhang S, editor. Diagnostic Imaging Lung Cancers [Internet]. Singapore: Springer Nature Singapore; 2023. page 3–49. Available from: https://doi.org/10.1007/978-981-99-6815-2_1

11. Guo L, Zhu C, Cai L, Zhang X, Fang Y, Chen H, et al. Global burden of lung cancer in 2022 and projected burden in 2050. Chin Med J (Engl). China; 2024;137:2577–82.

12. Zhang S, Dou T, Li H, Yu H, Zhang W, Sun L, et al. Knockdown of IGF2BP2 overcomes cisplatin-resistance in lung cancer through downregulating Spon2 gene. 2024;1–15.

13. Li D, Hu S, Ye J, Zhai C, Liu J, Wang Z, et al. The Emerging Role of IGF2BP2 in Cancer Therapy Resistance: From Molecular Mechanism to Future Potential. Int J Mol Sci. 2024;25:1–25.

14. Chai R, Yin Y, Cai X, Fu X, Zhang Q. Patterns of Failure in Patients With Advanced Non-Small Cell Lung Cancer Treated With Immune Checkpoint Inhibitors. Front Oncol. 2021;11:1–7.

15. Cassetta L, Kitamura T. Targeting tumor-associated macrophages as a potential strategy to enhance the response to immune checkpoint inhibitors. Front Cell Dev Biol. 2018;6:1–6.

16. Liu W, Zeng H. IGF2BP2 attenuates intestinal epithelial cell ferroptosis in colitis by stabilizing m6A-modified GPX4 mRNA. Cytokine [Internet]. Elsevier Ltd; 2024;173:156388. Available from: https://doi.org/10.1016/j.cyto.2023.156388

17. Nan Y, Chen M, Wu W, Huang R, Sun W, Lu Q, et al. IGF2BP2 regulates the inflammation of fibroblast-like synoviocytes via GSTM5 in rheumatoid arthritis. Cell Death Discov. 2024;10:1–11.

18. Ma XX, Zhou XY, Feng MG, Ji YT, Song FF, Tang QC, et al. Dual Role of IGF2BP2 in Osteoimmunomodulation during Periodontitis. J Dent Res. United States; 2024;103:208–17.

19. Simon Y, Kessler SM, Gemperlein K, Bohle RM, Müller R, Haybaeck J, et al. Elevated free cholesterol in a p62 overexpression model of non-alcoholic steatohepatitis. World J Gastroenterol. 2014;20:17839–50.

20. Schymik HS, Dahlem C, Barghash A, Kiemer AK. Comment on: The m6A Reader IGF2BP2 Regulates Macrophage Phenotypic Activation and Inflammatory Diseases by Stabilizing TSC1 and PPARγ. Adv Sci. 2022;9:2–5.

21. Hoppstädter J, Hachenthal N, Valbuena-Perez JV, Lampe S, Astanina K, Kunze MM, et al. Induction of Glucocorticoid-induced Leucine Zipper (GILZ) Contributes to anti-inflammatory effects of the natural product curcumin in macrophages. J Biol Chem. 2016;291:22949–60.

22. Hoppstädter J, Dembek A, Höring M, Schymik HS, Dahlem C, Sultan A, et al. Dysregulation of cholesterol homeostasis in human lung cancer tissue and tumour-associated macrophages. EBioMedicine. 2021;72.

23. Legroux TM, Schymik HS, Gasparoni G, Mohammadi S, Walter J, Libert C, et al. Immunomodulation by glucocorticoid-induced leucine zipper in macrophages: enhanced

phagocytosis, protection from pyroptosis, and altered mitochondrial function. Front Immunol. 2024;15:1–16.

24. Quiros PM, Goyal A, Jha P, Auwerx J. Analysis of mtDNA/nDNA Ratio in Mice. Curr Protoc Mouse Biol. 2017;7:47–54.

25. Kessler SM, Pokorny J, Zimmer V, Laggai S, Lammert F, Bohle RM, et al. IGF2 mRNA binding protein p62/IMP2-2 in hepatocellular carcinoma: Antiapoptotic action is independent of IGF2/PI3K signaling. Am J Physiol - Gastrointest Liver Physiol. 2013;304:328–36.

26. Lu M, Nakamura RM, Dent EDB, Zhang JY, Nielsen FC, Christiansen J, et al. Aberrant expression of fetal RNA-binding protein p62 in liver cancer and liver cirrhosis. Am J Pathol [Internet]. American Society for Investigative Pathology; 2001;159:945–53. Available from: http://dx.doi.org/10.1016/S0002-9440(10)61770-1

27. Hoppstädter J, Diesel B, Linnenberger R, Hachenthal N, Flamini S, Minet M, et al. Amplified host defense by toll-like receptor-mediated downregulation of the glucocorticoid-induced leucine zipper (GILZ) in macrophages. Front Immunol. 2019;10:1–15.

28. Dahlem C, Siow WX, Lopatniuk M, Tse WKF, Kessler SM, Kirsch SH, et al. Thioholgamide A, a new anti-proliferative anti-tumor agent, modulates macrophage polarization and metabolism. Cancers (Basel). 2020;12:E1288.

29. Hoppstädter J, Dembek A, Linnenberger R, Dahlem C, Barghash A, Fecher-Trost C, et al. Toll-Like Receptor 2 Release by Macrophages: An Anti-inflammatory Program Induced by Glucocorticoids and Lipopolysaccharide. Front Immunol. 2019;10:1634.

30. Linnenberger R, Hoppstädter J, Wrublewsky S, Ampofo E, Kiemer AK. Statins and bempedoic acid: Different actions of cholesterol inhibitors on macrophage activation. Int J Mol Sci. 2021;22.

31. Bligh, E.G. and Dyer WJ. Canadian Journal of Biochemistry and Physiology. Can J Biochem Physiol. 1959;37.

32. Liebisch G, Lieser B, Rathenberg J, Drobnik W, Schmitz G. High-throughput quantification of phosphatidylcholine and sphingomyelin by electrospray ionization tandem mass spectrometry coupled with isotope correction algorithm. Biochim Biophys Acta - Mol Cell Biol Lipids. 2004;1686:108–17.

33. Liebisch G, Drobnik W, Lieser B, Schmitz G. High-Throughput Quantification of Lysophosphatidylcholine by Electrospray Ionization Tandem Mass Spectrometry. Methods Mol Biol. 2002;580:29–37.

34. Matyash V, Liebisch G, Kurzchalia T V., Shevchenko A, Schwudke D. Lipid extraction by methyl-terf-butyl ether for high-throughput lipidomics. J Lipid Res [Internet]. Â© 2008 ASBMB. Currently published by Elsevier Inc; originally published by American Society for Biochemistry and Molecular Biology.; 2008;49:1137–46. Available from: http://dx.doi.org/10.1194/jlr.D700041-JLR200

35. Liebisch G, Drobnik W, Reil M, Trümbach B, Arnecke R, Olgemöller B, et al. Quantitative

measurement of different ceramide species from crude cellular extracts by electrospray ionization tandem mass spectrometry (ESI- MS/MS). J Lipid Res. 1999;40:1539–46.

36. Zemski Berry KA, Murphy RC. Electrospray ionization tandem mass spectrometry of glycerophosphoethanolamine plasmalogen phospholipids. J Am Soc Mass Spectrom. 2004;15:1499–508.

37. Scherer M, Schmitz G, Liebisch G. Simultaneous quantification of cardiolipin, bis(monoacylglycero)phosphate and their precursors by hydrophilic interaction LC-MS/MS including correction of isotopic overlap. Anal Chem. 2010;82:8794–9.

38. Höring M, Ejsing CS, Krautbauer S, Ertl VM, Burkhardt R, Liebisch G. Accurate quantification of lipid species affected by isobaric overlap in Fourier-transform mass spectrometry. J Lipid Res [Internet]. The Authors; 2021;62:100050. Available from: https://doi.org/10.1016/j.jlr.2021.100050

39. Höring M, Ejsing CS, Hermansson M, Liebisch G. Quantification of Cholesterol and Cholesteryl Ester by Direct Flow Injection High-Resolution Fourier Transform Mass Spectrometry Utilizing Species-Specific Response Factors. Anal Chem. 2019;91:3459–66.

40. Ampofo E, Rudzitis-Auth J, Dahmke IN, Rössler OG, Thiel G, Montenarh M, et al. Inhibition of protein kinase CK2 suppresses tumor necrosis factor (TNF)-α-induced leukocyte-endothelial cell interaction. Biochim Biophys Acta - Mol Basis Dis [Internet]. Elsevier B.V.; 2015;1852:2123–36. Available from: http://dx.doi.org/10.1016/j.bbadis.2015.07.013

41. Hoffmann JN, Vollmar B, Laschke MW, Inthorn D, Fertmann J, Schildberg FW, et al. Microhemodynamic and cellular mechanisms of activated protein C action during endotoxemia. Crit Care Med. 2004;32:1011–7.

42. Nalbach L, Müller D, Wrublewsky S, Metzger W, Menger MD, Laschke MW, et al. Microvascular fragment spheroids: Three-dimensional vascularization units for tissue engineering and regeneration. J Tissue Eng. 2021;12.

43. Bailey TL, Grant CE. SEA: simple enrichment analysis of motifs. BioRxiv. Cold Spring Harbor Laboratory; 2021;2008–21.

44. Stovner EB, Sætrom P. PyRanges: efficient comparison of genomic intervals in Python. Bioinformatics [Internet]. 2019;36:918–9. Available from: https://doi.org/10.1093/bioinformatics/btz615

45. Çelik MH, Mortazavi A. Analysis of alternative polyadenylation from long-read or short-read RNA-seq with LAPA. bioRxiv [Internet]. 2022;2022.11.08.515683. Available from: http://biorxiv.org/content/early/2022/11/08/2022.11.08.515683.abstract

46. Zaccara S, Ries RJ, Jaffrey SR. Reading, writing and erasing mRNA methylation. Nat Rev Mol cell Biol. Nature Publishing Group UK London; 2019;20:608–24.

47. Bailey TL, Johnson J, Grant CE, Noble WS. The MEME suite. Nucleic Acids Res. Oxford University Press; 2015;43:W39–49.

48. Korn SM, Ulshöfer CJ, Schneider T, Schlundt A. Structures and target RNA preferences of the RNA-binding protein family of IGF2BPs: An overview. Structure. United States; 2021;29:787–803.

49. Kierans SJ, Taylor CT. Regulation of glycolysis by the hypoxia-inducible factor (HIF): implications for cellular physiology. J Physiol. 2021;599:23–37.

50. Ren Y, Wang M, Yuan H, Wang Z, Yu L. A novel insight into cancer therapy: Lipid metabolism in tumor-associated macrophages. Int Immunopharmacol [Internet]. Elsevier B.V.; 2024;135:112319. Available from: https://doi.org/10.1016/j.intimp.2024.112319

51. Wu H, Han Y, Rodriguez Sillke Y, Deng H, Siddiqui S, Treese C, et al. Lipid droplet-dependent fatty acid metabolism controls the immune suppressive phenotype of tumor-associated macrophages. EMBO Mol Med. 2019;11:1–17.

52. Chanmee T, Ontong P, Konno K, Itano N. Tumor-associated macrophages as major players in the tumor microenvironment. Cancers (Basel). 2014;6:1670–90.

53. Joyce JA, Pollard JW. Microenvironmental regulation of metastasis. Nat Rev Cancer. 2009;9:239–52.

54. Grouleff J, Irudayam SJ, Skeby KK, Schiøtt B. The influence of cholesterol on membrane protein structure, function, and dynamics studied by molecular dynamics simulations. Biochim Biophys Acta - Biomembr [Internet]. Elsevier B.V.; 2015;1848:1783–95. Available from: http://dx.doi.org/10.1016/j.bbamem.2015.03.029

55. Harayama T, Shimizu T. Roles of polyunsaturated fatty acids, from mediators to membranes. J Lipid Res [Internet]. Copyright © 2020 Harayama and Shimizu.; 2020;61:1150–60. Available from: http://dx.doi.org/10.1194/jlr.R120000800

56. Subczynski W, Pasenkiewicz-Gierula M, Widomska J, Mainali L, Raguz M. High Cholesterol/Low Cholesterol: Effects in Biological Membranes: A Review. Cell Biochem Biophys [Internet]. 2017;75:369–85. Available from: https://consensus.app/papers/high-cholesterollow-cholesterol-effects-in-biological-subczynski-pasenkiewicz-gierula/c71b470fd2fd51e0ae6720eb57f33f5d/

57. Clausen BE, Burkhardt C, Reith W, Renkawitz R, Förster I. Conditional gene targeting in macrophages and granulocytes using LysMcre mice. Transgenic Res. 1999;8:265–77.

58. Viola A, Munari F, Sánchez-Rodríguez R, Scolaro T, Castegna A. The metabolic signature of macrophage responses. Front Immunol. 2019;10:1–16.

59. Rottenberg H. The Reduction in the Mitochondrial Membrane Potential in Aging: The Role of the Mitochondrial Permeability Transition Pore. Int J Mol Sci. 2023;24.

60. Zhou Y, Yan J, Huang H, Liu L, Ren L, Hu J, et al. The m6A reader IGF2BP2 regulates glycolytic metabolism and mediates histone lactylation to enhance hepatic stellate cell activation and liver fibrosis. Cell Death Dis. Springer US; 2024;15.

61. Wu S, Chi C, Weng S, Zhou W, Liu Z. IGF2BP2 promotes lncRNA DANCR stability

mediated glycolysis and affects the progression of FLT3-ITD + acute myeloid leukemia. Apoptosis. 2023;28:1035–47.

62. Cunningham CE, Vizeacoumar FS, Zhang Y, Kyrylenko L, Both S, Maranda V, et al. Identification of targetable vulnerabilities of PLK1-overexpressing cancers by synthetic dosage lethality. Cell Genomics. 2025;

63. Summer M, Riaz S, Ali S, Noor Q, Ashraf R, Khan RRM. Understanding the Dual Role of Macrophages in Tumor Growth and Therapy: A Mechanistic Review. Chem Biodivers. 2025;

64. Duan Z, Luo Y. Targeting macrophages in cancer immunotherapy. Signal Transduct Target Ther [Internet]. Springer US; 2021;6:1–21. Available from: http://dx.doi.org/10.1038/s41392-021-00506-6

65. Mashayekhi V, Schomisch A, Rasheed S, Puerta EA, Risch T, Yildiz D, et al. The RNA binding protein IGF2BP2 / IMP2 alters the cargo of cancer cell - derived extracellular vesicles supporting tumor - associated macrophages. Cell Commun Signal [Internet]. BioMed Central; 2024;1–25. Available from: https://doi.org/10.1186/s12964-024-01701-y

66. Li J, Jiang Y, Ma M, Wang L, Jing M, Yang Z, et al. IGF2BP2 Shapes the Tumor Microenvironment by Regulating Monocyte and Macrophage Recruitment in Bladder Cancer. Cancer Med. 2024;13:1–17.

67. Wang X, Ji Y, Feng P, Liu R, Li G, Zheng J, et al. The m6A Reader IGF2BP2 Regulates Macrophage Phenotypic Activation and Inflammatory Diseases by Stabilizing TSC1 and PPARγ. Adv Sci. 2021;2100209:1–14.

68. Wang X, Ji Y, Feng P, Liu R, Li G, Zheng J, et al. The m6A Reader IGF2BP2 Regulates Macrophage Phenotypic Activation and Inflammatory Diseases by Stabilizing TSC1 and PPARγ. Adv Sci. 2021;8:1–14.

69. Du X, Guo Y, Zhao X, Zhang L, Fan R, Li Y. METTL3-mediated TIM1 promotes macrophage M1 polarization and inflammation through IGF2BP2-dependent manner. J Biochem Mol Toxicol. 2024;38:1–9.

70. Schroder K, Irvine KM, Taylor MS, Bokil NJ, Le Cao KA, Masterman KA, et al. Conservation and divergence in Toll-like receptor 4-regulated gene expression in primary human versus mouse macrophages. Proc Natl Acad Sci U S A. 2012;109.

71. Vijayan V, Pradhan P, Braud L, Fuchs HR, Gueler F, Motterlini R, et al. Human and murine macrophages exhibit differential metabolic responses to lipopolysaccharide - A divergent role for glycolysis. Redox Biol [Internet]. Elsevier B.V.; 2019;22:101147. Available from: https://doi.org/10.1016/j.redox.2019.101147

72. Friedman-DeLuca M, Karagiannis GS, Condeelis JS, Oktay MH, Entenberg D. Macrophages in tumor cell migration and metastasis. Front Immunol. 2024;15:1–16.

73. Liu D, Xia AD, Wu LP, Li S, Zhang K, Chen D. IGF2BP2 promotes gastric cancer progression by regulating the IGF1R-RhoA-ROCK signaling pathway. Cell Signal [Internet]. Elsevier Inc.; 2022;94:110313. Available from: https://doi.org/10.1016/j.cellsig.2022.110313

74. Holthuis JCM, Menon AK. Lipid landscapes and pipelines in membrane homeostasis. Nature. England; 2014;510:48–57.

75. Ernst R, Ejsing CS, Antonny B. Homeoviscous Adaptation and the Regulation of Membrane Lipids. J Mol Biol. Netherlands; 2016;428:4776–91.

76. Harayama T, Antonny B. Beyond Fluidity: The Role of Lipid Unsaturation in Membrane Function. Cold Spring Harb Perspect Biol. United States; 2023;15.

77. Ecker J, Liebisch G, Englmaier M, Grandl M, Robenek H, Schmitz G. Induction of fatty acid synthesis is a key requirement for phagocytic differentiation of human monocytes. Proc Natl Acad Sci U S A. United States; 2010;107:7817–22.

78. Zhou L, Li H, Cai H, Liu W, Pan E, Yu D, et al. Upregulation of IGF2BP2 Promotes Oral Squamous Cell Carcinoma Progression That Is Related to Cell Proliferation, Metastasis and Tumor-Infiltrating Immune Cells. Front Oncol. 2022;12:1–16.

79. Kesapragada M, Sun Y-H, Recendez C, Fregoso D, Yang H, Isseroff R, et al. Establishing cell motility patterns as predictors of macrophage subtypes and their relation to cell morphology. bioRxiv [Internet]. 2022;2022.11.29.518400. Available from: https://www.biorxiv.org/content/10.1101/2022.11.29.518400v1%0Ahttps://www.biorxiv.org/content/10.1101/2022.11.29.518400v1.abstract

80. Kesapragada M, Sun Y-H, Zhu K, Recendez C, Fregoso D, Yang H-Y, et al. A data-driven approach to establishing cell motility patterns as predictors of macrophage subtypes and their relation to cell morphology. PLoS One. United States; 2024;19:e0315023.

Supplement

IGF2BP2 Deficiency in Macrophages Induces Metabolic Reprogramming and Impairs Tumor Progression

Hanna S. Schymik[1], Selina Wrublewsky[2], Marcus Höring[3], Gerhard Liebisch[3], Gilles Gasparoni[4], Caroline Bickelmann[2], Hanah Robertson[1], Charlotte Dahlem[1], Jörn Walter[4], Volkhard Helms[1], Matthias W. Laschke[2,5,6], Emmanuel Ampofo[2], Jessica Hoppstädter[1], Alexandra K. Kiemer[1,5,6*]

[1]Department of Pharmacy, Pharmaceutical Biology, Saarland University, Saarbrücken, Germany.

[2] Institute for Clinical & Experimental Surgery, Saarland University, Homburg, Germany.

[3] Institute of Clinical Chemistry and Laboratory Medicine, University Hospital Regensburg, Regensburg, Germany.

[4] Department of Genetics/Epigenetics, Saarland University, Saarbrücken, Germany.

[5] Center for Gender-Specific Biology and Medicine, Saarland University, Homburg, Germany.

[6] Pharma Science Hub, Saarland University, Saarbrücken, Germany.

***Correspondence:**
Alexandra Kathrin Kiemer, Pharmaceutical Biology, Saarland University, D-66123 Saarbrücken, Germany. E-mail: pharm.bio.kiemer@uni-saarland.de.

Supplemental Tables

Table 1: Primer Sequences

Gene	Accession number	Primer forward sequence	Primer reverse sequence
Acss2	NM_019811.3	TATGTGACCGGAGATGGCTGC	TCGTGTTCCACAAGTGCCGA
Aldh2	NM_001308450	GGACCTACCTAGCGGCCTTG	TGGTACTTGTCAGCCCAGCC
Aldoc	NM_001303423	CATCTGCCAGCAGAATGGGAT	GCTTGAGCAGAGTCCCTTCG
Bpgm1	NM_007563.5	GTCTGCAGCACGGCGTTAC	CAAGAACAGCAGTATATCTGCAAGG
Cxcl1	NM_008176.3	AACCGAAGTCATAGCCACACT	CCGTTACTTGGGGACACCTT
Fgf2	NM_008006.2	GCTCTACTGCAAGAACGGCG	TAACACACTTAGAAGCCAGCAGC
Gapdh	NM_001289726.2	TCGGTGTGAACGGATTTGGC	TGAAGGGGTCGTTGATGGCA
Gpi1	NM_008155.4	CCTGTCTACGAACACGGCCA	GCTGACCACAGCGAATAGCG
Hif1a	NM_001313919	TCAAGCAGCAGGAATTGGAACAT	TCATCCATTGACTGCCCCAGC
Hk2 (genomic DNA)	NC_000072.7	GCCAGCCTCTCCTG ATTTTAGTGT	GGGAACACAAAAGACCTCTTCTGG
Il1ß	NM_008361.3	CCAAAAGATGAAGGGCTGCTT	GGAAGGTCCACGGGAAAGAC
Il6	NM_031168.2	AAGAAATGATGGATGCTACCAAACTG	GTACTCCAGAAGACCAGAGGAAATT
Igf2bp2	NM_183029.2	TTGGATGGGCTGTTGGCTGA	GTGACGTTGACAACGGCAGTT
Mito 16S	AP014886.1	CCGCAAGGGAAAGATGAAAGAC	TCGTTTGGTTTCGGGGTTTC
Mito Nd1	AP014886.1	CTAGCAGAAACAAACCGGGC	CCGGCTGCGTATTCTACGTT
Mmp2	NM_008610.2	CATCGCTGCACCATCGC	GCATGGTCTCGATGGTGTTC
Mmp9	NM_013599.3	GCCGACTTTTGTGGTCTTCC	TACAAGTATGCCTCTGCCAGC
Mrc1	NM_008625.2	TTCAGCTATTGGACGCGAGG	GAATCTGACACCCAGCGGAA
Nos2	NM_010927.3	CTTCCTGGACATTACGACCC	TACTCTGAGGGCTGACACAA
Pgk1	NM_008828.3	CAAGCTGGACGTGAAGGGGAA	AACAGCAGCCTTGATCCTTTGGT
Ppia	NM_008907.1	GCGTCTCCTTCGAGCTGTTT	CACCCTGGCACATGAATCCT
RNA18S	NR_003278.3	AGGTCTGTGATGCCCTTAGA	GAATGGGGTTCAACGGGTTA
Tgfb	NM_011577.1	ACCCTGCCCCTATATTTGGA	CGGGTTGTGTTGGTTGTAGAG
Tnf	NM_013693.2	CCATTCCTGAGTTCTGCAAAGG	AGGTAGGAAGGCCTGAGATCTTATC
Vegfa	NM_001025250.3	CCACCATGCCAAGTGGTCCC	ACCAGGGTCTCAATCGGACG

Supplemental Figures

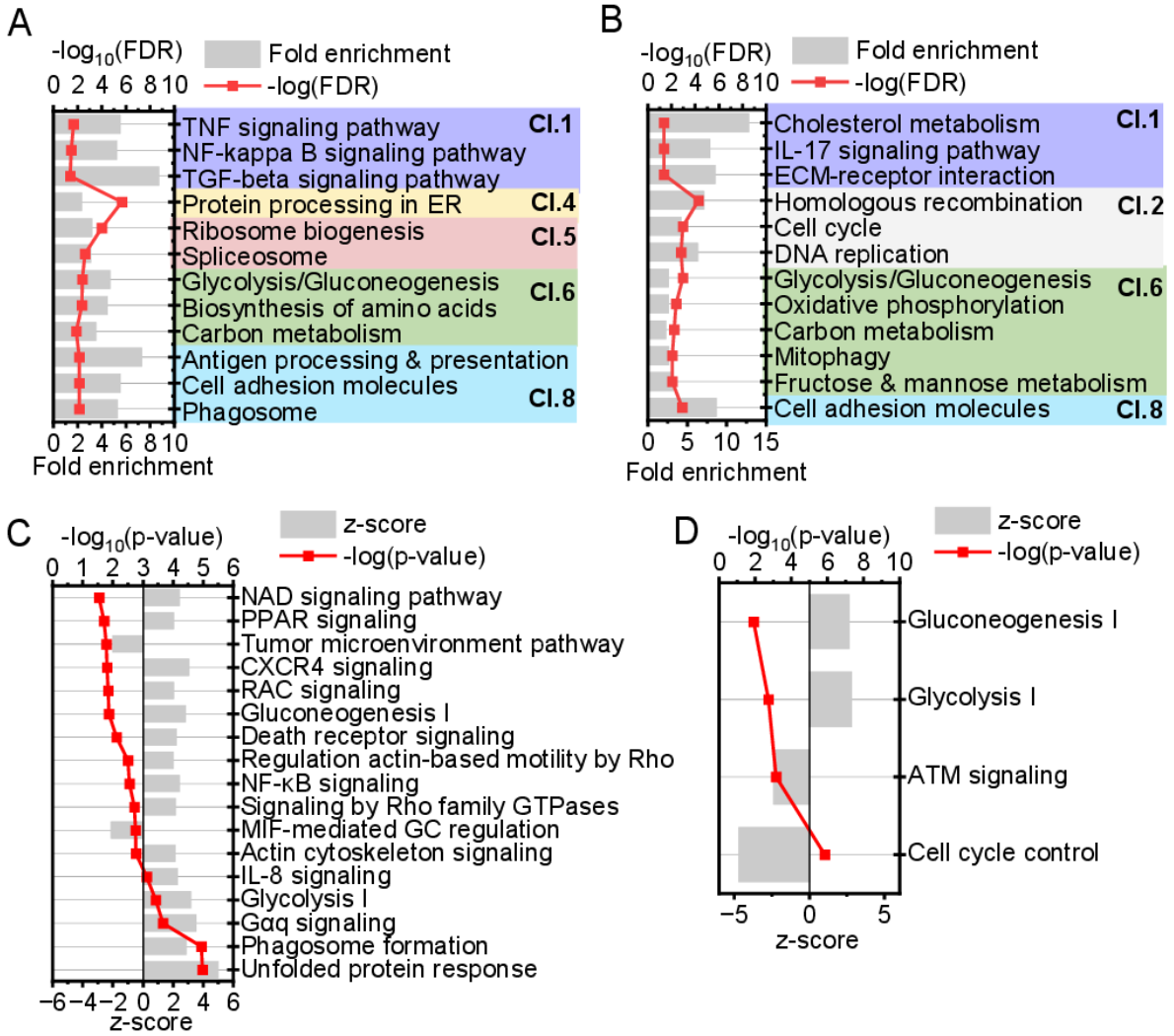

Supplemental Figure 1. Pathway Analysis in WT and IGF2BP2 KO Macrophages.
(A, B) Selected KEGG pathways enriched in clusters (Cl) identified as shown in Figure 1C and 1D. Pathway enrichment significance is shown by false discovery rate (FDR) values (fold change > 2, FDR < 0.05). **(C, D)** Ingenuity Pathway Analysis (IPA) of differentially expressed genes (DEGs; $p < 0.05$) in untreated **(A, C)** and IL-4-treated (8 h, 20 ng/ml) (B, D) BMMs (n = 3 mice per group) from WT and IGF2BP2 MΦ-KO mice n = 3 mice per group). Pathways are ranked by activation z-scores (z-score > 2, *p*-value < 0.05), indicating predicted pathway activation states.

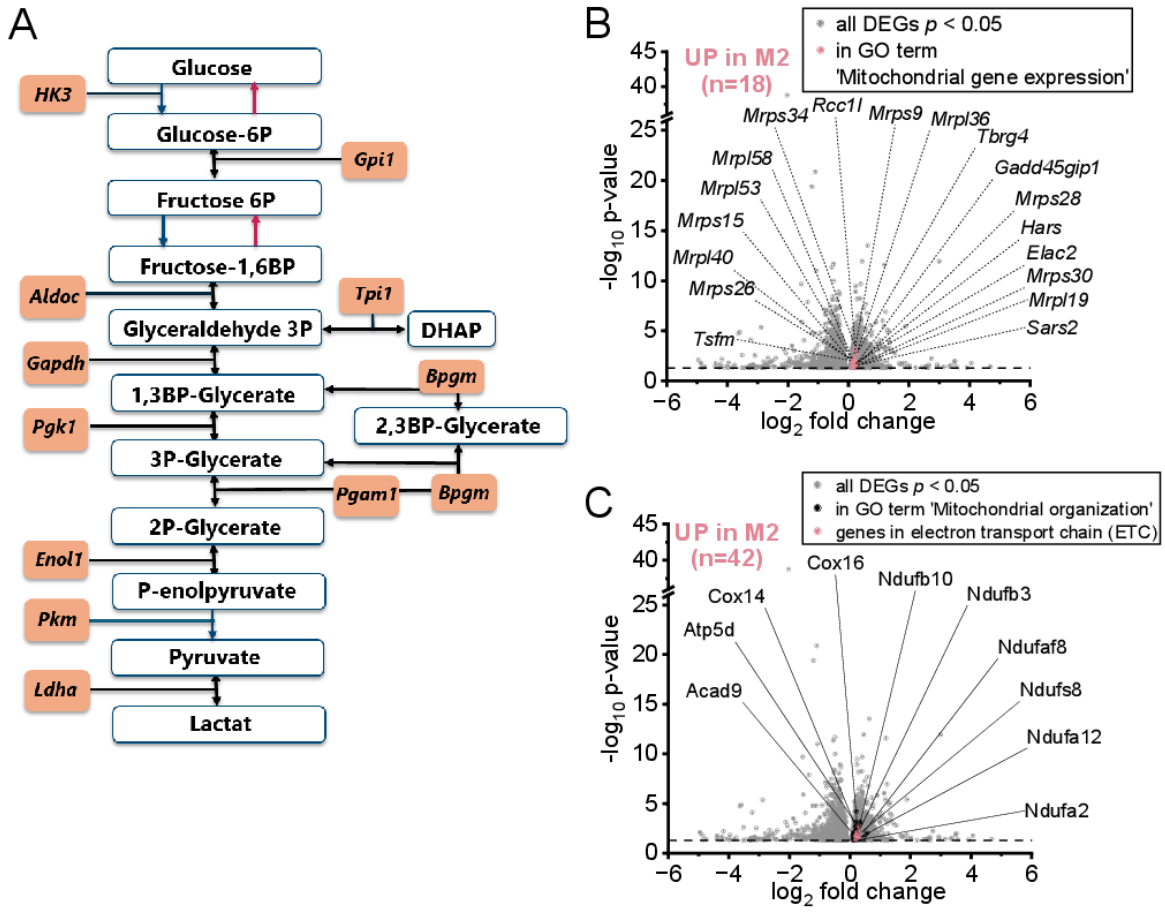

Supplemental Figure 2. Alterations in Glycolytic and Mitochondrial Pathways in IGF2BP2 KO Macrophages. (A) Schematic representation of the glycolytic pathway, highlighting genes (purple) that are significantly upregulated ($p < 0.05$) in IGF2BP2 KO M2-polarized macrophages in KEGG pathway "Glycolysis" **(B, C)** Volcano plots of DEGs (shown in gray) of KO M2 vs. WT M2 macrophages, with significantly upregulated genes in **(B)** the GO term "Mitochondrial gene expression" (GO:0140053) highlighted in purple, and **(C)** the GO term "Mitochondrial gene expression" (GO:0140053) shown in black, with a subset of genes from the electron transport chain (ETC) highlighted in purple (n = 3 mice per group).

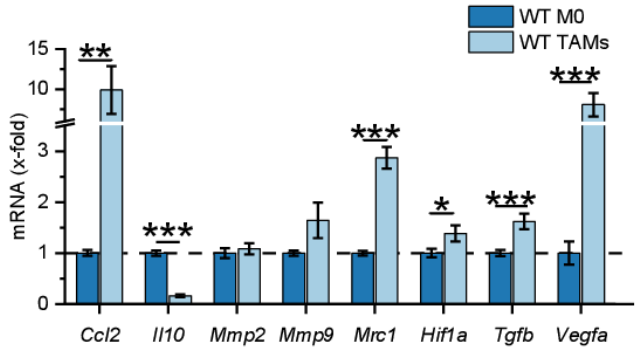

Supplemental Figure 3. Elevated TAM Marker Expression in LLC1 TAM-like Macrophages. BMMs were cultured in standard medium (M0) or TCM from LLC1 cells (TAM-like) for 8 hours. mRNA expression was measured by qPCR and normalized to *Ppia*. Expression of TAM-like macrophage markers is shown as a fold change of WT M0 (n = 6 mice per group, duplicates). Data are presented as mean ± SEM. Statistical significance was determined by Student's t-test (*$p < 0.05$; **$p < 0.01$; ***$p < 0.001$).

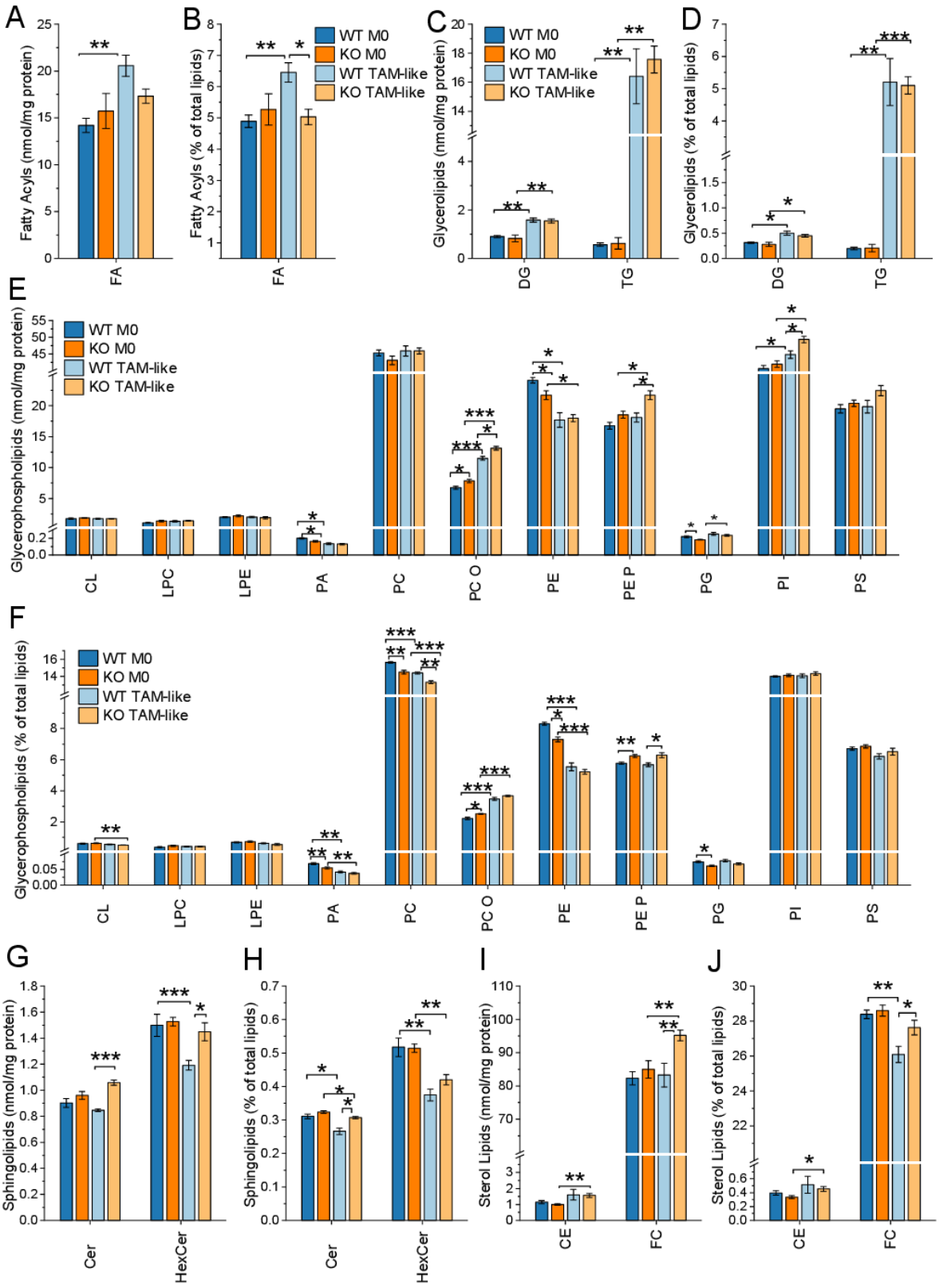
A
Fatty Acyls (nmol/mg protein)
FA
B
Fatty Acyls (% of total lipids)
FA
WT M0
KO M0
WT TAM-like
KO TAM-like
C
Glycerolipids (nmol/mg protein)
DG
TG
D
Glycerolipids (% of total lipids)
DG
TG
E
Glycerophospholipids (nmol/mg protein)
CL
LPC
LPE
PA
PC
PC O
PE
PE P
PG
PI
PS
F
Glycerophospholipids (% of total lipids)
CL
LPC
LPE
PA
PC
PC O
PE
PE P
PG
PI
PS
G
Sphingolipids (nmol/mg protein)
Cer
HexCer
H
Sphingolipids (% of total lipids)
Cer
HexCer
I
Sterol Lipids (nmol/mg protein)
CE
FC
J
Sterol Lipids (% of total lipids)
CE
FC

Supplemental Figure 4. Lipid Classes in WT and IGF2BP2 KO Macrophages (M0 and TAM-like macrophages). BMMs were cultured either in standard medium (M0) or in TCM from LLC1 cells for 24 hours to induce TAM-like polarization. Lipid concentrations in WT and IGF2BP2 KO M0 and TAM-like macrophages were analyzed by mass spectrometry. Data are displayed as **(A, C, E, G, I)** absolute concentrations (nmol/mg protein) and **(B, D, F, H, J)** relative abundance, expressed as a percentage of total detected lipids. Lipid categories: **(A-B)** Fatty acyls, **(C-D)** Glycerolipids, **(E-F)** Glycerophospholipids, **(G-H)** Sphingolipids, **(I-J)** Sterol lipids. Data are presented as mean ± SEM (n = 4 mice per group). Statistical significance was determined by ANOVA with Bonferroni's post hoc test (*$p < 0.05$; **$p < 0.01$; ***$p < 0.001$).

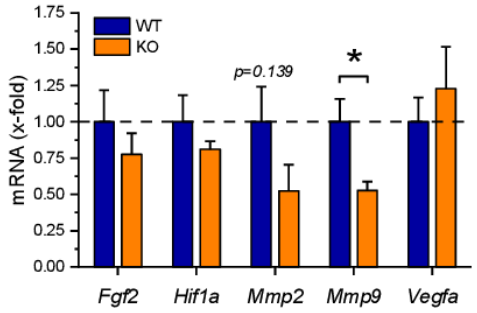

Supplemental Figure 5. Expression of Angiogenesis-related Genes in IGF2BP2 MΦ-KO Tumors. RNA was isolated from tumor tissue and mRNA expression levels of *Fgf2*, *Hif1a*, *Mmp2*, *Mmp9*, and *Vegfa* were normalized to *Ppia* and expressed as fold change relative to WT tumor tissue. Data are presented as mean ± SEM (n = 8 WT, n = 6 KO). Statistical analysis was performed using Student's t-test (*$p < 0.05$; **$p < 0.01$; ***$p < 0.001$).

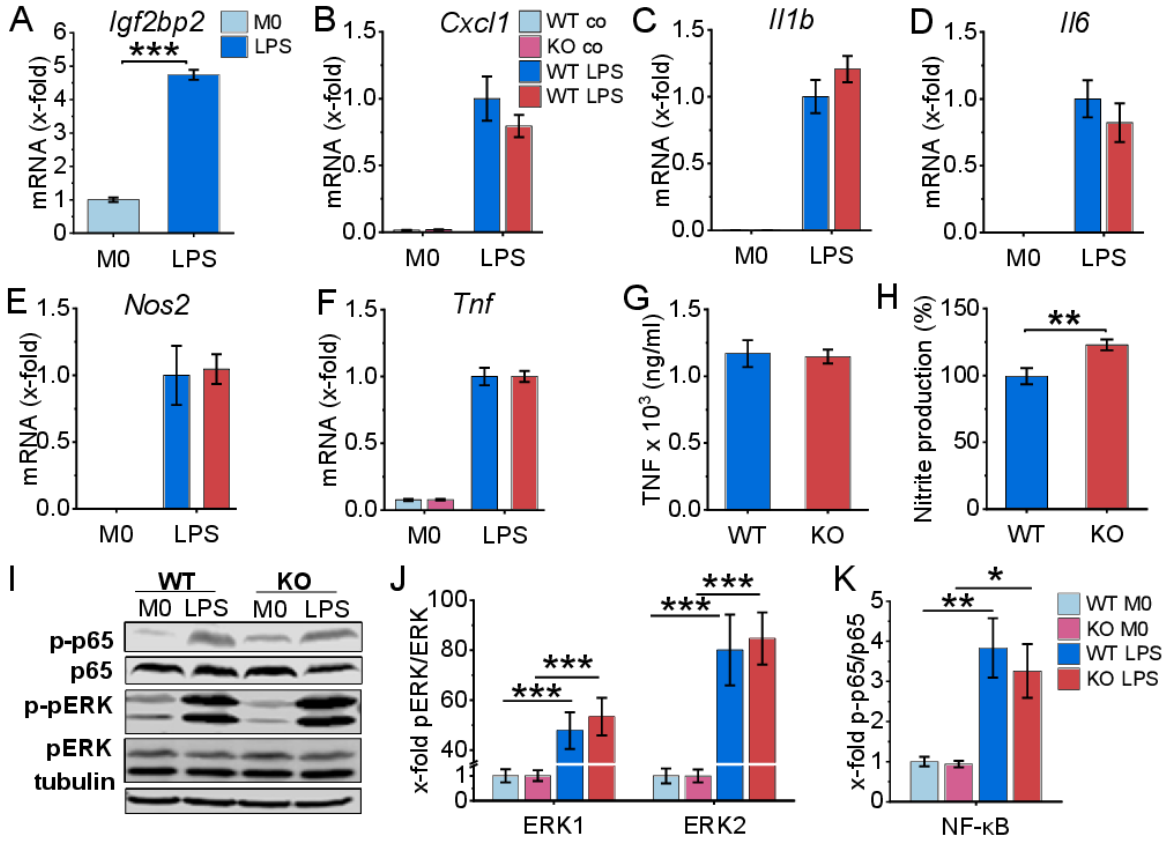

Supplemental Figure 6. Regulation and Role of IGF2BP2 in LPS-activated BMMs (A-G) BMMs were treated with 100 ng/ml LPS for 4 hours. **(A, B)** mRNA expression data were normalized to *Ppia* and expressed as x-fold of untreated WT control. A: *Igf2bp2* expression (n = 8 mice per group, duplicates). **(B)** Expression of *Cxcl1*, *Il1b*, *Il6*, *Nos2*, and *Tnf* (n = 5 mice per group, duplicates). **(G)** TNF secretion was measured by ELISA in LPS-treated BMMs (n = 8 mice per group, duplicates). **(H)** The relative nitrite production in LPS/IFN-γ (100 ng/ml;25 ng/ml; 24 h) treated BMMs was measured by Griess assay, with data normalized to WT (set to 100%) (n = 8 mice per group, triplicates). **(E)** ERK and NF-κB activation in WT and IGF2BP2 KO BMMs were assessed by Western blotting after 15 minutes of LPS (100 ng/ml) treatment. Phosphorylated ERK (pERK) and phosphorylated p65 (pp65) signal intensities were quantified and normalized to their respective total (unphosphorylated) protein levels. Tubulin served as a loading control (n = 5 mice per group, duplicates). Data are presented as means ± SEM. Statistical analysis was performed using ANOVA with Bonferroni's post hoc test (J,K) or Student's *t*-test (A, H) ($p < 0.05$; *$p < 0.01$; **$p < 0.001$).

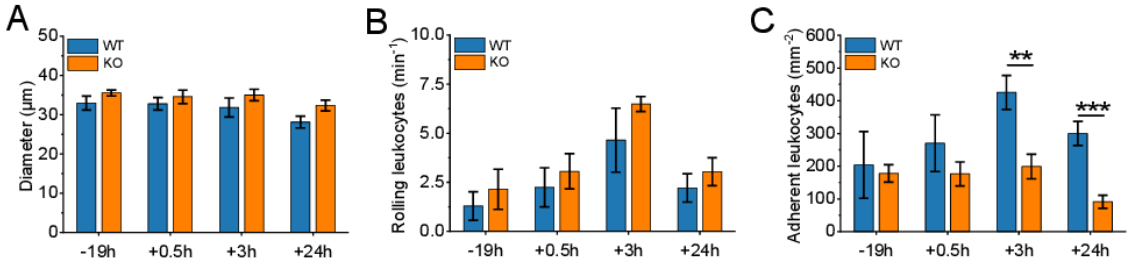

Supplemental Figure 7. IGF2BP2 Modulates Leukocyte Adherence in Arterioles. Intravital fluorescence microscopy of arterioles was used to assess microcirculatory changes. Quantification includes **(A)** arteriolar diameter (µM), **(B)** rolling leukocytes, and **(C)** adherent leukocytes in dorsal skinfold chambers of WT and IGF2BP2 MΦ-KO mice (n = 8 mice per group). Mice were exposed to LPS treatment for 0.5 hours, and WT and IGF2BP2 MΦ-KO animals were analyzed simultaneously. Measurements were obtained using intravital fluorescence microscopy and computer-assisted image analysis. Data are presented as mean ± SEM, with statistical significance determined using Student's t-test for individual time points (*$p < 0.05$; **$p < 0.01$; ***$p < 0.001$).

3.2 Author Contributions

I conceptualized the study, designed and performed all experiments unless otherwise specified, and conducted data analysis and interpretation. I was responsible for drafting the manuscript, preparing all figures, and coordinating collaboration and communication with co-authors throughout the review and revision process.

Selina Wrublewsky performed the dorsal skinfold chamber experiments, analyzed the resulting data, and assisted in establishing and executing the murine LLC1 tumor model. She also contributed to drafting and revising the manuscript. Marcus Höring and Gerhard Liebisch conducted the lipidomics analyses, including sample processing, mass spectrometry, and data analysis. They also contributed to writing and editing the lipidomics results section. Gilles Gasparoni and Jörn Walter contributed to the RNA sequencing data; Gilles Gasparoni performed the RNA-Seq data processing and analysis. Hanah Robertson and Volkhard Helms conducted the m^6A-related analyses. Caroline Bickelmann prepared the histological tumor sections and conducted the corresponding analyses. Charlotte Dahlem assisted with the supervision of selected experimental procedures. Matthias W. Laschke provided laboratory infrastructure and reviewed the manuscript. Emmanuel Ampofo supervised the LLC1 tumor model and the dorsal skinfold chamber experiments.

Jessica Hoppstädter co-supervised the project, contributed to manuscript writing, and was involved in reviewing experimental data and manuscript content, including RNA-Seq analyses.

Alexandra K. Kiemer initiated and supervised the project, provided conceptual and scientific guidance, acquired funding, and contributed substantially to the writing and review of the manuscript. The project was funded by the Deutsche Forschungsgemeinschaft (grant KI702).

Additional acknowledgments are included in the original publication.

4 Part III: Sex-Dependent Tumor Progression and Macrophage Function: The Role of IGF2BP2

4.1 Introduction

Sex-based differences in immune responses, driven by both genetic and hormonal factors, significantly shape disease prevalence, progression, and clinical outcomes, including in cancer. Women typically mount stronger immune responses to infections and vaccines, while men experience higher incidence and mortality rates across many cancer types (Rubin et al., 2020; Wilkinson et al., 2022). However, this increased immune activity in women also increases their susceptibility to autoimmune and inflammatory diseases. This heightened immune activity in females is partially attributed to immune-related genes on the X chromosome (e.g., *FOXP3*, *IL2RG*, *TLR7*, *TLR8*, and *CD40L*) and the immunomodulatory effects of sex hormones, particularly estrogen and progesterone (Desai and Brinton, 2019; Markle and Fish, 2014; Merrheim et al., 2020). Recent evidence suggests that the loss of the Y chromosome in tumor-infiltrating immune cells, particularly $CD8^+$ and $CD4^+$ T cells, impairs antitumor immune responses and is associated with worse cancer outcomes in men (Mcgranahan and Roychoudhuri)

Recent studies have revealed sex-specific differences in gene expression within immune cells, particularly macrophages, which play crucial roles in immune regulation and tumor progression. Female macrophages have been reported to express higher levels of Fc receptor-associated genes, which may contribute to increased phagocytic capacity and enhanced immune activation (Gomez et al., 2001; Hukara et al., 2024). Additionally, estrogen exerts protective effects in female macrophages, reducing susceptibility to stress-induced cell death, whereas in male macrophages, estrogen exposure may induce apoptotic pathways under similar conditions (Jog and Caricchio, 2013; Ortona et al., 2014). Female macrophages also exhibit an elevated expression of interferon-responsive genes, which enhances early immune defenses but may increase the risk of autoimmune disease (Gal-Oz et al., 2019). In general, females exhibit stronger baseline inflammatory responses, including rapid polarization toward the M1 macrophage phenotype, which is beneficial for pathogen clearance but may be detrimental due to increased inflammatory damage (Spencer and Sanchez Guillen, 2022). In contrast, male macrophages and monocytes exhibit increased migratory activity in response to obesity-associated chemokines, particularly under high-fat diet conditions, contributing to sex differences in metabolic inflammation (Chen et al., 2021; Varghese et al., 2022).

These sex-specific immune differences extend to TAMs, which exhibit distinct gene expression signatures in several cancer types, including bladder, colorectal, and non-small cell lung cancer

(NSCLC) (Chenard et al., 2021; Ray et al., 2020; Yang et al., 2021). In bladder cancer, female patients often exhibit increased immune cell infiltration, particularly increased $CD163^+$ M2-like macrophages, compared to male tumors (Chenard et al., 2021; Toren et al., 2024). In colorectal cancer, females mount a distinct immune response characterized by increased M1 macrophage activity and pro-inflammatory cytokine production, which may explain their lower disease incidence and delayed onset compared to males (Jang et al., 2024). In NSCLC, female-derived TAMs exhibit increased interferon signaling and enhanced antigen-presenting capacities, whereas male-derived TAMs favor immunosuppressive phenotypes, characterized by upregulation of genes, SPP1 and PPARs, involved in extracellular matrix remodeling and tumor progression (Yang et al., 2021).

Lung cancer remains one of the leading causes of cancer-related mortality globally, with five-year survival rates of around 21% for women and 15% for men despite therapeutic advances (Kaatsch et al., 2020). Sex differences in lung cancer are well known; for example, non-smoking women have a 2- to 2.5-fold higher risk of developing lung cancer than non-smoking men. Preclinical studies suggest that steroid hormone pathways, including those involving progesterone receptors, contribute to these disparities (Novello et al., 2018). Understanding the molecular mechanisms underlying sex-specific tumor behavior is essential for precision medicine and optimizing therapeutic strategies for both sexes.

Preliminary investigations using gender-specific analyses from The Cancer Genome Atlas (TCGA) database have indicated a correlation between elevated IGF2BP2 expression and reduced survival rates, particularly in women, across multiple cancer types, including lung adenocarcinoma (LUAD), liver hepatocellular carcinoma (LIHC), and colorectal adenocarcinoma (CoAD) (data unpublished, C. Dahlem, Figure 7).

TCGA data analysis of NSCLC subtypes revealed distinct prognostic implications of IGF2BP2 expression. In LUAD, high IGF2BP2 expression was significantly associated with poor prognosis, whereas in lung squamous cell carcinoma (LUSC), the trend was reversed, with elevated IGF2BP2 levels correlating with slightly improved survival (Figure 7A-C). Further stratification of the LUAD cohort by sex highlighted a stronger negative correlation between high IGF2BP2 expression and decreased survival in female patients. While survival rates remained comparable between men and women in the low-expression group, a pronounced disparity was observed in individuals with high expression (Figure 7C). Interestingly, although IGF2BP2 expression levels appeared higher in LUAD tumors from male patients, the trend

toward an adverse prognostic effect of elevated IGF2BP2 was more noticeable in female patients (Figure 7D). Possible explanations include slightly higher basal IGF2BP2 protein levels in women and other mechanistic factors contributing to these sex-specific differences.

A similar correlation between high IGF2BP2 expression and poor prognosis in women was also observed in LIHC (Figure 1E-H) and CoAD (Figure 7I-K).

Considering these findings, this part of the study (Part III) aimed to examine tumor growth and progression in male WT and IGF2BP2 KO mice using the LLC1 tumor model. These results will be compared with tumor growth and progression in female WT and IGF2BP2 KO mice analyzed in Part II. By elucidating the role of IGF2BP2 in sex-specific tumor progression, this study aims to improve our understanding of the molecular mechanisms underlying the sex differences in lung cancer.

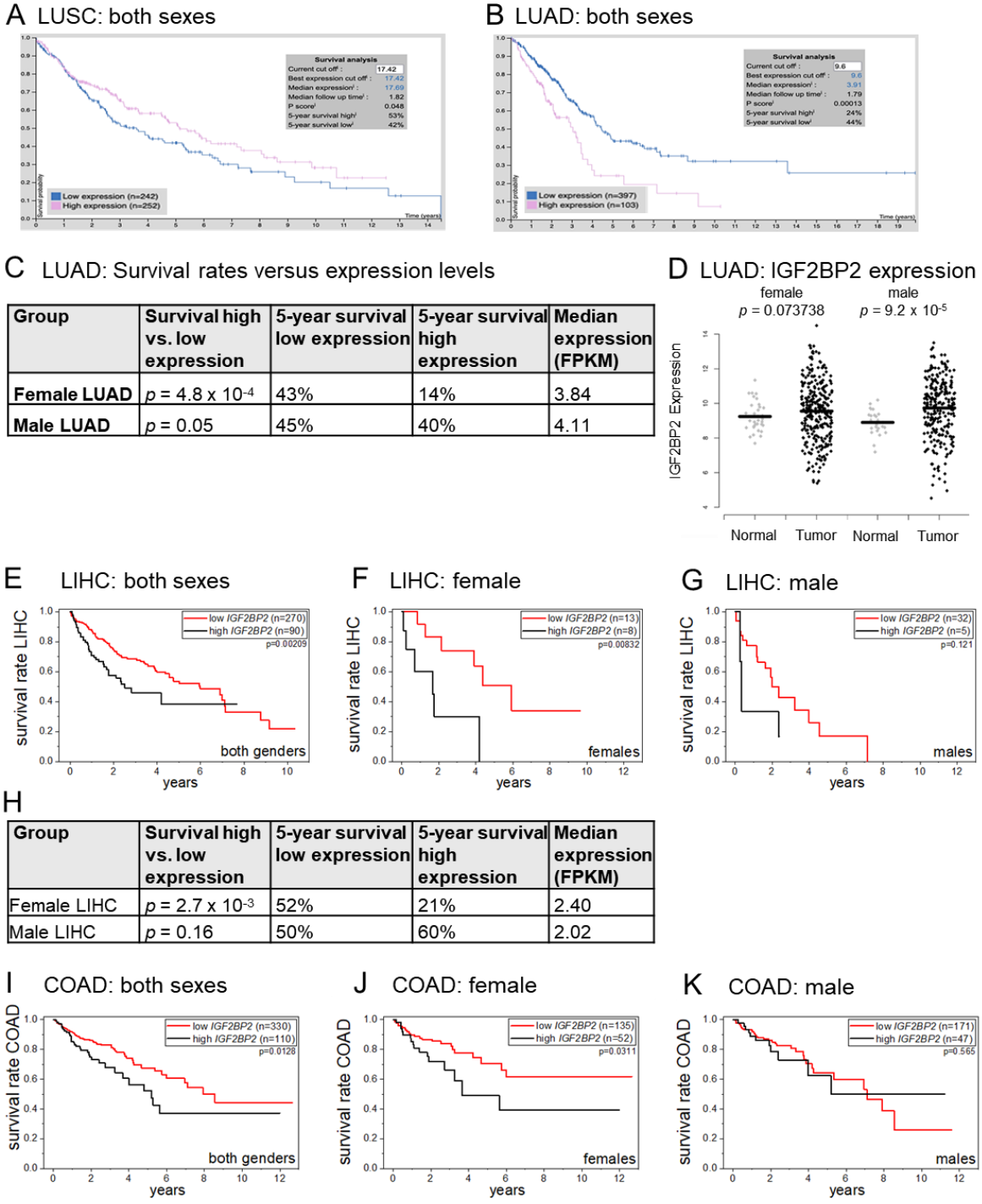

Group	Survival high vs. low expression	5-year survival low expression	5-year survival high expression	Median expression (FPKM)
Female LUAD	$p = 4.8 \times 10^{-4}$	43%	14%	3.84
Male LUAD	$p = 0.05$	45%	40%	4.11

Group	Survival high vs. low expression	5-year survival low expression	5-year survival high expression	Median expression (FPKM)
Female LIHC	$p = 2.7 \times 10^{-3}$	52%	21%	2.40
Male LIHC	$p = 0.16$	50%	60%	2.02

Figure 7. Gender-dependent analysis of IGF2BP2 expression across different cancer types. **(A-D)** NSCLC Analysis: Survival analysis of **(A)** LUSC patients and **(B)** LUAD patients, based on IGF2BP2 expression levels (blue: low expression, pink: high expression). **(C)** Sex-specific analysis of the correlation between IGF2BP2 expression and survival in LUAD patients, including p-values, 5-year survival rates in low-expressing cohorts, and median expression levels. **(D)** IGF2BP2 expression levels in LUAD tumor patients, separated by sex. Data obtained from proteinatlas.org. **(E-H)** LIHC Analysis: Survival analysis based on IGF2BP2 expression (red: low expression, black: high expression) presented for **(E)** combined gender data, **(F)** female patients, and **(G)** male patients. **(H)** Sex-specific differences in the correlation of IGF2BP2 expression with survival, showing p-values and 5-year survival rates for cohorts with low IGF2BP2 expression. **(I-K)** COAD Analysis: Survival analysis in COAD patients related to IGF2BP2 expression levels (red: low expression, black: high expression) shown for **(I)** all

patients combined, **(J)** female patients, and **(K)** male patients. (A-C, E-K) Data sourced from the TCGA database. All analyses and figure compilation were performed by Charlotte Dahlem.

4.2 Results

Given the sex-specific differences in TAMs and tumor progression, as well as the previously demonstrated differential effects of increased IGF2BP2 expression on lung tumor survival rates (Figure 7), we conducted a separate analysis of lung tumors in male mice. To investigate the role of IGF2BP2 in these sex-dependent variations within the TME, we utilized the LLC1 tumor model, as described in Part II, for female mice. In this part of the study, we followed the same experimental approach by subcutaneously injecting luciferase-expressing LLC1 cells into male WT and IGF2BP2 KO mice.

As shown in Figure 8A–C, IGF2BP2 KO mice developed tumors with similar volumes and weights compared to WT controls. Bioluminescence imaging on day 14 confirmed a comparable tumor burden in KO mice, with a slight but non-significant increase in radiance and photon flux quantification (Figure 8D).

We performed flow cytometric analysis to characterize the immune cell composition within the tumors. The percentage of TAMs, defined as $CD11b^{+}F4/80^{+}$, was similar between IGF2BP2 KO and WT (Figure 8E, F). Further, phenotypic characterization using CD86 and CD206 markers revealed no significant differences in the proportions of $CD86^{+}CD206^{-}$ (M1-like, pro-inflammatory) and $CD86^{-}CD206^{+}$ (M2-like, immunosuppressive) populations (Figure 8G- J).

Beyond macrophages, other immune cell populations remained essentially unchanged. While $CD4^{+}$ helper T cells, $CD8^{+}$ cytotoxic T cells, and $NK1.1^{+}$ cells showed a slight reduction in KO tumors compared to WT, these differences were not statistically significant (Figure 8K–P).

To evaluate tumor vascularization, we conducted CD31 immunofluorescence staining, which revealed a comparable CD31-positive endothelial cell area in both KO and WT tumors (Figure 8Q, R). Similarly, Ki67 immunohistochemical staining, which marks proliferative cells, revealed no significant difference in the number of $Ki67^{+}$ cells, indicating that IGF2BP2 deletion does not significantly affect tumor cell proliferation (Figure 8S, T).

Gene expression analysis of angiogenesis markers showed no changes in *Hif1a* and *Mmp9* expression, while *Vegfa* was slightly increased in KO tumors (Figure 8U). Likewise, inflammation markers *Cxcl10*, *Il6*, and *Tgfb* remained unchanged, although *Tnf* expression

exhibited a modest increase in KO tumors (Figure 8V). We analyzed key proliferation and apoptotic markers to investigate further the impact of IGF2BP2 KO on tumor cell proliferation and survival. *Bcl2*, *Cdk1*, *Myc*, and *Pten* expression showed a slight increase in KO tumors, suggesting potential alterations in cell survival and cell cycle regulation. However, no significant differences between WT and KO tumors were observed in *Bak*, *Bax*, or *Cdkn1a* expression (Figure 8W).

These results suggest that the impact of IGF2BP2 depletion on tumor progression is sex-specific, potentially reflecting fundamental differences in macrophage biology between males and females. Such differences may contribute to the sex-dependent prognostic effects observed in patients.

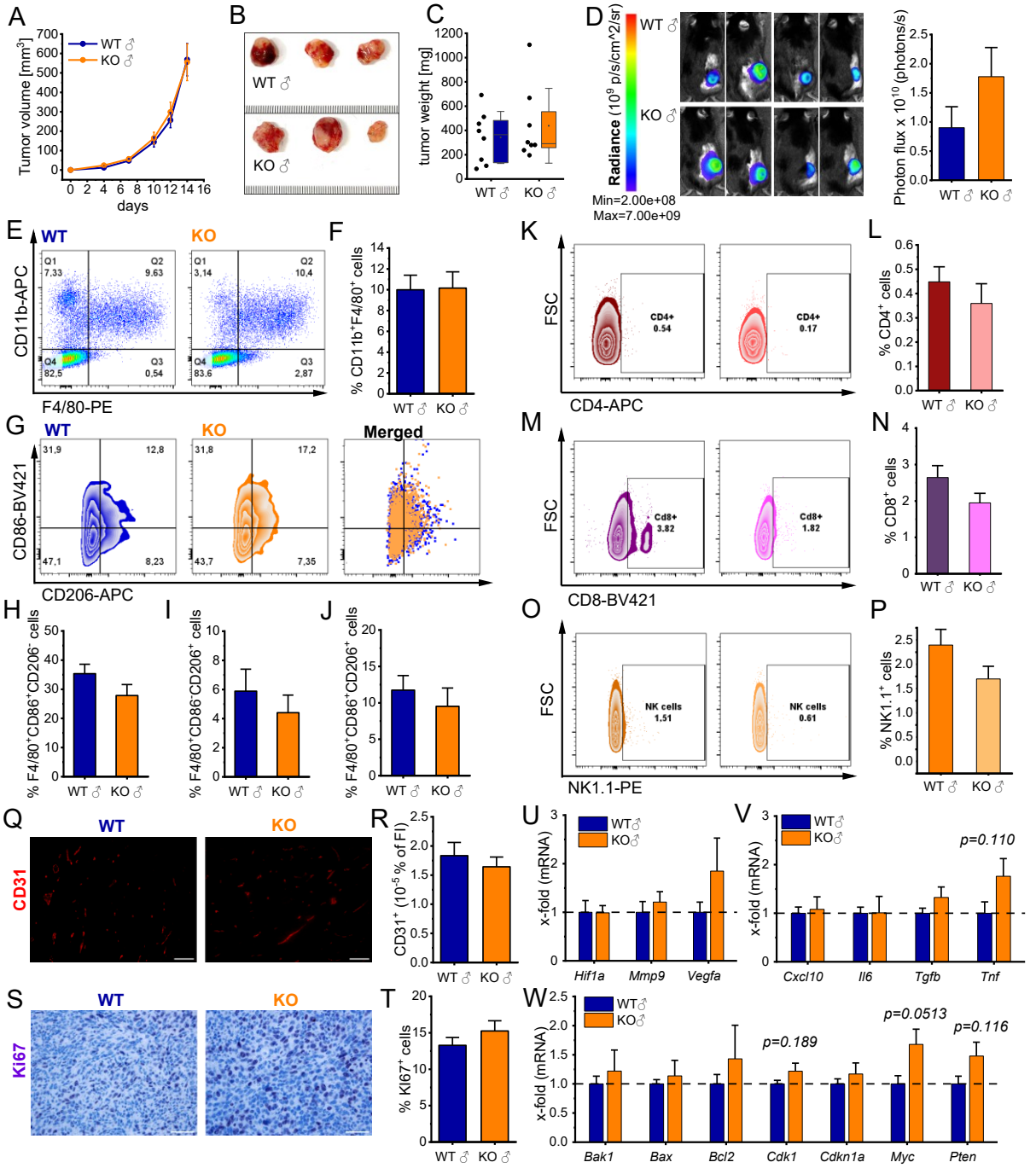

Figure 8. Tumor growth, progression, and immune cell infiltration are comparable between WT and IGF2BP2 KO male mice in LLC1 tumors. Luciferase-expressing LLC1 cells were injected subcutaneously into WT and IGF2BP2 KO male mice. **(A)** Tumor volume over time. **(B)** Representative images of resected subcutaneous tumors (scale bar: 1 mm per line). **(C)** Comparison of tumor weights **(D)** Bioluminescence imaging of luciferase-expressing LLC1 cells following luciferin injection, with photon flux intensity quantified on day 14. **(E-J)** Flow cytometric analysis of tumors collected and dissociated on day 14. **(E, left panel)** Representative dot plots showing TAMs, gated as $CD11b^+F4/80^+$ populations. **(F, right panel)** TAM quantification. **(G)** TAMs classified into three subpopulations: $F4/80^+CD86^+CD206^-$, $F4/80^+CD86^+CD206^+$, and $F4/80^+CD86^-CD206^+$ and the representative flow cytometry plots. **(H-J)** Quantification of TAM subpopulations. **(K-P)** Quantification of $CD4^+$, $CD8^+$, and $NK1.1^+$ immune cell populations. **(K, M, O, left panel)** Representative flow cytometry plots. **(L, N, P, right panel)** Quantification data. **(Q)** Representative image of fluorescently stained CD31-positive endothelial cells (red). **(R)** Quantification of the CD31-positive endothelial cell area. **(S)** Representative image of Ki67 immunohistochemical staining. **(T)** Quantification of Ki67-positive cells (scale bar:

100 µm). **(U-W)** RNA was isolated from tumor tissue, and mRNA expression was normalized to *Ppia* and expressed as fold change relative to WT tumor tissue. **(U)** Angiogenesis markers. **(V)** Inflammation markers. **(W)** Proliferation markers. Data are presented as mean ± SEM. (A-T: n = 8 mice per group; U-W: n = 8 WT, n = 6 KO mice per group, from two independent experiments). Statistical significance was determined using Student's t-test (*$p < 0.05$; **$p < 0.01$; ***$p < 0.001$).

4.3 Discussion

Sex-specific differences in tumor progression are increasingly recognized, and IGF2BP2 has been implicated as a potential regulator of tumor development and inflammatory processes. However, its contribution to sex-related disparities remains to be fully understood. In this study, we aimed to expand our understanding of these variations by examining IGF2BP2 deletion in male mice, complementing the results obtained in female mice.

4.3.1 IGF2BP2 KO Leads to Divergent Effects on Tumor Growth in Male and Female Mice

Findings from Part II demonstrated that myeloid-specific IGF2BP2 KO in female mice resulted in significantly reduced tumor growth, as evidenced by smaller tumor volumes and lower tumor weights than WT female controls. This tumor suppression was associated with a notable reduction in TAMs and a shift toward an M1-like (pro-inflammatory) phenotype, reduced $CD4^+$ and $CD8^+$ T cell infiltration, and impaired tumor vascularization. In contrast, our results in male mice (Part III) indicate that IGF2BP2 KO does not significantly affect tumor size, weight, or progression. Despite the same experimental conditions, no significant differences were observed between male WT and KO tumors in immune cell infiltration, angiogenesis, or proliferation markers. These results suggest that IGF2BP2 may have a more decisive tumor-promoting role in female mice than in males, potentially due to sex-specific immune regulation.

4.3.2 Challenges and Considerations in Male Mice Experiments

Home-cage aggression among group-housed male mice poses significant concerns regarding animal welfare and the validity of research outcomes. Factors such as social rank, housing conditions, and genetic background influence aggression levels, with interventions like cage dividers showing mixed effects on reducing variability and stabilizing social hierarchies (Streiff et al., 2024; Theil et al., 2020).

The complexity of the social dynamics of male mice can lead to stress-induced hormonal changes, particularly elevated testosterone levels, which may affect tumor growth and

progression. Elevated testosterone has been associated with increased incidence and accelerated progression of lung cancer in human studies (Chan et al., 2017). This hormonal tumor-promoting environment, combined with the inherently faster tumor growth observed in males, with a mean tumor volume of approximately 600 mm^3 versus 400 mm^3 in females at 14 days, may confound the detection of subtle genotype-specific effects such as those induced by IGF2BP2 deficiency. Consequently, aggression-related stress and endocrine variability contribute to increased inter-individual heterogeneity, potentially masking immune or metabolic phenotypes and complicating the interpretation of sex-specific roles of IGF2BP2 in tumor progression.

It is also essential to recognize that the experiments with male and female mice were conducted at different times, although identical experimental protocols were followed. This temporal difference introduces potential batch effects and variations in environmental conditions, which limit the direct comparability of results between male and female experimental cohorts. Consequently, caution should be exercised when interpreting the observed findings across sex.

4.3.3 Potential Mechanisms Underlying Sex-Specific Differences in IGF2BP2 Function

Previous research has demonstrated sex-specific differences in TAMs. Female TAMs exhibit more substantial immunogenic characteristics, whereas male TAMs tend toward an immunosuppressive phenotype (Yang et al., 2021). Male tumors contained approximately 10% TAMs ($CD11b^+F4/80^+$ cells) compared to only 6% in female wild-type tumors. Additionally, male tumors exhibited a slightly higher proportion of M2-TAMs ($F4/80^+CD86^-CD206^+$), approximately 6%, compared to 4% in females. The increased number and higher proportion of immunosuppressive TAMs in males may significantly contribute to enhanced tumor growth, potentially counteracting the beneficial effects of IGF2BP2 KO.

The minimal changes in TAM composition observed in male IGF2BP2 KO and WT mice suggest that IGF2BP2 plays a less critical role in TAM recruitment and differentiation in males. Differences in the immune microenvironment may contribute to this difference. In addition, male TAMs have been reported to be more migratory and immunosuppressive (Varghese et al., 2022; Yang et al., 2021). Therefore, they may be less affected by IGF2BP2 deletion than female TAMs, resulting in a reduced impact on their polarization and infiltration.

In humans, elevated IGF2BP2 expression correlates with poorer prognosis in female LUAD patients but not in males, despite males exhibiting slightly higher IGF2BP2 protein levels. This discrepancy implies that additional regulatory mechanisms, potentially involving estrogen signaling pathways, influence IGF2BP2-driven tumor progression in females. Increased estrogen and progesterone receptor expression has been associated with decreased infiltration of activated T cells essential for anti-tumor immunity (Diao et al., 2025; Oh et al., 2021). Estrogen further modulates the immune microenvironment, affecting macrophages and dendritic cells, thus promoting a pro-tumorigenic environment (Smida et al., 2020). Notably, IGF2BP2 has been identified as a key maternal activator of zygotic genome activation, underscoring its involvement in early developmental regulation and suggesting that sex-specific effects may be imprinted at very early stages (Liu et al., 2019). These observations support the hypothesis that estrogen-mediated immune regulation may underlie the more pronounced impact of IGF2BP2 on tumor progression in female mice compared to males.

4.3.4 Conclusion

Overall, our data indicate that IGF2BP2 deletion has significant tumor-suppressive effects in female mice, whereas minimal or no effect in male mice regarding tumor growth and immune infiltration. These findings suggest the potential for sex-specific roles of IGF2BP2 within the tumor microenvironment. Future research should further investigate the underlying molecular and immunological mechanisms, taking into account sex-specific factors, to better understand the role of IGF2BP2 in tumor biology.

5 Part IV: IGF2BP2 Inhibition Alters Human TAM-like Polarization and Metabolic Function

5.1 Introduction

RBPs regulate key post-transcriptional processes, including mRNA stability, localization, and translation, and are increasingly recognized as therapeutic targets in cancer and inflammatory diseases (Goel & Saraogi, 2025; Joseph et al., 2023; Wu, 2020). Structurally, RBPs contain RRMs and KH domains, which enable specific mRNA interactions, while their flexibility allows for diverse regulatory functions. Though historically challenging to target, advances in small-molecule inhibitors and RNA-based therapies are unlocking new therapeutic possibilities (Lu et al., 2023).

Among the diverse RBPs, IGF2BP2 has particularly captured attention for its role in cancer progression. Pivotal work from our research team has identified potent small-molecule inhibitors specifically targeting IGF2BP2. Utilizing advanced biophysical and biochemical approaches, such as fluorescence polarization assays, thermal shift analyses, and STD-NMR, Ali Abuhaliema (Pharmaceutical Biology, Saarland University) successfully identified and characterized promising inhibitors, notably compounds 4, 6, and 9 (Dahlem et al., 2021). These molecules demonstrated significant biological specificity and potent anti-cancer effects *in vitro* by inhibiting tumor growth in colorectal (HCT116, SW480), hepatocellular (Huh7), and lung (LLC1) cancer cell lines (Chanda et al., 2024; Dahlem et al., 2021). Furthermore, compound treatment reduced the expression of IGF2BP2 downstream targets, including *DANCR*, *MYC*, and *HMGA1.* Notably, our studies further validated these findings *in vivo*, where compounds effectively suppressed tumor xenograft growth in zebrafish embryo models.

In this study, we investigated the therapeutic potential of IGF2BP2 inhibition in modulating human macrophage polarization and associated metabolic functions using three validated IGF2BP2 inhibitors (compounds 4, 6, 9).

5.2 Results

To investigate the effects of IGF2BP2 inhibition on macrophage function, we treated murine RAW-Blue™ cells with IGF2BP2 inhibitors (10 μM and 25 μM) and assessed NF-κB/AP-1 activity following LPS treatment. Treatment with all three inhibitors significantly enhanced NF-κB/AP-1 activity, indicating an induced inflammatory response (Figure 9A–C).

We further evaluated the effects of these inhibitors in human monocyte-derived macrophages (HMDMs) and TAM-like macrophages, polarized using TCM derived from the A549 cell line, following a previously established and validated protocol (Hoppstädter et al., 2021). qPCR analysis revealed increased expression of classical TAM-associated markers, including *HIF1A* and *VEGFA*, upon polarization (Figure 9D). Notably, treatment with compounds 4 and 9 reduced *CCL2* and *MMP9* expressions in M0 macrophages, while HIF1A expression decreased following treatment with compound 9 (Figure 9E). All inhibitors (compounds 4, 6, and 9) significantly downregulated VEGFA expression in TAM-like macrophages (Figure 9F). Compound 4 further reduced the expression of *CCL2*, *IL8*, *MMP9*, and *TGFB* compared to untreated TAM-like macrophages (Figure 9F).

To assess the potential metabolic effects of IGF2BP2 inhibition in human macrophages, we performed a Mito Stress Test in inhibitor-treated M0 and TAM-like macrophages (Figure 9G-L). Notably, TAM-like macrophages showed an elevated reserve respiratory capacity, which could be reduced to M0 levels by inhibitor treatment (Figure 9I). In addition, compounds 4 and 9 significantly decreased maximal respiration in TAM-like macrophages, indicating impaired mitochondrial function (Figure 9J). Assessment of glycolytic activity through ECAR measurements revealed a significant decrease in basal ECAR levels in M0 macrophages treated with compounds 4, 6, and 9 (Figure 9K). Consistently, glycolytically derived ATP (glycoATP) levels were also reduced following inhibitor treatment in M0 macrophages (Figure 9L). However, human macrophages showed no significant changes in glycolytic rate, glycolytic capacity, or glycolytic reserve upon inhibitor treatment when performing a glycolysis stress test (Figure 9M-O). Furthermore, a modest, though not statistically significant, reduction in basal acidification was noted following inhibitor treatment in TAM-like macrophages (Figure 9O). This discrepancy between basal ECAR levels observed in mitochondrial stress tests and glycolytic stress tests might arise because basal acidification in the glycolytic stress test is evaluated under glucose-starved conditions.

These findings indicate that IGF2BP2 inhibitors selectively impair mitochondrial function and induce metabolic reprogramming, specifically in TAM-like macrophages.

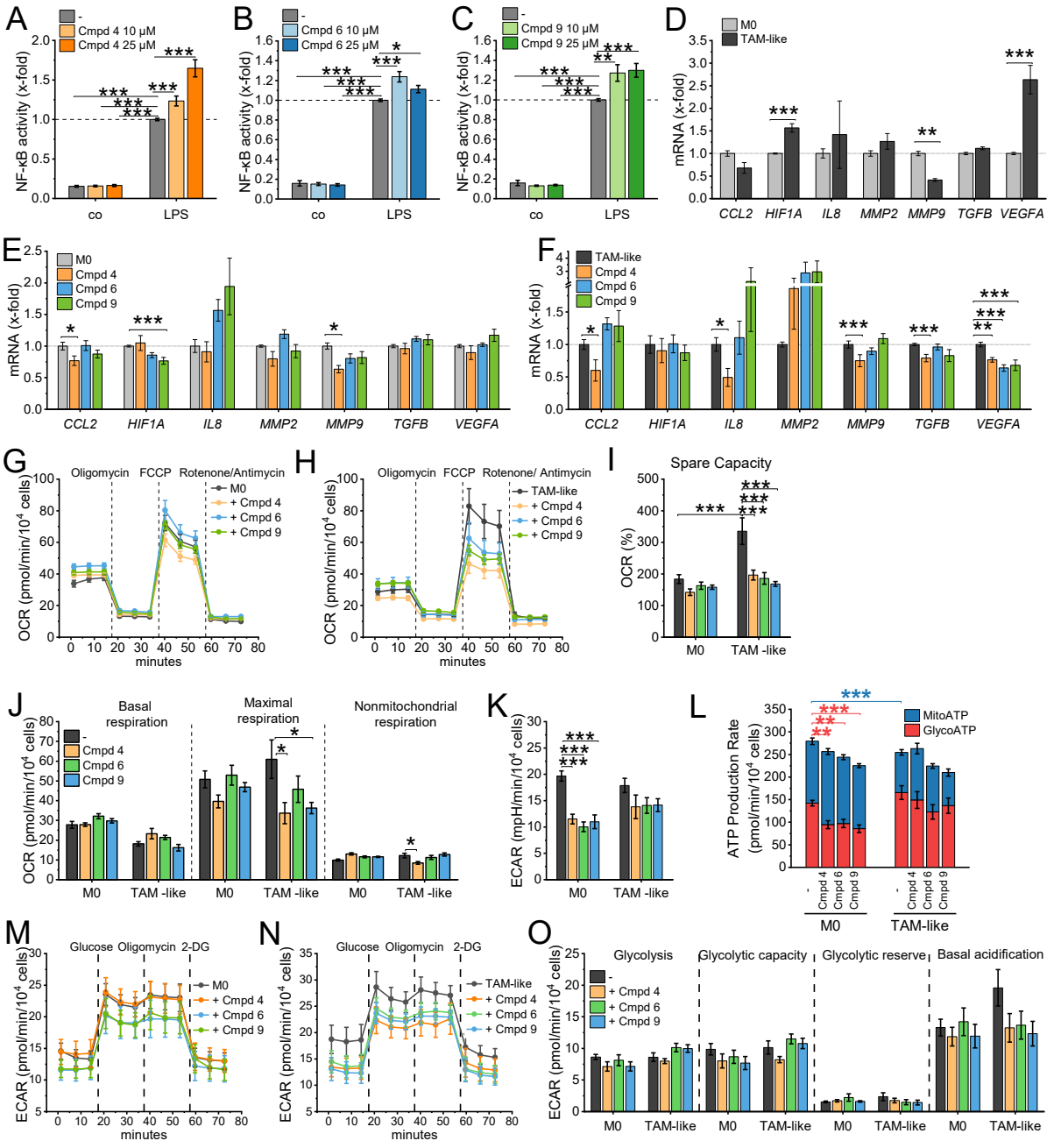

Figure 9. IGF2BP2 inhibitors reprogram human TAM-like macrophages. (A-C) Murine RAW-Blue™ cells were pre-treated for 24 hours with IGF2BP2 inhibitors (Compounds 4, 6, or 9), followed by treatment with LPS (100 ng/mL) for an additional 22 hours. NF-κB/AP-1 activity was quantified by measuring secreted embryonic alkaline phosphatase (SEAP) levels. Co = solvent control (n = 4, triplicates). **(D-P)** HMDMs were cultured either in standard medium (M0) or A549 tumor-conditioned medium (TAM-like) for 24 hours in the absence or presence of IGF2BP2 inhibitors (10 µM). **(D-F)** mRNA expression levels of selected genes normalized to *RNA18S* expression are shown as: **(D)** Fold-change of TAM-like macrophages compared to untreated M0 macrophages; **(E)** Fold-change of inhibitor-treated M0 macrophages relative to untreated M0 macrophages; **(F)** Fold-change of inhibitor-treated TAM-like macrophages relative to untreated TAM-like macrophages (n = 4, duplicates). **(G-L)**

OCR and ECAR parameters were obtained from the Mito Stress test **(M-O)** ECAR parameters obtained from glycolysis stress tests using the Seahorse XF Pro Analyzer (n = 3, triplicates). Data are presented as mean ± SEM. Statistical significance was determined using one-way ANOVA followed by Bonferroni post-hoc tests (*$p < 0.05$; **$p < 0.01$; ***$p < 0.001$).

5.3 Discussion

In this study, we demonstrated that IGF2BP2 inhibitors significantly modulate macrophage polarization and metabolic functions, explicitly targeting human TAM-like macrophages. These findings expand our understanding of IGF2BP2, suggesting its critical involvement beyond cancer progression to include significant roles in immune modulation and macrophage function.

The enhanced inflammatory response observed in murine RAW-Blue cells treated with IGF2BP2 inhibitors suggests a shift towards a pro-inflammatory phenotype. This aligns with our previously published RNA sequencing data, which indicated increased NF-κB and TNF signaling in untreated IGF2BP2 KO macrophages. Despite these transcriptional changes, Western blot analysis of LPS-treated BMMs revealed no significant differences in ERK or NF-κB phosphorylation between WT and IGF2BP2 KO.

Furthermore, treating human TAM-like macrophages with IGF2BP2 inhibitors resulted in reduced expression of *VEGFA*, a key factor in angiogenesis and immune suppression within the tumor microenvironment. VEGFA-expressing TAMs have been shown to facilitate the intravasation of cancer cells into blood vessels, thereby enhancing their metastatic potential (Banerjee et al., 2023; Ferreira et al., 2022). This finding aligns with our previous observations in murine IGF2BP2 KO macrophages, which exhibited decreased *Mrc1*, *Mmp2*, and *Il10* expression in TAM-like cells polarized with TCM from LLC1 cells.

Metabolic profiling revealed that IGF2BP2 inhibitors selectively disrupted mitochondrial function in human TAM-like macrophages. Treatment with these inhibitors significantly reduced the reserve respiratory capacity of TAM-like macrophages and diminished maximal respiration, indicating mitochondrial dysfunction. This metabolic shift mirrors findings in murine IGF2BP2 KO macrophages, which exhibited reduced mitochondrial respiration alongside increased glycolytic capacity. However, in human macrophages, IGF2BP2 inhibition did not significantly affect glycolysis, suggesting species-specific metabolic differences. These disparities may be attributed to fundamental differences in macrophage bioenergetics between species. Unlike murine macrophages, which shift towards glycolysis upon LPS treatment,

human macrophages primarily rely on OXPHOS for ATP production and do not undergo significant metabolic reprogramming towards glycolysis (Maoldomhnaigh et al., 2021; Vijayan et al., 2019). These findings underscore the complexity of IGF2BP2's role in macrophage metabolism across species.

Collectively, our findings highlight the therapeutic potential of IGF2BP2 inhibitors in reprogramming TAMs, modulating their inflammatory profiles, and disrupting tumor-promoting metabolic pathways. Further mechanistic studies and *in vivo* validations are crucial to fully elucidating IGF2BP2's role in macrophage-driven tumor progression.

6 Supplements

6.1 Materials & Methods

This thesis includes manuscripts [Part I, Part II] containing detailed methodology. Methods unique to additional results presented in this thesis and not included in these publications are described below.

6.1.1 Materials

All materials and reagents used were obtained from commercial suppliers. RPMI-1640 cell culture media (#R0833) and DMEM (high Glucose) cell culture media (#D6546-0500) were purchased from Sigma-Aldrich, along with L-glutamine (#G7513), Penicillin/Streptomycin (#P4333), Accutase (#A6964), Trypsin-EDTA (#T3924), Dihydroethidium (DHE) (#37291), and Bafilomycin A1 from Streptomyces griseus (#B1793-2UG). Filtrated bovine serum (FBS, #P040-37500) was obtained from PAN Biotech. Blasticidin S hydrochloride (#R21001) and the High Capacity cDNA Reverse Transcription Kit (#4368813) were acquired from Thermo Fisher Scientific. Leucosep tubes (#227290) from Greiner. Lymphocyte separation medium 1077 (#C-44010) from Promocell. Recombinant human M-CSF (#130-096-492), mouse M-CSF (#130-101-704), recombinant murine interleukin-4 (IL-4) (#130-093-921), anti-CD14 microbeads (#130-050-201), LS columns (#130-042-401), and the Murine Tumor Dissociation Kit (#130-096-730) were obtained from Miltenyi Biotech. Recombinant murine IFNγ (#87389.20) was sourced from Biomol, as was Rockland Blocking Buffer (#MB-70). Ultrapure LPS from E. coli K12 (#tlrl-peklps), ATP (#tlrl-atpl), Rapamycin (#tlrl-rap), and QUANTI-Blue™ solution (#rep-qbs) were purchased from Invivogen. Antibody anti-α-tubulin monoclonal antibody (DM1A, #T6199) was obtained from Sigma-Aldrich. Antibody LC3B Antibody (CST, #2775) and anti-mouse Ki67 antibody (D3B5, #12202) were procured from Cell Signaling Technology. IRDye 680 (#926-68071) and IRDye 800 (#926-32210) conjugated secondary antibodies were purchased from LI-COR Biosciences. Additional reagents included the protease inhibitor mix (cOmplete®; #04693124001) from Roche Diagnostics (Basel, Switzerland). Immobilon FL-PVDF membranes (#IPFL00010) from Millipore (Burlington, MA, USA), and the High Pure RNA Isolation Kit (#11828665001) from Roche. The Total RNA Quick-RNA Miniprep Kit (#R1055) was obtained from Zymo Research. RNase inhibitor (#10777-019) was from Invitrogen. BD Fc Block™ (#553142) was purchased from BD Biosciences. The CD31 primary antibody (SZ31, #DIA310) was obtained from Dianova, and the Cy3-conjugated goat anti-rat secondary antibody (# 712-165-153) was acquired from Jackson ImmunoResearch Labs. 5× HotFirePol EvaGreen qPCR Plus Mix (no ROX) (#082500020) was from Solis BioDyne. Zombie Yellow viability dye (#423101) was from BioLegend. Glycolytic and Mito Stress Test kits (#103020-100, #103010-100) and Seahorse XF96 cell culture microplates (#103793-100) were purchased from Agilent. TE buffer (#A0386.1000) and DMSO (#A3672-0250) were from AppliChem. Primers for qRT-PCR were purchased from Eurofins Genomics. Other chemicals were obtained from either Sigma-Aldrich or Carl Roth unless stated otherwise.

6.1.2 Mice

Mice were housed under a 12-hour light/dark cycle and *ad libitum* access to food and water. Myeloid-specific IGF2BP2 KO mice were generated by crossing B6.Cg-Igf2bp2tm1.1Thor/J mice (The Jackson Laboratory), which carry loxP sites flanking exons 4 and 5 of the *Igf2bp2* gene, with 29P2-Lyz2tm1(cre)Ifo/J mice (The Jackson Laboratory). Control WT mice were littermates that did not carry floxed alleles and either expressed or lacked Cre recombinase. IGF2BP2-KO mice were validated by assessing protein and mRNA levels. Sex- and age-matched littermates were used for all experiments. All animal procedures were approved by the local animal welfare committee (approval no. 35/2024; Saarland State Office for Social Affairs, Health, and Consumer Protection).

6.1.3 LLC-Tumor Model

A murine cancer model was established by subcutaneous injection of luciferase-expressing Lewis lung carcinoma (LLC1) cells (CRL-1642-LUC2™, ATCC) into 8- to 10-week-old female and male WT and IGF2BP2 MΦ-KO mice. ATCC authenticated the LL2-Luc cell line for viability, growth characteristics, mycoplasma contamination, species identity, and sterility. Cells were cultured under standard conditions according to ATCC guidelines. Before injection, subconfluent LLC1 cells were maintained for 2-3 weeks, harvested, filtered through a 40 µm cell strainer (BD Biosciences), washed, and resuspended in phosphate-buffered saline (PBS). Tumor induction was performed by subcutaneous injection of 5×10^5 cells into the right flank of each mouse. Tumor growth was monitored by measuring tumor dimensions with digital calipers, and volumes were calculated using the formula: $(\text{height} \times \text{width}^2)/2$.

Bioluminescence imaging (BLI) was conducted on day 14 post-injection to assess tumor burden. Mice were administered 3 mg of D-luciferin potassium salt (Revvity, #122799) *via* subcutaneous injection, and bioluminescent signals were captured using the IVIS Spectrum *in vivo* imaging system (PerkinElmer). Image acquisition and quantification were performed using Living Image 4.5 software (PerkinElmer).

6.1.4 Histology and Immunohistochemistry

Tumor tissues were fixed in 4% PFA at 4°C for 24 hours, then dehydrated, embedded in paraffin, and sectioned into 3-µm slices. Antigen retrieval was performed using citrate buffer (pH 6.0) at 95°C for 30 minutes. To block non-specific binding, sections were incubated with goat serum for 1 hour at room temperature. CD31 expression was detected using a primary anti-CD31 antibody (1:300, SZ31, Dianova, #DIA310) incubated overnight at 4°C, followed by a

Cy3-conjugated goat anti-rat secondary antibody (1:1000, Jackson ImmunoResearch Labs, #712-165-153) for 1 hour at room temperature. To assess tumor cell proliferation, sections were stained with a rabbit anti-mouse Ki67 antibody (1:500, D3B5, Cell Signaling Technology, #12202). Detection was performed using a biotin-conjugated secondary antibody (Abcam, #ab64256) and horseradish peroxidase (HRP)-conjugated streptavidin (Abcam, #ab210901). Signal development was achieved with the peroxidase substrate 3-amino-9-ethylcarbazole (Abcam, #ab142228), and sections were counterstained with Mayer's hemalum solution (Merck, #109249). Twelve fields per section were imaged at 400 × magnification using a BX60 fluorescence microscope (Olympus). CD31-positive cells were quantified using FIJI software (NIH), and the percentage of Ki67-positive and cleaved caspase-3-positive tumor cells were analyzed. The procedure was performed as previously described Gu et al. (2022).

6.1.5 Cell Culture Conditions

Cells were cultured at 37°C in a humidified 5% CO_2 atmosphere in RPMI-1640 or DMEM supplemented with 10% FBS, 2 mM L-glutamine, and 100 units/ml penicillin G, 100 µg/ml streptomycin, unless stated otherwise.

6.1.6 Cultivation of Tumor Cell Lines

Tumor cell lines, including A549 and LLC1, were cultured in RPMI-1640, whereas Luc-LLC1 was maintained in DMEM, both supplemented with 10% FBS, 2 mM L-glutamine, 100 U/mL penicillin, and 100 µg/mL streptomycin. Subculturing was performed according to ATCC recommendations. Cells were washed with PBS buffer (2.7 mM KCl, 1.8 mM KH_2PO_4, 137 mM NaCl, and 10 mM Na_2HPO_4; pH 7.4, autoclaved) and detached using trypsin. The enzymatic reaction was stopped by adding fresh culture medium, and the cell suspension was centrifuged at 250 × g for 5 minutes. The resulting pellet was resuspended in complete growth medium and used for subsequent seeding and passaging.

6.1.7 Cell Freezing and Thawing

Cells were washed, detached, and centrifuged at 200 × *g* for 5 minutes. The pellet was resuspended in FCS supplemented with 10% dimethyl sulfoxide (DMSO) and aliquoted into cryovials. Cells were gradually frozen to -80°C using a Mr. Frosty™ freezing container (ThermoFisher Scientific) before being transferred to liquid nitrogen for long-term storage.

For thawing, cryovials were rapidly warmed in a 37°C water bath until only a tiny ice pellet remained. The cell suspension was immediately transferred to pre-warmed culture medium to minimize DMSO toxicity, then centrifuged at 200 × *g* for 5 minutes. After removing the

supernatant, the pellet was resuspended in a fresh culture medium and maintained under standard culture conditions.

6.1.8 Genotyping

Genomic DNA for genotyping was extracted from ear biopsies using proteinase K (Roche, #03115836001) digestion in Taq buffer (Genscript, #E00007) at 55°C for 1 hour. The presence of LysM-Cre was detected by PCR using Kapa2G Fast HS Genotyping Mix (Sigma, #KK5621) with the primers listed in Supplemental Table 1. The PCR conditions were as follows: initial denaturation at 95°C for 3 min, followed by 40 cycles of 95°C for 15 s, primer-specific annealing for 15 s, and 72°C for 20 s, with a final extension at 72°C for 2 min. The annealing temperature was set to 64°C for oIMR3067 and oIMR3068 and 62°C for oIMR3066 and oIMR3067.

To confirm the presence of floxed *Igf2bp2*, PCR was performed following the Jackson Laboratory protocol for B6.Cg-Igf2bp2 (Stock: 032494). The PCR was performed using 2x Kapa2G Fast HS Genotyping Mix with the primers listed in Supplemental Table 1. The PCR conditions consisted of an initial denaturation at 95°C for 3 min, followed by 40 cycles of 95°C for 15 s, 60°C for 15 s, and 72°C for 30 s, with a final extension at 72°C for 1 min.

Specific PCR products were validated for all genotyping reactions using agarose gel electrophoresis, with results compared against positive and negative controls.

Supplemental Table 1. Primers used for mouse genotyping

Name	Primer sequence (5′→3′)	Target
oIMR3066	CCCAGAAATGCCAGATTACG	Detects LysMCre (750 bp) with oIMR3066 and oIMR3067. Detects WT (350 bp) with oIMR3067 and oIMR3068.
oIMR3067	CTTGGGCTGCCAGAATTTCTC	
oIMR3068	TTACAGTCGGCCAGGCTGAC	
Igf2bp2_Fw	GCTTCCTCTAGCGTATTTATCCAC	WT (370 bp), heterozygous (490 bp and 370 bp), mutant (490 bp)
Igf2bp2_Rev	CACCTCACAGGAAACAGACG	

6.1.9 Isolation and Cultivation of Bone Marrow-Derived Macrophages

Bone marrow cells were isolated from three- to four-month-old WT or IGF2BP2 KO mice. Cells were flushed from femurs and tibias using a standard medium (RPMI 1640 supplemented with 10% FCS, 100 U/ml penicillin G, 100 µg/ml streptomycin, and 2 mM glutamine). After centrifugation at 200 × *g* for 10 minutes, erythrocytes were lysed by incubation in hypotonic buffer (155 mM NH_4Cl, 10 mM $KHCO_3$, and 1 mM Na_2EDTA) for 3 minutes at 37°C. The remaining cells were resuspended in a standard medium supplemented with macrophage colony-stimulating factor (M-CSF, 50 ng/ml) and transferred to a 75 cm² culture flask overnight for initial attachment. Non-adherent cells were collected the following day and cultured in a 150 cm² culture flask for 5-6 days in an M-CSF-containing medium to promote differentiation into BMMs, as described before (Hoppstädter et al., 2016). Differentiated cells were detached using Accutase, resuspended in a standard medium supplemented with 50 ng/ml M-CSF, and seeded as indicated. To polarize BMMs, the differentiation media was supplemented with 20 ng/ml IL4 for M2 polarization or left without further supplementation for M0 macrophages. TAM-like macrophages were generated with TCM supplemented with 50 ng/ml M-CSF. TCM was generated by seeding 0.5-1 × 10^6 murine LLC1 cells into a T75 culture flask and growing until confluency for three days. Subsequently, the supernatant was discarded, and a standard growth medium was added to the cells. After 48 hours, the medium was sterile-filtered (0.22 µm) to remove cell debris and used immediately for macrophage polarization.

6.1.10 Isolation and Cultivation of Human Monocyte-Derived Macrophages

Peripheral blood mononuclear cells (PBMCs) were isolated using Leucosep tubes (Greiner, #227290) by density gradient centrifugation with lymphocyte separation medium 1077 (Promocell, #C-44010). According to the manufacturer's instructions, monocytes were then separated from the PBMC fraction using anti-CD14 microbeads and LS columns (Miltenyi Biotec, #130-042-401). The isolated monocytes were seeded at a density of 5 × 10^5 cells per well in a 12-well plate (1 ml/well) or 5 × 10^4 cells per well in a 96-well plate or Seahorse plate (Agilent,#103725-100) (200 µL/well) in complete RPMI-1640 growth medium supplemented with 20 ng/ml recombinant human M-CSF to promote differentiation. Differentiation was performed for six days, with a medium change after four days.

TAM-like macrophages were generated by culturing the cells in TCM supplemented with 20 ng/ml M-CSF. TCM was prepared by culturing A549 lung adenocarcinoma cells in a T75 flask for up to 3 days, followed by incubation with 20 ml of fresh medium for 48 hours. The

collected medium was filtered through a 0.22 µm membrane to remove cell debris before being used for polarization, as previously described (Hoppstädter et al., 2021). M0 macrophages were generated using a standard medium supplemented with 20 ng/mL M-CSF.

For IGF2BP2 inhibitor treatment, polarized macrophages were incubated for 24 hours with the indicated inhibitor concentrations in the respective polarization medium. Cell viability following IGF2BP2 inhibitor treatment was assessed using the MTT assay to ensure that only non-toxic concentrations were used.

6.1.11 Seahorse Measurement

The Glycolytic and Mito Stress Tests (Agilent, #103020-100, #103010-100) were conducted using the Agilent Seahorse® XF96 Analyzer and corresponding assay kits, following the manufacturer's protocols. Cells were seeded into Agilent Seahorse XF96 cell culture microplates (#103793-100), and the culture medium was replaced with Seahorse assay medium one hour prior to measurement.

During the Mito Stress Test, cells were treated with 1.5 µM carbonyl cyanide-4-(trifluoromethoxy)phenylhydrazone (FCCP). Oxygen consumption rate (OCR) and extracellular acidification rate (ECAR) were quantified using the Seahorse Wave software (Agilent Technologies). Data normalization was performed based on cell counts obtained from brightfield images, analyzed with Gen5 software (version 3.14) on a Cytation 1 imaging system (BioTek).

6.1.12 NF-κB Reporter Assay

RAW-Blue cells (InvivoGen, #raw-sp), which express secreted embryonic alkaline phosphatase (SEAP) under the control of an IFNκ minimal promoter fused to five NF-κB and AP-1 binding sites, were used to assess NF-κB/AP-1 activity. RAW-Blue macrophages were seeded in a 96-well plate at a density of 1×10^5 cells and incubated according to the manufacturer's instructions. The cells were pre-treated with the respective IGF2BP2 inhibitor additive for 24 hours, including 22 hours of treatment with 100 ng/ml LPS. After incubation, the supernatant was collected, and SEAP activity was measured using QUANTI-Blue™ solution according to the manufacturer's instructions. SEAP levels were quantified using a microplate reader (Promega™ GloMax®) at 600 nm.

6.1.13 Staining and Quantification of F-Actin

BMMs were seeded at a density of 2×10^5 cells per well in a 12-well plate on an 18 mm Ø coverslip (Geyer, #WQ-0692) and incubated overnight. The following day, cells were fixed with 3.7% PFA, washed with PBS, and permeabilized for 10 minutes with 0.25% Triton X-100. After additional PBS washes, cells were blocked with 1% bovine serum albumin (BSA) for 30 minutes at room temperature. For F-actin staining, cells were incubated with phalloidin-tetramethylrhodamine isothiocyanate (TRITC, 10 µg/mL, 30 minutes, 4°C, in darkness) (Sigma, #P1951–Aldrich). Nuclei were counterstained with DAPI (1 µg/mL, 5 minutes, room temperature) (Sigma, #D9542). Coverslips were mounted using a mounting buffer, and images were acquired using an LSM900 microscope with Airyscan 2 (Zeiss). All images were analyzed using Fiji (ImageJ).

6.1.14 Real-time Deformability Cytometry (RT-DC)

Real-time deformability cytometry (RT-DC; Zellmechanik Dresden) was performed to assess the mechanical properties of BMMs, following the method described by Yanamandra et al. (2024). Briefly, BMMs were seeded in a T75 cm^2 flask at a density of 8 $x10^6$ cells. Before measurement, cells were resuspended in a cell carrier solution (Zellmechanik Dresden, #ZM-C-CC-049-6CL) at a concentration of 1 $x\ 10^6$ cells per 100 µL. For RT-DC analysis, a microfluidic polydimethylsiloxane (PDMS) chip with a 20 µm-wide channel (Zellmechanik, #ZM-C-F20-Flic20) was mounted onto the stage of an inverted Zeiss microscope. The cell suspension was introduced into the chip using a syringe pump at a controlled flow rate of 0.16 µl/s. As cells passed through the microfluidic channel, they experienced shear stress and a pressure gradient, leading to cell deformation. Each event was captured in real-time using a CMOS camera, with a minimum of 5000 events recorded per condition. The mechanical properties of the cells were analyzed using ShapeOut 2 software (Zellmechanik Dresden), which applies linear mixed models to determine statistical significance.

6.1.15 pHrodo™ S.aureus Phagocytosis Assay

BMMs were seeded at a density of 0.75 $x\ 10^5$ cells per well in a 96-well plate and incubated overnight. pHrodo™ Red *Staphylococcus aureus* (S.aureus) Bioparticles™ (Thermo Scientific, #A10010) were resuspended in PBS and sonicated in a water bath at 37°C for 15 minutes. Subsequently, 2 µg of Bioparticles were added to each well. Real-time imaging was performed using the Incucyte® S3 Live-Cell Analysis System (Essen BioScience), capturing brightfield and red fluorescence channels (10 × objective, 400 ms acquisition time). Phagocytic capacity

was quantified as the total red object integrated intensity (RCU × µm²/image), normalized to initial cell confluency (%), following the method described by Linnenberger et al. (2021).

6.1.16 pHrodo™-Labeled Tumor Cell Phagocytosis Assay

BMMs were seeded at a density of 0.75×10^5 cells per well in a 96-well plate and incubated overnight. LLC1 cells were cultured in a T75 flask at a density of 5×10^5 cells and maintained for five days until confluency, with a media change on day three. For labeling, the pHrodo™ Red Cell Labeling Kit for Phagocytosis (Sartorius, #46469) was used according to the manufacturer's instructions. LLC1 cells were detached using trypsin and resuspended in pHrodo® labeling buffer. The cells were then incubated at 37°C for 1 hour at a concentration of 1×10^6 cells in 200 ng/ml pHrodo™ Red cell labeling dye. Following labeling, the LLC1 cells were incubated with 10 µg/ml of CD47 purified anti-mouse antibody (BioLegend, #127502) in PBS for 1 hour at 4°C. Following antibody incubation, LLC1 labeled cells were resuspended in fresh medium and co-cultured with BMMs at a ratio of 1:2.7 by adding 200 µl containing 2×10^5 LLC1 labeled cells per well onto pre-seeded BMMs (0.75×10^5 cells per well, after aspiration of the previous medium).

6.1.17 Real-time Caspase-3/7 Activity and Cytotoxicity Detection

BMMs were seeded at a density of 5×10^4 per well in 96-well plates and allowed to adhere overnight. Cells were treated with 100 ng/ml LPS for 4 hours, followed by 2 mM ATP to induce pyroptosis. Real-time imaging was initiated immediately after LPS treatment using the Incucyte® S3 Live-Cell Analysis System (Essen BioScience), capturing images in brightfield as well as red and green fluorescence channels (10 × objective lens, acquisition time: 300 ms for the green channel, 400 ms for the red channel). To monitor caspase-3/7 activation and cytotoxicity, the culture medium was supplemented with 4 µM CellEvent™ Caspase-3/7 Green Detection Reagent (Invitrogen, #C10723) and 0.25 µM Incucyte® Cytotox Red Reagent (Essen BioScience, #4632). Fluorescence intensities (total red and green object integrated intensities, GCU or RCU × µm²/Image) were normalized to the initial cell confluency (%) within each well. Baseline fluorescence was uniformly set to zero at the start of the experiment. Per the manufacturer's guidelines, spectral unmixing was applied, with 1.5% of the red signal removed from the green channel. The procedure was performed as previously described (Legroux et al., 2024).

6.1.18 Detection of Reactive Oxygen Species (ROS)

BMMs were seeded at a density of 0.75×10^5 cells per well in 96-well plates and incubated overnight. Cells were cultured in the standard medium as a control, while the experimental group was treated with 100 ng/ml LPS for 4 hours. Following LPS treatment, the culture medium was replaced with fresh medium containing 2 mM ATP and 10 µM dihydroethidium (DHE) to assess ROS production. Real-time imaging was initiated immediately after DHE treatment using the Incucyte® S3 Live-Cell Analysis System (Essen BioScience), capturing images in brightfield and red fluorescence channels (10× objective lens, 400 ms acquisition time). ROS levels were quantified as the total red object integrated intensity (RCU × µm²/Image) after 30 minutes and normalized to the initial cell confluency (%) at the start of the assay. The procedure was performed as previously described (Legroux et al., 2024).

6.1.19 Flow Cytometric Analysis of Macrophage Polarization

BMMs were seeded at a density of 1×10^6 cells per well in a 6-well plate and incubated overnight. The following day, cells were polarized for 24 hours under different conditions: M0 macrophages were maintained in a standard culture medium, M2 macrophages were treated with IL-4 (20 ng/ml), and TAM-like macrophages were treated with TCM from LLC1 cells. After polarization, cells were detached with Accutase and resuspended in 100 µl FACS Wash Buffer (PBS supplemented with 2.5% FCS and 0.05% sodium azide). BD Fc Block™ (#553142, BD Biosciences, 1 µg/ml) was added to prevent non-specific antibody binding. After incubation for 10 minutes at room temperature, specific antibodies were added. Cells were incubated with fluorophore-conjugated antibodies for 30 minutes in the dark on ice for extracellular staining. The following antibodies were used: APC Rat IgG2a, κ Isotype Control Antibody (Clone RTK2758, BioLegend, #400511, 2.5 µg/ml), APC anti-mouse CD206 (MMR) (Clone C068C2, BioLegend, #141707, 2.5 µg/ml), Brilliant Violet 421™ Rat IgG2a, κ Isotype Control Antibody (Clone RTK2758, BioLegend, #400535, 1 µg/ml), Brilliant Violet 421™ anti-mouse CD86 (Clone GL-1, BioLegend, #105031, 1 µg/ml), FITC Armenian Hamster IgG Isotype Control (Clone HTK888, BioLegend, #400905, 2 µg/ml), and FITC anti-mouse CD80 (Clone 16-10A1, BioLegend, #104705, 2 µg/ml), PE Rat IgG2a, κ Isotype Control Antibody (Clone RTK2758, BioLegend, #400507, 5 µg/ml) and PE anti-mouse CD163 (Clone S15049I, BioLegend, #155307, 5 µg/ml). Following staining, cells were washed once with FACS Wash Buffer and resuspended in 1% PFA in PBS.

Flow cytometric analysis was performed using a BD LSRFortessa™ (BD Biosciences). Data acquisition and analysis were conducted using BD FACSDiva™ software (BD Biosciences).

Surface marker expression was quantified by determining the median fluorescence intensity (MFI) of singlet cells. The relative MFI was calculated by subtracting the MFI of the respective isotype control from that of the stained sample.

6.1.20 Flow Cytometric Analysis of Cells Isolated from Tumor Tissue

Tumor cells were isolated from murine tumor tissue on day 14 after subcutaneous injection. Tumors were enzymatically dissociated using the Murine Tumor Dissociation Kit (#130-096-730, Miltenyi Biotec) and the gentleMACS Octo Dissociator (Miltenyi Biotec), according to the manufacturer's instructions. Following dissociation, cells were washed with PBS, resuspended in 100 µl PBS, and stained with Zombie Yellow viability dye (#423101, BioLegend) at a 1:100 dilution for 20 minutes at room temperature in the dark. A blocking step was performed using BD Fc Block™ (#553142, BD Biosciences,1 µg/ml) for 10 minutes at room temperature. For extracellular staining, cells were incubated with fluorophore-conjugated antibodies in FACS Wash buffer (PBS containing 2.5% fetal calf serum [FCS] and 0.05% sodium azide) for 30 minutes in the dark on ice. The following antibodies were used: APC anti-mouse/human CD11b (Clone M1/70, BioLegend, 2 µg/mL), PE anti-mouse F4/80 (Clone BM8, BioLegend, 2.5 µg/mL), APC anti-mouse CD206 (MMR) (Clone C068C2, BioLegend, 2.5 µg/mL), Brilliant Violet 421™ anti-mouse CD86 (Clone GL-1, BioLegend, 2 µg/mL), APC anti-mouse CD4 (Clone RM4-5, BioLegend, 2 µg/mL), Brilliant Violet 421™ anti-mouse CD8a (Clone 53-6.7, BioLegend, 5 µg/mL), and PE anti-mouse NK-1.1 (Clone PK136, BioLegend, 2 µg/mL). Following staining, cells were washed once with FACS Wash Buffer and resuspended in 1% PFA in PBS. For intracellular CD68 staining, cells were fixed in 1% PFA for 30 minutes on ice, followed by permeabilization with saponin buffer (FACS Wash supplemented with 0.2% [w/v] saponin) for 10 minutes at room temperature. Subsequently, cells were blocked in PBS supplemented with 20% FCS and 0.02% saponin for 30 minutes at room temperature, then incubated with Alexa Fluor® 594 anti-mouse CD68 (Clone FA-11, BioLegend, 5 µg/mL) for an additional 30 minutes on ice in the dark. Following staining, cells were washed once with FACS Wash Buffer and resuspended in 1% PFA in PBS.

Flow cytometric analysis was performed using a BD LSRFortessa™ (BD Biosciences). Data acquisition and analysis were conducted using BD FACSDiva™ software (BD Biosciences), and median fluorescence intensities of singlet cells were used to quantify surface marker expression.

6.1.21 Quantitative Real-Time PCR (qRT-PCR)

BMMs were seeded at 5×10^5 cells per well in 12-well plates. Total RNA was isolated using the High Pure RNA Isolation Kit (Roche; #11828665001) or the Total RNA Quick-RNA Miniprep Kit (Zymo Research; #R1055), following the manufacturer's protocols. The concentration and purity of the isolated RNA were assessed using a NanoDrop™ spectrophotometer (Thermo Fisher Scientific). Equal amounts of RNA were reverse transcribed into complementary DNA (cDNA) using the High-Capacity cDNA Reverse Transcription Kit (Thermo Fisher Scientific; #4368813) with the addition of an RNase inhibitor (Invitrogen; #10777-019), as per the manufacturer's instructions. Quantitative real-time PCR (qRT-PCR) was performed using 5× HotFirePol EvaGreen qPCR Plus Mix (no ROX) (Solis BioDyne; #082500020), as described previously (Dahlem et al., 2020; Hoppstädter et al., 2019a), and primers listed in Supplemental Table 2. Reactions were conducted in a CFX96 Touch™ Real-Time PCR Detection System (Bio-Rad). Gene expression data were normalized to the housekeeping genes *RNA18S*, or *Ppia*.

Supplemental Table 2. Primer sequences

Gene	Accession number	Primer forward sequence	Primer reverse sequence
Abca1	NM_013454.3	ACAAGTCCATCGTGTCTCGC	GGGATGCTTGATCTGCCGTA
Abcg1	NM_009593.2	ACACCGATGTGAACCCGTTT	CAGATGTGTCAGGACCGAGT
Arhgef5	NM_133674.2	CAAGCTGCTGCTCCAGAACAT	CGCCGCATTCTCTGCACATT
Atp5i	NM_013795.5	GCCAAGGTTGAGCTGGTTCC	GCCACCAAACCATTCAGCACA
Atp5l	NM_007507.3	CGCCAAGCGCTACAGTTACC	TGTCATCTTGAGCTTCCGCCA
Bak1	NM_007523.3	CCCGTCCCCTTCTGAACAGC	ACCCACCTGACCCAAGATGC
Bax	NM_007527.4	GCCCGAGCTGATCAGAACCA	CATGTGGGGGTCCCGAAGTA
Bcl2	NM_009741.5	CAGGATAACGGAGGCTGGGATG	CCTCACTTGTGGCCCAGGTAT
CCL2	NM_002982	TTGATGTTTTAAGTTTATCTTTCATGG	CAGGGGTAGAACTGTGGTTCA
Cdk1	NM_007659.4	CACTCCCGGCGAGT TCTTCA	ACAGCGTCACTACC TCGTGT
Cdkn1a (p21)	NM_007669.5	CAGACCAGCCTGACAGATTTCTA	GAGTGAGGGCTAAGGCCGAA
Cdkn2a (p16)	NM_001040654.1	ATTCAGGTGATGATGATGGGCAACG	GGTAGTGGGGTCCTCGCAGT
Cox7b	NM_025379.2	GCCCAAGCATGGTGACTTCTC	TGACCCAGTGGGCTCCTAAAA
Ctsb	NM_007798.3	GCACGGGAACAATGGTCCAA	CTGCCCCAAATGCCCAACAAG
Ctsk	NM_007802.4	CACCCTTAGTCTTCCGCTCA	CTTGAACACCCACATCCTGCT
Ctsl	NM_001428555.1	CCTATGAAGCGAAGGACGGA	AGGGCTTTCTCTTGCTGAGG
Cxcl1	NM_008176.3	AACCGAAGTCATAGCCACACT	CCGTTACTTGGGGACACCTT
Cxcl10	NM_021274.2	GCCCACGTGTTGAGATCATTGCC	TCTCTGCTGTCCATCCATCGC
Diaph2	NM_172493.3	TCAGTGAGGCCCTAATCCAGAATC	ATGCTCGTGAGACGAGGACG
Fbxo32	NM_026346.3	TGACCGACCTCAGCAGTTAC	TTCTCTTCTTGGCTGCGACG
Foxo3	NM_001376967.1	GAAATGGGCAAAGCAGACCCT	GGATCACTGTCCACTTGCTGA
HIF1A	NM_001530.4	CGGGGACCGATTCACCAT	TTTCGACGTTCAGAACTTATCTTTT
Hif1a	NM_001313919	TCAAGCAGCAGGAATTGGAACAT	TCATCCATTGACTGCCCCAGC
Ifny	NM_008337	CAAGTTTGAGGTCAACAACCC	ACTCCTTTTCCGCTTCCTGA
Igf2bp2	NM_183029.2	TTGGATGGGCTGTTGGCTGA	GTGACGTTGACAACGGCAGTT
Il10	NM_010548.2	GCCCAGAAATCAAGGAGCAT	GAAATCGATGACAGCGCCT
Il6	NM_031168.2	AAGAAATGATGGATGCTACCAAACTG	GTACTCCAGAAGACCAGAGGAAATT
IL-8	NM_000584.4	GAGAAGTTTTTGAAGAGGGCTGA	GCTTGAAGTTTCACTGGCATCT
Itga1	NM_001033228.3	TTGGCCAACCCAAAGCAAGA	GGGCCCACATGCCAGAAATC
Itgb3	NM_016780.2	GGCGTTGTTGTTGGAGAGTCC	GGGGTGAGCCCTGAGACAAA
Lc3	NM_025735.3	CTCCGACCGGCCTTTCAA	TGATCACCG GGATCTTACTGG
Mmp2	NM_008610.2	CATCGCTGCACCATCGC	GCATGGTCTCGATGGTGTTC
MMP2	NM_001302510.1	CGTCGCCCATCATCAAGTTC	GAAGGTGTTCAGGTATTGCACTG
Mmp9	NM_013599.3	GCCGACTTTTGTGGTCTTCC	TACAAGTATGCCTCTGCCAGC
MMP9	NM_004994.2	TTCTGCCCGGACCAAGGATA	ACATAGGGTACATGAGCGCC
Myc	NM_001177353.1	TCGCCCAAATCCTGTACCTCG	GCCTCTTCTCCACAGACACCA
Ndudaf4	NM_010886.3	GCAAGCCAAGAAGCATCCCA	GTGCCAAGCGCATCACATACA
Ndufa3	NM_025348.3	GCCTGTGAGAGATGACGGGAA	TTGGAGAGCAACAGGGAAGGG
Ndufab1	NM_028177.4	GGATGTGGCTGCTGACTGGAA	TGACTAGGCCAGATGTGTGGG
Neat1	NR_131212.1; NR_003513.3	TGACAAAACCAGCAGACCC	CCACACCCAAATTACATACCAC
Nlrp3	NM_145827.3	AGCCTTCCAGGATCCTCTTC	CTTGGGCAGCAGTTTCTTTC
Ppia	NM_008907.1	GCGTCTCCTTCGAGCTGTTT	CACCCTGGCACATGAATCCT
Pten	NM_008960.2	GTGAGGATGGTAGGGGAAT	CACCACGCTTCAAAGAGAAA
Rac1	NM_009007.2	GCGAAAGAGATCGGTGCTGT	GACAGAGAACCGCTCGGATAG
RhoB	NM_007483.3	CGTGCCTGCTGATCGTGTTC	GACGTCGGTGTCCGGATAGG
RNA18S	NR_003278.3	AGGTCTGTGATGCCCTTAGA	GAATGGGGTTCAACGGGTTA
Tgfb	NM_011577.1	ACCCTGCCCCTATATTTGGA	CGGGTTGTGTTGGTTGTAGAG
TGFB	NM_000660	GTGGACATCAACGGG TTCACT	CGCACGCAGCAGTTCTTCTC
Tnf	NM_013693.2	CCATTCCTGAGTTCTGCAAAGG	AGGTAGGAAGGCCTGAGATCTTATC
VEGFA	NM_001171623.1	CGCTTACTCTCACCTGCTTCTG	GGTCAACCACTCACACACACAC
Vegfa	NM_001025250.3	CCACCATGCCAAGTGGTCCC	ACCAGGGTCTCAATCGGACG

6.1.22 RNA Stability Assay

To measure mRNA stability, 5×10^5 BMMs per well were seeded into 12-well plates, treated with 5 µg/mL Actinomycin D (Sigma, #A9415), and collected at the indicated time points. Total RNA was extracted using the RNA Quick-RNA Miniprep Kit (Zymo Research; #R1055) and analyzed by qRT-PCR.

6.1.23 Small RNA Sequencing

BMMs were seeded 1 x 10^6 cells per well on a 6-well plate and incubated overnight. RNA was isolated using miRNeasy Mini kit (#217004, Qiagen), respectively, according to the manufacturer's protocols. The RNA concentration was quantified by a Nanodrop spectrometer (ThermoFisher Scientific) at 260 nm. The small RNA library was prepared using the MGIEasy small RNA library preparation kit (#1000005269, MGI Tech). After 3' and 5' adapter ligation, cDNA was synthesized. After PCR amplification, the product was loaded onto a 6% TBE PAGE gel, and the portion of the gel corresponding to the appropriate size (100–120 bp) was extracted. The purified PCR product was subjected to denaturation and single-strand circularization, followed by enzymatic digestion and cleanup. The purified product was quantified with a Qubit ssDNA assay kit (#Q10212, Invitrogen). Fastq sequencing files were analyzed using the miRMaster pipeline with default parameters, as previously described (Fehlmann et al., 2021), with miRBase (release 22.1) as the reference database (Kozomara et al., 2019). As output, miRMaster generated a list of all mapped miRNAs, with expression values normalized to reads per million (RPM) of miRNA-mapped reads. Differential expression analysis was performed on normalized values using a two-tailed Student's t-test, with multiple testing corrections applied using the Benjamini-Hochberg method. The procedure was conducted as previously described (Mashayekhi et al., 2024).

6.1.24 Western Blot

BMMs were seeded at 1 x 10^6 cells per well in a 6-well plate and incubated overnight. Cells were lysed in a lysis buffer (50 mM Tris-HCl, 1% SDS, 10% glycerol, 5% 2-mercaptoethanol, 0.004% bromophenol blue) supplemented with a protease inhibitor mix (cOmplete; Roche Diagnostics, #04693124001). Western Blot was performed as previously described (Hoppstädter et al., 2019b). The lysates were sonicated, centrifuged at 10,000 × *g* for 10 min at 4°C, and stored at -80°C until further use. Before gel electrophoresis, all samples were denatured at 95°C for 5 min and placed on ice. SDS-polyacrylamide gel electrophoresis (PAGE) was performed using 4% stacking and 12% resolving polyacrylamide gels with the

Mini-PROTEAN® system (Bio-Rad). A prestained protein ladder (ThermoFisher Scientific, #26616) was used for molecular mass estimation. Electrophoresis was performed at 80 V for 15 min and then at 120 V for 1.5 h. After SDS-PAGE, the gel was placed on a Trans-Blot Turbo Midi Transfer Sandwich (#1704157, Bio-Rad). The transfer was performed using the Trans-Blot Transfer System (Bio-Rad), using Bio-Rad's Mixed Molecular Weight protocol, at 25 V and 2.5 A for 7 min. After membrane transfer, the membrane was blocked with Rockland Blocking Buffer (#MB-070, Rockland) for at least 1 hour at RT. Membranes were incubated overnight at 4°C with primary antibodies (1:1000 dilution in Rockland blocking buffer), followed by a 1.5-hour incubation at room temperature with IRDye 680- or IRDye 800-conjugated secondary antibodies (1:10,000 dilution in Rockland blocking buffer).

6.2 Results

6.2.1 IGF2BP2 KO in Myeloid Cells Does Not Affect Body Weight

In contrast to the complete IGF2BP2 KO mice, the myeloid-specific IGF2BP2 KO mice showed no reduction in body weight (Supplemental Figure 1). Dai et al. (2015) reported that mice with a complete IGF2BP2 KO weighed approximately 25% less than their WT littermates by 30 weeks of age and already exhibited a 2-gram reduction in body weight by 10 weeks.

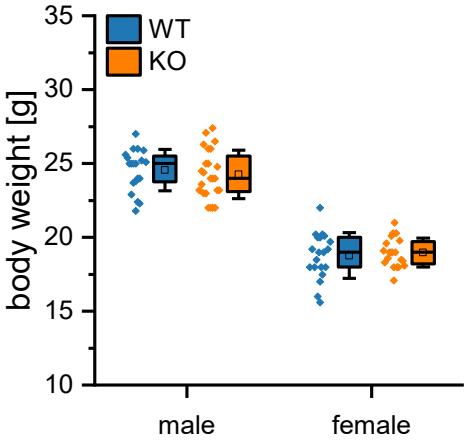

Supplemental Figure 1. Body weight in WT and IGF2BP2 KO mice. Eight-week-old mice were weighed (n = 20 mice per group). Box plots represent the 25th–75th percentiles (box), the median (line), and the standard deviation (whiskers). Squares indicate the mean, while bars represent the mean ± SEM.

6.2.2 Actin Cytoskeleton Organization Remains Unchanged in IGF2BP2 KO Macrophages

IGF2BP1 is known to selectively bind mRNAs encoding key proteins involved in cytoskeletal integrity and dynamics, such as ACTB and CD44 (Stöhr and Hüttelmaier, 2012). Similarly, IGF2BP2 has been implicated in regulating cell motility *via* pathways like PI3K/Akt and FAK/Src, which are critical for cell invasion and migration (Lin et al., 2024b; Yu et al., 2023). Our RNA-Seq analysis revealed the enrichment of GO terms related to cell migration and motility (Schymik, 2025, unpublished work). Additionally, Ingenuity Pathway Analysis (IPA) indicated significant activation of the KEGG Actin Cytoskeleton pathway, with 13 genes upregulated and 7 genes downregulated in IGF2BP2 KO macrophages (Supplemental Figure 2A).

To validate these findings, we analyzed the mRNA expression of *Arhgef5*, *Diaph2*, *Itga1*, *Itgb3*, *Rac1*, and *Rhob*. No significant differences were observed between WT and IGF2BP2 KO macrophages, except for *Itga1*, which was significantly upregulated in IGF2BP2 KO M2-polarized macrophages treated with IL-4 compared to WT M2 (Supplemental Fig. 2B).

To assess the impact of IGF2BP2 loss on cytoskeletal organization, we performed F-actin staining using rhodamine-phalloidin and visualized macrophages via confocal laser scanning microscopy (CLSM) (Supplemental Fig. 2C-F). Quantifying F-actin intensity showed no significant differences in total F-actin levels or nuclear F-actin intensity between WT and KO macrophages. However, KO macrophages exhibited a slight increase in the elongation index (Supplemental Fig. 2F).

We conducted real-time deformability cytometry (RT-DC) to examine mechanical properties, which measure cell deformation under shear stress as cells pass through a microfluidic channel. No significant changes were detected in the cell area, deformation, or Young's modulus between WT and IGF2BP2 KO macrophages (Supplemental Fig. 2G-J).

Although our findings indicate that myeloid-specific IGF2BP2 KO does not significantly alter actin cytoskeleton organization in macrophages, further studies are needed to explore potential compensatory mechanisms and long-term effects on macrophage function.

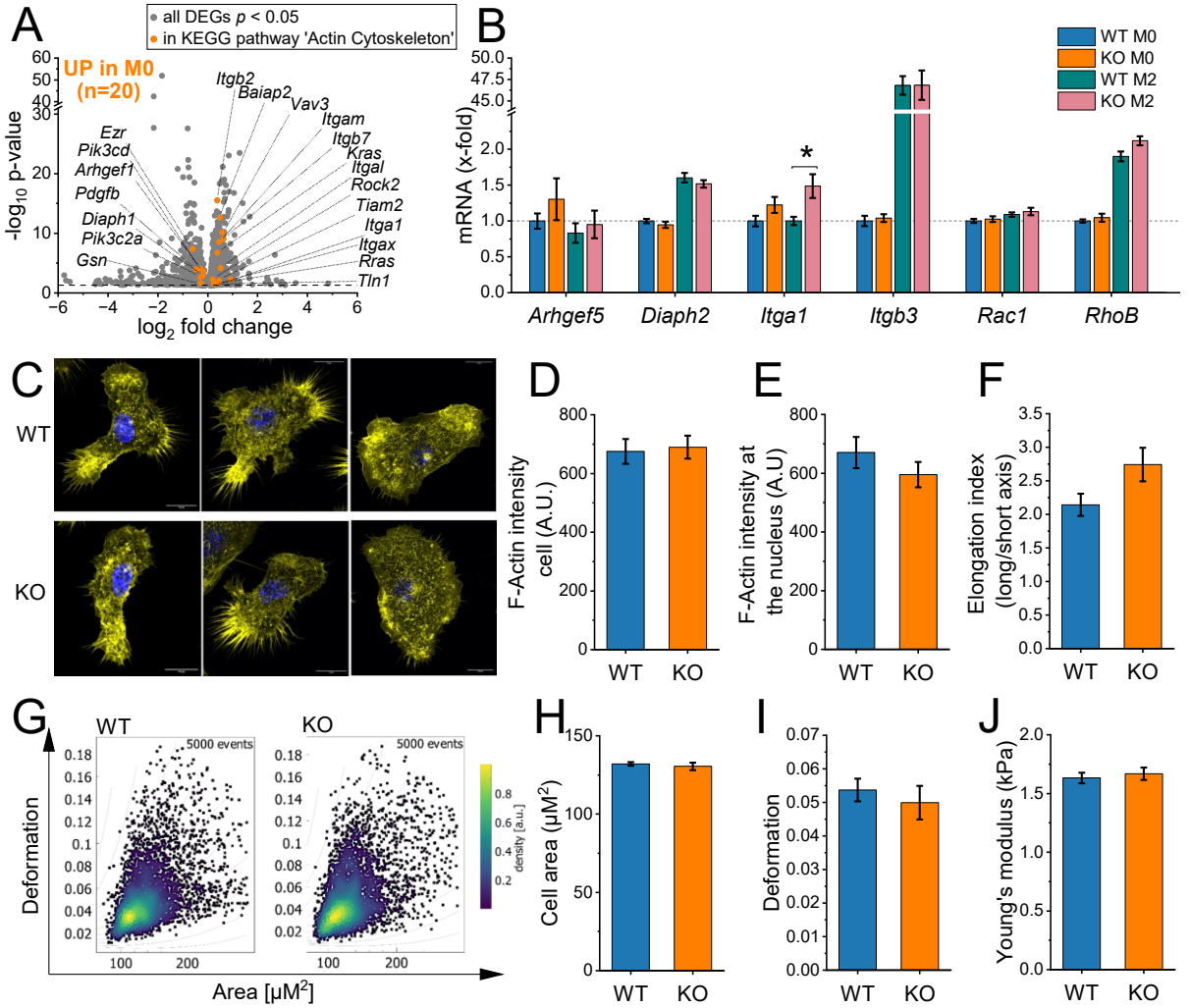

Supplemental Figure 2. Analysis of actin cytoskeleton organization and mechanical properties in WT and IGF2BP2 KO BMMs. (A) Volcano plot displaying differentially expressed genes (DEGs; $p < 0.05$, shown in gray) in untreated IGF2BP2 KO BMMs compared with WT BMMs. Genes associated with the KEGG actin cytoskeleton pathway are highlighted in orange (n = 3 mice per group). **(B)** mRNA expression analysis of BMMs cultured in standard media (M0) or treated with IL-4 (20 ng/ml, 8 h) to induce M2 polarization. mRNA was normalized to *Ppia* and is shown as fold change relative to untreated WT controls. **(C)** F-actin was stained with rhodamine-phalloidin (yellow) and nuclei with DAPI (blue). Images were acquired using confocal laser scanning microscopy (CLSM) (scale bar = 10 µm). **(D–F)** Quantification of actin cytoskeleton properties: **(D)** Total F-actin intensity. **(E)** F-actin intensity at the nucleus expressed in arbitrary units (A.U.). **(F)** Elongation index, calculated as the ratio of the long cellular axis to the short axis (n = 4 mice per group, 5 cells analyzed per mouse). **(G–K)** RT-DC was used to assess the mechanical properties of WT and IGF2BP2 KO BMMs: **(H)** cell size **(I)** cell deformation, representing the extent of cell shape changes under shear stress. **(J)** Young's modulus (kPa), indicating cellular stiffness (n = 4 mice per group). Data are presented as mean ± SEM. Statistical significance was determined using one-way ANOVA followed by Bonferroni post hoc tests (B) (*$p < 0.05$; **$p < 0.01$; ***$p < 0.001$).

6.2.3 IGF2BP2 KO Reduces the Phagocytic Capacity of Macrophages

Macrophages are central to host defense, not only by producing cytokines but also through phagocytosis, a key mechanism for eliminating pathogens and tumor cells. To assess phagocytic capacity, we performed live-cell imaging using pHrodo™ *S. aureus* bioparticles, which fluoresce upon engulfment. As shown in Supplemental Figure 3A, quantitative analysis revealed that IGF2BP2 KO macrophages exhibited significantly reduced phagocytic activity compared to WT macrophages.

To further investigate the role of IGF2BP2 in tumor cell phagocytosis, we labeled LLC1 tumor cells with pHrodo™ and incubated them with macrophages. Since CD47, a well-established "don't eat me" signal, is expressed on tumor cells to inhibit phagocytosis, we used anti-CD47 antibodies to enhance their engulfment by macrophages (Nam et al., 2019). Notably, KO macrophages displayed a significantly lower capacity to engulf tumor cells, indicating that IGF2BP2 deficiency impairs macrophage-mediated tumor clearance (Supplemental Figure 3B).

Our findings demonstrate that IGF2BP2 deficiency impairs macrophage phagocytosis of bacteria and tumor cells. Rather than enhancing engulfment, IGF2BP2 KO macrophages exhibited a reduction in phagocytic capacity, suggesting a crucial role for IGF2BP2 in macrophage-mediated clearance.

Previous studies have highlighted the enhanced phagocytic capacity of M2-like macrophages, particularly in the context of *E. coli* and tumor cells (Kapellos et al., 2016b; Li et al., 2024c). Jaggi et al. (2020) further highlight the enhanced phagocytic role of M2 macrophages during HSV-1 infection. These findings support the conventional role of M2 macrophages in tissue remodeling and clearance of apoptotic cell clearance, processes that require efficient phagocytosis (Wynn and Vannella, 2016).

However, this apparent superiority is not universally observed. Lam et al. (2016) reported that while M2 macrophages appeared to internalize more *E. coli* particles under the microscope, pHrodo-based assays indicated lower effective phagocytosis. This may suggest that rapid phagosomal acidification in M2 macrophages promotes degradation pathways better suited for apoptotic debris than for the processing and elimination of live bacteria. This observation is supported by Canton et al. (2014), who found that M2 macrophages prioritize fast acidification over microbial killing, thereby limiting their antimicrobial efficacy.

In contrast, M1 macrophages, although sometimes exhibiting lower phagocytic rates, are characterized by strong bactericidal properties mediated by the production of reactive ROS and the release of proinflammatory cytokines (Chakraborty and Diwan, 2024; Kohno et al., 2021; Rabani et al., 2018). In other studies, M1 macrophages show effective clearance of gram-negative bacteria such as *P. gingivalis* and *E. coli* (Lam et al., 2016; Schulz et al., 2019), and also exhibit enhanced phagocytosis of tumor cells (Zhang et al., 2016).

If IGF2BP2 KO macrophages exhibit a shift toward a more inflammatory, M1-like phenotype, the observed reduction in phagocytic activity is paradoxical and not easily explained by the existing literature. Impaired cytoskeletal remodeling may explain the reduced phagocytosis in IGF2BP2 KO macrophages. Efficient phagocytosis requires actin polymerization for the formation of filopodia and lamellipodia (Mei et al., 2023). In addition, myosin-Ie/f stabilizes F-actin at the phagocytic cup, while myosin-II generates contractile forces for cup closure, both of which may be impaired in IGF2BP2 KO macrophages (Barger et al., 2022; Vorselen et al., 2021).

While our findings highlight IGF2BP2 as a key regulator of macrophage phagocytosis, the precise mechanisms by which it influences cytoskeletal remodeling, inflammatory signaling, and receptor regulation remain unclear and warrant further investigation.

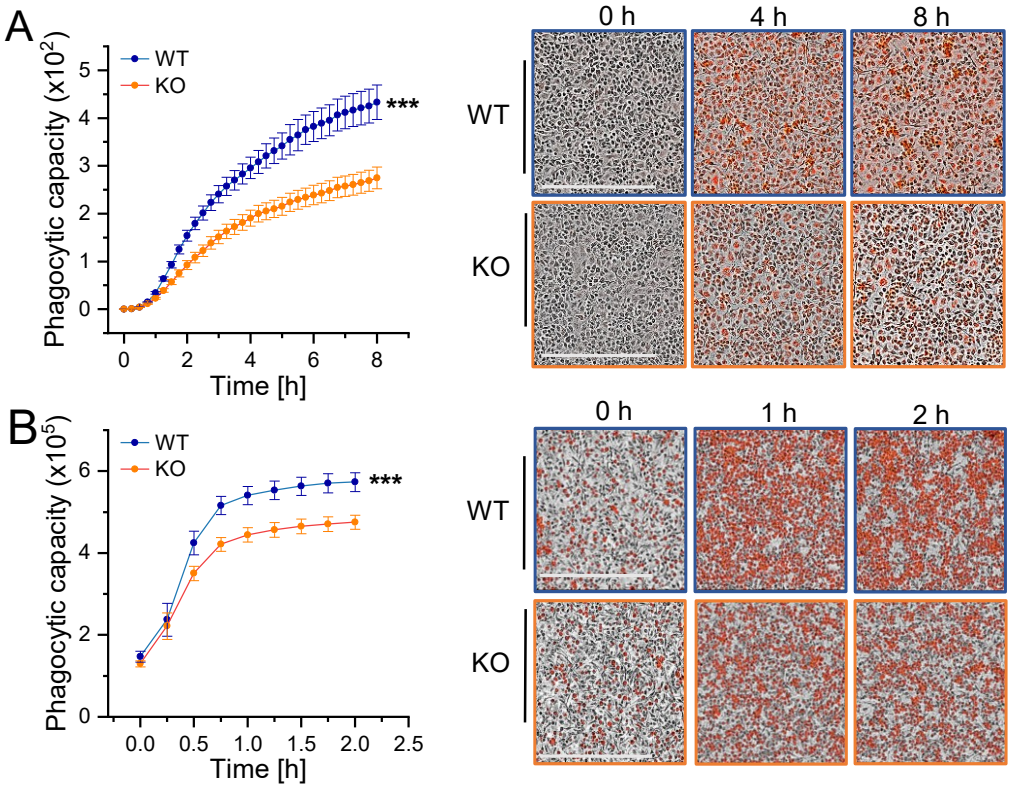

Supplemental Figure 3. IGF2BP2 KO macrophages exhibit reduced bacterial and tumor cell

engulfment. (A) Phagocytosis of pHrodo™ particles (n = 4 mice per group, quadruplicates), **(B)** Tumor cell phagocytosis of pHrodo™-labeled LLC1 cells (n = 4 mice per group, triplicates) was assessed using live-cell imaging with the Incucyte® S3 system. Representative images are shown. The fluorescent signal is shown in the color red. Phagocytic capacity was quantified as the total red object integrated intensity (RCU × µm²/image), normalized to initial cell confluency (%) Scale bar: 400 µm. Statistical significance was determined using two-way ANOVA followed by Bonferroni post hoc tests (*$p < 0.05$; **$p < 0.01$; ***$p < 0.001$).

6.2.4 Autophagy Regulation in IGF2BP2 KO Macrophages

Autophagy plays a critical role in macrophage function, contributing to the elimination of intracellular pathogens, regulation of cytokine production, and control of inflammatory responses (Bah and Vergne, 2017; Wu and Lu, 2020). It enhances the ability of macrophages to eliminate pathogens, mainly intracellular pathogens such as mycobacteria, by promoting their antimicrobial functions (Tatano et al., 2024). In addition, autophagy regulates cytokine production, ensuring a balanced inflammatory response that prevents excessive tissue damage (Vitaliti et al., 2024).

Autophagy plays a key role in TAM polarization by regulating the balance between pro-inflammatory (M1) and anti-inflammatory (M2) states, which can either promote or inhibit tumor growth (Jing et al., 2023). Inhibiting autophagy in TAMs has been shown to enhance their M1 phenotype, improving anti-tumor immunity. Targeted modulation of autophagy pathways may help reverse their immunosuppressive phenotype, leading to better therapeutic outcomes in cancers such as urothelial carcinoma (Singh et al., 2024; Yu et al., 2024).

Furthermore, IGF2BP2 has been implicated in autophagy regulation, particularly in glioma, where its depletion enhances autophagic activity (Li et al., 2024b).

In our study, genes within the KEGG Autophagy pathway were significantly upregulated in IGF2BP2 KO macrophages (Supplemental Fig. 4A). Notably, several core autophagy-related genes (ATGs), including *Atg4c*, *Atg13*, *Atg2a*, *Atg4a*, *Atg7*, and *Atg9a*, were induced in KO macrophages. To functionally assess the autophagic flux, we treated BMMs with bafilomycin A1, an inhibitor of lysosomal degradation, and measured LC3-II accumulation *via* Western blot. Quantifying LC3-II protein levels relative to Tubulin revealed a significant induction in KO compared to WT BMMs (Supplemental Figure 4B, C), indicating enhanced autophagic processing in the absence of IGF2BP2.

Given the influence of the tumor microenvironment on macrophage autophagy, we next cultured BMMs in TCM from LLC1 cells for 8 hours to induce a TAM-like phenotype. Under these conditions, *Lc3* mRNA expression was significantly induced in WT and KO macrophages (Supplemental Figure 4D).

To further investigate the role of IGF2BP2 in autophagy under metabolic stress, we subjected BMMs to nutrient starvation or treatment with the autophagy inducer rapamycin. KO BMMs exhibited significantly lower *Lc3* gene expression following rapamycin treatment than WT cells

(Supplemental Figure 4E). Given the known regulation of IGF2BP2 by cellular stress, such as hypoxia, we next examined whether its expression is influenced by starvation. Notably, *Igf2bp2* gene expression significantly increased in WT BMMs upon nutrient deprivation (Supplemental Figure. 4F).

In addition, we examined the expression of F-box only protein 32 (FBXO32), a FOXO3-regulated ubiquitin ligase involved in autophagosome-lysosome fusion (Murdoch et al., 2016). *Fbxo32* and *Foxo3* were downregulated in KO macrophages, regardless of condition (M0, starvation, or Rapamycin treatment) (Supplemental Figure 4G).

Following autophagosome-lysosome fusion, lysosome-derived cathepsins play a critical role in degrading engulfed contents, a process essential for autophagy (Man and Kanneganti, 2016). Expression analysis of *Ctsb* and *Ctsk* revealed a significant reduction in KO macrophages under basal (M0), starvation, and Rapamycin-treated conditions. However, *Ctsb* expression did not significantly differ between WT and KO macrophages (Supplemental Figure 4H).

Ultimately, these results present a partially contradictory pattern: while RNA-seq and LC3-II Western blot analyses indicate increased autophagic activity and flux, expression levels of specific autophagy-related genes (e.g., *Foxo3*, *Fbxo32*, *Ctsk*) were reduced under basal and stress conditions. This discrepancy suggests that IGF2BP2 may play a complex, context-dependent role in regulating macrophage autophagy. Further studies are needed to clarify its precise mechanistic contribution.

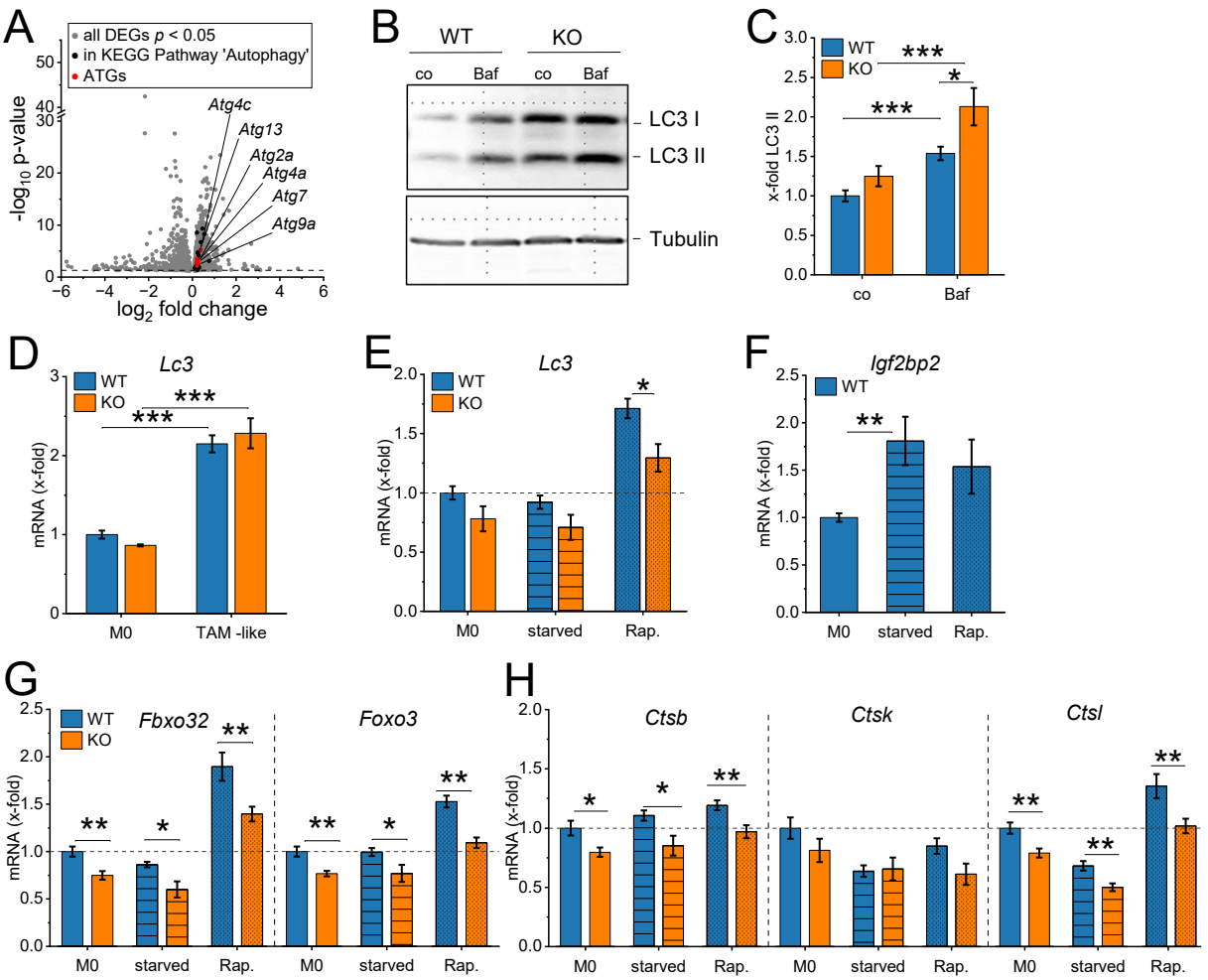

Supplemental Figure 4. Autophagy-related gene expression and functional analysis in IGF2BP2 KO macrophages. (A) Volcano plot showing DEGs ($p < 0.05$, shown in gray) in untreated IGF2BP2 KO BMMs compared with WT BMMs. Genes associated with the KEGG autophagy pathway are highlighted in black, and autophagy-related genes (ATG) are marked in red (n = 3 mice per group). **(B, C)** BMMs were treated with bafilomycin A1 (10 nM) for 4 h to induce autophagy. LC3-II protein levels were measured and normalized to Tubulin (n = 5 mice per group, duplicates). **(D)** BMMs were cultured in standard medium (M0) or TCM from LLC1 cells (TAM-like) for 8 h (n = 4 mice per group, duplicate). **(E-H)** BMMs were treated with medium supplemented with 1% FCS (starved), or Rapamycin (100 nM) for 24 h (n = 5, duplicate). **(D-H)** mRNA expression was normalized to *Ppia* and is expressed as x-fold-change to untreated WT controls. Data are presented as mean ± SEM. Statistical significance was determined using one-way ANOVA followed by Bonferroni post hoc tests (*$p < 0.05$; **$p < 0.01$; ***$p < 0.001$).

6.2.5 Pyroptosis and Inflammasome Regulation in IGF2BP2 KO Macrophages

Inflammatory responses are central to the pathogenesis of many diseases. One of the key mechanisms involved in the activation of the NLRP3 inflammasome is the induction of pyroptosis, a pro-inflammatory form of programmed cell death (Blevins et al., 2022). Emerging evidence suggests that IGF2BP2 plays a critical role in modulating NLRP3 inflammasome activation through post-transcriptional regulation across different pathological contexts.

In Alzheimer's disease and acute lung injury, IGF2BP2 functions as a positive regulator of NLRP3 inflammasome activation by stabilizing *NLRP3* mRNA. Inhibition of IGF2BP2 in these conditions has been shown to reduce *NLRP3* expression, thereby mitigating pyroptosis and inflammation (Cao et al., 2024; Jingrui et al., 2025).

In contrast, in ischemic stroke, IGF2BP2 appears to exert an opposite effect, acting as an inflammasome suppressor in microglia. In this context, IGF2BP2, in concert with FTO, has been reported to inhibit NLRP3 inflammasome activation by decreasing the m^6A modification of NLRP3 transcripts. Notably, TMAO treatment downregulates IGF2BP2 expression, leading to enhanced NLRP3 activation and exacerbated neurological injury (Ge et al., 2023).

In our study, GO analysis of the term "pyroptosis" revealed no significant induction. Among the DEGs with a fold change >1.5, we observed an upregulation of *Tlr4* and *Tlr5*, whereas *Nfkb2*, *Tlr2*, *Nlrp3*, *Tnf,* and *Il1b* were downregulated (Supplemental Figure 5A). Notably, *Nlrp3* expression exhibited a slight but significant reduction in KO IGF2BP2 macrophages, as validated by qPCR (Supplemental Figure 5B). To assess whether IGF2BP2 affects *Nlrp3* mRNA stability, BMMs were treated with the transcription inhibitor actinomycin D. However, no significant differences in *Nlrp3* mRNA degradation rates were observed between WT and IGF2BP2 KO BMMs (Supplemental Figure 5B, C).

Contrarily, the long non-coding RNA *Neat1*, known to promote inflammasome activation in macrophages (Zhang et al., 2019), was upregulated in IGF2BP2 KO BMMs (Supplemental Figure 5D).

To further evaluate the impact of IGF2BP2 on inflammasome-mediated cell death, we assessed caspase-3/7 activity and membrane integrity in BMMs after LPS priming and ATP treatment. Live cell imaging revealed a significant increase in caspase-3/7 activity in IGF2BP2 KO macrophages compared to WT cells (Supplementary Figure 5E). In contrast, cytotoxicity, as measured by Cytotox Red fluorescence, a marker of compromised plasma membrane integrity,

was equally elevated in both genotypes upon treatment (Supplementary Figure 5F), indicating comparable levels of terminal membrane damage. The disproportion between increased caspase-3/7 activation and unchanged membrane damage in IGF2BP2 KO macrophages suggests a shift towards apoptotic signaling rather than enhanced pyroptosis. As caspase-3 is not a canonical mediator of pyroptosis, and pyroptotic cell death is typically characterized by gasdermin (GSDM) D activation downstream of caspase-1, these results point to an inflammasome-independent form of programmed cell death (Yu et al., 2021). The potential involvement of GSDME-mediated secondary pyroptosis seems unlikely in this context, given the lack of increased membrane permeability in the KO group.

Additionally, the production of reactive oxygen species (ROS), which act as upstream activators of the NLRP3 inflammasome, was significantly reduced in IGF2BP2 KO macrophages following LPS and ATP treatment (Supplemental Figure 5G). This finding aligns with the observed downregulation of *Nlrp3* mRNA (Figure 5A, B) and supports the notion of attenuated inflammasome activity in IGF2BP2-deficient cells.

Together, these findings suggest that IGF2BP2 deficiency does not enhance canonical inflammasome activation or pyroptosis but may sensitize macrophages to apoptosis or alternative caspase-3/7-driven, non-lytic forms of cell death under inflammasome-activating conditions.

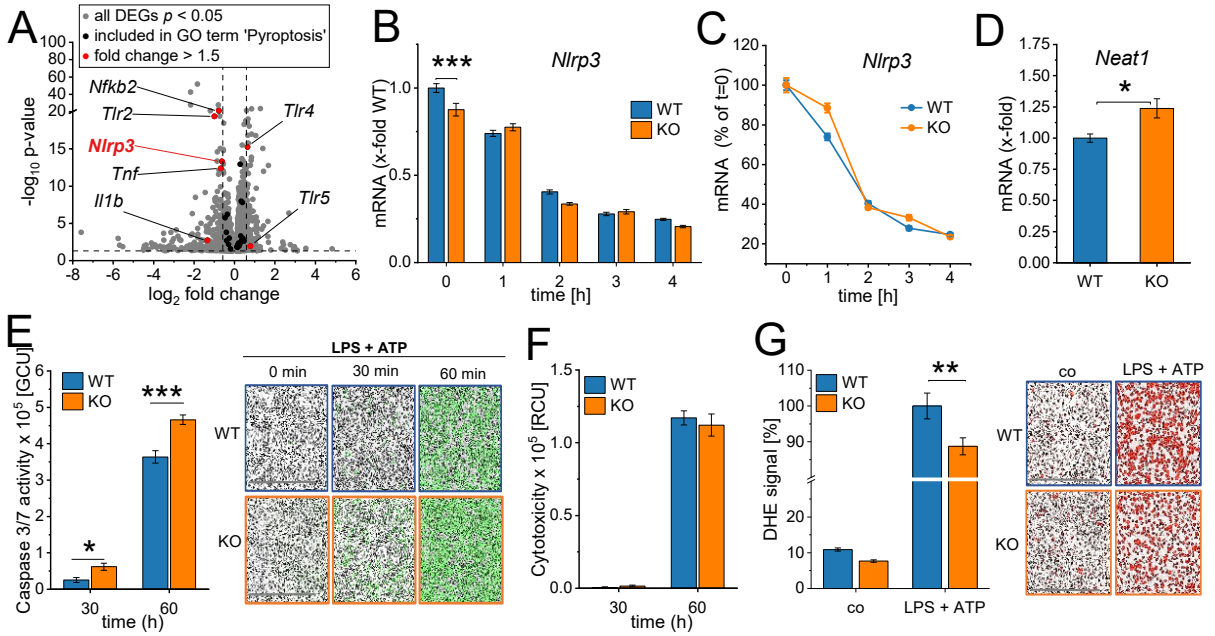

Supplemental Figure 5. Analysis of inflammasome activation in IGF2BP2 KO and WT BMMs. **(A)** Volcano plot displaying DEGs ($p < 0.05$, shown in gray) in untreated IGF2BP2 KO BMMs compared to WT BMMs. Genes associated with the GO term "pyroptosis" (GO:0008219) are highlighted in black, while those with a fold change > 1.5 are marked in red (n = 3 mice per group). **(B)** *Nlrp3* mRNA degradation in BMMs treated with actinomycin D for the indicated time points, expressed as fold change relative to untreated WT controls. **(C)** Residual RNA levels were normalized to 0 h and set 100% (n = 4 mice per group, duplicates). **(D)** mRNA expression of *Neat1* in WT and KO BMMs normalized to *Ppia* (n = 4 mice per group, duplicates). **(E)** Caspase-3/7 activity (green fluorescence) and **(F)** cytotoxicity (red fluorescence) in LPS-primed BMMs after ATP treatment, measured by real-time live cell imaging using the Incucyte® S3 system (n = 4 mice per group, triplicates). **(G)** Detection of ROS by DHE fluorescence in untreated BMMs (co) and 30 min after ATP treatment in LPS-treated BMMs. Fluorescence intensity was normalized to treated WT controls (set to 100%, n = 4 mice per group, quadruplicates). Scale bar: 400 µm. p-values were determined using one-way ANOVA followed by Bonferroni post-hoc tests (E, G) or student's t-test (B, D) (*$p < 0.05$; **$p < 0.01$; ***$p < 0.01$).

6.2.6 Differential miRNA Expression in IGF2BP2 KO BMMs

IGF2BP2 has emerged as a multifaceted regulator of post-transcriptional gene expression, particularly through its interactions with microRNAs (miRNAs). These interactions occur through several distinct mechanisms, allowing IGF2BP2 to both influence and be influenced by miRNA-mediated regulation.

One prominent mechanism involves IGF2BP2 functioning as a co-regulator of miRNA activity. Qian et al. (2021) demonstrated that IGF2BP2 forms a complex with AGO2 to enhance the repressive activity of miR-133a on its targets during cardiac development and hypertrophy. This effect depends on m^6A modifications at the miR-133a binding sites, which facilitate stronger miRNA-mRNA interactions, highlighting IGF2BP2's role as a reader of m^6A in modulating miRNA function.

In addition to supporting miRNA function, IGF2BP2 is a direct target of several tumor-suppressive miRNAs. For example, miR-129-5p directly binds and downregulates IGF2BP2 in glioblastoma cells, leading to reduced proliferation, increased apoptosis, and enhanced chemosensitivity (Wang et al., 2021d). Similarly, miR-188 targets IGF2BP2 in glioma, suppressing tumor cell growth, migration, and invasion (Ding et al., 2017).

Moreover, IGF2BP2 can act as a competitive binder at shared mRNA sites, thereby reducing the regulatory impact of miRNAs. Notably, genes that are co-targeted by IGF2BP2 and multiple miRNAs tend to be upregulated in IGF2BP2-overexpressing livers, suggesting that IGF2BP2 may shield these transcripts from miRNA-mediated repression by competing for overlapping binding sites (Dehghani Amirabad et al., 2018).

To further elucidate the impact of IGF2BP2 deficiency on miRNA regulation in macrophages, we performed miRNA-Seq analysis in IGF2BP2 KO and WT BMMs. This analysis identified 3 significantly upregulated and 22 significantly downregulated miRNAs (Supplemental Figure 6).

Notably, three members of the *let-7* family (*let-7c-2-3p*, *let-7a-1-3p*, and *let-7b-3p*) were significantly downregulated in IGF2BP2 KO BMMs. Mechanistically, IGF2BP2 has been shown to bind to the *let-7* miRNA response element and inhibit let-7 miRNA-mediated RNA degradation (Cao et al., 2021). This suggests that in IGF2BP2 KO BMMs, the loss of IGF2BP2 leads to reduced stability or impaired biogenesis of *let-7* miRNAs, resulting in their overall downregulation. Interestingly, IGF2BP2 itself is a direct target of *let-7* family members, specifically *let-7b* and *let-7i*, which post-transcriptionally regulate its expression and

downstream signaling pathways (Fawzy et al., 2016). Furthermore, *let-7b* has been demonstrated to inhibit cell migration in keratinocytes by targeting IGF2BP2 (Wu et al., 2017).

We identified several miRNAs with anti-inflammatory properties that were downregulated in IGF2BP2 KO cells, including *miR-146b-5p*, *let-7c*, and *miR-26a-2-3p*. *miR-146b-5p* acts as an inhibitor of NF-κB-mediated inflammation and is required for the anti-inflammatory effects of high levels of globular adiponectin (Song et al., 2013). *Let-7c* promotes the transition from pro-inflammatory (M1) to anti-inflammatory (M2) macrophages, mainly through the PTEN-mediated PI3K/Akt pathway (Lu et al., 2024). Additionally, *let-7c* suppresses the production of pro-inflammatory cytokines such as IL-1β, IL-6, and TNF, suggesting its therapeutic potential in inflammatory diseases such as osteoarthritis and rheumatoid arthritis (Law et al., 2021). *miR-26a-2-3p* inhibits NF-κB and STAT3 activation, leading to a reduction in IL-6 production in macrophages, which is crucial for regulating intestinal inflammation and preventing colitis-associated cancer (Zhang et al., 2021). In monocytes, *miR-26a-2-3p* also regulates interferon-stimulated genes, modulating inflammation in systemic sclerosis (Ciechomska et al., 2020). The downregulation of these miRNAs in IGF2BP2 KO BMMs suggests that IGF2BP2 deficiency promotes a pro-inflammatory macrophage phenotype.

To further understand the functional impact of these differentially expressed miRNAs, we conducted KEGG pathway enrichment analysis using miRPathDB (Supplemental Table 3, 4). The analysis revealed that downregulated miRNAs target pathways such as “Regulation of the Actin Cytoskeleton,” “Endocytosis,” and “Protein Processing in the Endoplasmic Reticulum”. Interestingly, mRNA transcripts associated with these pathways were upregulated, as shown by RNA-Seq data (Schymik et al., 2025, submitted; see Part II). These findings suggest a potential compensatory mechanism, where IGF2BP2 depletion alters miRNA expression.

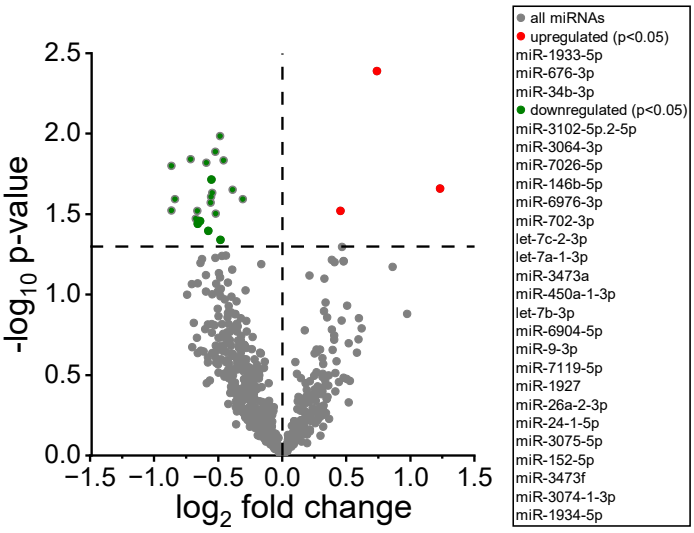

Supplemental Figure 6. Differential miRNA expression in IGF2BP2 KO BMMs. miRNA-Seq analysis was performed to identify differentially expressed miRNAs in untreated IGF2BP2 KO BMMs compared to WT BMMs. The volcano plot displays $\log_2$ fold change against $-\log_{10}$ *p*-value. Red indicates miRNAs that are upregulated in IGF2BP2 KO BMMs ($p < 0.05$), while green represents downregulated miRNAs ($p < 0.05$) (n = 4 mice per group).

Supplemental Table 3. KEGG Pathway Analysis for Upregulated miRNAs. KEGG pathway analysis was performed using miRPathDB. Pathways were identified by sorting KEGG annotations for each upregulated miRNA.

KEGG pathways from miRNA downregulated	**Number of miRNAs Targeting Pathway**	**miRNAs Involved**
Calcium signaling pathway	2	*miR-676-3p, miR-1933-5p*
Ras signaling pathway	2	*miR-1933-5p*
Endocytosis	1	*miR-1933-5p*
Focal adhesion	1	*miR-1933-5p*
FoxO signaling pathway	1	*miR-34b-3p*
mTOR signaling pathway	1	*miR-1933-5p*
Peroxisome	1	*miR-1933-5p*
Ubiquitin mediated proteolysis	1	*miR-34b-3p*

Supplemental Table 4. KEGG Pathway Analysis for Downregulated miRNAs. KEGG pathway analysis was performed using miRPathDB. Pathways were identified by sorting KEGG annotations for each downregulated miRNA.

KEGG pathways from miRNA downregulated	Number of miRNAs Targeting Pathway	miRNAs Involved
Foxo signaling pathway	17	*miR-3064-3p, miR-7026-5p, miR-146b-5p, miR-6976-3p, miR-702-3p, let-7c-2-3p, miR-3473a, miR-450a-1-3p, let-7b-3p, miR-6904-5p, miR-9-3p, miR-7119-5p, miR-26a-2-3p, miR-3075-5p, miR-152-5p, miR-3473f, miR-1934-5p*
Rap1 signaling pathway	17	*miR-3102-5p.2-5p, miR-3064-3p, miR-7026-5p, miR-6976-3p, miR-702-3p, let-7c-2-3p, miR-3473a, miR-450a-1-3p, let-7b-3p, miR-6904-5p, miR-9-3p, miR-7119-5p, miR-26a-2-3p, miR-24-1-5p, miR-3075-5p, miR-152-5p, miR-1934-5p*
Calcium signaling pathway	15	*miR-3102-5p.2-5p, miR-3064-3p, miR-7026-5p, miR-6976-3p, miR-702-3p, let-7c-2-3p, miR-3473a, miR-450a-1-3p, miR-6904-5p, miR-7119-5p, miR-26a-2-3p, miR-24-1-5p, miR-3075-5p, miR-152-5p, miR-1934-5p*
Hippo signaling pathway	15	*miR-3102-5p.2-5p, miR-3064-3p, miR-7026-5p, miR-146b-5p, miR-6976-3p, miR-702-3p, let-7c-2-3p, miR-450a-1-3p, miR-6904-5p, miR-9-3p, miR-7119-5p, miR-26a-2-3p, miR-3075-5p, miR-3473f, miR-1934-5p*
Wnt signaling pathway	14	*miR-3102-5p.2-5p, miR-3064-3p, miR-7026-5p, miR-6976-3p, miR-702-3p, miR-3473a, miR-450a-1-3p, miR-6904-5p, miR-7119-5p, miR-26a-2-3p, miR-24-1-5p, miR-3075-5p, miR-3473f, miR-1934-5p*
Endocytosis	14	*miR-3102-5p.2-5p, miR-3064-3p, miR-7026-5p, miR-146b-5p, miR-6976-3p, miR-702-3p, let-7c-2-3p, miR-3473a, let-7b-3p, miR-6904-5p, miR-7119-5p, miR-26a-2-3p, miR-3075-5p, miR-3473f*
PI3K-Akt signaling pathway	14	*miR-3102-5p.2-5p, miR-3064-3p, miR-146b-5p, miR-6976-3p, miR-702-3p, let-7c-2-3p, miR-3473a, miR-450a-1-3p, let-7b-3p, miR-7119-5p, miR-26a-2-3p, miR-3075-5p, miR-152-5p, miR-3473f*
Focal adhesion	14	*miR-7026-5p, miR-146b-5p, miR-702-3p, let-7c-2-3p, miR-3473a, miR-450a-1-3p, let-7b-3p, miR-6904-5p, miR-9-3p, miR-7119-5p, miR-3075-5p, miR-152-5p, miR-3473f, miR-1934-5p*
mTOR signaling pathway	13	*miR-3064-3p, miR-6976-3p, miR-702-3p, miR-3473a, miR-450a-1-3p, miR-6904-5p, miR-9-3p, miR-7119-5p, miR-26a-2-3p, miR-3075-5p, miR-152-5p, miR-3473f, miR-1934-5p*
MAPK signaling pathway	13	*miR-3064-3p, miR-7026-5p, miR-6976-3p, miR-702-3p, miR-3473a, miR-450a-1-3p, miR-6904-5p, miR-7119-5p, miR-26a-2-3p, miR-3075-5p, miR-152-5p, miR-3473f, miR-1934-5p*
Regulation of actin cytoskeleton	12	*miR-7026-5p, miR-146b-5p, miR-6976-3p, miR-702-3p, let-7c-2-3p, miR-3473a, let-7b-3p, miR-9-3p, miR-7119-5p, miR-3075-5p, miR-3473f, miR-1934-5p*
Other types of O-glycan biosynthesis	8	*miR-3064-3p, miR-6976-3p, miR-702-3p, miR-6904-5p, miR-9-3p, miR-7119-5p, miR-26a-2-3p, miR-1934-5p*
Ubiquitin mediated proteolysis	8	*miR-3064-3p, miR-7026-5p, miR-702-3p, let-7c-2-3p, miR-450a-1-3p, let-7b-3p, miR-6904-5p, miR-9-3p*
TGF-beta signaling pathway	8	*miR-6976-3p, miR-702-3p, let-7c-2-3p, let-7b-3p, miR-9-3p, miR-7119-5p, miR-3075-5p, miR-3473f*
Phosphatidylinositol signaling system	8	*miR-3064-3p, miR-146b-5p, miR-702-3p, miR-3473a, miR-450a-1-3p, miR-6904-5p, miR-7119-5p, miR-3075-5p*

Protein processing in endoplasmic reticulum	8	*miR-702-3p, let-7c-2-3p, miR-3473a, let-7b-3p, miR-6904-5p, miR-9-3p, miR-152-5p, miR-3473f*
HIF-1 signaling pathway	6	*miR-702-3p, let-7c-2-3p, miR-450a-1-3p, miR-6904-5p, miR-7119-5p, miR-3075-5p*
TNF signaling pathway	6	*miR-3064-3p, miR-6976-3p, miR-3473a, miR-450a-1-3p, miR-7119-5p, miR-3473f*
Chemokine signaling pathway	5	*miR-450a-1-3p, miR-6904-5p, miR-7119-5p, miR-152-5p, miR-1934-5p*
Hedgehog signaling pathway	5	*miR-6976-3p, miR-702-3p, miR-6904-5p, miR-3075-5p, miR-3473f*
Jak-STAT signaling pathway	4	*miR-3064-3p, miR-7119-5p, miR-152-5p, miR-3473f*
VEGF signaling pathway	4	*miR-702-3p, miR-3473a, miR-6904-5p, miR-7119-5p*
Fc gamma R-mediated phagocytosis	3	*miR-9-3p, miR-7119-5p, miR-3075-5p*
Peroxisome	3	*miR-702-3p, miR-450a-1-3p, miR-26a-2-3p*

6.2.7 Surface Marker Expression in IGF2BP2 KO Macrophages

To further characterize and distinguish WT and IGF2BP2 KO macrophages across different polarization states, we performed a flow cytometric analysis of CD80 and CD86, which are expressed on inflammatory (M1) macrophages, as well as CD163 and CD206, which are markers of anti-inflammatory (M2) macrophages. BMMs from WT and IGF2BP2 KO mice were polarized into M0 (unstimulated), M2 (IL-4-treated), or TAM-like (treated with TCM from LLC1 cells).

CD80 and CD163 expression levels remained comparable across different polarization states, indicating no significant modulation of these markers. CD86 expression was significantly elevated in WT TAM-like macrophages compared to WT M0, indicating a partly inflammatory phenotype in response to TCM. CD206 expression was markedly increased in M2 macrophages compared to WT M0, reinforcing its role as an M2 marker. In contrast, CD80 and CD86 expression levels were significantly reduced in IGF2BP2 KO M2 macrophages compared to WT M2, indicating a potential impairment in M2 polarization (Supplemental Figure 7).

Interestingly, the reduced expression of CD80 and CD86 in KO M2 macrophages does not align with our initial hypothesis. This unexpected result suggests that additional markers should be investigated to further clarify the phenotype.

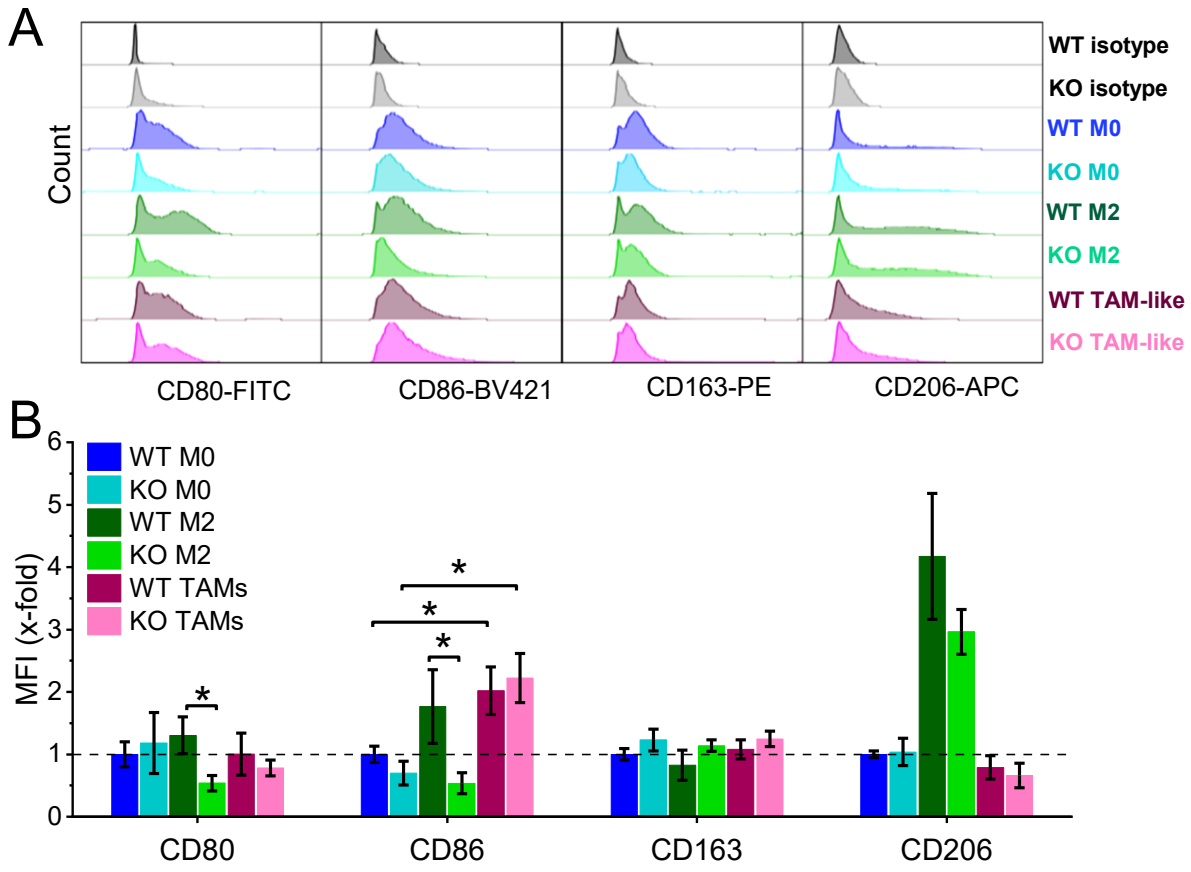

Supplemental Figure 7. Surface marker expression profiles of WT and IGF2BP2 KO macrophages. BMMs were polarized with standard media (M0), IL-4 (M2), or TCM of LLC1 cells (TAM-like) for 24 h, and surface marker expression was quantified by flow cytometry. **(A)** Representative histograms. **(B)** Median fluorescence intensities (MFIs) were expressed as x-fold of unpolarized M0 cells (n = 4 mice per group, duplicates). ANOVA followed by Bonferroni post-hoc tests (*$p < 0.05$; **$p < 0.01$; ***$p < 0.01$).

6.2.8 Expression of Respiratory Chain Genes in IGF2BP2 KO Macrophages

As previously reported (Schymik et al., 2025, submitted, see Part II), IGF2BP2 KO macrophages exhibit increased glycolysis and impaired mitochondrial function, characterized by reduced OCR and mitochondrial membrane potential. Despite unchanged mtDNA content, a compensatory upregulation of genes related to mitochondrial translation and electron transport chain components was observed at the transcriptomic level.

To validate the regulation of ETC-associated genes, we performed qPCR analysis on selected targets in untreated M0 and TAM-like macrophages from WT and IGF2BP2 KO BMMs. The expression levels of *Atp5i*, *Atp5l*, *Cox7b*, *Ndufa3*, and *Ndufa4* showed no significant differences between genotypes. However, *Ndufab1* expression was significantly increased in KO M0 macrophages compared to WT M0, suggesting potential alterations in mitochondrial complex I assembly or function (Supplemental Figure 8A, B).

Further analysis of additional ETC-related genes should be conducted to gain a more comprehensive understanding of mitochondrial adaptations in IGF2BP2 KO macrophages.

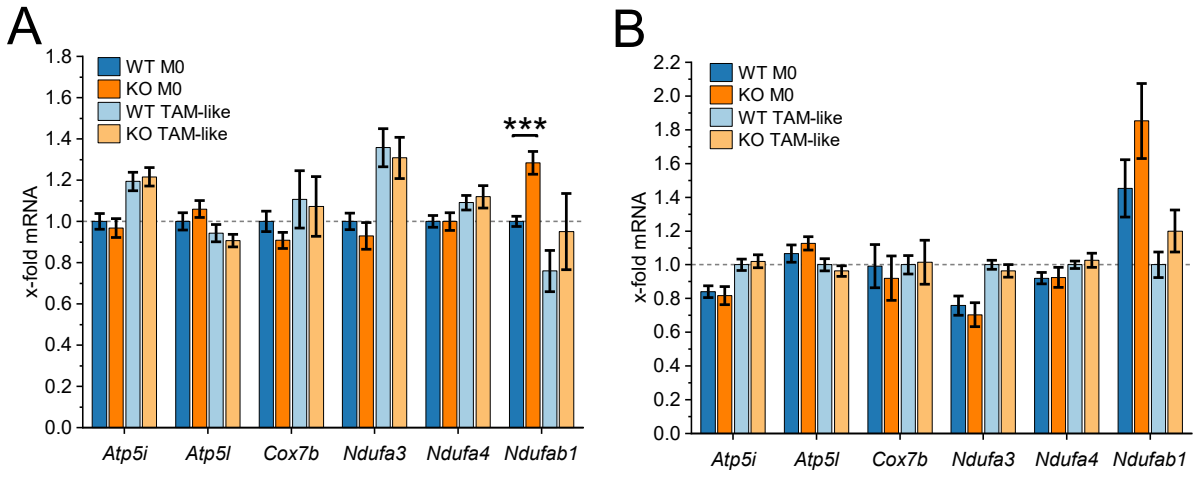

Supplemental Figure 8. Expression of mitochondrial respiratory chain genes in WT and IGF2BP2 KO macrophages. BMMs were cultured in standard medium (M0) or TCM from LLC1 cells (TAM-like) for 8 hours. **(A)** The expression of markers is shown as an x-fold change to WT M0, and (B) an x-fold change to WT TAM-like macrophages. mRNA expression was normalized to *Ppia* (n = 4 mice per group, duplicates). Data are presented as mean ± SEM. Statistical significance was determined by ANOVA with Bonferroni's post hoc test (*$p < 0.05$; **$p < 0.01$; ***$p < 0.001$).

6.2.9 *Expression of Cholesterol Transporters in IGF2BP2 KO Macrophages*

Previous studies have demonstrated that IGF2BP2 overexpression reduces *ABCA1* expression and increases cholesterol levels, indicating a direct role in cholesterol transport regulation (Yang et al., 2020). Additionally, our previous findings showed that the cholesterol transporters *ABCA1* and *ABCG1* are induced in TAMs from human lung tumors and macrophages treated with A549-conditioned medium (TAM-like macrophages), suggesting their involvement in TAM polarization and function (Hoppstädter et al., 2021).

As previously reported (Schymik et al., 2025, submitted, see Part II), qPCR analysis of TAM-associated genes revealed an increased expression of several TAM markers (*Ccl2*, *Hif1a*, *Mmp9*, *Mrc1*, *Tgfb*, *Vegfa*) in murine TAM-like macrophages generated by treating BMMs with LLC1-conditioned medium. Conversely, IGF2BP2 KO TAM-like macrophages exhibited a significant reduction in key TAM markers, including *Mrc1*, *Mmp2*, and *Il10*, indicating an impaired TAM-like phenotype.

To further investigate the role of IGF2BP2 in cholesterol transporter regulation, we analyzed the expression of *Abca1* and *Abcg1* in WT and IGF2BP2 KO TAM-like macrophages. *Abcg1* expression was significantly upregulated in TAM-like macrophages, reinforcing its association with TAM polarization. However, no significant differences in *Abca1* or *Abcg1* expression were observed between WT and IGF2BP2 KO macrophages (Supplemental Figure 9), suggesting that IGF2BP2 does not directly regulate these cholesterol transporters in TAM-like conditions.

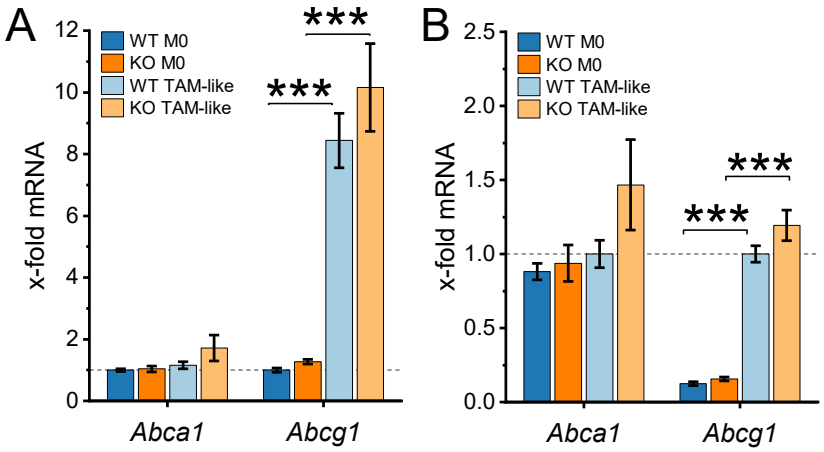

Supplemental Figure 9. Expression of cholesterol transporters in WT and IGF2BP2 KO TAM-like macrophages. BMMs were cultured in standard medium (M0) or TCM from LLC1 cells (TAM-like) for 8 hours. **(A)** *Abca1* and *Abcg1* expressions are shown as x-fold change relative to WT M0 macrophages and **(B)** as fold change relative to WT TAM-like macrophages. mRNA expression was normalized to *Ppia* (n = 4 mice per group, duplicates). Data are presented as mean ± SEM. Statistical significance was determined by ANOVA with Bonferroni's post hoc test (*$p < 0.05$; **$p < 0.01$; ***$p < 0.001$).

6.2.10 Tumor Growth and Inflammation Markers in IGF2BP2 KO Female Mice

Previous findings demonstrated that myeloid-specific IGF2BP2 deletion in a murine LLC1 tumor model led to a significant reduction in tumor growth, characterized by smaller tumor volume, decreased tumor weight, and lower bioluminescence signals in female mice (Schymik et al., 2025, submitted, see Part II). To further investigate the molecular mechanisms underlying these effects, we analyzed the expression of key inflammatory and tumor proliferation markers in tumor tissues of WT and IGF2BP2 KO mice.

Gene expression analysis of tumor tissues revealed alterations in inflammatory cytokines. *Cxcl10* expression was significantly elevated in KO tumors, while *Tnf* levels were markedly reduced. No significant differences were observed in the expression of *Ifng*, *Il6*, *Il10*, or *Tgfb* between WT and KO tumors. The upregulation of *Cxcl10*, a known pro-inflammatory chemokine, suggests a potential shift in the tumor immune landscape upon IGF2BP2 KO. In contrast, the downregulation of *Tnf* might indicate a reduction in tumor-associated inflammation (Supplemental Figure 10A).

We examined the expression of key pro-tumor and anti-tumor markers to assess the impact of IGF2BP2 KO on tumor cell proliferation and survival. The pro-apoptotic genes *Bak1* and *Bax* exhibited no significant changes between WT and KO tumors. Conversely, *Bcl2*, an anti-apoptotic regulator that inhibits Bax- and Bak-mediated apoptosis, showed a slight decrease in KO tumors, suggesting a potential increase in apoptotic susceptibility (Supplemental Figure 10B).

Regarding cell cycle regulation, *Cdk1* and *Myc*, both pro-tumor markers that promote cell cycle progression and metabolism, remained unchanged in KO tumors. Additionally, the expression of *Cdkn1a* and *Cdkn2a*, which function as anti-tumor regulators by inhibiting CDKs and restricting cell cycle progression, showed no significant differences between WT and KO tumors (Supplemental Figure 10B).

Furthermore, *Pten,* a well-established tumor suppressor involved in cell cycle inhibition and apoptosis through the negative regulation of PI3K/AKT signaling, exhibited a slight decrease in KO tumors (Supplemental Figure 10B). Finally, immunohistochemical staining for Ki67, a marker of cellular proliferation, revealed no significant differences in the number of Ki67-positive cells between WT and KO tumors (Supplemental Figure 10C).

Although we observed no significant differences in classical proliferation markers (Ki67, Myc, Cdk1) or apoptotic regulators (Bak1, Bax, Bcl2) between WT and KO tumors, IGF2BP2-deficient tumors were consistently smaller in size and weight. This suggests that the reduction in tumor growth is unlikely to be driven by intrinsic changes in tumor cell proliferation or survival.

As previously shown, IGF2BP2 KO resulted in a decreased presence of immunosuppressive TAMs and impaired tumor vascularization (see Part II), which could limit tumor nutrient supply and promote immune-mediated tumor control, even in the absence of overt changes in proliferation or apoptosis markers. Thus, tumor size reduction may reflect a complex interplay of microenvironmental constraints rather than direct tumor cell-intrinsic effects.

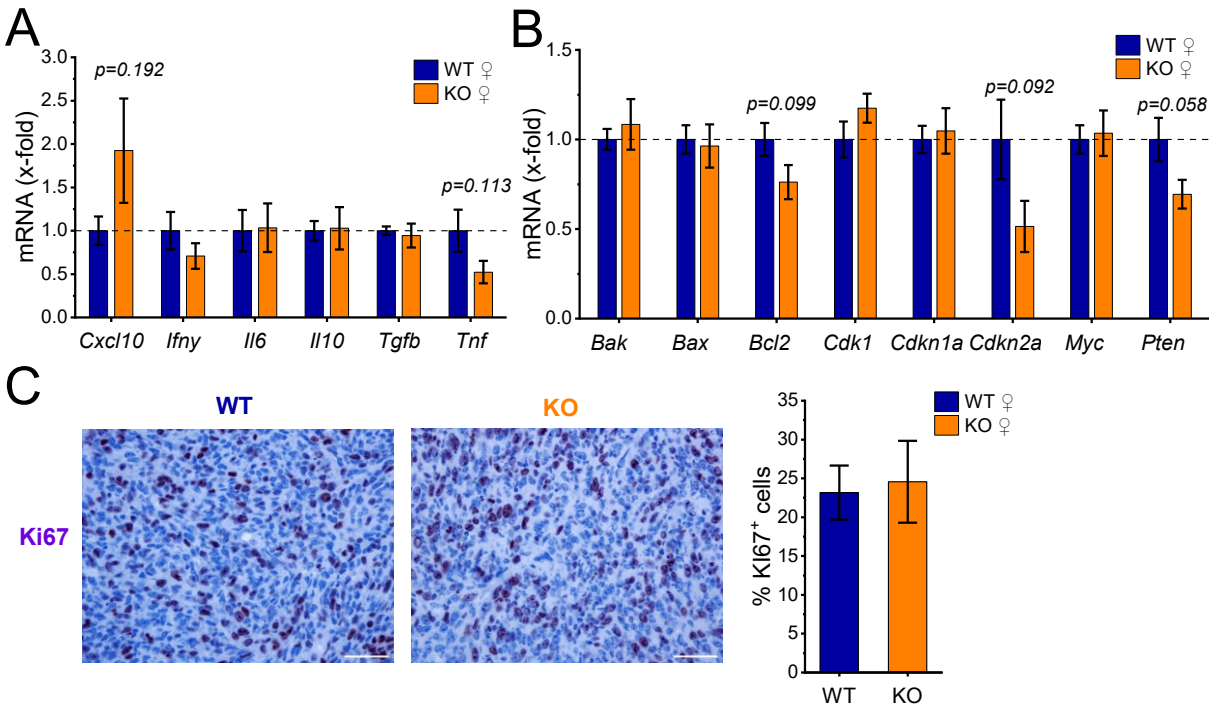

Supplemental Figure 10. Expression of tumor proliferation and inflammatory markers in female LLC1 tumors of WT and IGF2BP2 KO mice. (A, B) mRNA was isolated from tumor tissue, normalized to *Ppia*, and expressed as fold change relative to WT tumor tissue. (A) Inflammatory and (B) Proliferation markers. (C) Representative images and quantification of Ki67 immunohistochemical staining (scale bar = 100 µm) (n = 8 WT, n = 6 KO mice, from two independent experiments). Data are presented as mean ± SEM. Statistical significance was determined using Student's *t*-test for each gene (*$p < 0.05$; **$p < 0.01$; ***$p < 0.001$).

7 Summary and Conclusion

This thesis investigates the multifaceted role of IGF2BP2 in macrophage biology, focusing on its impact on immune modulation and tumor progression. The work includes a comparative analysis of human and mouse macrophages, the consequences of myeloid-specific IGF2BP2 deficiency, sex-dependent effects in tumor models, and therapeutic interventions using small molecule inhibitors.

Initial studies revealed a significant species-specific regulation of IGF2BP2 in response to inflammatory stimuli. While murine macrophages upregulated IGF2BP2 upon LPS treatment, human macrophages showed decreased *IGF2BP2* mRNA levels under similar conditions, whereas protein levels remained largely unchanged. Interestingly, under anti-inflammatory conditions, IGF2BP2 expression was consistently induced in both human and murine M2-polarized macrophages, suggesting a conserved upregulation in alternatively activated phenotypes. This observation prompted a deeper investigation into the functional consequences of IGF2BP2 regulation in macrophage polarization and TAM biology.

Using IGF2BP2-deficient murine macrophages, we demonstrated profound functional and metabolic changes, particularly in TAM-like macrophages. These IGF2BP2-deficient TAM-like macrophages exhibited a pronounced shift towards aerobic glycolysis, accompanied by impaired mitochondrial respiration and a significant reduction in TAM markers such as *Mrc1*, *Il10*, and *Mmp2* expression. Transcriptomic and lipidomic analyses further revealed the downregulation of genes related to cell motility and alterations in membrane lipid composition, namely decreased polyunsaturated phospholipids and increased cholesterol levels, contributing to reduced membrane fluidity and impaired migratory capacity. Functionally, these changes led to defective migration *in vitro* and *in vivo*, as confirmed by wound healing assays and intravital microscopy in a dorsal skinfold chamber model.

In vivo experiments using a subcutaneous Lewis lung carcinoma (LLC1) model in female mice substantiated these findings. IGF2BP2 deletion significantly reduced tumor growth, decreased infiltration of immunosuppressive macrophages, and shifted macrophage polarization toward an anti-tumorigenic phenotype. Interestingly, similar experiments performed in male mice did not reveal significant differences, suggesting notable sex-specific differences in the role of IGF2BP2, possibly mediated by hormonal or immunological differences between the sexes.

Finally, therapeutic evaluations with IGF2BP2 inhibitors demonstrated their potential to modulate human macrophage polarization and metabolic function. These inhibitors selectively impaired mitochondrial function and reprogrammed macrophages toward a less tumor-supportive phenotype, offering promising avenues for cancer therapy targeting the tumor microenvironment.

In conclusion, IGF2BP2 emerges as a key regulator of macrophage function, shaping their metabolic programming, migratory behavior, and immune phenotype. These findings deepen our understanding of immune regulation in cancer and present IGF2BP2 as a promising target for reprogramming the tumor microenvironment in future immunotherapeutic strategies.

8 References

Allavena, P., Digifico, E., and Belgiovine, C. (2021). Macrophages and cancer stem cells: a malevolent alliance. Mol. Med. *27*, 121.

An, Y., and Duan, H. (2022). The role of m6A RNA methylation in cancer metabolism. Mol. Cancer *21*, 1–24.

Arlauckas, S.P., Garren, S.B., Garris, C.S., Kohler, R.H., Oh, J., Pittet, M.J., and Weissleder, R. (2018). Arg1 expression defines immunosuppressive subsets of tumor-associated macrophages. Theranostics *8*, 5842–5854.

Arneth, B. (2020). Tumor microenvironment. Med. *56*.

Attiq, A., and Afzal, S. (2023). Trinity of inflammation, innate immune cells and cross-talk of signalling pathways in tumour microenvironment. Front. Pharmacol. *14*, 1–19.

Augoff, K., Hryniewicz-Jankowska, A., Tabola, R., and Stach, K. (2022). MMP9: A Tough Target for Targeted Therapy for Cancer. Cancers (Basel). *14*, 1–28.

Azizi, E., Carr, A.J., Plitas, G., Cornish, A.E., Konopacki, C., Prabhakaran, S., Nainys, J., Wu, K., Kiseliovas, V., Setty, M., et al. (2018). Single-Cell Map of Diverse Immune Phenotypes in the Breast Tumor Microenvironment. Cell *174*, 1293-1308.e36.

Bah, A., and Vergne, I. (2017). Macrophage autophagy and bacterial infections. Front. Immunol. *8*, 1–9.

Bailetti, D., Sentinelli, F., Prudente, S., Cimini, F.A., Barchetta, I., Totaro, M., Di Costanzo, A., Barbonetti, A., Leonetti, F., Cavallo, M.G., et al. (2022). Deep Resequencing of 9 Candidate Genes Identifies a Role for ARAP1 and IGF2BP2 in Modulating Insulin Secretion Adjusted for Insulin Resistance in Obese Southern Europeans. Int. J. Mol. Sci. *23*, 1–13.

Banerjee, K., Kerzel, T., Bekkhus, T., de Souza Ferreira, S., Wallmann, T., Wallerius, M., Landwehr, L.S., Agardy, D.A., Schauer, N., Malmerfeldt, A., et al. (2023). VEGF-C-expressing TAMs rewire the metastatic fate of breast cancer cells. Cell Rep. *42*.

Bao, X., Shi, R., Zhao, T., Wang, Y., Anastasov, N., Rosemann, M., and Fang, W. (2021). Integrated analysis of single-cell RNA-seq and bulk RNA-seq unravels tumour heterogeneity plus M2-like tumour-associated macrophage infiltration and aggressiveness in TNBC. Cancer Immunol. Immunother. *70*, 189–202.

Barger, S.R., Vorselen, D., Gauthier, N.C., Theriot, J.A., and Krendel, M. (2022). F-actin organization and target constriction during primary macrophage phagocytosis is balanced by competing activity of

myosin-I and myosin-II. Mol. Biol. Cell *33*, 1–10.

Basak, U., Sarkar, T., Mukherjee, S., Chakraborty, S., Dutta, A., Dutta, S., Nayak, D., Kaushik, S., Das, T., and Sa, G. (2023). Tumor-associated macrophages: an effective player of the tumor microenvironment. Front. Immunol. *14*.

Bhargav, A., Bhalla, N., Manoharan, S., Singh, G., Yadav, S.K., and Singh, A.K. (2023). Role of Various Immune Cells in the Tumor Microenvironment. Dis. & Res. *3*, 30–40.

Blevins, H.M., Xu, Y., Biby, S., and Zhang, S. (2022). The NLRP3 Inflammasome Pathway: A Review of Mechanisms and Inhibitors for the Treatment of Inflammatory Diseases. Front. Aging Neurosci. *14*, 1–27.

Boussios, S., Sheriff, M., and Ovsepian, S. V. (2024). Molecular Biology of Cancer—Interplay of Malignant Cells with Emerging Therapies. Int. J. Mol. Sci. *25*, 1–20.

Van Broeckhoven, J., Sommer, D., Dooley, D., Hendrix, S., and Franssen, A.J.P.M. (2021). Macrophage phagocytosis after spinal cord injury: When friends become foes. Brain *144*, 2933–2945.

Canton, J., Khezri, R., Glogauer, M., and Grinstein, S. (2014). Contrasting phagosome pH regulation and maturation in human M1 and M2 macrophages. Mol. Biol. Cell *25*, 3330–3341.

Cao, F., Chen, G., Xu, Y., Wang, X., Tang, X., Zhang, W., Song, X., Yang, X., Zeng, W., and Xie, J. (2024). METTL14 contributes to acute lung injury by stabilizing NLRP3 expression in an IGF2BP2-dependent manner. Cell Death Dis. *15*, 1–15.

Cao, J., Mu, Q., and Huang, H. (2018). The roles of insulin-like growth factor 2 mRNA-binding protein 2 in cancer and cancer stem cells. Stem Cells Int. *2018*.

Cao, J., Yan, W., Ma, X., Huang, H., and Yan, H. (2021). Insulin-like Growth Factor 2 mRNA-Binding Protein 2-a Potential Link between Type 2 Diabetes Mellitus and Cancer. J. Clin. Endocrinol. Metab. *106*, 2807–2818.

Cassetta, L., and Kitamura, T. (2018). Targeting tumor-associated macrophages as a potential strategy to enhance the response to immune checkpoint inhibitors. Front. Cell Dev. Biol. *6*, 1–6.

Cendrowicz, E., Sas, Z., Bremer, E., and Rygiel, T. (2021). The Role of Macrophages in Cancer Development and Therapy. Cancers (Basel). *13*.

Chakraborty, A., and Diwan, A. (2024). International Journal of Research in Oncology Nanopolymer-Mediated Targeting Cancer with M1 Macrophage Polarizing Factors : A Unique Strategy to Fight against Cancer. *3*.

Chan, Y.X., Alfonso, H., Chubb, S.A.P., Handelsman, D.J., Fegan, P.G., Hankey, G.J., Golledge, J.,

Flicker, L., and Yeap, B.B. (2017). Higher Dihydrotestosterone Is Associated with the Incidence of Lung Cancer in Older Men. Horm. Cancer *8*, 119–126.

Chanda, S., Lepikhov, K., Dahlem, C., Schymik, H.S., Hoppstädter, J., Geber, A.K., Wagner, K., Kessler, S.M., Empting, M., and Kiemer, A.K. (2024). Gene Editing and Small Molecule Inhibitors of the RNA Binding Protein IGF2BP2/IMP2 Show its Potential as an Anti-Cancer Drug Target. Front. Biosci. - Landmark *29*, 1–16.

Chanu, M.T., and Singh, A.S. (2024). Different types of Cancer treatment , its advancement , benefits , and side effects Different types of Cancer treatment , its advancement , benefits , and side effects.

Chen, J., Zhao, D., Zhang, L., Zhang, J., Xiao, Y., Wu, Q., Wang, Y., and Zhan, Q. (2024). Tumor-associated macrophage (TAM)-secreted CCL22 confers cisplatin resistance of esophageal squamous cell carcinoma (ESCC) cells via regulating the activity of diacylglycerol kinase α (DGKα)/NOX4 axis. Drug Resist. Updat. *73*, 101055.

Chen, K.-H.E., Lainez, N.M., and Coss, D. (2021). Sex Differences in Macrophage Responses to Obesity-Mediated Changes Determine Migratory and Inflammatory Traits. J. Immunol. *206*, 141–153.

Chen, Y., Song, Y., Du, W., Gong, L., Chang, H., and Zou, Z. (2019a). Tumor-associated macrophages: an accomplice in solid tumor progression. J. Biomed. Sci. *26*.

Chen, Y., Song, Y., Du, W., Gong, L., Chang, H., and Zou, Z. (2019b). Tumor-associated macrophages: An accomplice in solid tumor progression. J. Biomed. Sci. *26*, 1–13.

Chenard, S., Jackson, C., Vidotto, T., Chen, L., Hardy, C., Jamaspishvilli, T., Berman, D., Siemens, D.R., and Koti, M. (2021). Sexual Dimorphism in Outcomes of Non–muscle-invasive Bladder Cancer: A Role of CD163+ Macrophages, B cells, and PD-L1 Immune Checkpoint. Eur. Urol. Open Sci. *29*, 50–58.

Chettri, D., Satapathy, B.P., Yadav, R., Uttam, V., Jain, A., and Prakash, H. (2024). CAR-macrophages: tailoring cancer immunotherapy. Front. Immunol. *15*, 1–4.

Choo, Y.W., Kang, M., Kim, H.Y., Han, J., Kang, S., Lee, J., Jeong, G.-J., Kwon, S., Song, S., Go, S.-H., et al. (2018). M1 Macrophage-Derived Nanovesicles Potentiate the Anticancer Efficacy of Immune Checkpoint Inhibitors. ACS Nano *12 9*, 8977–8993.

Ciechomska, M., Wojtas, B., Swacha, M., Olesinska, M., Benes, V., and Maslinski, W. (2020). Global miRNA and mRNA expression profiles identify miRNA-26a-2-3p-dependent repression of IFN signature in systemic sclerosis human monocytes. Eur. J. Immunol. *50*, 1057–1066.

Coussens, L., Zitvogel, L., and Palucka, A. (2013). Neutralizing Tumor-Promoting Chronic Inflammation: A Magic Bullet? Science (80-.). *339*, 286–291.

Crusz, S.M., and Balkwill, F.R. (2015). Inflammation and cancer: advances and new agents. Nat. Rev. Clin. Oncol. *12*, 584–596.

Cui, J., Tian, J., Wang, W., He, T., Li, X., Gu, C., Wang, L., Wu, J., and Shang, A. (2021). IGF2BP2 promotes the progression of colorectal cancer through a YAP-dependent mechanism. Cancer Sci. *112*, 4087–4099.

Cunningham, C.E., Vizeacoumar, F.S., Zhang, Y., Kyrylenko, L., Gao, P., Maranda, V., Dong, H., Price, J.D.W., Ganapathysamy, A., Hari, R., et al. (2024). Identification of targetable vulnerabilities of PLK1-overexpressing cancers by synthetic dosage lethality. BioRxiv.

Cunningham, C.E., Vizeacoumar, F.S., Zhang, Y., Kyrylenko, L., Both, S., Maranda, V., Dong, H., Price, J.D.W., Gao, P., Wagner, K., et al. (2025). Identification of targetable vulnerabilities of PLK1-overexpressing cancers by synthetic dosage lethality. Cell Genomics.

Czepukojc, B., Abuhaliema, A., Barghash, A., Tierling, S., Naß, N., Simon, Y., Körbel, C., Cadenas, C., van Hul, N., Sachinidis, A., et al. (2019). IGF2 mRNA Binding Protein 2 Transgenic Mice Are More Prone to Develop a Ductular Reaction and to Progress Toward Cirrhosis. Front. Med. *6*, 1–16.

Dahlem, C., Siow, W.X., Lopatniuk, M., Tse, W.K.F., Kessler, S.M., Kirsch, S.H., Hoppstädter, J., Vollmar, A.M., Müller, R., Luzhetskyy, A., et al. (2020). Thioholgamide A, a new anti-proliferative anti-tumor agent, modulates macrophage polarization and metabolism. Cancers (Basel). *12*, E1288.

Dahlem, C., Abuhaliema, A., Kessler, S.M., Kr, T., Zoller, B.G.E., Chanda, S., Wu, Y., Both, S., Mu, F., Lepikhov, K., et al. (2021). First Small-Molecule Inhibitors Targeting the RNA-Binding Protein IGF2BP2/IMP2 for Cancer Therapy.

Dahlem, C., Abuhaliema, A., Kessler, S.M., Kröhler, T., Zoller, B.G.E., Chanda, S., Wu, Y., Both, S., Müller, F., Lepikhov, K., et al. (2022). First Small-Molecule Inhibitors Targeting the RNA-Binding Protein IGF2BP2/IMP2 for Cancer Therapy. ACS Chem. Biol.

Dai, N., Zhao, L., Wrighting, D., Krämer, D., Majithia, A., Wang, Y., Cracan, V., Borges-Rivera, D., Mootha, V.K., Nahrendorf, M., et al. (2015). IGF2BP2/IMP2-deficient mice resist obesity through enhanced translation of Ucp1 mRNA and other mRNAs encoding mitochondrial proteins. Cell Metab. *21*, 609–621.

Degrauwe, N., Suvà, M.L., Janiszewska, M., Riggi, N., and Stamenkovic, I. (2016). Imps: An RNA-binding protein family that provides a link between stem cell maintenance in normal development and cancer. Genes Dev. *30*, 2459–2474.

Dehghani Amirabad, A., Ramasamy, P., Wierz, M., Nordström, K., Kessler, S.M., Schulz, M.H., and Simon, M. (2018). Transgenic expression of the RNA binding protein IMP2 stabilizes miRNA targets

in murine microsteatosis. Biochim. Biophys. Acta - Mol. Basis Dis. *1864*, 3099–3108.

Deryugina, E.I., Zajac, E., Juncker-Jensen, A., Kupriyanova, T.A., Welter, L., and Quigley, J.P. (2014). Tissue-Infiltrating Neutrophils Constitute the Major In Vivo Source of Angiogenesis-Inducing MMP-9 in the Tumor Microenvironment. Neoplasia (United States) *16*, 771–788.

Desai, M., and Brinton, R. (2019). Autoimmune Disease in Women: Endocrine Transition and Risk Across the Lifespan. Front. Endocrinol. (Lausanne). *10*.

Diao, M., Wang, Y., Wu, S., He, S., and Liao, Y. (2025). Estrogen, estrogen receptor and the tumor microenvironment of NSCLC. Int. J. Cancer 1501–1508.

Ding, L., Wang, L., and Guo, F. (2017). microRNA-188 acts as a tumour suppressor in glioma by directly targeting the IGF2BP2 gene. Mol. Med. Rep. *16 5*, 7124–7130.

Doyle, E.H., Vaughan, H.J., and Mariani, S.A. (2024). From drosophila to humans: a journey through macrophage development. Exp. Hematol. *136*, 1–9.

Du, X., Guo, Y., Zhao, X., Zhang, L., Fan, R., and Li, Y. (2024). METTL3-mediated TIM1 promotes macrophage M1 polarization and inflammation through IGF2BP2-dependent manner. J. Biochem. Mol. Toxicol. *38*, 1–9.

Edwardson, D.W., Parissenti, A.M., and Kovala, A.T. (2019). Chemotherapy and Inflammatory Cytokine Signalling in Cancer Cells and the Tumour Microenvironment. Adv. Exp. Med. Biol. *1152*, 173–215.

Evren, E., Ringqvist, E., and Willinger, T. (2019). Origin and ontogeny of lung macrophages: from mice to humans. Immunology *160*.

Fawzy, I.O., Hamza, M.T., Hosny, K.A., Esmat, G., and Abdelaziz, A.I. (2016). Abrogating the interplay between IGF2BP1, 2 and 3 and IGF1R by let-7i arrests hepatocellular carcinoma growth. Growth Factors *34*, 42–50.

Fehlmann, T., Kern, F., Laham, O., Backes, C., Solomon, J., Hirsch, P., Volz, C., Müller, R., and Keller, A. (2021). miRMaster 2.0: multi-species non-coding RNA sequencing analyses at scale. Nucleic Acids Res. *49*, W397–W408.

Ferlay, J., Colombet, M., Soerjomataram, I., Parkin, D.M., Piñeros, M., Znaor, A., and Bray, F. (2021). Cancer statistics for the year 2020: An overview. Int. J. Cancer *149*, 778–789.

Fu, D., Shi, X., Yi, X., Wu, D., He, H., Zhou, W., and Cheng, W. (2024). m6A reader IGF2BP2 promotes M2 macrophage polarization and malignant biological behavior of bladder cancer by stabilizing NRP1 mRNA expression. BMC Urol. *24*, 1–12.

Gal-Oz, S.T., Maier, B., Yoshida, H., Seddu, K., Elbaz, N., Czysz, C., Zuk, O., Stranger, B.E., Ner-Gaon, H., and Shay, T. (2019). ImmGen report: sexual dimorphism in the immune system transcriptome. Nat. Commun. *10*.

Galli, F., Aguilera, J.V., Palermo, B., Markovic, S.N., Nisticò, P., and Signore, A. (2020). Relevance of immune cell and tumor microenvironment imaging in the new era of immunotherapy. J. Exp. Clin. Cancer Res. *39*, 1–21.

Gao, C., Li, L., Jin, X., Song, X., Li, H., Xu, X., Dong, C., and Ma, B. (2022). The Involvement of Insulin-Like Growth Factor 2 Messenger Ribonucleic Acid-Binding Protein 2 in the Regulation of the Expression of Breast Cancer-Related Genes. Breast Cancer (Dove Med. Press. *14*, 311–322.

Ge, P., Duan, H., Tao, C., Niu, S., Hu, Y., Duan, R., Shen, A., Sun, Y., and Sun, W. (2023). TMAO Promotes NLRP3 Inflammasome Activation of Microglia Aggravating Neurological Injury in Ischemic Stroke Through FTO/IGF2BP2. J. Inflamm. Res. *16*, 3699–3714.

Goel, K., and Saraogi, I. (2025). Harnessing RNA-Protein Interactions for Therapeutic Interventions. Chem. - An Asian J. *202401117*.

Goenka, A., Khan, F., Verma, B., Sinha, P., Dmello, C.C., Jogalekar, M.P., Gangadaran, P., and Ahn, B.C. (2023). Tumor microenvironment signaling and therapeutics in cancer progression. Cancer Commun. *43*, 525–561.

Goldmann, T., Wieghofer, P., Jordão, M., Prutek, F., Hagemeyer, N., Frenzel, K., Amann, L., Staszewski, O., Kierdorf, K., Krueger, M., et al. (2016). Origin, fate and dynamics of macrophages at central nervous system interfaces. Nat. Immunol. *17*, 797–805.

Gomez, F., Ruiz, P., Bernal, J.A., Escobar, M., Garcia-Egido, A., and Lopez-Saez, J.J. (2001). Enhancement of splenic-macrophage Fcgamma receptor expression by treatment with estrogens. Clin. Diagn. Lab. Immunol. *8*, 806–810.

Greten, F.R., and Grivennikov, S.I. (2019). Inflammation and Cancer: Triggers, Mechanisms, and Consequences. Immunity *51*, 27–41.

Gu, Y., Becker, V., Qiu, M., Tang, T., Ampofo, E., Menger, M.D., and Laschke, M.W. (2022). Brassinin Promotes the Degradation of Tie2 and FGFR1 in Endothelial Cells and Inhibits Triple-Negative Breast Cancer Angiogenesis. Cancers (Basel). *14*.

Gunassekaran, G.R., Vadevoo, S.M.P., Baek, M., and Lee, B. (2021). M1 macrophage exosomes engineered to foster M1 polarization and target the IL-4 receptor inhibit tumor growth by reprogramming tumor-associated macrophages into M1-like macrophages. Biomaterials *278*, 121137.

Gyorffy, B., Menyhart, O., Kothalawala, W., and Santarpia, L. (2024). CancerHallmarks.com: A tool

for the enrichment analysis of the cancer hallmarks. J. Clin. Oncol. *42*, e15079–e15079.

Han, J., Yu, X., Wang, S., Wang, Y., Liu, Q., Xu, H., and Wang, X. (2022a). IGF2BP2 Induces U251 Glioblastoma Cell Chemoresistance by Inhibiting FOXO1-Mediated PID1 Expression Through Stabilizing lncRNA DANCR. Front. Cell Dev. Biol. *9*, 1–16.

Han, L., Lei, G., Chen, Z., Zhang, Y., Huang, C., and Chen, W. (2022b). IGF2BP2 Regulates MALAT1 by Serving as an N6-Methyladenosine Reader to Promote NSCLC Proliferation. Front. Mol. Biosci. *8*, 1–8.

Hanahan, D., and Weinberg, R.A. (2011). Hallmarks of cancer: The next generation. Cell *144*, 646–674.

Hasan, M.N., Capuk, O., Patel, S.M., and Sun, D. (2022). The Role of Metabolic Plasticity of Tumor-Associated Macrophages in Shaping the Tumor Microenvironment Immunity. Cancers (Basel). *14*.

He, Z., and Zhang, S. (2021). Tumor-Associated Macrophages and Their Functional Transformation in the Hypoxic Tumor Microenvironment. Front. Immunol. *12*, 741305.

He, X., Li, W., Liang, X., Zhu, X., Zhang, L., Huang, Y., Yu, T., Li, S., and Chen, Z. (2018). IGF2BP2 overexpression indicates poor survival in patients with acute myelocytic leukemia. Cell. Physiol. Biochem. *51*, 1945–1956.

Herb, M., and Schramm, M. (2021). Functions of ros in macrophages and antimicrobial immunity. Antioxidants *10*, 1–39.

Herrera, M., Galindo-Pumariño, C., García-Barberán, V., and Peña, C. (2019). A snapshot of the tumor microenvironment in colorectal cancer: The liquid biopsy. Int. J. Mol. Sci. *20*, 1–27.

Hinshaw, D., and Shevde, L. (2019). The Tumor Microenvironment Innately Modulates Cancer Progression. Cancer Res.

Hirohashi, T., Beck, J.T., McDermott, J.D., Abbruzzese, J.L., Doi, T., Ingram, K., Li, R., and Subbiah, V. (2023). Trials in progress: TAM kinase inhibitor PF-07265807 and sasanlimab plus axitinib in patients with advanced or metastatic renal cell carcinoma—A phase 1, open-label, pharmacokinetic, safety and tolerability study. J. Clin. Oncol. *41*, TPS743–TPS743.

Hoeffel, G., and Ginhoux, F. (2015). Ontogeny of Tissue-Resident Macrophages. Front. Immunol. *6*.

Hoppstädter, J., Hachenthal, N., Valbuena-Perez, J.V., Lampe, S., Astanina, K., Kunze, M.M., Bruscoli, S., Riccardi, C., Schmid, T., Diesel, B., et al. (2016). Induction of Glucocorticoid-induced Leucine Zipper (GILZ) Contributes to anti-inflammatory effects of the natural product curcumin in macrophages. J. Biol. Chem. *291*, 22949–22960.

Hoppstädter, J., Dembek, A., Linnenberger, R., Dahlem, C., Barghash, A., Fecher-Trost, C., Fuhrmann,

G., Koch, M., Kraegeloh, A., Huwer, H., et al. (2019a). Toll-Like Receptor 2 Release by Macrophages: An Anti-inflammatory Program Induced by Glucocorticoids and Lipopolysaccharide. Front. Immunol. *10*, 1634.

Hoppstädter, J., Diesel, B., Linnenberger, R., Hachenthal, N., Flamini, S., Minet, M., Leidinger, P., Backes, C., Grässer, F., Meese, E., et al. (2019b). Amplified host defense by toll-like receptor-mediated downregulation of the glucocorticoid-induced leucine zipper (GILZ) in macrophages. Front. Immunol. *10*, 1–15.

Hoppstädter, J., Dembek, A., Höring, M., Schymik, H.S., Dahlem, C., Sultan, A., Wirth, N., Al-Fityan, S., Diesel, B., Gasparoni, G., et al. (2021). Dysregulation of cholesterol homeostasis in human lung cancer tissue and tumour-associated macrophages. EBioMedicine *72*.

Huang, H., Li, G., He, Y., Chen, J., Yan, J., Zhang, Q., Li, L., and Cai, X. (2024). Cellular succinate metabolism and signaling in inflammation: implications for therapeutic intervention. Front. Immunol. *15*, 1404441.

Huang, Y., Du, Y., Zheng, Y., Wen, C., Zou, H., Huang, J., Zhou, H., Zhao, H., and Wu, L. (2022). Ct-OATP1B3 promotes high-grade serous ovarian cancer metastasis by regulation of fatty acid beta-oxidation and oxidative phosphorylation. Cell Death Dis. *13*.

Hukara, A., Bonazza, G.A., Tabib, T., Micheroli, R., Jordan, S., Bürki, K., Rudnik, M., Ciurea, A., Distler, O., Lafyatis, R., et al. (2024). Elevated Fcy receptor expression augments pro-inflammatory macrophage phagocytosis in systemic sclerosis and associated rheumatic diseases. Rheumatology (Oxford). 1–14.

Huo, Y., Zhang, H., Sa, L., Zheng, W., He, Y., Lyu, H., Sun, M., Zhang, L., Shan, L., Yang, A., et al. (2023). M1 polarization enhances the antitumor activity of chimeric antigen receptor macrophages in solid tumors. J. Transl. Med. *21*, 225.

Hwang, I., Kim, J., Ylaya, K., Chung, E., Kitano, H., Perry, C., Hanaoka, J., Fukuoka, J., Chung, J., and Hewitt, S. (2020). Tumor-associated macrophage, angiogenesis and lymphangiogenesis markers predict prognosis of non-small cell lung cancer patients. J. Transl. Med. *18*.

Jääskeläinen, M., Tumelius, R., Hämäläinen, K., Rilla, K., Oikari, S., Rönkä, A., Selander, T., Mannermaa, A., Tiainen, S., and Auvinen, P. (2024). High Numbers of CD163+ Tumor-Associated Macrophages Predict Poor Prognosis in HER2+ Breast Cancer. Cancers (Basel). *16*.

Jackman, J.M., Yibrehu, B., Doyle, A., Alatise, O.I., Wuraola, F.O., Olasehinde, O., and Peter Kingham, T. (2024). Updates in global oncology: Advancements and future directions. J. Surg. Oncol. *129*, 1374–1383.

Jaggi, U., Yang, M., Matundan, H., Hirose, S., Shah, P., Sharifi, B., and Ghiasi, H. (2020). Increased phagocytosis in the presence of enhanced M2-like macrophage responses correlates with increased primary and latent HSV-1 infection. PLoS Pathog. *16*.

Jang, S., Han, H., Oh, Y., and Kim, Y. (2024). Sex differences in inflammation correlated with estrogen and estrogen receptor-β levels in azoxymethane/dextran sodium sulfate-induced colitis-associated colorectal cancer mice. Heliyon *10*.

Janiszewska, M., Suvà, M.L., Riggi, N., Houtkooper, R.H., Auwerx, J., Clément-Schatlo, V., Radovanovic, I., Rheinbay, E., Provero, P., and Stamenkovic, I. (2012). Imp2 controls oxidative phosphorylation and is crucial for preserving glioblastoma cancer stem cells. Genes Dev. *26*, 1926–1944.

Jing, G., Yang, L., Wang, H., Niu, J., Wang, H., Gao, Y., Li, Y., Wei, B., Qian, Y., and Wang, S. (2023). Blocked Autophagy is Involved in Layered Double Hydroxide-Induced Repolarization and Immune Activation in Tumor-Associated Macrophages. Adv. Healthc. Mater. *12*, 1–13.

Jingrui, W., Haihui, Y., Jinjin, Y., and Le, F. (2025). IGF2BP2 Regulates the Progression of Alzheimer's Disease Through m6A-Mediated NLRP3 Inflammasome. Immunity, Inflamm. Dis. *13*, 1–10.

Jog, N.R., and Caricchio, R. (2013). Differential regulation of cell death programs in males and females by Poly (ADP-Ribose) Polymerase-1 and 17β estradiol. Cell Death Dis. *4*, e758.

Jorquera-Cordero, C., Lara, P., Cruz, L.J., Schomann, T., van Hofslot, A., de Carvalho, T.G., Guedes, P.M.D.M., Creemers, L., Koning, R.I., Chan, A.B., et al. (2022). Extracellular Vesicles from M1-Polarized Macrophages Combined with Hyaluronic Acid and a β-Blocker Potentiate Doxorubicin's Antitumor Activity by Downregulating Tumor-Associated Macrophages in Breast Cancer. Pharmaceutics *14*.

Joseph, B.P., Weber, V., Knüpfer, L., Giorgetti, A., Alfonso-Prieto, M., Krauß, S., Carloni, P., and Rossetti, G. (2023). Low Molecular Weight Inhibitors Targeting the RNA-Binding Protein HuR. Int. J. Mol. Sci. *24*.

Jumaniyazova, E., Lokhonina, A., Dzhalilova, D., Miroshnichenko, E., Kosyreva, A., and Fatkhudinov, T. (2025). The Role of Macrophages in Various Types of Tumors and the Possibility of Their Use as Targets for Antitumor Therapy. Cancers (Basel). *17*, 1–27.

Kaatsch, P., Spix, C., Katalinic, A., Hentschel, S., Luttmann, S., Waldeyer-Sauerland, Mechthild Waldmann, A., Christ, M., Folkerts, J., Hansmann, J., Klein, S., et al. (2020). Cancer in Germany in 2015/2016.

Kapellos, T.S., Taylor, L., Lee, H., Cowley, S.A., James, W.S., Iqbal, A.J., and Greaves, D.R. (2016a).

A novel real time imaging platform to quantify macrophage phagocytosis. Biochem. Pharmacol. *116*, 107–119.

Kapellos, T.S., Taylor, L., Lee, H., Cowley, S.A., James, W.S., Iqbal, A.J., and Greaves, D.R. (2016b). A novel real time imaging platform to quantify macrophage phagocytosis. Biochem. Pharmacol. *116*, 107–119.

Kendzia, S., Franke, S., Kröhler, T., Golob-Schwarzl, N., Schweiger, C., Toeglhofer, A.M., Skofler, C., Uranitsch, S., El-Heliebi, A., Fuchs, J., et al. (2023). A combined computational and functional approach identifies IGF2BP2 as a driver of chemoresistance in a wide array of pre-clinical models of colorectal cancer. Mol. Cancer *22*, 1–14.

Kessler, S.M., Pokorny, J., Zimmer, V., Laggai, S., Lammert, F., Bohle, R.M., and Kiemer, A.K. (2013a). IGF2 mRNA binding protein p62/IMP2-2 in hepatocellular carcinoma: Antiapoptotic action is independent of IGF2/PI3K signaling. Am. J. Physiol. - Gastrointest. Liver Physiol. *304*.

Kessler, S.M., Pokorny, J., Zimmer, V., Laggai, S., Lammert, F., Bohle, R.M., and Kiemer, A.K. (2013b). IGF2 mRNA binding protein p62/IMP2-2 in hepatocellular carcinoma: Antiapoptotic action is independent of IGF2/PI3K signaling. Am. J. Physiol. - Gastrointest. Liver Physiol. *304*, 328–336.

Kessler, S.M., Laggai, S., Barghash, A., Schultheiss, C.S., Lederer, E., Artl, M., Helms, V., Haybaeck, J., and Kiemer, A.K. (2015). IMP2/p62 induces genomic instability and an aggressive hepatocellular carcinoma phenotype. Cell Death Dis. *6*, e1894-12.

Kohno, K., Koya-Miyata, S., Harashima, A., Tsukuda, T., Katakami, M., Ariyasu, T., Ushio, S., and Iwaki, K. (2021). Inflammatory M1-like macrophages polarized by NK-4 undergo enhanced phenotypic switching to an anti-inflammatory M2-like phenotype upon co-culture with apoptotic cells. J. Inflamm. (United Kingdom) *18*, 1–14.

Komohara, Y., Fujiwara, Y., Ohnishi, K., and Takeya, M. (2016). Tumor-associated macrophages: Potential therapeutic targets for anti-cancer therapy. Adv. Drug Deliv. Rev. *99*, 180–185.

Korn, S.M., Ulshöfer, C.J., Schneider, T., and Schlundt, A. (2021). Structures and target RNA preferences of the RNA-binding protein family of IGF2BPs: An overview. Structure *29*, 787–803.

Kozomara, A., Birgaoanu, M., and Griffiths-Jones, S. (2019). miRBase: from microRNA sequences to function. Nucleic Acids Res. *47*, D155–D162.

Krumbein, M., Oberman, F., Cinnamon, Y., Golomb, M., May, D., Vainer, G., Belzer, V., Meir, K., Fridman, I., Haybaeck, J., et al. (2023). RNA binding protein IGF2BP2 expression is induced by stress in the heart and mediates dilated cardiomyopathy. Commun. Biol. *6*, 1–14.

Kzhyshkowska, J., Shen, J., and Larionova, I. (2024). Targeting of TAMs: can we be more clever than

cancer cells? (Springer US).

Laggai, S., Kessler, S.M., Boettcher, S., Lebrun, V., Gemperlein, K., Lederer, E., Leclercq, I.A., Mueller, R., Hartmann, R.W., Haybaeck, J., et al. (2014a). The IGF2 mRNA binding protein p62/IGF2BP2-2 induces fatty acid elongation as a critical feature of steatosis. J. Lipid Res. *55*, 1087–1097.

Laggai, S., Kessler, S.M., Boettcher, S., Lebrun, V., Gemperlein, K., Lederer, E., Leclercq, I.A., Mueller, R., Hartmann, R.W., Haybaeck, J., et al. (2014b). The IGF2 mRNA binding protein p62/IGF2BP2-2 induces fatty acid elongation as a critical feature of steatosis. J. Lipid Res. *55*, 1087–1097.

Lam, R.S., O'Brien-Simpson, N.M., Holden, J.A., Lenzo, J.C., Fong, S.B., and Reynolds, E.C. (2016). Unprimed, M1 and M2 macrophages differentially interact with Porphyromonas gingivalis. PLoS One *11*, 1–17.

Larionova, I., Kazakova, E., Gerashchenko, T., and Kzhyshkowska, J. (2021). New angiogenic regulators produced by tams: Perspective for targeting tumor angiogenesis. Cancers (Basel). *13*, 1–40.

Latifkar, A., Wang, F., Mullmann, J.J., Panizza, E., Fernandez, I.R., Ling, L., Miller, A.D., Fischbach, C., Weiss, R.S., Lin, H., et al. (2022). IGF2BP2 promotes cancer progression by degrading the RNA transcript encoding a v-ATPase subunit. Proc. Natl. Acad. Sci. U. S. A. *119*.

Laviron, M., and Boissonnas, A. (2019). Ontogeny of Tumor-Associated Macrophages. Front. Immunol. *10*, 1799.

Law, Y.Y., Lee, W.F., Hsu, C.J., Lin, Y.Y., Tsai, C.H., Huang, C.C., Wu, M.H., Tang, C.H., and Liu, J.F. (2021). miR-let-7c-5p and miR-149-5p inhibit proinflammatory cytokine production in osteoarthritis and rheumatoid arthritis synovial fibroblasts. Aging (Albany. NY). *13*, 17227–17236.

Lee, K.Y. (2019). M1 and M2 polarization of macrophages: a mini-review. Med. Biol. Sci. Eng. *2*, 1–5.

Legroux, T.M., Schymik, H.S., Gasparoni, G., Mohammadi, S., Walter, J., Libert, C., Diesel, B., Hoppstädter, J., and Kiemer, A.K. (2024). Immunomodulation by glucocorticoid-induced leucine zipper in macrophages: enhanced phagocytosis, protection from pyroptosis, and altered mitochondrial function. Front. Immunol. *15*, 1–16.

Lei, X., Lei, Y., Li, J.-K., Du, W.-X., Li, R.-G., Yang, J., Li, J., Li, F., and Tan, H.-B. (2020). Immune cells within the tumor microenvironment: Biological functions and roles in cancer immunotherapy. Cancer Lett. *470*, 126–133.

Li, H., Jiang, T., Li, M.-Q., Zheng, X.-L., and Zhao, G.-J. (2018). Transcriptional Regulation of

Macrophages Polarization by MicroRNAs. Front. Immunol. *9*.

Li, J., Jiang, Y., Ma, M., Wang, L., Jing, M., Yang, Z., Wang, L., Qiu, Q., Song, R., Pu, Y., et al. (2024a). IGF2BP2 Shapes the Tumor Microenvironment by Regulating Monocyte and Macrophage Recruitment in Bladder Cancer. Cancer Med. *13*, 1–17.

Li, N., Deng, L., Zhang, Y., Tang, X., Lei, B., and Zhang, Q. (2024b). IGF2BP2 modulates autophagy and serves as a prognostic marker in glioma. Ibrain *10*, 19–33.

Li, T., Hu, P.-S., Lin, J.-F., Ju, H.-Q., and Xu, R.-H. (2019). IDDF2019-ABS-0290 IGF2BP2 facilitates tumor progression via an m6A-dependent mechanism in colorectal carcinoma. Gut *68*, A30 LP-A30.

Li, Y., Xiao, Z., Wang, Y., Zhang, D., and Chen, Z. (2024c). The m6A reader IGF2BP2 promotes esophageal cell carcinoma progression by enhancing EIF4A1 translation. Cancer Cell Int. *24*, 1–12.

Li, Z., Lao, Y., Yan, R., Guan, X., Bai, Y., Li, F., and Dong, Z. (2024d). N6-methyladenosine (m6A) modification in inflammation: a bibliometric analysis and literature review. PeerJ *12*, e18645.

Lin, C.-W., Yang, W.-E., Su, C.-W., Lu, H.-J., Su, S.-C., and Yang, S.-F. (2024a). IGF2BP2 promotes cell invasion and epithelial-mesenchymal transition through Src-mediated upregulation of EREG in oral cancer. Int. J. Biol. Sci. *20*, 818–830.

Lin, C.W., Yang, W.E., Su, C.W., Lu, H.J., Su, S.C., and Yang, S.F. (2024b). IGF2BP2 promotes cell invasion and epithelial-mesenchymal transition through Src-mediated upregulation of EREG in oral cancer. Int. J. Biol. Sci. *20*, 818–830.

Lin, Y., Xu, J., and Lan, H. (2019). Tumor-associated macrophages in tumor metastasis: Biological roles and clinical therapeutic applications. J. Hematol. Oncol. *12*, 1–16.

Linnenberger, R., Hoppstädter, J., Wrublewsky, S., Ampofo, E., and Kiemer, A.K. (2021). Statins and bempedoic acid: Different actions of cholesterol inhibitors on macrophage activation. Int. J. Mol. Sci. *22*.

Liu, W., and Zeng, H. (2024). IGF2BP2 attenuates intestinal epithelial cell ferroptosis in colitis by stabilizing m6A-modified GPX4 mRNA. Cytokine *173*, 156388.

Liu, D., Xia, A.D., Wu, L.P., Li, S., Zhang, K., and Chen, D. (2022a). IGF2BP2 promotes gastric cancer progression by regulating the IGF1R-RhoA-ROCK signaling pathway. Cell. Signal. *94*, 110313.

Liu, H. Bin, Muhammad, T., Guo, Y., Li, M.J., Sha, Q.Q., Zhang, C.X., Liu, H., Zhao, S.G., Zhao, H., Zhang, H., et al. (2019). RNA-Binding Protein IGF2BP2/IMP2 is a Critical Maternal Activator in Early Zygotic Genome Activation. Adv. Sci. *6*.

Liu, Y., Shi, M., He, X., Cao, Y., Liu, P., Li, F., Zou, S., Wen, C., Zhan, Q., Xu, Z., et al. (2022b).

LncRNA-PACERR induces pro-tumour macrophages via interacting with miR-671-3p and m6A-reader IGF2BP2 in pancreatic ductal adenocarcinoma. J. Hematol. Oncol. *15*, 1–18.

Lu, C., Xu, G., and Ma, J. (2023). Targeting RNA-binding proteins for cancer therapy. Clin. Transl. Discov. *3*.

Lu, D., Zhang, X., Ye, H., Wang, J., and Han, D. (2024). Milk-Derived Extracellular Vesicles Carrying ssc-let-7c Alleviate Early Intestinal Inflammation and Regulate Macrophage Polarization via Targeting the PTEN-Mediated PI3K/Akt Pathway. J. Agric. Food Chem.

Luan, H.H., and Medzhitov, R. (2016). Food Fight: Role of Itaconate and Other Metabolites in Antimicrobial Defense. Cell Metab. *24*, 379–387.

Luo, S., Yang, G., Ye, P., Cao, N., Chi, X., Yang, W.-H., and Yan, X. (2022). Macrophages Are a Double-Edged Sword: Molecular Crosstalk between Tumor-Associated Macrophages and Cancer Stem Cells. Biomolecules *12*.

Ma, X.X., Zhou, X.Y., Feng, M.G., Ji, Y.T., Song, F.F., Tang, Q.C., He, Q., and Zhang, Y.F. (2024). Dual Role of IGF2BP2 in Osteoimmunomodulation during Periodontitis. J. Dent. Res. *103*, 208–217.

Malier, M., Gharzeddine, K., Lavérriere, M., Marsili, S., Thomas, F., Decaens, T., Roth, G., and Millet, A. (2020). Hypoxia Drives Dihydropyrimidine Dehydrogenase Expression in Macrophages and Confers Chemoresistance in Colorectal Cancer. Cancer Res. *81*, 5963–5976.

Malier, M., Gharzeddine, K., Laverriere, M.H., Marsili, S., Thomas, F., Decaens, T., Roth, G., and Millet, A. (2021). Hypoxia drives dihydropyrimidine dehydrogenase expression in macrophages and confers chemoresistance in colorectal cancer. Cancer Res.

Man, S.M., and Kanneganti, T.D. (2016). Regulation of lysosomal dynamics and autophagy by CTSB/cathepsin B. Autophagy *12*, 2504–2505.

Mantovani, A., Biswas, S., Galdiero, M., Sica, A., and Locati, M. (2013). Macrophage plasticity and polarization in tissue repair and remodelling. J. Pathol. *229*.

Mantovani, A., Marchesi, F., Malesci, A., Laghi, L., and Allavena, P. (2017). Tumour-associated macrophages as treatment targets in oncology. Nat. Rev. Clin. Oncol. *14*, 399–416.

Marchesi, F., Cirillo, M., Bianchi, A., Gately, M., Olimpieri, O., Cerchiara, E., Renzi, D., Micera, A., Balzamino, B., Bonini, S., et al. (2015). High density of CD68+/CD163+ tumour-associated macrophages (M2-TAM) at diagnosis is significantly correlated to unfavorable prognostic factors and to poor clinical outcomes in patients with diffuse large B-cell lymphoma. Hematol. Oncol. *33*, 110–112.

Markle, J.G., and Fish, E.N. (2014). SeXX matters in immunity. Trends Immunol. *35*, 97–104.

Marrone, L., Romano, S., Malasomma, C., Di Giacomo, V., Cerullo, A., Abate, R., Vecchione, M.A., Fratantonio, D., and Romano, M.F. (2024). Metabolic vulnerability of cancer stem cells and their niche. Front. Pharmacol. *15*, 1–18.

Mashayekhi, V., Schomisch, A., Rasheed, S., Puerta, E.A., Risch, T., Yildiz, D., Koch, M., Both, S., Ludwig, N., Legroux, T.M., et al. (2024). The RNA binding protein IGF2BP2 / IMP2 alters the cargo of cancer cell - derived extracellular vesicles supporting tumor - associated macrophages. Cell Commun. Signal. 1–25.

Maueröder, C., Munoz, L.E., Chaurio, R.A., Herrmann, M., Schett, G., and Berens, C. (2014). Tumor immunotherapy: lessons from autoimmunity. Front. Immunol. *5*, 212.

McDermott, J.D., Subbiah, V., Beck, J.T., Doi, T., Hirohashi, T., Ingram, K., Li, R., and Abbruzzese, J.L. (2023). Trials in progress: A phase 1, open-label, pharmacokinetic, safety and tolerability study of PF-07265807 (selective TAM kinase inhibitor) alone or with sasanlimab in patients with advanced or metastatic solid tumors. J. Clin. Oncol. *41*, TPS270–TPS270.

Mcgranahan, N., and Roychoudhuri, R. News & views Y-chromosome loss in immune cells drives cancer. 1–2.

McWhorter, R., and Bonavida, B. (2024). The Role of TAMs in the Regulation of Tumor Cell Resistance to Chemotherapy. Crit. Rev. Oncog. *29 4*, 97–125.

Mehrotra, P., and Ravichandran, K.S. (2022). Drugging the efferocytosis process: concepts and opportunities. Nat. Rev. Drug Discov. *21*, 601–620.

Mei, J., Huang, X., Fan, C., Fang, J., and Jiu, Y. (2023). Cytoskeleton network participates in the anti-infection responses of macrophage. BioEssays *45*, 1–11.

Meirson, T., Gil-Henn, H., and Samson, A.O. (2020). Invasion and metastasis: the elusive hallmark of cancer. Oncogene *39*, 2024–2026.

Merrheim, J., Villegas, J., Van Wassenhove, J., Khansa, R., Berrih-Aknin, S., Panse, L., and Dragin, N. (2020). ESTROGEN, ESTROGEN-LIKE MOLECULES AND AUTOIMMUNE DISEASES. Autoimmun. Rev. 102468.

Mills, E.L., and O'Neill, L.A. (2016). Reprogramming mitochondrial metabolism in macrophages as an anti-inflammatory signal. Eur. J. Immunol. *46*, 13–21.

Montoya, D., Mehta, M., Ferguson, B.G., Teles, R.M.B., Krutzik, S.R., Cruz, D., Pellegrini, M., and Modlin, R.L. (2019). Plasticity of antimicrobial and phagocytic programs in human macrophages. Immunology *156*, 164–173.

Murdoch, J.D., Rostosky, C.M., Gowrisankaran, S., Arora, A.S., Soukup, S.F., Vidal, R., Capece, V., Freytag, S., Fischer, A., Verstreken, P., et al. (2016). Endophilin-A Deficiency Induces the Foxo3a-Fbxo32 Network in the Brain and Causes Dysregulation of Autophagy and the Ubiquitin-Proteasome System. Cell Rep. *17*, 1071–1086.

Murray, P.J. (2017). Macrophage Polarization. Annu. Rev. Physiol. *79*, 541–566.

Nakamura, K., and Smyth, M. (2019). Myeloid immunosuppression and immune checkpoints in the tumor microenvironment. Cell. Mol. Immunol. *17*, 1–12.

Nam, G.H., Hong, Y., Choi, Y., Kim, G.B., Kim, Y.K., Yang, Y., and Kim, I.S. (2019). An optimized protocol to determine the engulfment of cancer cells by phagocytes using flow cytometry and fluorescence microscopy. J. Immunol. Methods *470*, 27–32.

Nan, Y., Chen, M., Wu, W., Huang, R., Sun, W., Lu, Q., Gu, Z., Mao, X., Xu, H., and Wang, Y. (2024). IGF2BP2 regulates the inflammation of fibroblast-like synoviocytes via GSTM5 in rheumatoid arthritis. Cell Death Discov. *10*, 1–11.

Neophytou, C.M., Panagi, M., Stylianopoulos, T., and Papageorgis, P. (2021a). The role of tumor microenvironment in cancer metastasis: Molecular mechanisms and therapeutic opportunities. Cancers (Basel). *13*.

Neophytou, C.M., Panagi, M., Stylianopoulos, T., and Papageorgis, P. (2021b). The Role of Tumor Microenvironment in Cancer Metastasis: Molecular Mechanisms and Therapeutic Opportunities. Cancers (Basel). *13*.

Novello, S., Stabile, L.P., and Siegfried, J.M. (2018). 5 - Gender-Related Differences in Lung Cancer. In IASLC Thoracic Oncology (Second Edition), H.I. Pass, D. Ball, and G. V Scagliotti, eds. (Philadelphia: Elsevier), pp. 30-45.e5.

Ó Maoldomhnaigh, C., Cox, D.J., Phelan, J.J., Malone, F.D., Keane, J., and Basdeo, S.A. (2021). The Warburg Effect Occurs Rapidly in Stimulated Human Adult but Not Umbilical Cord Blood Derived Macrophages. Front. Immunol. *12*, 1–13.

Oh, M.S., Anker, J.F., and Chae, Y.K. (2021). High gene expression of estrogen and progesterone receptors is associated with decreased t cell infiltration in patients with NSCLC. Cancer Treat. Res. Commun. *27*, 100317.

Ortona, E., Matarrese, P., and Malorni, W. (2014). Taking into account the gender issue in cell death studies. Cell Death Dis. *5*, e1121.

Palmieri, E.M., Gonzalez-Cotto, M., Baseler, W.A., Davies, L.C., Ghesquière, B., Maio, N., Rice, C.M., Rouault, T.A., Cassel, T., Higashi, R.M., et al. (2020). Nitric oxide orchestrates metabolic rewiring in

M1 macrophages by targeting aconitase 2 and pyruvate dehydrogenase. Nat. Commun. *11*.

Pan, Y., Yu, Y., Wang, X., and Zhang, T. (2020). Tumor-Associated Macrophages in Tumor Immunity. Front. Immunol. *11*, 583084.

Park, M., Silvin, A., Ginhoux, F., and Merad, M. (2022). Macrophages in health and disease. Cell *185*, 4259–4279.

Pathria, P., Louis, T.L., and Varner, J.A. (2019). Targeting Tumor-Associated Macrophages in Cancer. Trends Immunol. *40*, 310–327.

Pérez, S., and Rius-Pérez, S. (2022). Macrophage Polarization and Reprogramming in Acute Inflammation: A Redox Perspective. Antioxidants *11*.

Piskovatska, V., Buheruk, V., Strilbytska, O., Zayachkivska, A., and Lushchak, O. V (2023). Chapter 10 - Nonsteroidal anti-inflammatory drugs. In Anti-Aging Pharmacology, V.K. Koltover, ed. (Academic Press), pp. 227–243.

Pyarilal, S., Aathira, S., Arpitha, A., Arvind, K., and and Pal, U.M. (2025). Early detection of carcinoma: correlating quantifiable tumor biomarkers with High-Resolution Microscopy (HRME) findings. Expert Rev. Mol. Diagn. *25*, 33–45.

Qian, B., Wang, P., Zhang, D., and Wu, L. (2021). m6A modification promotes miR-133a repression during cardiac development and hypertrophy via IGF2BP2. Cell Death Discov. *7*, 157.

Qian, L., Ji, Z., Mei, L., and Zhao, J. (2024). IGF2BP2 promotes lung adenocarcinoma progression by regulating LOX1 and tumor-associated neutrophils. Immunol. Res. *73*, 16.

Rabani, R., Volchuk, A., Jerkic, M., Ormesher, L., Garcés-Ramírez, L., Canton, J., Masterson, C., Gagnon, S., Tatham, K., Marshall, J., et al. (2018). Mesenchymal stem cells enhance NOX2-dependent reactive oxygen species production and bacterial killing in macrophages during sepsis. Eur. Respir. J. *51*.

Rajabalee, N.B.M.H., Siushansian, H., Weerapura, M., Berton, S., Berbatovci, F., Hooks, B., Geoffrion, M., Yang, D., Harper, M., Rayner, K., et al. (2023). ATF2 orchestrates macrophage differentiation and activation to promote antibacterial responses. J. Leukoc. Biol.

Ramos-Inza, S., Ruberte, A.C., Sanmartín, C., Sharma, A.K., and Plano, D. (2021). NSAIDs: Old Acquaintance in the Pipeline for Cancer Treatment and Prevention-Structural Modulation, Mechanisms of Action, and Bright Future. J. Med. Chem. *64*, 16380–16421.

Rasheed, A., and Koyyala, V. (2020). The tumor microenvironment. Curr. Biol. *30*.

Ray, A.L., Nofchissey, R.A., Khan, M.A., Reidy, M.A., Lerner, M.R., Wu, X., Guo, S., Hill, S.L.,

Weygant, N., Adams, S.F., et al. (2020). The role of sex in the innate and adaptive immune environment of metastatic colorectal cancer. Br. J. Cancer *123*, 624–632.

Regué, L., Zhao, L., Ji, F., Wang, H., Avruch, J., and Dai, N. (2021). RNA m6A reader IMP2/IGF2BP2 promotes pancreatic β-cell proliferation and insulin secretion by enhancing PDX1 expression. Mol. Metab. *48*, 101209.

Regué, L., Wang, W., Ji, F., Avruch, J., Wang, H., and Dai, N. (2023). Human T2D-Associated Gene IMP2/IGF2BP2 Promotes the Commitment of Mesenchymal Stem Cells Into Adipogenic Lineage. Diabetes *72*, 33–44.

Ren, X., Zhang, L., Zhang, Y., Li, Z., Siemers, N., and Zhang, Z. (2021). Insights Gained from Single-Cell Analysis of Immune Cells in the Tumor Microenvironment. Annu. Rev. Immunol. *39*, 583–609.

Riabov, V., Gudima, A., Wang, N., Mickley, A., Orekhov, A., and Kzhyshkowska, J. (2014). Role of tumor associated macrophages in tumor angiogenesis and lymphangiogenesis. Front. Physiol. *5*.

Ritchie, H., Roser, M., and Rodés-Guirao, L. (2023). Burden of disease by cause.

Rubin, J.B., Lagas, J.S., Broestl, L., Sponagel, J., Rockwell, N., Rhee, G., Rosen, S.F., Chen, S., Klein, R.S., Imoukhuede, P., et al. (2020). Sex differences in cancer mechanisms. Biol. Sex Differ. *11*, 1–29.

Schulz, D., Severin, Y., Zanotelli, V., and Bodenmiller, B. (2019). In-Depth Characterization of Monocyte-Derived Macrophages using a Mass Cytometry-Based Phagocytosis Assay. Sci. Rep. *9*.

Shao, W., Zhao, H., Zhang, S., Ding, Q., Guo, Y., Hou, K., Kan, Y., Deng, F., and Xu, Q. (2023). A pan-cancer landscape of IGF2BPs and their association with prognosis, stemness and tumor immune microenvironment. Front. Oncol. *12*, 1–16.

Shapouri-Moghaddam, A., Mohammadian, S., Vazini, H., Taghadosi, M., Esmaeili, S.A., Mardani, F., Seifi, B., Mohammadi, A., Afshari, J.T., and Sahebkar, A. (2018). Macrophage plasticity, polarization, and function in health and disease. J. Cell. Physiol. *233*, 6425–6440.

Sheng, J., Ruedl, C., and Karjalainen, K. (2015). Most Tissue-Resident Macrophages Except Microglia Are Derived from Fetal Hematopoietic Stem Cells. Immunity *43 2*, 382–393.

Simon, Y., Kessler, S.M., Bohle, R.M., Haybaeck, J., and Kiemer, A.K. (2014a). The insulin-like growth factor 2 (IGF2) mRNA-binding protein p62/IGF2BP2-2 as a promoter of NAFLD and HCC? Gut *63*, 861–863.

Simon, Y., Kessler, S.M., Gemperlein, K., Bohle, R.M., Müller, R., Haybaeck, J., and Kiemer, A.K. (2014b). Elevated free cholesterol in a p62 overexpression model of non-alcoholic steatohepatitis. World J. Gastroenterol. *20*, 17839–17850.

Singh, A., Raja, K.D., Singh, P., Seth, A., Kaushal, S., and Sharma, A. (2024). 38P Targeting autophagy in tumor-associated macrophages effects the phenotype and tumor progression in urothelial carcinoma of bladder. ESMO Open *9*, 102373.

Smida, T., Bruno, T.C., and Stabile, L.P. (2020). Influence of Estrogen on the NSCLC Microenvironment: A Comprehensive Picture and Clinical Implications. Front. Oncol. *10*, 1–15.

Song, H., Wang, Q., Guo, Y., Liu, S., Song, R., Gao, X., Dai, L., Li, B., Zhang, D., and Cheng, J. (2013). Microarray analysis of MicroRNA expression in peripheral blood mononuclear cells of critically ill patients with influenza A (H1N1). BMC Infect. Dis. *13*.

Soto-Heredero, G., Gómez de las Heras, M.M., Gabandé-Rodríguez, E., Oller, J., and Mittelbrunn, M. (2020). Glycolysis – a key player in the inflammatory response. FEBS J. *287*, 3350–3369.

de Souza Ferreira, S., Wallmann, T., Kerzel, T., Wallerius, M., Schauer, N., Landwehr, L.-S., Agardy, D.A., Bergh, J., Bartish, M., Hartman, J., et al. (2022). VEGF-C expressing Tumor Associated Macrophages decrease hematogenous metastatic dissemination and normalizes the tumor vasculature. BioRxiv 2022.01.26.468593.

Spencer, C.T., and Sanchez Guillen, M.A. (2022). Increased M1 macrophage activity makes females more sensitive to Francisella tularensis infection. J. Immunol. *208*, 50.16-50.16.

Sreejit, G., Fleetwood, A., Murphy, A., and Nagareddy, P. (2020). Origins and diversity of macrophages in health and disease. Clin. Transl. Immunol. *9*.

Stöhr, N., and Hüttelmaier, S. (2012). IGF2BP1: A post-transcriptional “driver” of tumor cell migration. Cell Adhes. Migr. *6*, 312–318.

Streiff, C., Herrera, A., Voelkl, B., Palme, R., Würbel, H., and Novak, J. (2024). The impact of cage dividers on mouse aggression, dominance and hormone levels. PLoS One *19*, 1–17.

Strizova, Z., Benešová, I., Bartolini, R., Novysedlak, R., Čečrdlová, E., Foley, L.K., and Stříž, I. (2023a). M1/M2 macrophages and their overlaps – myth or reality? Clin. Sci. (Lond). *137*, 1067–1093.

Strizova, Z., Benesova, I., Bartolini, R., Novysedlak, R., Cecrdlova, E., Foley, L.K., and Striz, I. (2023b). M1/M2 macrophages and their overlaps - myth or reality? Clin. Sci. *137*, 1067–1093.

Summer, M., Riaz, S., Ali, S., Noor, Q., Ashraf, R., and Khan, R.R.M. (2025). Understanding the Dual Role of Macrophages in Tumor Growth and Therapy: A Mechanistic Review. Chem. Biodivers.

Sun, Y., Wu, J., Sun, W., Liu, C., and Shi, X. (2024). Novel insights into the interaction between IGF2BPs and ncRNAs in cancers. Cancer Cell Int. *24*.

Taban, Q., Mumtaz, P.T., Masoodi, K.Z., Haq, E., and Ahmad, S.M. (2022). Scavenger receptors in host

defense: from functional aspects to mode of action. Cell Commun. Signal. *20*, 2.

Tang, D., Han, B., He, C., Xu, Y., Liu, Z., Wang, W., Huang, Z., Xiao, Z., and He, F. (2024). Electrospun Poly-L-Lactic Acid Membranes Promote M2 Macrophage Polarization by Regulating the PCK2/AMPK/mTOR Signaling Pathway. Adv. Healthc. Mater.

Tatano, Y., Shimizu, T., Sano, C., and Tomioka, H. (2024). Roles of autophagy in killing of mycobacterial pathogens by host macrophages - Effects of some medicinal plants. Eur. J. Microbiol. Immunol. *14*, 26–36.

Tečić Vuger, A., Separovic, R., Tolaney, S.M., and Trapani, D. (2024). Globalization of clinical research in oncology: Status, challenges, and future directions. J. Cancer Policy *42*, 100500.

Theil, J.H., Ahloy-Dallaire, J., Weber, E.M., Gaskill, B.N., Pritchett-Corning, K.R., Felt, S.A., and Garner, J.P. (2020). The epidemiology of fighting in group-housed laboratory mice. Sci. Rep. *10*, 1–10.

Thiruchenthooran, V., Sánchez-López, E., and Gliszczyńska, A. (2023). Perspectives of the Application of Non-Steroidal Anti-Inflammatory Drugs in Cancer Therapy: Attempts to Overcome Their Unfavorable Side Effects. Cancers (Basel). *15*, 1–24.

Tong, N., He, Z., Ma, Y., Wang, Z., Huang, Z., Cao, H., Xu, L., Zou, Y., Wang, W., Yi, C., et al. (2021). Tumor Associated Macrophages, as the Dominant Immune Cells, Are an Indispensable Target for Immunologically Cold Tumor-Glioma Therapy? Front. Cell Dev. Biol. *9*, 706286.

Toren, P., Wilkins, A., Patel, K., Burley, A., Gris, T., Kockelbergh, R., Lodhi, T., Choudhury, A., and Bryan, R.T. (2024). The sex gap in bladder cancer survival — a missing link in bladder cancer care? Nat. Rev. Urol. *21*, 181–192.

Tybl, E., Shi, F.D., Kessler, S.M., Tierling, S., Walter, J., Bohle, R.M., Wieland, S., Zhang, J., Tan, E.M., and Kiemer, A.K. (2011). Overexpression of the IGF2-mRNA binding protein p62 in transgenic mice induces a steatotic phenotype. J. Hepatol. *54*, 994–1001.

Varghese, M., Clemente, J., Lerner, A., Abrishami, S., Islam, M., Subbaiah, P., and Singer, K. (2022). Monocyte Trafficking and Polarization Contribute to Sex Differences in Meta-Inflammation. Front. Endocrinol. (Lausanne). *13*, 1–13.

Velmurugan, S., Deshmukh, V.R., Sontakke, B.R., Chandrasekaran, K., and Subbaraj, G.K. (2025). Polymorphisms of IGF2BP2 and SIRT1 genes in type 2 diabetes mellitus: A comprehensive meta-analysis and statistical power analysis. World Acad. Sci. J. *7*, 1–14.

Vempati, R.K., and Malla, R.R. (2020). Autophagy-Induced Drug Resistance in Liver Cancer. Crit. Rev. Oncog. *25*, 21–30.

Vijayan, V., Pradhan, P., Braud, L., Fuchs, H.R., Gueler, F., Motterlini, R., Foresti, R., and Immenschuh, S. (2019). Human and murine macrophages exhibit differential metabolic responses to lipopolysaccharide - A divergent role for glycolysis. Redox Biol. *22*, 101147.

Viola, A., Munari, F., Sánchez-Rodríguez, R., Scolaro, T., and Castegna, A. (2019). The metabolic signature of macrophage responses. Front. Immunol. *10*, 1–16.

Vitaliti, A., Reggio, A., and Palma, A. (2024). Macrophages and autophagy: partners in crime. FEBS J.

Vogel, A., and Weichhart, T. (2023). Tissue-resident macrophages — early passengers or drivers in the tumor niche? Curr. Opin. Biotechnol. *83*, 102984.

Vorselen, D., Barger, S.R., Wang, Y., Cai, W., Theriot, J.A., Gauthier, N.C., and Krendel, M. (2021). Phagocytic “teeth” and myosin-ii “jaw” power target constriction during phagocytosis. Elife *10*, 1–31.

Wang, J., Chen, L., and Qiang, P. (2021a). The role of IGF2BP2, an m6A reader gene, in human metabolic diseases and cancers. Cancer Cell Int. *21*, 1–11.

Wang, L., Wang, H., Yu, L., Jiang, H., and Xia, L. (2023a). MIF Regulates M1 Macrophage Polarization via CD74/CXCR2/JNK Pathway and Mediates Aortic Dissection in Mice. BioRxiv 2023.10.26.564292.

Wang, P., Wang, X., He, D., and Zhuang, C. (2023b). LncRNA AK142643 promotes hepatic lipid accumulation by upregulating CD36 via interacting with IGF2BP2. Gene *887*, 147747.

Wang, X., Ji, Y., Feng, P., Liu, R., Li, G., Zheng, J., Xue, Y., Wei, Y., Ji, C., Chen, D., et al. (2021b). The m6A Reader IGF2BP2 Regulates Macrophage Phenotypic Activation and Inflammatory Diseases by Stabilizing TSC1 and PPARγ. Adv. Sci. *2100209*, 1–14.

Wang, X., Ji, Y., Feng, P., Liu, R., Li, G., Zheng, J., Xue, Y., Wei, Y., Ji, C., Chen, D., et al. (2021c). The m6A Reader IGF2BP2 Regulates Macrophage Phenotypic Activation and Inflammatory Diseases by Stabilizing TSC1 and PPARγ. Adv. Sci. *8*, 1–14.

Wang, X., Li, X., Zhou, Y., Huang, X., and Jiang, X. (2021d). Long non-coding RNA OIP5-AS1 inhibition upregulates microRNA-129-5p to repress resistance to temozolomide in glioblastoma cells via downregulating IGF2BP2. Cell Biol. Toxicol.

Wang, Y., Lu, J.-H., Wu, Q.-N., Jin, Y., Wang, D.-S., Chen, Y.-X., Liu, J., Luo, X.-J., Meng, Q., Pu, H.-Y., et al. (2019). LncRNA LINRIS stabilizes IGF2BP2 and promotes the aerobic glycolysis in colorectal cancer. Mol. Cancer *18*, 174.

Watanabe, S., Watanabe, S., Alexander, M., Misharin, A., and Budinger, G. (2019). The role of macrophages in the resolution of inflammation. J. Clin. Invest. *130*.

Weng, H., Huang, F., Yu, Z., Chen, Z., Prince, E., Kang, Y., Zhou, K., Li, W., Hu, J., Fu, C., et al.

(2022). The m(6)A reader IGF2BP2 regulates glutamine metabolism and represents a therapeutic target in acute myeloid leukemia. Cancer Cell *40*, 1566-1582.e10.

Wilkinson, N.M., Chen, H.C., Lechner, M.G., and Su, M.A. (2022). Sex Differences in Immunity. Annu. Rev. Immunol. *40*, 75–94.

Wu, P. (2020). Inhibition of RNA-binding proteins with small molecules. Nat. Rev. Chem. *4*, 441–458.

Wu, M.Y., and Lu, J.H. (2020). Autophagy and macrophage functions: Inflammatory response and phagocytosis. Cells *9*, 1–25.

Wu, Y., Zhong, J.L., Hou, N., Sun, Y., Ma, B., Nisar, M.F., Teng, Y., Tan, Z., Chen, K., Wang, Y., et al. (2017). MicroRNA Let-7b inhibits keratinocyte migration in cutaneous wound healing by targeting IGF2BP2. Exp. Dermatol. *26*, 116–123.

Wynn, T., and Vannella, K. (2016). Macrophages in Tissue Repair, Regeneration, and Fibrosis. Immunity *44 3*, 450–462.

Xia, C., Li, Q., Cheng, X., Wu, T., Gao, P., and Gu, Y. (2022). Insulin-like growth factor 2 mRNA-binding protein 2-stabilized long non-coding RNA Taurine up-regulated gene 1 (TUG1) promotes cisplatin-resistance of colorectal cancer via modulating autophagy. Bioengineered *13*, 2450–2469.

Xia, T., Dai, X.Y., Sang, M.Y., Zhang, X., Xu, F., Wu, J., Shi, L., Wei, J.F., and Ding, Q. (2024). IGF2BP2 Drives Cell Cycle Progression in Triple-Negative Breast Cancer by Recruiting EIF4A1 to Promote the m6A-Modified CDK6 Translation Initiation Process. Adv. Sci. *11*, 1–15.

Xiao, Y., Wang, Z., Zhao, M., Deng, Y., Yang, M., Su, G., Yang, K., Qian, C., Hu, X., Liu, Y., et al. (2022). Single-Cell Transcriptomics Revealed Subtype-Specific Tumor Immune Microenvironments in Human Glioblastomas. Front. Immunol. *13*, 1–17.

Xu, X., Yu, Y., Zong, K., Lv, P., and Gu, Y. (2019). Up-regulation of IGF2BP2 by multiple mechanisms in pancreatic cancer promotes cancer proliferation by activating the PI3K/Akt signaling pathway. J. Exp. Clin. Cancer Res. *38*, 1–14.

Yanamandra, A.K., Zhang, J., Montalvo, G., Zhou, X., Biedenweg, D., Zhao, R., Sharma, S., Hoth, M., Lautenschläger, F., Otto, O., et al. (2024). PIEZO1-mediated mechanosensing governs NK-cell killing efficiency and infiltration in three-dimensional matrices. Eur. J. Immunol. *54*, e2350693.

Yang, M., Gallo-ebert, C., Hayward, M., Liu, W., Mcdonough, V., and Nickels, J.T. (2020a). crossm Increases MicroRNA 33a / b Inhibition of Liver ABCA1. *40*, 1–15.

Yang, M., Gallo-Ebert, C., Hayward, M., Liu, W., McDonough, V., and Nickels, J.T.J. (2020b). Human Insulin Growth Factor 2 mRNA Binding Protein 2 Increases MicroRNA 33a/b Inhibition of Liver

ABCA1 Expression and Alters Low-Density Apolipoprotein Levels in Mice. Mol. Cell. Biol. *40*.

Yang, Q., Guo, N., Zhou, Y., Chen, J., Wei, Q., and Han, M. (2020c). The role of tumor-associated macrophages (TAMs) in tumor progression and relevant advance in targeted therapy. Acta Pharm. Sin. B *10*, 2156–2170.

Yang, Q., Zhang, H., Wei, T., Lin, A., Sun, Y., Luo, P., and Zhang, J. (2021). Single-Cell RNA Sequencing Reveals the Heterogeneity of Tumor-Associated Macrophage in Non-Small Cell Lung Cancer and Differences Between Sexes. Front. Immunol. *12*, 1–18.

Yang, S., Zhao, M., and Jia, S. (2023). Macrophage: Key player in the pathogenesis of autoimmune diseases. Front. Immunol. *14*, 1–15.

Yao, Y., Xu, X.H., and Jin, L. (2019). Macrophage polarization in physiological and pathological pregnancy. Front. Immunol. *10*, 1–13.

Yin, S., Huang, J., Li, Z.-S., Zhang, J., Luo, J., Lu, C., Xu, H., and Xu, H.-M. (2017). The Prognostic and Clinicopathological Significance of Tumor-Associated Macrophages in Patients with Gastric Cancer: A Meta-Analysis. PLoS One *12*.

Yolal Ertural, D., Çınkır, Ü., and Aras, N. (2024). Investigation of Insulin-Like Growth Factor 2 mRNA Binding Protein 2 Gene Polymorphisms in Type 2 Diabetes Patients. Genel Tıp Derg. *34*, 332–336.

Yu, D., Xiao, Z., Zou, Z., Lin, L., Li, J., Tan, J., and Chen, W. (2023). IGF2BP2 promotes head and neck squamous carcinoma cell proliferation and growth via the miR-98-5p/PI3K/Akt signaling pathway. Front. Oncol. *13*, 1–13.

Yu, P., Zhang, X., Liu, N., Tang, L., Peng, C., and Chen, X. (2021). Pyroptosis: mechanisms and diseases. Signal Transduct. Target. Ther. *6*.

Yu, Q., Ding, J., Li, S., and Li, Y. (2024). Autophagy in cancer immunotherapy: Perspective on immune evasion and cell death interactions. Cancer Lett. *590*, 216856.

Yu, T., Gan, S., Zhu, Q., Dai, D., Li, N., Wang, H., Chen, X., Hou, D., Wang, Y., Pan, Q., et al. (2019). Modulation of M2 macrophage polarization by the crosstalk between Stat6 and Trim24. Nat. Commun. *10*.

Yuan, X., Zhang, J., Li, D., Mao, Y., Mo, F., Du, W., and Xuelei (2017). Prognostic significance of tumor-associated macrophages in ovarian cancer: A meta-analysis. Gynecol. Oncol. *147 1*, 181–187.

Yunna, C., Hu, M., Lei, W., and Chen, W. (2020). Macrophage M1/M2 polarization. Eur. J. Pharmacol. 173090.

Zhang, C., Yang, M., and Ericsson, A.C. (2021a). Function of Macrophages in Disease: Current

Understanding on Molecular Mechanisms. Front. Immunol. *12*, 1–12.

Zhang, L., Lu, X., Xu, Y., La, X., Tian, J., Li, A., Li, H., Wu, C., Xi, Y., Song, G., et al. (2023). Tumor-associated macrophages confer colorectal cancer 5-fluorouracil resistance by promoting MRP1 membrane translocation via an intercellular CXCL17/CXCL22–CCR4–ATF6–GRP78 axis. Cell Death Dis. *14*.

Zhang, M., Hutter, G., Kahn, S.A., Azad, T.D., Gholamin, S., Xu, C.Y., Liu, J., Achrol, A.S., Richard, C., Sommerkamp, P., et al. (2016). Anti-CD47 Treatment Stimulates Phagocytosis of Glioblastoma by M1 and M2 Polarized Macrophages and Promotes M1 Polarized Macrophages In Vivo. PLoS One *11*, e0153550.

Zhang, P., Cao, L., Zhou, R., Yang, X., and Wu, M. (2019). The lncRNA Neat1 promotes activation of inflammasomes in macrophages. Nat. Commun. *10*, 1–17.

Zhang, Q., Zhu, B., and Li, Y. (2017). Resolution of Cancer-Promoting Inflammation: A New Approach for Anticancer Therapy. Front. Immunol. *8*.

Zhang, W., Fu, X., Xie, J., Pan, H., Han, W., and Huang, W. (2021b). miR-26a attenuates colitis and colitis-associated cancer by targeting the multiple intestinal inflammatory pathways. Mol. Ther. Nucleic Acids *24*, 264–273.

Zhang, Z., Xing, Y., Gao, W., Yang, L., Shi, J., Song, W., and Li, T. (2022). N(6)-methyladenosine (m(6)A) reader IGF2BP2 promotes gastric cancer progression via targeting SIRT1. Bioengineered *13*, 11541–11550.

Zhao, H., Wu, L., Yan, G., Chen, Y., Zhou, M., Wu, Y., and Li, Y. (2021a). Inflammation and tumor progression: signaling pathways and targeted intervention. Signal Transduct. Target. Ther. *6*, 263.

Zhao, H., Wu, L., Yan, G., Chen, Y., Zhou, M., Wu, Y., and Li, Y. (2021b). Inflammation and tumor progression: signaling pathways and targeted intervention. Signal Transduct. Target. Ther. *6*.

Zhao, X., Ren, T., Li, S., Wang, X., Hou, R., Guan, Z., Liu, D., Zheng, J., and Shi, M. (2024). A new perspective on the therapeutic potential of tumor metastasis: targeting the metabolic interactions between TAMs and tumor cells. Int. J. Biol. Sci. *20*, 5109–5126.

Zhao, Y., Shen, M., Wu, L., Yang, H., Yao, Y., Yang, Q., Du, J., Liu, L., Li, Y., and Bai, Y. (2023). Stromal cells in the tumor microenvironment: accomplices of tumor progression? Cell Death Dis. *14*, 587.

Zhou, B., Luo, Y., Ji, N., Mao, F., Xiang, L., Bian, H., Zheng, M.-H., Hu, C., Li, Y., and Lu, Y. (2022a). Promotion of nonalcoholic steatohepatitis by RNA N(6)-methyladenosine reader IGF2BP2 in mice. Life Metab. *1*, 161–174.

Zhou, L., Li, H., Cai, H., Liu, W., Pan, E., Yu, D., and He, S. (2022b). Upregulation of IGF2BP2 Promotes Oral Squamous Cell Carcinoma Progression That Is Related to Cell Proliferation, Metastasis and Tumor-Infiltrating Immune Cells. Front. Oncol. *12*, 809589.

Zhou, L., Li, H., Cai, H., Liu, W., Pan, E., Yu, D., and He, S. (2022c). Upregulation of IGF2BP2 Promotes Oral Squamous Cell Carcinoma Progression That Is Related to Cell Proliferation, Metastasis and Tumor-Infiltrating Immune Cells. Front. Oncol. *12*, 1–16.

Zhu, T.Y., Hong, L.L., and Ling, Z.Q. (2023). Oncofetal protein IGF2BPs in human cancer: functions, mechanisms and therapeutic potential. Biomark. Res. *11*, 1–15.

Zorc, S., Munoz-Tello, P., O'Leary, T., Yu, X., Giridhar, M.N.K., Hansel-Harris, A., Forli, S., Griffin, P.R., Kojetin, D.J., Roy, R.N., et al. (2024). Structural insights into IMP2 dimerization and RNA binding. BioRxiv Prepr. Serv. Biol.

9 Appendix

Abbrevations

AKT	Protein kinase B (AKT serine/threonine kinase)
APC	Antigen-presenting cell
ATP	Adenosine triphosphate
BLI	Bioluminescence imaging
BMM	Bone marrow-derived macrophage
BSA	Bovine serum albumin
CAFs	Cancer-associated fibroblasts
CCL2	Chemokine ligand 2
CD	Cluster of differentiation
CE	Cholesteryl ester
CSCs	Cancer stem cells
cDNA	Complementary DNA
CXCL9	Chemokine (C-X-C motif) ligand 9
DMEM	Dulbecco's Modified Eagle's Medium
DMSO	Dimethyl sulfoxide
DPD	Dihydropyrimidine dehydrogenase
ECAR	Extracellular acidification rate
EDTA	Ethylenediaminetetraacetic acid
ELISA	Enzyme-linked immunosorbent assay
EMT	Epithelial-mesenchymal transition
ERK	Extracellular signal-regulated kinase
FACS	Fluorescence-activated cell sorting
FAO	Fatty-acid oxidation
FCCP	Carbonyl cyanide-4-(trifluoromethoxy)phenylhydrazone
FBS	Fetal bovine serum
FCS	Fetal calf serum

FSC	Forward scatter
GPX4	Glutathione peroxidase 4
h	Hour
H_2O bidest.	Aqua bidestillata
HCC	Hepatocellular carcinoma
HIF-1α	Hypoxia-inducible factor 1-alpha
HMDM	Human monocyte-derived macrophage
IFN-γ	Interferon-gamma
IGF2	Insulin-like growth factor 2
IGF2BP2/IMP2	Insulin-like growth factor 2 mRNA-binding protein 2
IGF2BPs/IMPs	IGF2 mRNA-binding proteins
IL	Interleukin
IPA	Ingenuity Pathway Analysis
KEGG	Kyoto Encyclopedia of Genes and Genomes
KH	hnRNP K homology
KLF12	Krüppel-like factor 12
KO	Knockout
lncRNA	Long non-coding RNA
LPS	Lipopolysaccharide
LUAD	Lung adenocarcinoma
LUSC	Lung squamous-cell carcinoma
M-CSF	Macrophage colony-stimulating factor
MFI	Mean fluorescence intensity
min	Minutes
miR	microRNA
MMP9	Matrix metalloproteinase 9
mRNA	Messenger RNA

mTOR	Mechanistic target of rapamycin
MTT	3-(4,5-dimethylthiazole-2-yl)-2,5 diphenyltetrazolium bromide
MΦ	Macrophage
NF-κB	Nuclear factor kappa-light-chain-enhancer of activated B cells
NK	Natural killer (cell)
NO	Nitric oxide
NSCLC	Non-small cell lung cancer
OCR	Oxygen consumption rate
OXPHOS	Oxidative phosphorylation
PBS	Phosphate-buffered saline
PCR	Polymerase chain reaction
PD-L1/2	Programmed death ligand 1/2
PDAC	Pancreatic ductal adenocarcinoma
PMA	Phorbol 12-myristate 13-acetate
PPARγ	Peroxisome proliferator-activated receptor gamma
qRT-PCR	Quantitative real-time polymerase chain reaction
RBPs	RNA-binding proteins
RIN	RNA integrity number
RNA	Ribonucleic acid
RNA-Seq	RNA sequencing
ROS	Reactive oxygen species
RPM	reads per million
RPMI	Roswell Park Memorial Institute 1640 Medium
RRM	RNA recognition motif
RT-DC	Real-time deformability cytometry
SRC	Spare respiratory capacity
TAM	Tumor-associated macrophage

TCA	Tricarboxylic acid
TCM	Tumor-conditioned medium
TME	Tumor microenvironment
TNF	Tumor necrosis factor
Treg	Regulatory T cell
TSC1	Tuberous sclerosis complex 1
VEGF	Vascular endothelial growth factor
WT	Wildtype

List of Figures

Part I: Published work: *Comment on: The m6A Reader IGF2BP2 Regulates Macrophage Phenotypic Activation and Inflammatory Diseases by Stabilizing TSC1 and PPARγ.*

Part II: Submitted work: *IGF2BP2 Deficiency in Macrophages Induces Metabolic Reprogramming and Impairs Tumor Progression.*

List of Tables

Part II: Submitted work: *IGF2BP2 Deficiency in Macrophages Induces Metabolic Reprogramming and Impairs Tumor Progression.*

Publications

1. Hoppstädter J, Dembek A, Höring M, **Schymik HS**, Dahlem C, Sultan A, Wirth N, Al-Fityan S, Diesel B, Gasparoni G, Walter J, Helms V, Huwer H, Simon M, Liebisch G, Schulz MH, Kiemer AK. *Dysregulation of cholesterol homeostasis in human lung cancer tissue and tumour-associated macrophages.* EBioMedicine. 2021 doi: 10.1016/j.ebiom.2021.103578.

2. **Schymik HS**, Dahlem C, Barghash A, Kiemer AK. *Comment on: The m6A Reader IGF2BP2 Regulates Macrophage Phenotypic Activation and Inflammatory Diseases by Stabilizing TSC1 and PPARγ*. Adv Sci (Weinh). 2022 doi: 10.1002/advs.202104372.

3. Dahlem C, Chanda S, Hemmer J, **Schymik HS**, Kohlstedt M, Wittmann C, Kiemer AK. *Characterization of Anti-Cancer Activities of Violacein: Actions on Tumor Cells and the Tumor Microenvironment.* Front Oncol. 2022 doi: 10.3389/fonc.2022.872223.

4. Chanda S, Lepikhov K, Dahlem C, **Schymik HS**, Hoppstädter J, Geber AK, Wagner K, Kessler SM, Empting M, Kiemer AK. *Gene Editing and Small Molecule Inhibitors of the RNA Binding Protein IGF2BP2/IMP2 Show its Potential as an Anti-Cancer Drug Target.* Front Biosci (Landmark Ed). 2024 doi: 10.31083/j.fbl2901041.

5. Legroux TM, **Schymik HS**, Gasparoni G, Mohammadi S, Walter J, Libert C, Diesel B, Hoppstädter J, Kiemer AK. *Immunomodulation by glucocorticoid-induced leucine zipper in macrophages: enhanced phagocytosis, protection from pyroptosis, and altered mitochondrial function.* Front Immunol. 2024 doi: 10.3389/fimmu.2024.1396827.

6. **Schymik HS**, Wrublewsky S, Höring M, Liebisch G, Gasparoni G, Bickelmann C, Robertson H, Dahlem C, Walter J, Helms V, Laschke MW, Ampofo E, Hoppstädter J, Kiemer AK. *IGF2BP2 Deficiency in Macrophages Impairs Migration, Reprograms Metabolism, and Limits Tumor Progression*. Manuscript submitted 2025.

Curriculum Vitae

Current position

Since 2020 **PhD student** Department of Pharmaceutical Biology, Saarland University
Dissertation title: *"Insulin-Like Growth Factor 2 mRNA-Binding Protein 2 as a Regulator of Macrophage Function: Potential Implications for Tumor Progression*"
Supervisor: Prof. Dr. Alexandra Kiemer
Teaching and Mentoring Experience:

- **Lecturer**, *Pharmaceutical Biology II* – Microscopic and macroscopic characteristics of pharmaceutical drugs
- **Student Supervision**: Mentorship of elective interns, pharmacy students, and laboratory trainees during practical projects

Education

2019-2020 **Master of Science (M.Sc.)** Saarland University
Thesis: "*Impact of the long non-coding RNA H19 on macrophage functions*" Supervisor: Prof. Dr. Alexandra Kiemer

2014-2020 **Pharmacist (Approbation)** Albert Ludwig University of Freiburg
Completed 1st, 2nd, and 3rd State Examinations (2016, 2019, 2020)

2006-2014 **Abitur (1.9)** Ludwig-Marum Gymnasium Pfinztal

Internship & Practical Experience

05-10/2019 **Pharmaceutical Internship** Holzmarkt Pharmacy, Freiburg
Supervisor: Suzanne S. Sennecke-Bölch (Duration: 6 months)

10/2018 **Research Internship** Helmholtz Center Munich
Project: Apoptosis in hematopoietic stem cells
Supervisor: Prof. Dr. Irmela Jeremias (Duration: 3 weeks)

08-09/2017 **Research Internship** University of Freiburg
Institute of Experimental and Clinical Pharmacology and Toxicology, Supervisor: Prof. Dr. Lutz Hein (Duration: 4 weeks)

Awards

- **Oral and Poster Presentation Award**
  Doctoral Research Symposium (DPhG), Bonn, Germany (2023)
- **Poster Award**
  15th World Congress on Inflammation, Rome, Italy (2022)

Abstracts and Conferences

- **Schymik HS**, Dahlem C, Gasparoni G, Ludwig N, Aparicio-Puerta E, Walter J, Meese E, Keller A, Hoppstädter J, Kiemer AK (2023). *The regulation and role of the RNA-binding protein IMP2 in macrophage activation and function.*
  Annual PhD/Postdoc Meeting, Bonn, Germany. *(Oral and poster presentation)*
- **Schymik HS**, Dahlem C, Kiemer AK (2022). *The regulation of the RNA-binding protein IMP2 in macrophage activation.*
  15th World Congress on Inflammation, Rome, Italy. *(Poster presentation)*

Danksagungen

An dieser Stelle möchte ich mich ganz herzlich bei Frau Prof. Dr. Alexandra K. Kiemer bedanken. Bereits während meiner Masterarbeit durfte ich von Ihrer engagierten Betreuung profitieren und auch während der Promotion haben Sie mich mit großer Unterstützung begleitet - sei es bei der Antragstellung, dem Verfassen von Abstracts, Konferenzbeiträgen oder dem Publikationsprozess. Auch für kurzfristige Anliegen hatten Sie immer ein offenes Ohr. Besonders dankbar bin ich Ihnen für Ihre Unterstützung bei größeren Projekten wie dem Tierversuchsantrag und für Ihr unerschütterliches Vertrauen in den Erfolg meines Promotionsvorhabens. Durch Ihre Begleitung konnte ich nicht nur viel lernen, sondern mich auch fachlich und persönlich weiterentwickeln.

Mein besonderer Dank gilt Herrn Prof. Dr. Christian Ducho für die Übernahme der Rolle des wissenschaftlichen Begleiters sowie für die stets angenehme Zusammenarbeit.

Ich danke zudem allen Co-Autorinnen und Co-Autoren für die erfolgreiche Zusammenarbeit im Rahmen zahlreicher gemeinsamer Projekte.

Ein herzliches Dankeschön an die gesamte Arbeitsgruppe Pharmazeutische Biologie. Die Zusammenarbeit mit Euch war nicht nur fachlich bereichernd, sondern auch menschlich eine große Freude. Für die vielen schönen und oft auch humorvollen gemeinsamen Stunden im Labor, im Büro und in den Pausen - aus denen echte Freundschaften entstanden sind - danke ich euch von ganzem Herzen.

Liebe Dr. Jessica Hoppstädter, ich möchte mich ganz besonders bei dir bedanken. Schon während meiner Masterarbeit warst du eine tolle Betreuerin und auch während meiner Promotion konnte ich viel von Dir lernen - vom Laboralltag über das Schreiben bis hin zum gemeinsamen Brainstorming. Aber auch der Aperol in Rom, mein erstes Fußballspiel und unsere tiefgründigen politischen Diskussionen bleiben unvergessen - danke für all das.

Vielen lieben Dank auch an Dr. Charlotte Dahlem für deine engagierte und stets verlässliche Betreuung, die ich sehr geschätzt habe.

Liebe Annika Schomisch und Ella Mitschang, danke für eure Freundschaft und den wertvollen Ausgleich außerhalb des Labors, besonders unsere gemeinsame Töpferzeit werde ich nie vergessen.

Ein besonderer Dank gilt meiner Bouldercrew – für gemeinsame Ausflüge, Rennradtouren, Urlaube und viele unbeschwerte Stunden in der Kletterhalle. Eure Freundschaft und die gemeinsamen Erlebnisse waren ein wertvoller Ausgleich zum Promotionsalltag.

Lieber Lukas Mengestu, danke, dass du immer an meiner Seite warst und mich in allen Lebenslagen unterstützt hast. Du hast dir unzählige Gespräche angehört, mir Mut gemacht und mir mit kluger, konstruktiver Kritik bei Entscheidungen geholfen. Dein Vertrauen, deine Wärme und deine Ruhe haben mir stets Kraft gegeben – dafür bin ich dir von Herzen dankbar.

Ein großes Dankeschön gilt meiner Familie. Ihr habt mich vom Studium bis zur Promotion begleitet, mir stets den Rücken gestärkt – auch in schwierigen Phasen.

Zum Abschluss möchte ich darauf hinweisen, dass zur finalen sprachlichen Überarbeitung dieser Arbeit (Rechtschreibung, Grammatik, Stil) unterstützend ein KI-basiertes Schreibtool (z. B. ChatGPT, Grammarly) verwendet wurde. Die inhaltliche Ausarbeitung und wissenschaftliche Verantwortung liegen ausschließlich bei der Autorin.